Development of Fluorescent Markers for Super-Resolution Microscopy at Cryogenic Temperature

Angela Mantovanelli

THÈSE

Pour obtenir le grade de

DOCTEUR DE L'UNIVERSITÉ GRENOBLE ALPES

École doctorale : CSV- Chimie et Sciences du Vivant
Spécialité : Chimie Physique Moléculaire et Structurale
Unité de recherche : Institut de Biologie Structurale

Développement de marqueurs fluorescents pour la microscopie super-résolution à température cryogénique

Development of Fluorescent Markers for Super-Resolution Microscopy at Cryogenic Temperature

Présentée par :

Angela Maria Regina MANTOVANELLI

Direction de thèse :

Dominique BOURGEOIS DIRECTEUR DE RECHERCHE, Université Grenoble Alpes	Directeur de thèse

Rapporteurs :

Agathe ESPAGNE
MAITRE DE CONFERENCES HDR, Ecole Normale Supérieure Paris
Brahim LOUNIS
PROFESSEUR DES UNIVERSITES, Université de Bordeaux

Thèse soutenue publiquement le **10 mars 2023**, devant le jury composé de :

Dominique BOURGEOIS DIRECTEUR DE RECHERCHE CNRS, Institut de Biologie Structurale Grenoble	Directeur de thèse
Agathe ESPAGNE MAITRE DE CONFERENCES HDR, Ecole Normale Supérieure Paris	Rapporteure
Brahim LOUNIS PROFESSEUR DES UNIVERSITES, Université de Bordeaux	Rapporteur
Marie ERARD PROFESSEUR DES UNIVERSITES, Université Paris-Saclay	Examinatrice
Antoine ROYANT DIRECTEUR DE RECHERCHE CNRS, Institut de Biologie Structurale Grenoble	Président
Eve DE ROSNY MAITRE DE CONFERENCES HDR, Université Grenoble Alpes	Examinatrice

Thesis

To obtain the degree of

Doctor of Natural Sciences
from the Grenoble Alpes University

Specialty: Biophysics

Thesis prepared at the Institute of Structural Biology Grenoble
Doctoral School: Chemistry and Life Science
Thesis director: Dr. Dominique Bourgeois

Presented on 10th March 2023 by

Angela Maria Regina Mantovanelli

Development of Fluorescent Markers for Super-resolution Microscopy at Cryogenic Temperature

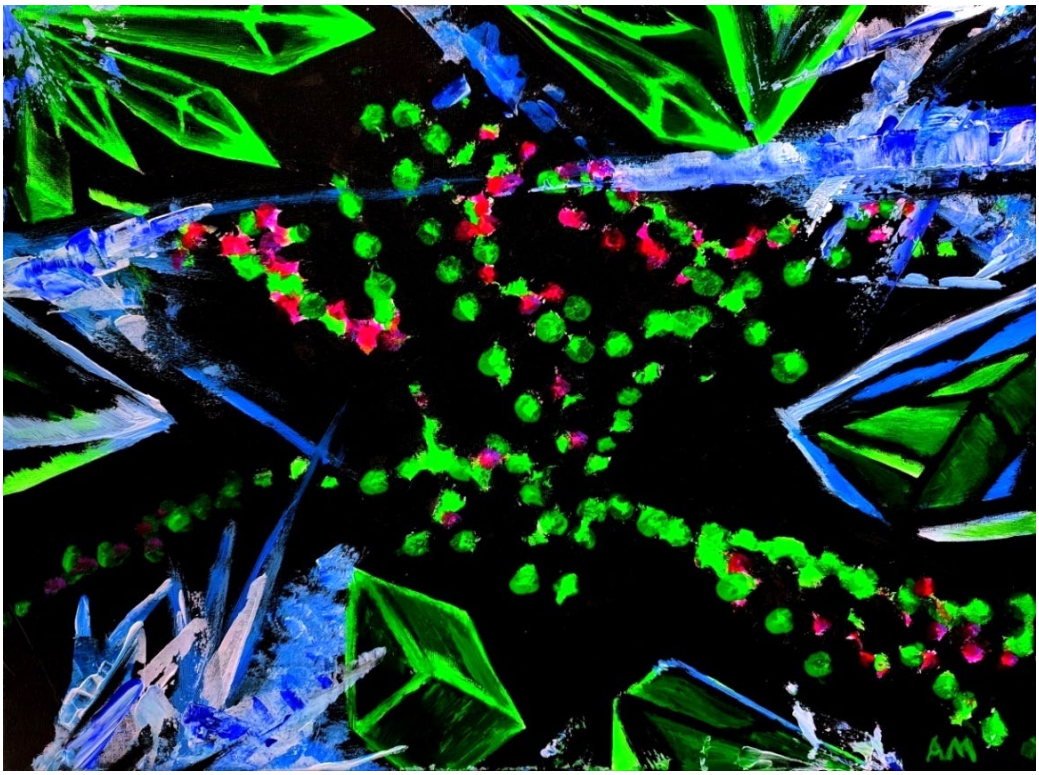

Examining jury:
Dr. Agathe Espagne: École Normale Supérieure Paris, Reviewer
Prof. Brahim Lounis: Bordeaux University, Reviewer
Dr. Antoine Royant: Institute of Structural Biology Grenoble, Jury President
Dr. Eve de Rosny: Grenoble Alpes University, Examiner
Prof. Marie Erard: Paris Saclay University, Examiner
Dr. Dominique Bourgeois: Institute of Structural Biology Grenoble, Supervisor

(Title page: painting by the author abstractly illustrating two-color single molecule localization microscopy in frozen conditions and fluorescent protein crystals)

Table of contents

List of abbreviations

ABD	Azobenzene derivative
CCD	Charge-coupled device
CCP4	Collaborative Computational Project Number 4
CIF	Crystallographic Information File
CNS	Crystallography and NMR system
CT	Cryogenic temperature
DC	Duty cycle
DMSO	Dimethyl sulfoxide
DNA	Desoxyribonucleic acid
DTT	Dithiothreitol
EGFP	Enhanced green fluorescent protein
EM	Electron microscopy
EMCCD	Electron multiplying charge-coupled device
ESRF	European Synchrotron Radiation Facility
ET	Electron tomography
EYFP	Enhanced yellow fluorescent protein
GFP	Green fluorescent protein
HBDI	p-hydroxybenzylideneimidazolidinone
HEPES	4-(2-hydroxyethyl)-1-piperazineethanesulfonic acid
ISC	Intersystem crossing
mEGFP	Monomeric EGFP
NR	Non-radiative relaxation
OD	Optical density
PAFPs	Photoactivatable fluorescent proteins
PA-GFP	Photoactivatable GFP
PALM	Photoactivated localization microscopy
PCFPs	Photoconvertible fluorescent proteins
PDB	Protein Data Bank
PM	Photomultiplier
PVA	Poly vinyl alcohol
RESOLFT	Reversible saturable optical fluorescence transitions
RISC	Reverse intersystem crossing
rsEGFP	Reversibly switchable enhanced green fluorescent protein
RSFPs	Reversibly switchable fluorescent proteins
RT	Room temperature
SFX	Serial femtosecond crystallography
SMLM	Single-molecule localization microscopy
STED	Stimulated emission depletion
STORM	Stochastic optical reconstruction microscopy
XDS	X-ray Detector Software

List of figures

List of tables

Abstract

Single-molecule localization microscopy is a powerful tool for studying biological processes at nanoscale resolution. However, in this technique, biological samples are typically fixed chemically to avoid motion blur. As the chemical fixation may produce artifacts at these high resolutions, alternative fixation strategies are of high demand. One solution is to freeze the samples at cryo-temperature, which also has other advantages as for example the possibility of performing cryo-correlative studies with cryo-EM. The main challenge of sample-freezing is the lack of fluorescent markers which can undergo efficient photo-switching at cryo-temperature. Organic dyes which are typically used in stochastic super-resolution microscopy cannot be used, because their switching is based on diffusion of STORM buffer molecules, which is hampered below the glass transition temperature. In addition, few organic fluorophores can cross the membrane of living cells, so chemical fixation is often necessary, even at cryogenic temperature. In contrast, fluorescent proteins are genetically encoded and can be expressed directly with the protein of interest and thus no fixation is necessary. Hence, they are the best candidates to be used as fluorescent markers for single-molecule localization microscopy at cryogenic temperature. However, strategies to photo-switch them more efficiently are required, as their conformational flexibility is reduced at such temperature.

We performed spectroscopic and structural investigations on the fluorescent protein rsEGFP2 and also studied other proteins (rsEGFP2-V151A, rsEGFP2-V151L, mEmerald and EGFP) at room- and cryo-temperature in order to understand their switching mechanisms, and we developed an illumination strategy to enhance their recovery from non-fluorescent to fluorescent states at cryo-temperature. We observed, that for rsEGFP2, the cryo-switching mechanism is structurally and spectroscopically different from the mechanism at room temperature. In contrast to a cis-trans isomerization at room temperature, no major structural changes between the on- and off-states were observed by X-ray crystallography for switching at cryogenic temperature. The absorbance and fluorescence microspectrophotometry investigations revealed two off-states arising upon cryo-off-switching, both blue shifted as compared to the off-state which is observed after room temperature switching. With the typically used 405 nm laser only one of the off-states is recoverable to the fluorescent on-state. We observed that with a 355 nm laser both off-states are recoverable and thus achieve a substantial enhancement of total recovery of the fluorescent state. Interestingly, the switching of mEmerald and EGFP at cryo- and room-temperature appear to be very similar to the rsEGFP2 switching at cryo-temperature, which indicates that this new switching mechanism could be general to proteins of the GFP family. Using a 355 nm laser for activating fluorescent proteins like rsEGFP2, mEmerald and EGFP at cryo-temperature could open the door to more efficient effective labeling in single-molecule localization microscopy applications at cryo-temperature.

Résumé

La microscopie à localisation de molécules uniques est une méthode puissante pour étudier les processus biologiques à une résolution nanométrique. Cependant, dans cette technique, les échantillons biologiques sont généralement fixés chimiquement pour éviter les mouvements. Comme la fixation chimique peut produire des artefacts à ces hautes résolutions, il est nécessaire de développer des stratégies de fixation alternatives. Une solution consiste à congeler les échantillons à une température cryogénique, ce qui présente également d'autres avantages, comme par exemple la possibilité de réaliser des études cryocorrélatives avec la cryo-EM. Un défi important est cependant le manque de marqueurs fluorescents capables de photocommuter efficacement à température cryogénique. Les fluorophores organiques qui sont généralement utilisés en microscopie ne peuvent pas être utilisés, car leur commutation est basée sur la diffusion des molécules du tampon STORM, qui est entravée en dessous de la température de transition vitreuse. En outre, peu de fluorophores organiques peuvent traverser la membrane des cellules vivantes, et une fixation chimique reste donc souvent nécessaire. A l'inverse, les protéines fluorescentes sont codées génétiquement et peuvent être exprimées directement avec la protéine d'intérêt et aucune fixation n'est donc nécessaire. Elles sont donc les meilleurs candidats pour être utilisées comme marqueurs fluorescents pour la microscopie de localisation de molécules uniques à température cryogénique, mais des stratégies pour les photocommuter plus efficacement sont nécessaires, car leur flexibilité conformationnelle est réduite à cette température.
Nous avons réalisé des études spectroscopiques et structurales sur la protéine fluorescente rsEGFP2 et nous avons également étudié d'autres protéines (rsEGFP2-V151A, rsEGFP2-V151L, mEmerald et EGFP) à température ambiante et à température cryogénique afin de comprendre leurs mécanismes de photocommutation Nous avons développé une stratégie d'illumination pour améliorer leur retour de l'état non-fluorescent à l'état fluorescent à température cryogénique. Nous avons observé que pour rsEGFP2, le mécanisme de photocommutation cryogénique est structuralement et spectroscopiquement différent du mécanisme à température ambiante. Contrairement à une isomérisation cis-trans à température ambiante, aucun changement structural majeur entre l'état fluorescent et l'état non-fluorescent n'a été observé par cristallographie aux rayons X à température cryogénique. Les études de microspectrophotométrie d'absorbance et de fluorescence ont mis en évidence deux états non-fluorescents différents qui se produisent lors de la photocommutation cryogénique, tous deux décalés vers le bleu par rapport à l'état non-fluorescent observé après la commutation à température ambiante. Avec le laser 405 nm généralement utilisé, seul l'un des états non-fluorescents peut être ramené à l'état fluorescent. Nous avons observé qu'avec un laser 355 nm, les deux états non-fluorescents sont récupérables, ce qui permet d'améliorer significativement le retour de l'état fluorescent. Il est intéressant de noter que la photocommutation de mEmerald et d'EGFP aux températures ambiantes et cryogéniques semble très similaire à la commutation de rsEGFP2 à température cryogénique, ce qui indique que ce nouveau mécanisme de commutation pourrait être général aux protéines de la famille GFP. L'utilisation d'un laser de 355 nm pour activer des protéines fluorescentes comme rsEGFP2, mEmerald et EGFP à cryo-température pourrait permettre d'obtenir un marquage effectif plus efficace dans les applications de microscopie de localisation de molécules uniques à cryo-température.

Zusammenfassung

Die Einzelmolekül-Lokalisierungsmikroskopie ist eine leistungsstarke Methode zur Untersuchung biologischer Prozesse mit einer Auflösung im Nanobereich. Dabei werden biologische Proben jedoch in der Regel chemisch fixiert, um unerwünschte Bewegungen zu vermeiden. Da die chemische Fixierung bei diesen hohen Auflösungen zu Artefakten führen kann, sind alternative Fixierungsstrategien sehr gefragt. Eine Lösung ist das Einfrieren der Proben bei Kryo-Temperatur, was darüber hinaus weitere Vorteile hat, wie zum Beispiel die Möglichkeit, Kryo-Korrelationsstudien mit Kryo-EM durchzuführen. Das größte Hindernis bei der Benutzung von Proben bei Kryo-Temperatur ist der Bedarf an fluoreszierenden Markern, die bei diesen tiefen Temperaturen einen effizienten Photo-Umschaltprozess durchlaufen können. Organische Farbstoffe, die typischerweise in der stochastischen Superauflösungs-mikroskopie verwendet werden, können nicht eingesetzt werden, da ihre Umschaltung auf Diffusion von STORM-Puffer-Molekülen beruht, welche unterhalb der Glasübergangstemperatur eingeschränkt ist. Darüber hinaus können nur wenige organische Farbstoffmoleküle die Membran lebender Zellen passieren, sodass meist eine chemische Fixierung erforderlich bleibt. Da fluoreszierende Proteine genetisch kodiert sind und direkt mit dem Protein von Interesse exprimiert werden können, ist hier keine Fixierung notwendig. Daher sind sie die beste Wahl für die Verwendung als fluoreszierende Marker für die Einzelmolekül-Lokalisierungsmikroskopie bei kryogener Temperatur, jedoch sind Strategien erforderlich, um sie effizienter zu schalten, da ihre Konformationen bei dieser Temperatur weniger flexibel sind.
Wir führten spektroskopische und strukturelle Untersuchungen am fluoreszierenden Protein rsEGFP2 durch und untersuchten auch andere Proteine (rsEGFP2-V151A, rsEGFP2-V151L, mEmerald und EGFP) bei Raum- und Kryo-Temperatur, um ihre Umschaltmechanismen zu verstehen, und wir entwickelten eine Belichtungsstrategie, um ihre Reaktivierung von nicht-fluoreszierenden zu fluoreszierenden Zuständen bei Kryo-Temperatur zu verbessern. Wir haben festgestellt, dass sich der Kryo-Umschaltmechanismus für rsEGFP2 strukturell und spektroskopisch von dem Mechanismus bei Raumtemperatur unterscheidet. Im Gegensatz zu einer cis-trans-Isomerisierung bei Raumtemperatur wurden bei der Umschaltung bei kryogener Temperatur mittels Röntgenkristallographie keine wesentlichen strukturellen Veränderungen zwischen dem Ein- und Aus-Zustand beobachtet. Die Absorptions- und Fluoreszenzmikrospektrophotometrie-Untersuchungen brachten zwei verschiedene Aus-Zustände zum Vorschein, die beim Kryo-Aus-Schalten entstehen, beide blau verschoben im Vergleich zu dem Aus-Zustand, der nach dem Umschalten bei Raumtemperatur beobachtet wird. Mit dem üblicherweise verwendeten 405-nm-Laser kann nur einer der Aus-Zustände in den fluoreszierenden Zustand zurückgeführt werden. Wir haben beobachtet, dass mit einem 355-nm-Laser beide Aus-Zustände wiederhergestellt werden können und somit eine wesentliche Verbesserung der Gesamtreaktivierung des fluoreszierenden Zustands erreicht wird. Interessanterweise scheint das Umschalten von mEmerald und EGFP bei Kryo- und Raumtemperatur dem Umschalten von rsEGFP2 bei Kryo-Temperatur sehr ähnlich zu sein, was darauf hindeutet, dass dieser neue Umschaltmechanismus für Proteine der GFP-Familie verallgemeinerbar sein könnte. Die Verwendung eines 355-nm-Lasers zur Aktivierung von fluoreszierenden Proteinen wie rsEGFP2, mEmerald und EGFP bei Kryo-Temperatur könnte ein effizienteres effektives Markieren bei Anwendungen der Einzelmolekül-Lokalisierungsmikroskopie bei Kryo-Temperatur ermöglichen.

I. State of the Art

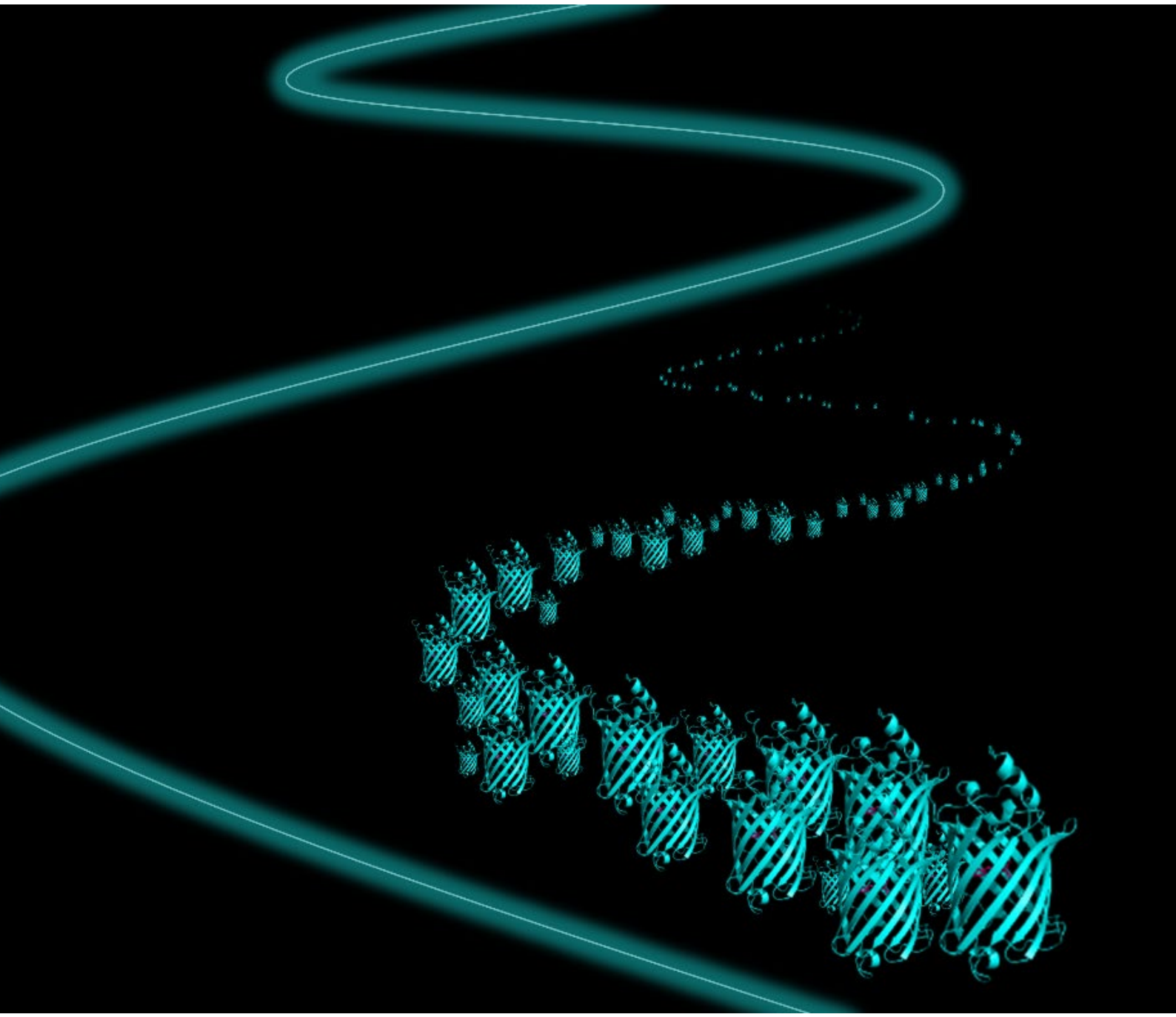

1. Fluorescent proteins and their photophysics

1.1. Motivation to study fluorescent proteins in this work

Fluorescent proteins are widely used as fluorescent markers in fluorescence microscopy. Their main advantages over other fluorophores are that they are fully genetically encoded and allow highly specific labelling. By the development of photoactivated localization microscopy (PALM) with fluorescent proteins (Betzig et al., 2006) it became possible to overcome the diffraction limit in microscopy. Many different super-resolution microscopy (nanoscopy) techniques using different kinds of fluorophores were developed since then. Moreover, there is a high demand on performing single-molecule localization microscopy (SMLM) at cryogenic temperature (CT) in order to avoid chemical cell fixation, which creates artifacts at high resolution (Whelan & Bell, 2015). For SMLM, efficiently switchable fluorophores, undergoing highly complete switching, are necessary but dynamics are hampered at CT and thus it is challenging to find suitable fluorophores. Fluorescent proteins have an advantage over fluorophores whose switching relies on the diffusion of buffer molecules, as diffusion is hampered below the glass transition temperature. However, also protein dynamics of fluorescent proteins are hampered at CT and it is challenging to find an efficiently switchable protein.

In this work, the focus is placed on investigating the CT switching mechanism of the reversibly switchable enhanced green fluorescent protein rsEGFP2, as its switching is known to be very fast at room temperature (RT) (Grotjohann et al., 2012) and thus rsEGFP2 could be a suitable candidate for single-molecule localization microscopy at CT. Moreover, the goal is to obtain more general understanding of the switching mechanisms and photophysical properties of GFP proteins at CT and to use this knowledge to enhance their switching efficiency at CT.

After an introduction to the principle of fluorescence, we discuss the origin and the properties of the green fluorescent protein (GFP) and phototransformable variants developed from it. The known RT photoswitching mechanisms of fluorescent proteins are explained in order to address the question which proteins could also undergo efficient photoswitching at CT to be usable for SMLM at CT. Finally, fluorescent proteins which were already demonstrated to be switchable at CT are reviewed in detail to figure out potential candidates which would be of interest for further investigations.

1.2. Fluorescence and dark state formation

Fluorescence is the emission of a photon of a certain energy by a molecule which has been excited by absorbing a photon of a higher energy. A molecule in the electronic ground state S_0 can reach the first excited state S_1 by absorbing a photon with a wavelength which corresponds to the energy difference between these two states (Figure 1). Each state consists of several sub-states with different vibrational energies. The molecule can vibrationally relax to sub-states of lower energy. From the S_1 state the molecule can reach the S_0 state either by non-radiative relaxation or by emitting a photon of the corresponding energy (fluorescence) (Figure 1). A third possibility is intersystem crossing (ISC) to the triplet state T_1 which involves an electron spin flip and is therefore considered as a so-called forbidden transition. This is also the case for the reverse intersystem crossing (RISC) from T_1 to S_1. For this reason, the triplet-state has a relatively long lifetime on the millisecond time scale, unlike the S_1 state which has a lifetime in the nanosecond range. The triplet state can reach the ground state by phosphorescence, i.e. the emission of a photon with a long wavelength corresponding to the energy gap or by non-radiative

relaxation (Figure 1). It was observed that the lifetime of the triplet-state is a few milliseconds in fluorescent proteins at RT (Byrdin et al., 2018) and also at CT (Rane et al., 2023). The triplet state can react further to radical dark-states (Figure 1) and thus opens the door to many reaction pathways and bleaching (see section 1.5) (Byrdin et al., 2018). The triplet state can bleach either directly or through the radical dark-states. The dark-states can also react back to the S_0 state upon electron transfer. This reaction can be favored by electron donors or acceptors (see section 1.5). Upon further excitation, higher energetic triplet states T_n can be reached, which also can react further to radical dark states.

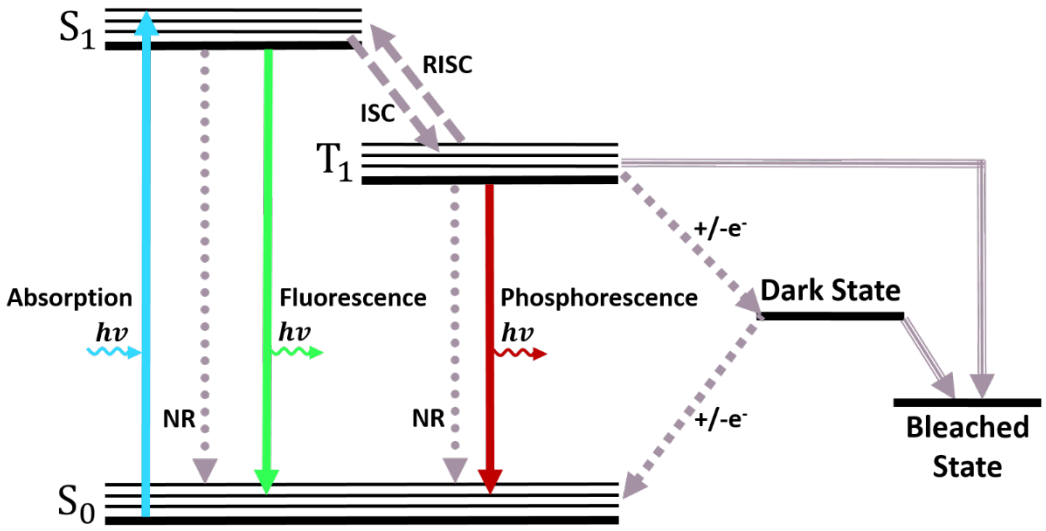

Figure 1: Simplified Jablonski diagram. By absorption of a photon with a particular wavelength a molecule can get excited from the electronic ground state S_0 to the first excited state S_1. By vibrational relaxation it can reach a lower energy vibrational state of S_1. From the latter one it can reach S_0 by non-radiative relaxation (NR), or by emission of a photon with the wavelength corresponding to the energy difference between the states or through intersystem crossing (ISC) to the triplet state T_1 and subsequent emission of a photon. T_1 can also undergo reverse intersystem crossing (RISC) to S_1 or bleach or further react to non-fluorescent radical states which can react back to S_0 or bleach. For simplicity, higher energy states (S_2 to S_n and T_2 to T_n) are not shown in this diagram.

1.3. Green Fluorescent Protein (GFP)

1.3.1 Discovery

The Green Fluorescent Protein (GFP) was discovered in the jellyfish *Aequorea victoria* (Figure 2) in 1962 by Osamu Shimomura, who was awarded with the Nobel Prize in 2008 together with Martin Chalfie and Roger Tsien “for the discovery and development of the green fluorescent protein” (Zimmer, 2009).

Figure 2: Painting by the author showing the jellyfish Aequorea victoria. Only the lateral edge of the umbrella is fluorescent.

The main advantage of GFP as compared to other fluorescent markers is that it is fully genetically encoded. This makes it possible to fuse the DNA of GFP to that of other proteins, which thus can be monitored by fluorescence detection without the need to add or attach other co-factors. GFP can be expressed by bacteria and be produced in large quantities. It was sequenced and cloned by Prasher et al. (1992) and expressed in C. elegans by Chalfie (Chalfie et al., 1994). Tsien developed a panoply of different fluorescent proteins which opened the door to many applications (Zimmer, 2009).

Fluorescent proteins were not only found in Aequorea Victoria, but similar proteins were discovered later in many other organisms, such as reef corals (Matz et al., 1999), which will be discussed in section 1.4.2.

1.3.2 Protein structure

GFP consists of a single chain composed of 238 residues, which is folded to eleven β-strands forming a cylinder of 24 Å diameter and 42 Å length (Ormö et al., 1996) (Figure 3).

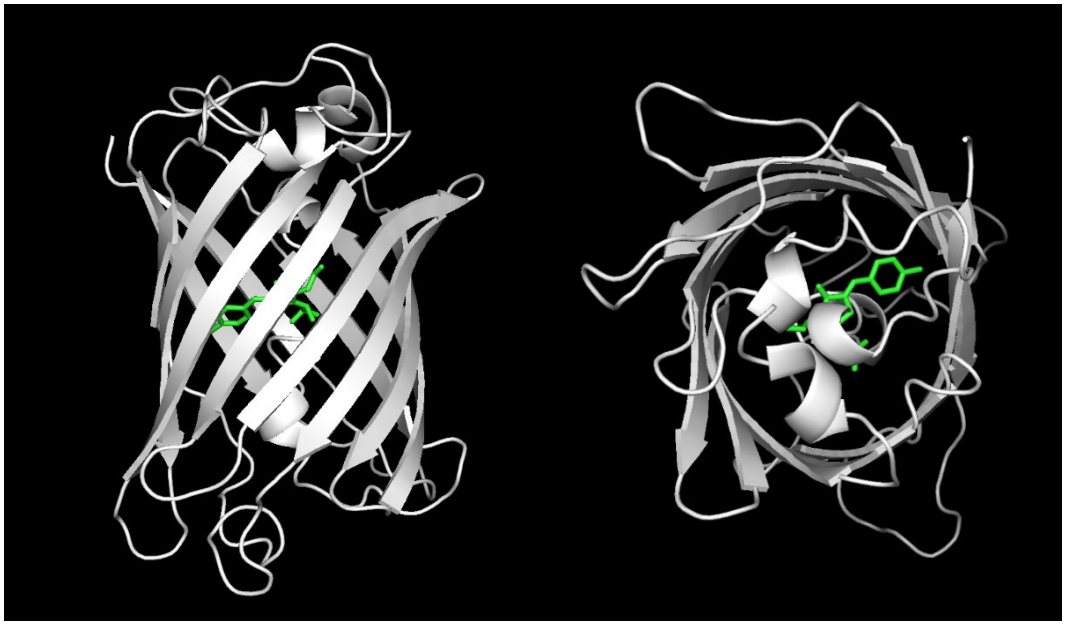

Figure 3: Protein Data Bank (PDB) structure 1EMA of GFP (Ormö et al., 1996) *side and front view. The chromophore is shown in green and the β-strands in white.*

The p-hydroxybenzylideneimidazolidinone (HBDI) chromophore (Cody et al., 1993) is tightly packed inside this β-barrel, to which it is connected by an α-helix, and thus is hampered to relax thermally from the excited state. This fact is essential, as it favors the chromophore to undergo fluorescence instead.

1.3.3 Chromophore

The chromophore of GFP is composed of three amino acids – serine (position 65 in the protein chain), tyrosine (position 66) and glycine (position 67) (Figure 4).

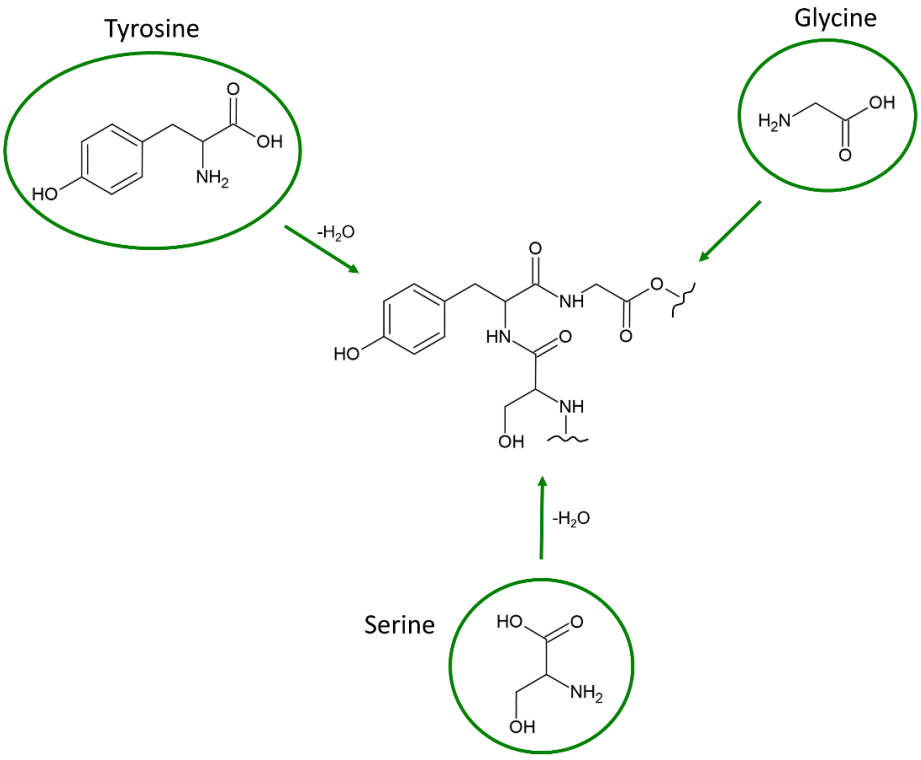

Figure 4: By peptide bonding, tyrosine 66, glycine 67 and serine 65 form the chromophore. The continuation of the amino acid chain is marked by a wavy line.

Zang et al. (2006) describe the formation of the imidazolinone ring as follows (Figure 5): In the first step a cyclization takes place, which is initiated by a hydrophilic attack of the glycine nitrogen onto the carbonyl of the serine that

leads to ring closure forming an intermediate state with a five-membered ring. It involves the movement of a hydrogen of the glycine to the oxygen of the serine. Oxygen present in the chromophore environment can react with two hydrogens from the five-membered ring to hydrogen peroxide. Further rearrangements of the atoms lead to the formation of a water molecule out of the hydroxyl group of the five-membered ring and a hydrogen of the tyrosine. An alternative mechanism was proposed by Tsien (1998), who describes that dehydration occurs before oxidation.

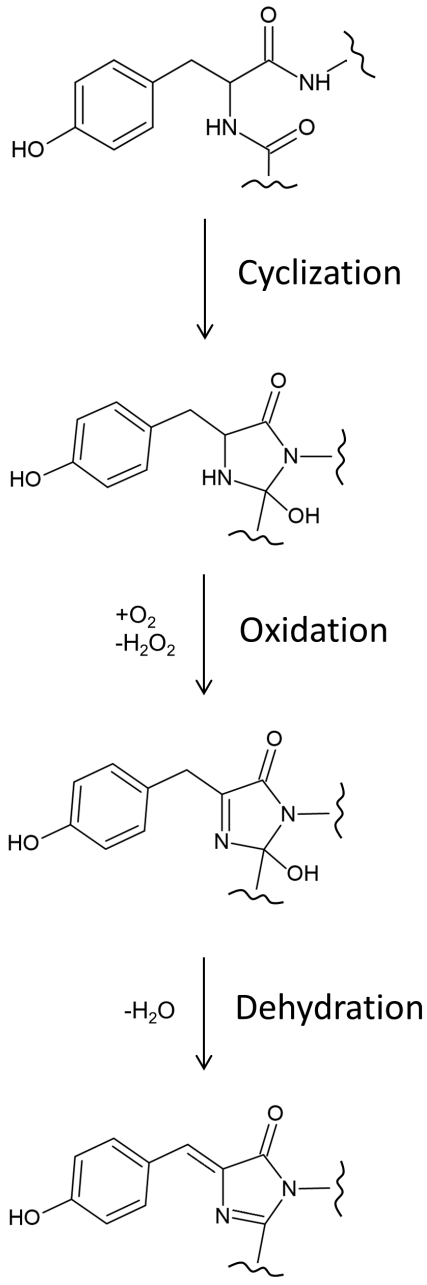

Figure 5 (based on Zhang et al., 2006*): Cyclization, oxidation and dehydration of the chromophore. For clarity, the continuing part of the chain which does not undergo changes is not shown and marked by a wavy line.*

The conjugation of the imidazolinone ring with the hydroxybenzylidene due to the connecting double bond allows a largely delocalized electron distribution in a π-electron conjugation system which can absorb visible light and thus is responsible for the photophysical properties of GFP.

Tsien (1998) measured absorption and emission spectra of GFP and found a maximum absorption at 395 nm with a shoulder at 475 nm. Tsien observed that excitation at 395 nm leads to a maximum fluorescence emission peak at 508 nm and excitation at 475 nm to a maximum peak at 503 nm. His data shows that upon excitation of GFP with 395 nm light the absorption peak at this wavelength decreases and the 475 nm shoulder increases. Kneen et al. (1998) observed that at higher pH, i.e. less protons available in the buffer, the 475 nm shoulder is substantially higher than at lower pH. These effects can be explained by the existence of two different states with different protonation, as it was proposed by Chattoraj et al. (1996). They suggest that these states can be interconverted fast in the light induced excited state via excited state proton transfer, but also on a slower time scale in the ground state. Brejc et al. (1997) provide a detailed scheme of this proton redistribution (Figure 6). The chromophore can be protonated at the hydroxyl group of the tyrosine end or stay in the anionic state, which makes a substantial difference to the chromophore properties because protonation involves the bonding of one electron which is thus not available for the electron conjugation system which is shared between the hydroxybenzylidene and the imidazolidinone. Upon absorption of a photon by the hydroxybenzylidene, an electron movement into the direction of the imidazolinone ring takes place. In the protonated state, this electron movement is less facilitated due to the attraction of the positive charge of the proton and thus more photon energy is necessary to make an absorption take place. Hence, in the protonated state the conjugated system has a higher energy gap between the S_0 and S_1 states and thus photons of shorter wavelengths are absorbed.

1.3.4 Enhanced GFP variants

The fluorescence brightness of GFP was improved and new variants as for example the Enhanced Green Fluorescent Protein (EGFP) were developed by including mutations, which was the starting point for many different variants.

(a) EGFP

GFP was enhanced by Heim & Tsien (1996) by mutation of the serine 65 of the chromophore to a threonine (mutation S65T), which led to a 6-fold fluorescence brightness enhancement. Brejc et al. (1997) propose a hydrogen bond network scheme for GFP and the S65T mutant (Figure 6) with which they explain that the threonine 65 stabilizes the hydrogen bond network of the deprotonated chromophore with the additional methyl group, which prevents ionization of glutamic acid 222. By this the chromophore can stay ionized and thus the protonated species, which is not fluorescent, can be suppressed and the fluorescence is enhanced.

Cormack et al. (1996) introduced an additional point mutation: phenylalanine 64 was substituted by a leucine. By this, they enhanced the brightness by a factor of about 30 as compared to the GFP wildtype. They express the hypotheses that these mutations could favor protein folding or chromophore formation or affect the absorption efficiency. G. Zhang et al. (1996) constructed a variant with these two mutations and with replaced codons which are suitable for high expression in mammalian cells, as compared to the jelly fish codons, and called it Enhanced Green Fluorescent Protein (EGFP). According to Tsien (1998), the F64L mutation might improve the GFP folding properties for temperatures above RT and thus lead to higher brightness.

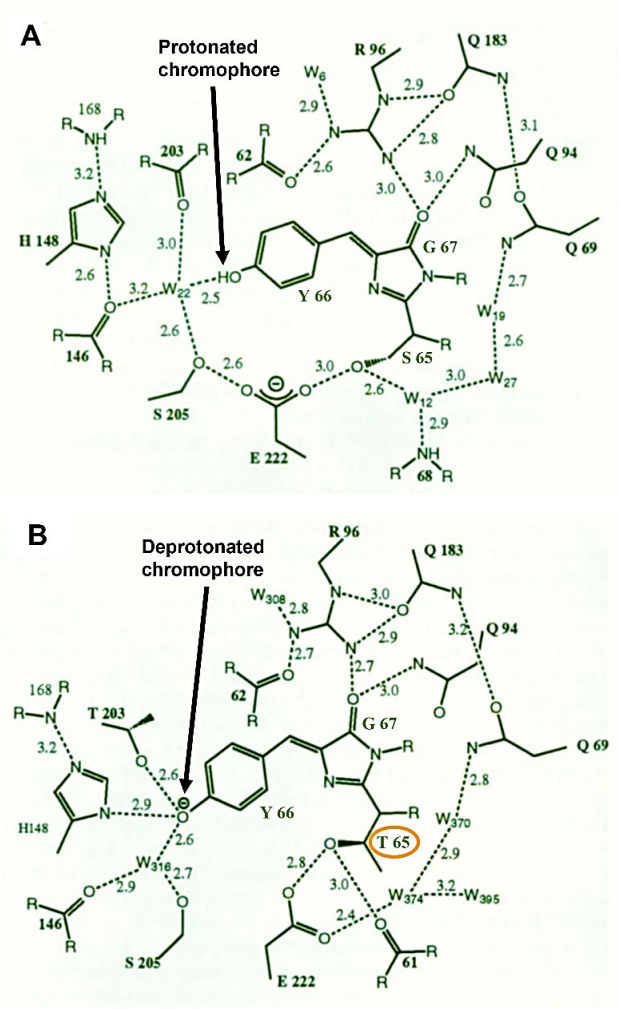

Figure 6 (adapted from Brejc et al., 1997*): Scheme of chromophore and its interaction with its environment in (A) GFP and (B) GFP-S65T. Hydrogen bonds are shown in dashed lines with the bond lengths indicated in Å.*

(b) mEmerald

The GFP variant Emerald (F64L, S65T, S72A, N149K, M153T, and I167T) is derived from EGFP and has similar properties but with improvements such as increased brightness and photostability and faster folding (Cubitt et al., 1999; Day & Davidson, 2009; Shaner et al., 2007). The monomeric variant mEmerald additionally contains the mutation A206K which inhibits dimer formation (Shaner et al., 2007). It was tried to photoswitch mEmerald at RT but a low contrast between the non-activated and activated state was

observed due to a bright non-activated state (Shaner et al., 2007). For SMLM of fusion proteins at RT, they obtained much higher numbers of localized molecules with other marker proteins such as mNeonGreen than with mEmerald (Shaner et al., 2013). However, it was observed that a cryogenic temperature mEmerald is efficiently switchable (Hoffman et al., 2020) (see 1.6 for more detailed description). Thus, it is considered as a fluorescent protein of high interest for this work.

1.4. Phototransformable fluorescent proteins

1.4.1 Overview

From GFP many different variants were developed by several mutations. An overview of the variants which are of particular interest in this work including their parent proteins is shown in Figure 7.

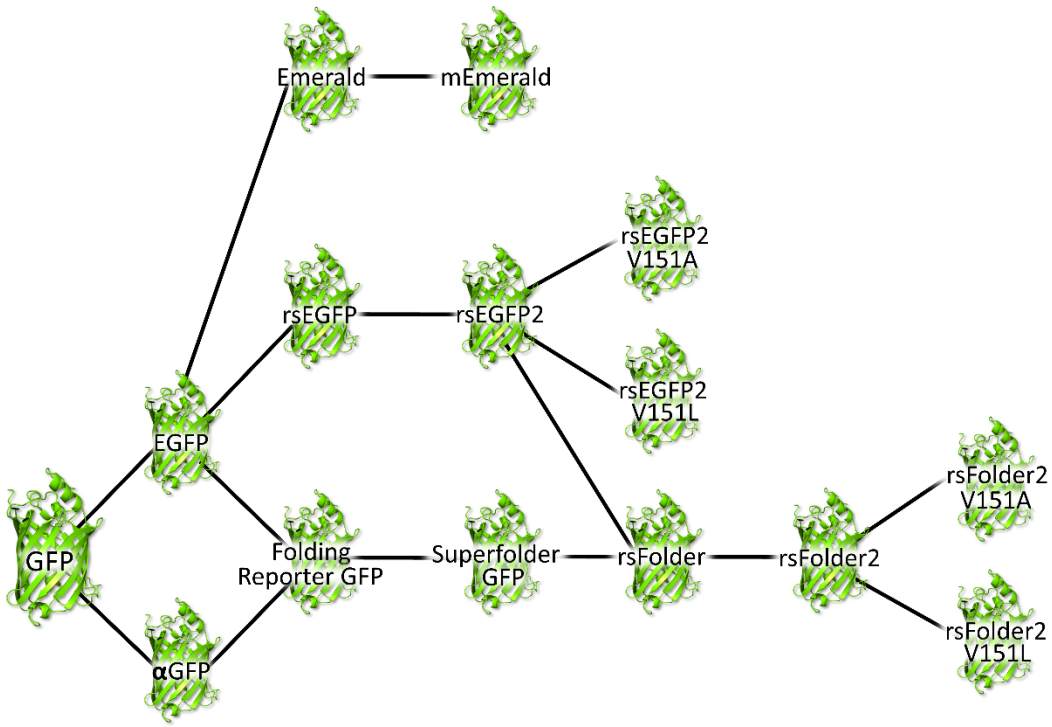

Figure 7: Development of different variants from left to right by mutagenesis of GFP.

By approaches to control the transition between the two different protonation states present in GFP and optimizing their properties, phototransformable proteins were developed. Photoactivatable fluorescent proteins (PAFPs) can be activated from a non-fluorescent state to a fluorescent state upon laser light illumination of a certain wavelength (typically 405 nm). This enables important applications such as photoactivated localization microscopy (see section 2.2).

Reversibly switchable fluorescent proteins (RSFPs) were engineered, as they are useful for many important applications, such as RESOLFT (see section 2.4). They can be switched back and forth between a fluorescent and a non-fluorescent state upon illumination with certain wavelengths of laser light (typically 405 nm and 488 nm). It was observed that in many RSFPs the underlying mechanism of switching between these states is a cis-trans isomerization of the chromophore (Andresen et al., 2005). From this knowledge more RSFPs could be developed, such as rsEGFP (Grotjohann et al., 2011) and rsEGFP2 (Grotjohann et al., 2012).

Moreover, photoconvertible fluorescent proteins (PCFPs), which can switch between states of different emission wavelengths were found in corals. For example, proteins of the Eos family can switch between a green and a red state (Wiedenmann et al., 2004).

In the following, engineering and applications of the variants which were used for this work, and which are important to understand the context are described.

1.4.2 Photoswitching in fluorescent proteins of anthozoan origin

The organisms which contain fluorescent proteins can be divided into two classes, the hydrozoa, to which *Aequorea victoria* and other jellyfishes belong to and the Anthozoa, which include corals and sea anemones. Anthozoa and Hydrozoa belong to the same Phylum – *Cnidaria* – and thus

contain fluorescent proteins of a similar origin. Matz et al. (1999) discovered proteins in reef corals which are homologous to GFP. They observed that the proteins also have a β-barrel structure but that it is more elliptical than for GFP. Also different spectral properties were observed for proteins of anthozoan origin, which typically have a more reddish color. Lukyanov et al. (2000) observed that the emission intensity of the protein asFP595 of the sea anemone *Anemonia sulcata* differs depending on the illumination wavelength, which was classified as the first description of efficient photoswitching (Bourgeois & Adam, 2012). Ando et al. (2004) developed the RSFP Dronpa, a variant originating from the coral *Echinophyllia sp. SC22*. It was the first fluorescent protein used as a reversibly switching fluorescent marker for biological samples in cryo-correlated studies of cryo-PALM and cryo-EM (B. Liu et al., 2015) (see section 2.5.3). Andresen et al. (2007) performed structural studies on Dronpa and observed that at RT it undergoes cis-trans isomerization, followed by rearrangements of neighboring amino acids (Figure 8).

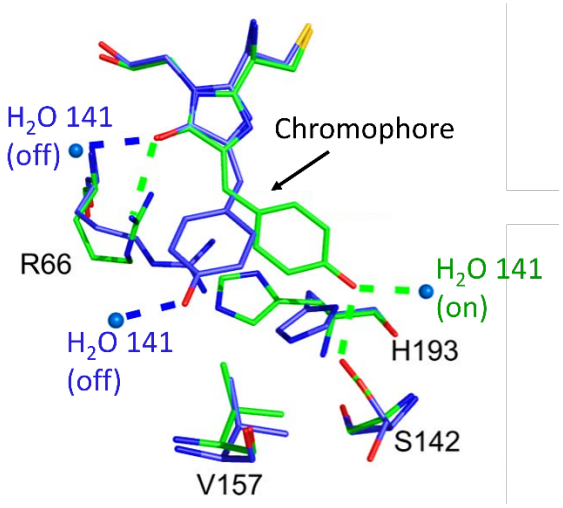

Figure 8 (adapted from Andresen et al. 2007): X-ray crystallography structure of Dronpa in the on-state (green) and in the off-state (blue).

Of note, they suggest that not the trans-conformation itself is the main reason for favoring protonation, which then inhibits fluorescence, but the non-planarity of the chromophore and that it is bound less strongly to the β-barrel. As described in section 1.3.2, tight bonding to the surrounding is

essential to favor fluorescence. Moreover, Andresen et al. (2008) generated other Dronpa variants, such as rsFastLime and Padron. Padron was the first RSFP for which a positive switching mechanism was observed (Andresen et al., 2008). It is in the non-fluorescent state in its non-illuminated form and can be switched to the fluorescent state by 488 nm light, which at the same time excites the on-state to fluoresce. By 405 nm light it can be switched back-off. This is the opposite behavior to what is observed for example in Dronpa and rsFastLime, which exhibit negative photoswitching. These proteins are initially in the on-state which is excited by 488 nm light, which at the same time causes off-switching. Back-on switching is achieved by 405 nm light. Andresen et al. (2008) show that Dronpa/rsFastLime and Padron together can be used for monochromatic multilabel super-resolution imaging by the use of only two illumination wavelengths.

Another fluorescent protein which is commonly used as a marker in SMLM imaging is the photoconvertible EosFP, which can irreversibly switch between a green and a red fluorescent state and was found in the coral *Lobophyllia hemprichii* (Wiedenmann et al., 2004). The red state is reached due to an extension of the conjugated system after backbone cleavage (Figure 9).

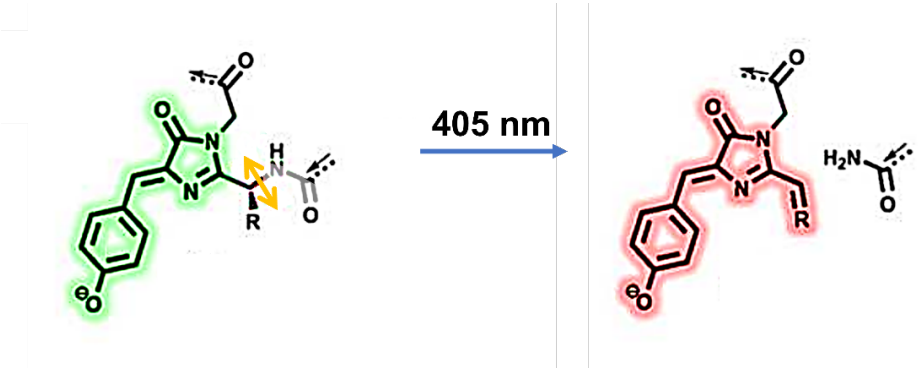

Figure 9 (adapted from Adam et al., 2014)*: Green-to-red photoconversion in EosFP. 405 nm light illumination causes breaking of a peptide bond which leads to an extension of the conjugated system to the histidine of EosFP (marked as R).*

EosFP was further enhanced to the mEos2 variant with higher brightness and photostability (McKinney et al., 2009) and to mEos3.1 and mEos3.2

with further improved properties such as brightness and maturation (M. Zhang et al., 2012). mEos4b was developed by Paez-Segala et al. (2015), which retains its fluorescence and photoconversion efficiency in heavily fixed samples as used for electron microscopy. Many other variants were developed from EosFP, such as IrisFP (Adam et al., 2008) and its monomeric form mIrisFP (Wiedenmann et al., 2011), which can be switched between a dark state and a green state, which upon 405 nm light illumination can irreversibly photoconvert to a red state and a corresponding dark state. A more complex model of switching in mEos4b was suggested by Wulffele et al. (2022), involving several dark states and bleached states (see non-linear bleaching in section 7.5).

In the reddish anemone *Entacmaea quadricolor* the red fluorescent protein eqFP578 was found (Merzlyak et al., 2007). Photoactivatable red variants such as PAmKate were engineered to bring forward multicolor imaging (Gunewardene et al., 2011).

1.4.3 Photoactivatable hydrozoan fluorescent proteins (PAFPs)

Patterson & Lippincott-Schwartz (2002) developed the first photoactivatable GFP (T203H) variant PA-GFP, which can be efficiently photoactivated by ~400 nm light. This variant shows a 100-fold increase of fluorescence upon 488 nm illumination, with respect to the non-activated state, which is a great enhancement compared to previous attempts to develop PAFPs (Elowitz et al., 1997; Marchant et al., 2001; Sawin & Nurse, 1997; Yokoe & Meyer, 1996 cited by Patterson & Lippincott-Schwartz, 2002). Patterson & Lippincott-Schwartz (2002) suggest that 413 nm laser light leads to decarboxylation of Glu222, which leads to a change in the hydrogen bond pattern that surrounds the chromophore and thus to a rotation of the T203 residue, which could be the reason for the change of the chromophore state from neutral to anionic, giving rise to the fluorescent state (Figure 10).

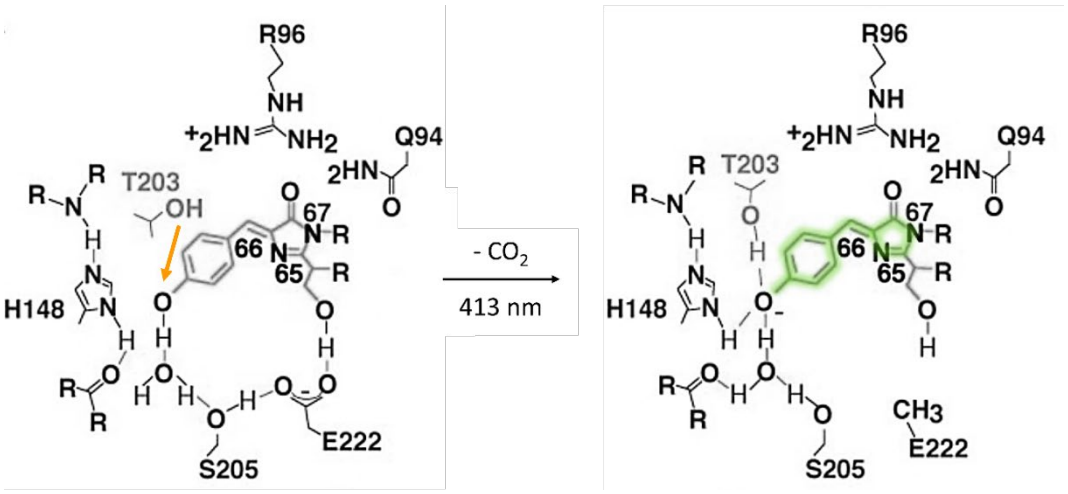

Figure 10 (adapted from Patterson & Lippincott-Schwartz, 2002): Illustration of photoactivation: PA-GFP chromophore switches from the non-activated state (left) to the fluorescent state (right) upon 413 nm illumination which causes decarboxylation of the neighboring glutamic acid 222 and thus a rearrangement of the hydrogen bond network.

1.4.4 Reversibly switchable hydrozoan fluorescent proteins (RSFPs)

Efficient reversible switching in fluorescent proteins was first observed in proteins of anthozoan origin (see section 1.4.2). As this work is focused on hydrozoan proteins, and in particular on rsEGFP2, the underlying switching mechanism and the development of RSFPs will be explained with the example of rsEGFP2 and similar variants.

Dickson et al. (1997) reported photoswitching in GFP-variants for the first time, albeit with a low efficiency. They used the yellow fluorescent EYFP variants GFP(S65G/S72A/T203F) and GFP(S65G/S72A/T203F), which they immobilized in gels. They observed at the single-molecule level that the proteins switch into a dark-state after extensive 488 nm illumination and can be switched back to an emissive state by 405 nm illumination.

Bizzarri et al. (2010) improved this efficiency substantially by replacing the highly conserved glutamic acid 222 with glutamine. This single mutation

prevents the irreversible decarboxylation and stabilizes the hydrogen bonding pattern such that the chromophore is less disturbed by it. This gives rise to an efficient cis-trans isomerization and thus efficient reversible photoswitching at the ensemble level (Bizzarri et al., 2010). However, the glutamic acid is a catalyzer in the chromophore maturation reaction and thus the replacement by glutamine might impair the maturation efficiency. The reasoning behind their approach was as follows: Since it was shown that the RSFP Dronpa switches between an anionic fluorescent state in cis-conformation to a neutral dark state in trans-conformation (Andresen et al., 2007), the idea was to modify the chromophore environment such that cis-trans isomerization becomes possible in GFP. In previous studies (Bizzarri et al., 2007), they observed that a fast proton transfer between the chromophore and Glu222 occurs in many proteins of the GFP-family which is often linked to structural rearrangements of the chromophore pocket, which could affect the ability of the fluorescent proteins to photoswitch. Instead, Gln222 has a stabilizing effect on the hydrogen network (Bizzarri et al., 2010).

(a) rsEGFP and rsEGFP2

Slightly after, the RSFP rsEGFP was developed (Grotjohann et al., 2011) using EGFP as a starting point. They substituted the amino acids which appeared to not favor cis-trans isomerization, because this – together with a change of the protonation state - appeared to be the typical photo-switching mechanism in RSFPs in various anthozoan and hydrozoan RSFPs (Adam et al., 2008; Andresen et al., 2005, 2007; Brakemann et al., 2010; Henderson et al., 2007 cited by Grotjohann et al., 2011). The exchange of glutamine 69 by a leucine was sufficient to make EGFP reversibly switchable, but more mutations (Q69L, V150A, V163S, S205N, and A206K) were introduced to optimize the properties of the protein, especially to enhance the on-to-off switching contrast (see definition of

switching contrast in section 2.2) (Grotjohann et al., 2011). The resulting protein was named rsEGFP. It was successfully applied as a marker for the super-resolution microscopy technique RESOLFT (see section 2.4) live-cell imaging with resolutions comparable to STED (see section 2.3), with the use of 10^6 times less light intensity, which has the advantage of reducing light-induced damage at the sample (Grotjohann et al., 2011).

rsEGFP2 is also a reversibly switchable EGFP variant and was developed later by Grotjohann et al. (2012). It can undergo much faster switching than rsEGFP. With rsEGFP2 they could perform RESOLFT studies with 25-250 times faster recording than with rsEGFP. The steps of developing rsEGFP2 were as follows (Grotjohann et al., 2012): Threonine 65 of the EGFP chromophore, which was a serine in the original GFP protein, was exchanged to an alanine. Already this single mutation had the effect that EGFP transformed into a reversibly switchable protein, which was switching fast. Again, the switching contrast was not optimal, thus the other mutations which were performed to produce rsEGFP were added to EGFP-T65A. Different combinations of mutations were tested to achieve a protein with the highest switching contrast, best resistance to photobleaching and fastest switching. EGFP(T65A/Q69L/V163S/A206K) led to the best results and was named rsEGFP2. They report an absorbance maximum at 483 nm and an emission maximum at 503 nm at RT. rsEGFP and rsEGFP2 are negative switchers. Off-switching in negative RSFPs is typically achieved by 488 nm light and on-switching by 405 nm light.

Structural investigations revealed that rsEGFP2 indeed undergoes a cis-trans isomerization (el Khatib et al., 2016) (Figure 11), as almost all RSFPs of hydrozoan and anthozoan origin. In addition to this, a protonation takes place upon on-to-off-switching. An exception of this common mechanism is the GFP variant Dreiklang, which switches based on a reversible hydration reaction and for which the fluorescence excitation spectrum is not coupled to the optical switching (Brakemann et al., 2011).

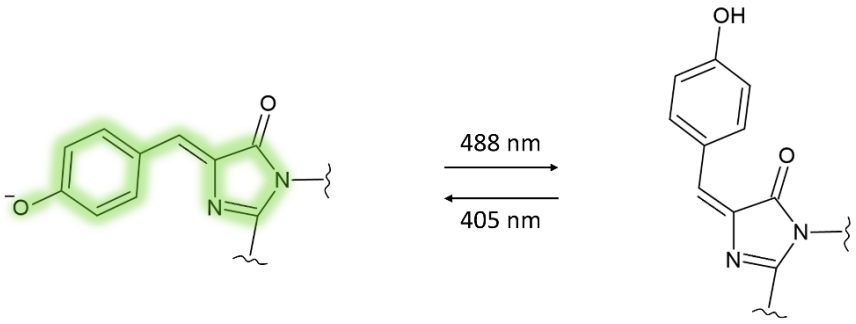

Figure 11: Illustration of photoswitchig: rsEGFP2 chromophore switches from the anionic on-state (left) to the protonated off-state (right) upon 488 nm illumination upon cis-trans isomerization. This process is reversed if 405 nm illumination is applied.

In contrast to other RSFPs such as Dronpa (Andresen et al., 2007) no major change of the chromophore pocket was observed upon switching (El Khatib et al., 2016). Tyrosine 146 and Histidine 149 exhibit a rearrangement in the direction of the chromophore movement (Figure 12).

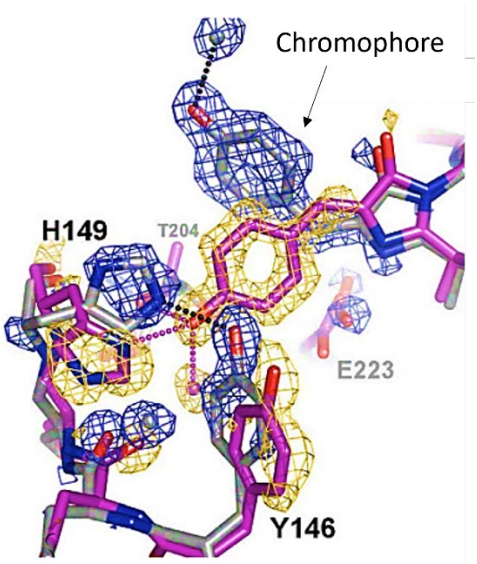

Figure 12 (adapted from El Khatib et al., 2016): rsEGFP2 chromophore pocket upon cis-trans isomerization with the fluorescent state (purple) in cis-conformation and the off-switched state (grey) in trans-conformation. The F_{obs}(off)-F_{obs}(on) difference map displayed at ±4.5 σ, indicates the motions from the on- to the off-state (yellow: negative density, blue: positive density).

Moreover, the chromophore twisting during trans-cis isomerization in rsEGFP2 was observed by time-resolved serial femtosecond crystallography (SFX) (Coquelle et al., 2018). On-to-off switching could not be studied in the same way due to the much lower switching quantum yield. Their data suggests that the chromophore undergoes a hula-twist upon off-to-on switching from the trans-conformation to an intermediate state I. This is a simultaneous twist of two bonds as shown in Figure 13 A in contrast to a one bond flip. In fluorescent proteins the isomerization between cis- and trans- conformations might either involve a one bond flip or a hula-twist or a combination of both. A hula-twist would require less space, as it does not involve a complete rotation. Therefore, at CT, where major conformational changes are inhibited, hula-twists eventually might occur more likely than one bond flips. In Figure 13 B the principle of a hula-twist is illustrated by showing how two subsequent rotations of single bonds would lead to the same final conformation as after a hula-twist (R. S. Liu & Asato, 1985).

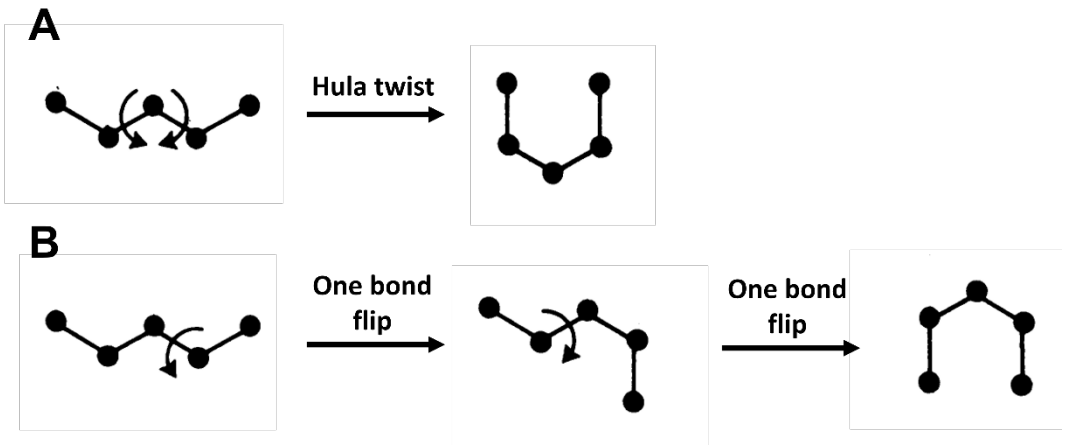

Figure 13 (adapted from R. S. Liu & Asato, 1985): A molecule in a w-shape can reach a u-shaped conformation by (A) a simultaneous twist of the two central bonds involving a down-stream motion (hula-twist) or (B) by two subsequent one bond flips which involve a rotation of single bond each.

Further, in a combination of pump-probe spectroscopy studies at nanosecond resolution with time-resolved SFX, intermediate states of the off-to-on switching were revealed, showing that rsEGFP2 first undergoes trans-cis isomerization which is followed by deprotonation in the ground state (Woodhouse et al., 2020). The intermediate state, which is reached after 10 ns, reveals a chromophore in cis-conformation but with differences in the chromophore pocket, notably histidine 149, which is twisted, as compared to the histidine in the final state (Figure 14). According to their spectroscopy measurements this state is protonated. Deprotonation then would occur on a microsecond time scale in correlation with the conformational change of the histidine (Woodhouse et al., 2020). Similar studies on Dronpa suggested that the cis-conformation could be only observed after ~90 ns (Laptenok et al., 2018).

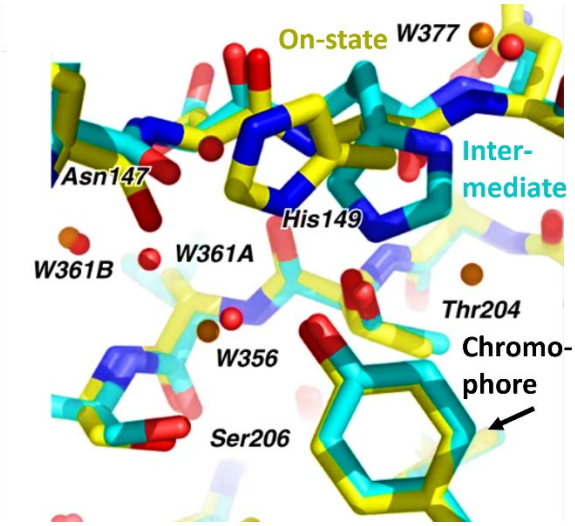

Figure 14 (adapted from Woodhouse et al., 2020*): Intermediate state of off-to-on switching in rsEGFP2 resolved by SFX studies in cyan and the on-state in yellow.*

(b) rsFolder and rsFolder2

rsFolder was developed by El Khatib et al. (2016) by hybridization of rsEGFP2 and Superfolder-GFP. For many GFP variants the problem was encountered that they misfolded when they were expressed as a fusion with another protein or when they were in oxidative conditions. For this reason,

Waldo et al. (1999) developed variants with more robust folding properties. Folding Reporter GFP of Waldo et al., which has the combination of the mutations of α-GFP (F99S, M153T and V163A) and EGFP (S65T and F64L), was used as a starting variant for the engineering of Superfolder-GFP (Pédelacq et al., 2006). α-GFP is a variant developed by Crameri et al. (1996) with a 45-fold enhancement of fluorescence signal in cells. Pédelacq et al. (2006) kept the mutations of Folding Reporter GFP and added six new mutations (S30R, Y39N, N105T, Y145F, I171V and A206V) and obtained the more resistant and faster folding variant called Superfolder-GFP.

El Khatib et al. (2016) aimed to combine the improved folding of Superfolder-GFP with the fast switching-kinetics of rsEGFP2 which resulted in the development of rsFolder. It showed the desired properties but had a reduced switching contrast. El Khatib et al. (2016) found that the on-to-off switching contrast of rsEGFP2 is higher because its off-to-on switching quantum yield and the extinction coefficient of the off-state at 488 nm is lower than for rsFolder. To address this issue the differences between rsEGFP2 and rsFolder were studied by El Kathib et al.: Their data showed that rsFolder and rsEGFP2 show relatively similar switching kinetics. Both undergo efficient negative photoswitching and have similar absorption and fluorescence emission spectra. On the structural level it was revealed that in both cases a cis-trans isomerization without major rearrangement of the surrounding hydrogen network occurs upon on-to-off switching. However, the off-state chromophore of rsFolder is much tighter connected to the β-barrel by hydrogen bonds (Figure 15) and appears in a slightly different trans-configuration than rsEGFP2 (see trans1 and trans2 states in results section 6). Possibly, the trans-conformation in rsFolder is reached by hula-twist and the rsEGFP2 trans-conformation by a one bond flip. The residue 146 appeared to play a key role in the difference of the two off-switching mechanisms and thus Phe146 was replaced by Tyr146 to obtain a protein with a switching mechanism more similar to rsEGFP2, which was named rsFolder2. rsFolder2 indeed displays a higher switching contrast than rsFolder.

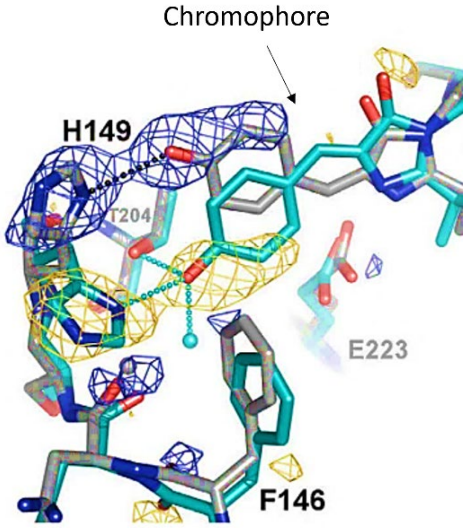

Figure 15 (adapted from El Khatib et al., 2016): rsFolder chromophore pocket upon cis-trans isomerization with the on-state (cyan) in cis-conformation and the off-state (grey) in trans-conformation. The F_{obs}(off)-F_{obs}(on) difference map is displayed at ±4.5 σ and indicates the motions from the on-state to the off-switched state (yellow: negative density, blue: positive density).

1.5. Photobleaching and photoblinking

Fluorescent proteins are illuminated with laser light to excite fluorescence or to make them switch between different states. This can cause damage on the chromophore or its surrounding, such that it irreversibly loses its ability to fluoresce, which is called photobleaching. A high photostability – the ability of a fluorescent protein to repeatedly emit fluorescence upon excitation with light – is an important measure for studies where dynamics are studied over time or for other studies where a long acquisition time is necessary. Thus, for improving the photostability it is important to understand the underlying photobleaching mechanisms.

Many different pathways of photobleaching were reported. Due to its long-lived nature, the triplet state is suggested to be a likely starting point for

bleaching pathways (Byrdin et al., 2018) but also photobleaching from the singlet state was reported (Bell et al., 2003). Byrdin et al. (2018) report that the addition of oxidative and reducing co-factors reduces photobleaching of the triplet state in EGFP, similar to effects observed for organic STORM (Stochastic Optical Reconstruction Microscopy) dyes (Chapagain et al., 2011) and explain this by a fast depopulation of the reactive intermediate states.

It was often reported that the presence of oxygen can lower the photostability of fluorophores, as for example by Chapagain et al. (2011), Roy et al. (2010), Schwartz et al., (2007) and Zheng et al. (2014). As the oxygen ground state is a triplet state it can highly react with the triplet state of the chromophore. This leads to the formation of reactive oxygen species which can cause destructions in the chromophore pocket (Ha & Tinnefeld, 2012).

Also non-linear bleaching processes which involve the absorption of two subsequent photons were reported (Wulffele et al., 2022).

In SMLM (see section 2.2) photobleaching determines the number of collectable photons per molecule. At the single molecule level also another phenomenon – photoblinking – is observed, which is caused by stochastic switching between reversible dark-states and fluorescent states upon continuous illumination. These can be different long-lived or short-lived dark-states, from which the molecules can recover either thermally or by light-induced pathways. One of these dark-states which can cause blinking are the triplet state and the radical states to which it can react (see section 1.2). Oxygen acts as an electron acceptor and thus quenches the triplet state, such that shorter off-times are observed as without oxygen (Ha & Tinnefeld, 2012). Many other triplet state quenchers can be used to achieve a similar effect (Henrikus et al., 2021). Long-lived blinking is typically caused by photoswitching upon cis-trans isomerization (de Zitter et al., 2019).

1.6. Photoswitching at cryogenic temperature

Several fluorescent proteins have been successfully switched at CT, though with much lower efficiency and speed than at RT. To understand why the switching efficiency and speed are reduced and how this can be improved, it is crucial to understand the cryo-switching mechanisms. As of now, not many investigations have been carried out to address this issue and the switching mechanism is poorly understood.

Organic dyes can be advantageous for many RT applications due to their small size and high brightness. However, for many organic dyes photoswitching relies on diffusion of buffer molecules, which is hampered at CT, and thus they are not suitable for SMLM applications at CT. Further, many dyes cannot cross membranes of living cells and thus the cells often have to be perforated and for this purpose to be fixed chemically despite sample freezing, which can create artifacts in high-resolution imaging (see section 2.5.1). Hulleman et al. (2018) tested several organic dyes and did not observe any significant photoswitching or photoactivation at CT. They suggest that instead of reaching sparsity of fluorescent labels by photoswitching, other approaches could be used for organic dyes at CT. (Moser et al., 2019) propose cryogenic super-resolution optical fluctuation imaging (cryo-SOFI), which is based on statistical analysis of temporal fluctuations between fluorescent states and short-lived dark states (Dertinger et al., 2009).

While photoswitching of RSFPs becomes less efficient at CT, some advantageous properties have also been noted. At CT all photochemical reaction rates are reduced (Hulleman et al., 2018), such as the photobleaching rate of fluorophores, as observed by Schwartz et al. (2007). Schwartz et al. suggest that oxygen diffusion is hampered at CT and thus oxygen molecules do not collide with the chromophore. At RT this would lead to formation of reactive oxygen species which could lead to destructions in the chromophore pocket (see section 1.5). Therefore, there is less bleaching at CT as compared to RT, as observed by Weisenburger

et al. (2013) and (Li et al., 2015). As a result, more photons per molecule can be detected. Also a higher quantum yield is observed at CT because major motions are hampered below the glass transition temperature and thus the decay to the ground state by thermal relaxation is less favored and therefore decay upon fluorescence becomes more favored.

The first study on photoswitching of GFP at cold temperature was carried out by Creemers et al. (1999). They observed different spectral properties at 1.6 K and at RT (Figure 16). The protonated peak appears to be red-shifted at CT and the anionic peak blue-shifted. They further report that at both temperatures photoswitching between different states is possible. (Creemers et al., 2000) also investigated other variants: GFP(S65T), from which EGFP was derived, RS-GFP (Delagrave et al., 1995), a red-shifted variant and EYFP and report that cryo-switching is also possible for these variants.

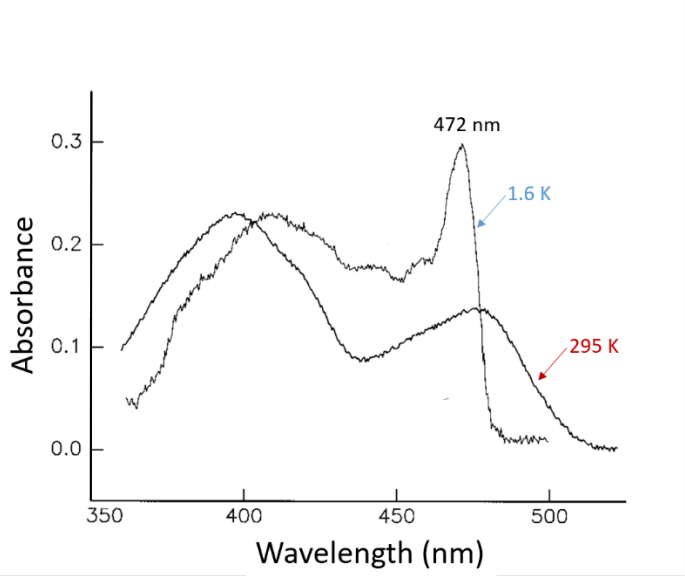

Figure 16 (adapted from Creemers et al., 1999)*: Absorption spectrum of wildtype GFP at 295 K and 1.6 K.*

Investigations on the photoswitching mechanism of fluorescent proteins at CT were carried out on Dronpa, IrisFP and EYFP (Regis Faro et al., 2010). They reported that at the ensemble level at RT, IrisFP is efficiently reversibly switchable, Dronpa is intermediately efficient but slow switching, and EYFP

almost not reversibly switchable. Interestingly, they observed that by using 355 nm light instead of 405 nm light for recovery of EYFP at RT, more efficient backswitching could be obtained, which has also been reported by McAnaney et al. (2005).

The data of Regis Faro et al. (2010) obtained at CT shows that IrisFP, Dronpa and EYFP all undergo reversible photoswitching at CT (upon illumination with 514 and 405 nm light). They report very low quantum yields ($\Phi = 10^{-6}$ for EYFP, 4×10^{-7} for Dronpa and 9×10^{-8} for IrisFP) for off-switching with 300 W/cm² at 100K but consider them as significant in relation to the reduced rate of photobleaching at CT. The initial yellow fluorescent state of EYFP with an absorption maximum at ~510 nm could be switched to a blue fluorescent state with two absorption maxima at 385 and 410 nm, with absorption into the UV range. The build-up rate of this state was demonstrated to be linear dependent on the used laser power, and thus processes where two subsequent photons are absorbed were excluded. Regis Faro et al. (2010) suggest that at CT off-switching of the yellow fluorescent state in EYFP, as well as the off-switching of IrisFP and Dronpa, might be based on photoinduced protonation of the chromophore with small structural changes without involving a cis-trans isomerization as the switching at RT. They express further that this protonation possibly takes place in the long-lived triplet state, as suggested by Mizuno et al. (2008), and that at RT the switching mechanism might compete with cryo-switching pathways.

In further structural studies, Regis Faro et al. (2011) demonstrated that indeed no cis-trans isomerization occurs for Dronpa at CT. Their data shows the same isomeric state for the off-state as for the on-state. Interestingly, they observed that trans-cis isomerization of Padron is maintained at CT. They explain this by the finding that cis-trans isomerization in Dronpa requires major conformational rearrangements, unlike in the case of Padron where only little rearrangements are necessary, which could be still possible at CT despite the hampered protein dynamics.

Some applications of fluorescent proteins in cryo-SMLM were demonstrated in the last years (see section 2.5.3). PA-GFP was reported to be photoactivatable at CT in a study of Chang et al. (2014). Tuijtel et al. (2019) suggest further that it is reversibly switchable at CT, although at RT it is only irreversibly switchable (see section 1.4.3). Chang et al. (2014) also tested several other fluorescent proteins such as Dronpa and PAmCherry, which was developped from DsRed (Subach et al., 2009), and could not successfully photoswitch them.

Kaufmann et al. (2014) reported cryo-switching for mEGFP (monomeric EGFP) and mVenus (Kremers et al., 2006), a monomeric, yellow fluorescent variant derived from EYFP. Dronpa was successfully applied as a reversibly switchable marker in PALM imaging at CT correlated with cryo-EM by Liu et al. (2015). Nahmani et al. (2017) used PA-GFP and PSmOrange, a photoconvertible orange fluorescent protein developed from DsRed (Subach et al., 2011), for their cryoPALM studies and report photoswitchability at CT.

PAmKate was characterized by Dahlberg et al. (2018) as an efficient photoswitcher at CT. As a control they also investigated PA-GFP at CT, which was also switchable, and PAmCherry, which was not switchable, as previously reported by Chang et al. (2014). They found similar switching efficiencies for PAmKate and PA-GFP as at RT. PAmKate was successfully applied by (Dahlberg et al., 2020) as a fluorescent marker in single-molecule active control microscopy correlated to cryo-ET.

Tuijtel et al. (2019) compared the switching kinetics of EGFP, PA-GFP, Dronpa, Padron, rsFastLime, rsEGFP2, mIrisFP at CT. Interestingly, they observed that all proteins exhibited similar kinetics and express the hypothesis that they may undergo the same switching mechanism at CT. The fastest switcher appeared to be rsEGFP2. Strikingly, even the positive switcher Padron became a negative switcher at CT, in contrast to the observations of Regis Faro et al. (2011). This hints at competing photoswitching pathways which depend on experimental conditions. Of note, the switching efficiency of Dronpa differed significantly as well in

different experiments. Whereas Tuijtel et al. (2019) and Liu et al. (2015) and Regis Faro et al. (2010) observed efficient switching at CT, Chang et al. (2014) could not observe significant switching. Experimental conditions as laser power and wavelength could be possible factors which impact the switching efficiency and led to different results.

In cryo-SMLM studies correlated with cryo-EM of Hoffman et al. (2020) several fluorescent proteins and organic dyes were analyzed. They report that the best images could be obtained using mEmerald. An unknown dark state was observed by Hoffman et al. (2020) for mEmerald and for the other tested fluorescent proteins, leading to a higher dynamic contrast (ratio between the times the molecule is in the off state and in the on-state), which allowed them to obtain cryo-SMLM images of high resolution. They express the hypothesis that this dark-state could be the triplet state T_1 or higher energy triplet states T_n reached after re-excitation, and that the lifetime of the triplet state might be increased at CT and thus would make this mechanism possible.

An overview of all fluorescent proteins, of which the ability to photoswitch at CT was investigated, is shown in Table 1 and 2. Remarkably, for most fluorescent proteins it was reported that they change their switching mechanism at CT to an efficient negative reversible switching mechanism, even if they are not switchable at RT.

Hydrozoan Fluorescent proteins switched at CT	Reference	Photoswitching at CT	Photoswitching at RT
GFP	Creemers et al. (1999)	Reversible photo-switching	Not phototransformable
GFP-S65T	Creemers et al. (1999)	Efficient negative reversible photo-switching	Not phototransformable
EGFP	Tuijtel et al. (2019)	Efficient negative reversible photo-switching	Not photo-transformable
mEGFP	Kaufmann et al. (2014)	Intermediately efficient negative photoswitching	Not photo-transformable
RS-GFP	Creemers et al. (1999)	Efficient negative reversible photo-switching	Not phototransformable
mEmerald	Hoffman et al. (2020)	Efficient negative reversible photo-switching	Not photo-transformable
rsEGFP2	Tuijtel et al. (2019)	Efficient	negative reversible photo-switching at RT and CT
PA-GFP	Chang et al. (2014)	Efficient photo-activation/ Efficient negative reversible photo-switching	Irreversibly photoactivatable
	Nahmani et al. (2017)		
	Dahlberg et al. (2018)		
	Tuijtel et al. (2019)		
EYFP		negative reversible photo-switching	Not efficiently photo-transformable
	Regis Faro et al. (2010)	Efficient	
	Creemers et al. (1999)	Efficient	
mVenus	Kaufmann et al. (2014)	Intermediately efficient negative photoswitching	Not photo-transformable

Table 1: Overview of fluorescent proteins of hydrozoan origin which were photoswitched at CT. The color scheme indicates the fluorescence colors of the proteins.

Anthozoan Fluorescent proteins switched at CT	Reference	Photoswitching at CT	Photoswitching at RT
Dronpa		negative reversible photoswitching	Negative reversible photoswitching
	Regis Faro et al. (2010)	Efficient	
	Tuijtel et al. (2019)	Efficient	
	Liu et al. (2015)	Efficient	
	Chang et al. (2014)	Low efficiency	
Padron	Regis Faro et al. (2010)	Positive reversible photoswitching with trans-cis isomerization	positive reversible photo-switching (trans-cis isomerization)
	Tuijtel et al. (2019)	Efficient negative reversible photo-switching	
rsFastLime	Tuijtel et al. (2019)	Efficient negative reversible photoswitching	Negative reversible photoswitching
IrisFP	Regis Faro et al. (2010)	Efficient negative reversible photo-switching	Photo-convertible
mIrisFP	Tuijtel et al. (2019)	Efficient negative reversible photo-switching	Photo-convertible
PAmKate	Dahlberg et al. (2018, 2020)	As efficient photo-activation as at RT	Irreversibly photoactivatable
PSmOrange	Nahmani et al. (2017)	Intermediately efficient negative photoswitching	Photoconvertible

Table 2: Overview of fluorescent proteins of anthozoan origin which were photoswitched at CT. The color scheme indicates the fluorescence colors of the proteins.

2. Super-resolution microscopy

In the last two decades microscopy was revolutionized by the development of plenty of super-resolution microscopy techniques, which allow resolutions on the nanometer scale and thus are also named as *nanoscopy techniques*.

In this chapter the two main groups of nanoscopy methods – wide-field single molecule localization microscopy (SMLM) and STED-like techniques based on target scanning - are summarized and possible applications at CT are discussed, considering advantages and limitations. In this context, also requirements for the fluorescent protein properties are tackled, as the goal of this work is to propose suitable fluorescent proteins for SMLM applications at CT.

2.1. Discovery

According to the Abbe equation

$$\Delta d_{min} = \frac{\lambda}{2n\ sin\ \alpha} \approx \frac{\lambda}{2}$$

With λ, the incoming light wavelength, n, the refractive index of the microscopy medium and α, the half aperture angle of the objective lens, two objects separated by the distance Δd_{min} smaller than half the wavelength of the incoming light cannot be resolved by a microscope. In 2014 the Nobel Prize in chemistry was awarded to Dr. Eric Betzig, Dr. Stefan Hell, and Dr. William E. Moerner for overcoming the diffraction limit by developing super-resolution fluorescence microscopy (Möckl et al., 2014). They developed two different approaches, independently from each other. Betzig and Moerner elaborated photo-activated localization microscopy (PALM) (Betzig et al., 2006), which is based on localization of single fluorescent proteins

and is a stochastic nanoscopy technique. The other approach, namely Stimulated Emission Depletion (STED) (Hell & Wichmann, 1994), was developed by Stefan Hell and is based on controlling the emission of excited fluorescent dyes by deexcitation induced by stimulated emission and is a deterministic nanoscopy method.

STED and other similar techniques based on different fluorophores and optical transitions are summarized with the term “reversible saturable optical (fluorescence) transitions” (RESOLFT) (Hell et al., 2004). Hofmann et al. (2005) describe the successful use of reversibly switchable proteins for RESOLFT. Brakemann et al. (2010) and Grotjohann et al. (2011) report biological imaging with RESOLFT using the reversible switchable proteins Dreiklang and rsEGFP. The speed of RESOLFT recordings with fluorescent proteins was substantially improved by the development of the fast switching protein rsEGFP2 by Grotjohann et al. (2012).

Besides PALM, many other single-molecule localization methods (SMLM) were developed, such as stochastic optical reconstruction microscopy (STORM), which is based on random switching of organic dyes (Rust et al., 2006) instead of photoactivation of fluorescent proteins as in PALM (Betzig et al., 2006).

In the following, the SMLM and the STED principles as well as the use of fluorescent proteins in RESOLFT are explained.

2.2. SMLM

In SMLM a low intensity activation laser (typically 405 nm wavelength) is used to switch on a fraction of single molecules and an excitation laser (561 nm for PALM in Betzig et al. (2006)) is applied to make them fluoresce until they bleach. This procedure is repeated many times to activate different molecules such that a stack of images gathering the fluorescent signal of nearly all emitters can be recorded. From each image the locations of the molecules are determined by a Gaussian fit. A final image is reconstructed

from the extracted localizations in the recorded frames (Figure 17). All SMLM techniques are based on this principle but use different fluorophores and lasers.

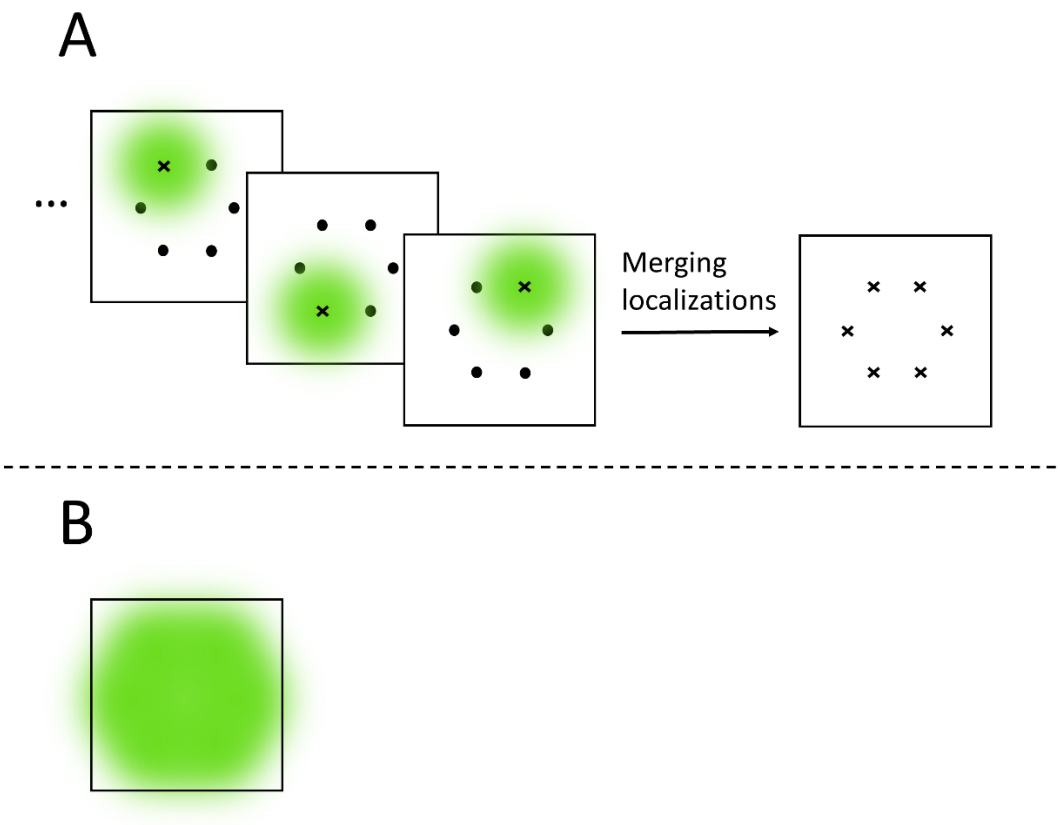

Figure 17: (A) Fluorescence of single molecules is recorded during excitation with laser light and several images are recorded. From each image the single molecules are localized separately, and the spatial information is merged in a final image. (B) In comparison, with conventional fluorescence microscopy single emitters which have a distance below 200 nm cannot be distinguished because they are all detected at the same time.

The precision of the Gaussian fit of the fluorescence signal depends on the signal to noise ratio, thus a high number of detected photons per localization improves the fit precision and therefore might enhance the image resolution. The higher brightness of the fluorescent markers, the better will be the signal. Further, the better the photostability of the markers, the more emission cycles of the same fluorophore and thus a higher photon number can be measured.

Another important measure for SMLM is the dynamic contrast of the fluorescent proteins, which is defined by the ratio between the times the fluorophores are in the off-state and in the on-state. For the localization precision in SMLM the off-time of the fluorophores is crucial to make it possible to distinguish between neighboring molecules.

At the ensemble level this corresponds to switching contrast of the fluorescent markers. It is defined as the ratio of molecules which are fluorescent after and before photoswitching. In case of on-to-off switching with 488 nm light, the off-state is partially switched back to the on-state by this laser as it absorbs in this wavelength range. The same rule applies vice versa for off-to-on recovery. One can distinguish between the photophysical switching contrast, which means the “real” switching contrast as a property of the fluorescent markers, and the apparent switching contrast, which is determined by measuring fluorescence decay or gain and can include bleaching effects.

The other parameter which influences the resolution is the labeling density which should be high enough to achieve a sufficient sampling. The effective labeling efficiency is a measure for successfully labeled sample positions with fluorescent markers with detectable signal and thus not only depends on the labeling efficiency but also on the brightness and photostability of the fluorophore.

2.3. STED

In the STED approach, an excitation beam immediately followed by a fluorescence depletion beam (STED beam) is focused on a sample and scanned over it. The excitation beam has a wavelength which is absorbed by the fluorophore and excites it from the ground state S_0 to the first excited state S_1 (Figure 18).

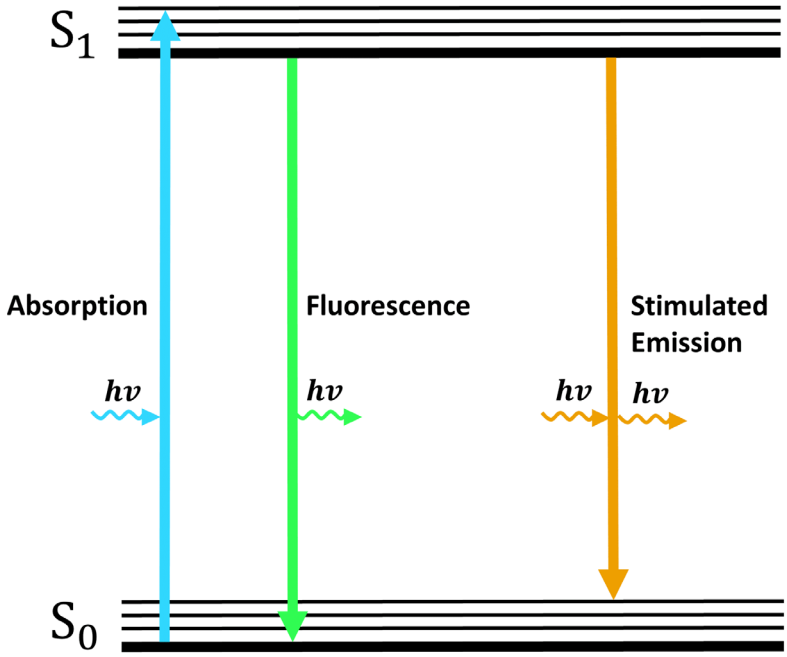

Figure 18 (based on Hell & Wichmann, 1994): Stimulated emission shown in a Jablonski diagram. After excitation to the S_1 state, the molecule can vibrationally relax to a lower energy level of the S_1 state and then be depleted by stimulated emission by irradiation with a wavelength corresponding to the energy gap to one of the energy levels of the S_0 state and will emit a photon of the same wavelength. If stimulated emission is induced, no spontaneous fluorescence will occur.

The STED beam has a wavelength that is not absorbed by the fluorophore in the S_0 state but corresponds to its emission spectrum and thus can deplete its S_1 state by stimulated emission. The STED beam has a 2-dimensional donut shape at the sample position (Figure 19). Thus, it can deplete the molecules in the outer regions before fluorescence can occur. Hence, only a small region of molecules in the inner part of the illumination fluoresces. In this way, the fluorescence emitting area is substantially reduced over conventional fluorescence excitation and a much higher image resolution can be achieved.

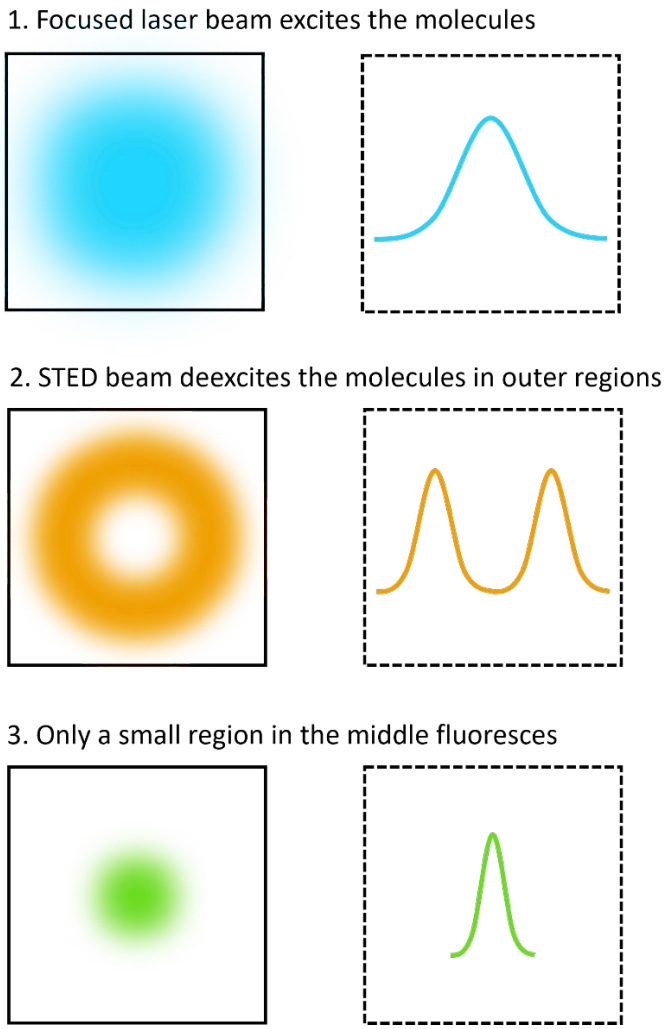

Figure 19 (based on Hell & Wichmann, 1994 and Klar & Hell, 1999): In the first step, a laser beam illuminates the sample in order to excite it to the S_1 state. Secondly, a STED beam, shaped like a 2-dimensional torus, is applied to deplete the excited state of the molecules in the outer regions by stimulated emission such that only a small region in the middle which is not exposed to the STED beam can undergo fluorescence. This illumination scheme is applied repeatedly for subsequent sample positions in order to reconstruct a full image.

2.4. RESOLFT with fluorescent proteins

RESOLFT (reversible saturable optical fluorescence transitions) is based on the STED principle but RSFPs are used as markers, which have long-lived on- and off-states. Thus, a different illumination scheme is applied. The

RSFPs, as for example rsEGFP2, are initially in the on-state. They are irradiated with a donut-shaped depletion beam – which is typically a 488 nm laser illumination – which switches the fluorescent proteins in the outer region to the off-state. Subsequently, the sample is irradiated with a conventional focused 488 nm laser beam. Hence, the inner region fluoresces while also switching to the off-state and this signal can be detected. In the next step a 405 nm laser is applied on the illuminated region to switch all fluorescent proteins back on such that the process can be repeated, and the sample can be scanned. This technique allows the use of laser intensities which are 10^6 times lower than in STED because of the longer lifetimes of the dark states (Grotjohann et al., 2011), which allows long sample irradiation without damaging it. As the fluorescent proteins are switched many times between the on- and off-state, one problem is that they can bleach leading to a continuous decrease of the fluorescence signal. Also the switching contrast influences the signal-to-noise ratio.

2.5. Super-resolution microscopy at cryo-temperature

2.5.1 Flash-freezing as fixation strategy

At the nanoscale artifacts of chemical fixation become especially visible and are not always recognizable as artifacts, as reported by Whelan & Bell (2015). Moreover, Tanaka et al. (2010) observed that chemical fixation is not always effective, and molecules can still be mobile.

One alternative fixation strategy is to freeze the samples at cryo-temperature. Cryo-techniques gained popularity in biological ultrastructure research in the 1960s-1990s (Afzelius & Maunsbach, 2004). Cryo-electron microscopy (cryo-EM) was developed in the 1970s by Taylor & Glaser (Dubochet et al., 1988). Cryo-EM is a type of transmission electron

microscopy applied to samples at CT. In contrast to conventional electron microscopy, there is no need for removing water of the sample because the sample is flash-frozen. Damage to the sample by freezing can be avoided by vitrification – i.e. fast freezing of a liquid such that the molecules become immobile before crystallization can occur – which was proposed by Gehenio & Luyet (1940). This was an important step for the successful application of cryo-EM (Dubochet et al., 1982). Cryo-EM can be extended to cryo-electron tomography (cryo-ET), where 3-dimensional data is collected by imaging the sample, typically cells, at different angles.

2.5.2 Correlative studies with cryo-EM

There is a high interest in correlative studies of cryo-EM and fluorescence microscopy techniques, as this combines specificity of fluorescence labelling with high-resolution of the cellular structure obtained by EM. However, to achieve this goal, it is advantageous to perform fluorescence imaging on frozen samples as well. Sartori et al. (2007) and Schwartz et al. (2007) report successful imaging of vitrified samples with fluorescent labels by fluorescence light microscopy and high preservation of the biological structures due to vitrification.

Moreover, in the last decade many investigations were conducted to bring forward cryo-nanoscopy and its correlation with cryo-EM as by this even smaller cell structures can be observed. Cryo-EM can provide near atomic resolution imaging of the structural context of a sample with fluorescent labels that allow identification of closely spaced particles and their localizations by nanoscopy (Wolff et al., 2016).

2.5.3 Cryo-SMLM and other single-molecule based approaches at CT

Chang et al. (2014) and Kaufmann et al. (2014) showed that complex macromolecular structures below the diffraction limit which were not understandable with cryo-EM can be resolved by cryo-PALM, and demonstrated that low-efficiency photoswitching at CT of the fluorescent proteins PA-GFP, mEGFP and mVenus is in principle sufficient for cryo-PALM. Liu et al. (2015) used the RSFP Dronpa as a fluorescent label, which is still switchable at CT, to obtain PALM images of thin cellular structures at CT and correlated them with cryo-EM data.

Many approaches of SMLM on vitrified samples have been demonstrated. However, there are many challenges in cryo-SMLM, such as the long data acquisition times over which the sample must be cooled, and its mechanical drift must be avoided. Strong laser powers can cause sample heating but on the other hand, a sufficient excitation of the fluorescent markers has to be guaranteed. Further, user-friendly instrumentation is not straightforward at CT. One of the main challenges is the lack of suitable fluorescent markers which can undergo efficient photoswitching at CT.

In the last years, several approaches have been established to address these issues and to improve cryo-SMLM. Nahmani et al. (2017) demonstrated the application of a high-numerical-aperture objective lens which are typically used at RT to a cryo-PALM setup, resulting in an increased photon yield. With their approach the objective can be held at RT and thus can be used on a conventional microscope.
Weisenburger et al. (2017) developed a technique to perform Cryogenic Optical Localization in 3D in vitro which they called COLD. It relies on the principle that different individual dyes fluoresce with different intensities. By this they resolved 3-dimensional positions of several fluorescent dyes attached to one small protein. Their approach has recently been advanced by Mazal et al. (2022), who use polarization encoding for identifying the fluorophores and thus make the technique compatible with a much broader range of fluorophores, including fluorescent proteins.

Xu et al. (2018) presented a setup with optimized temperature and sample stability. Tuijtel et al. (2019) studied the maximum laser power which can be used without risking sample devitrification and improved the registration accuracy by decreasing the cryostage drift. They demonstrate successful cryo-SMLM correlated with cryo-EM with rsEGFP2 as a fluorescent marker on mammalian cells. An approach to correlate 3-dimensional cryo-nanoscopy with block face cryo-EM on whole cells with mEmerald labels was developed by Hoffman et al. (2020). With their study they discovered valuable protein ultrastructure in mammalian cells.

2.5.4 Cryo-RESOLFT

The main challenge of performing STED at CT is the high laser intensity of the STED beam which is necessary for the depletion of the excited state, which can cause sample heating leading to unfreezing (Dahlberg & Moerner, 2021). RESOLFT with fluorescent protein markers allows the use of much lower intensities. However, as of now, RESOLFT with fluorescent proteins has not been demonstrated at cryogenic temperature (Dahlberg & Moerner, 2021). As the switching speed of fluorescent proteins is slowed down substantially at CT (see results section 7.1), data acquisition would be very slow for cryo-RESOLFT with fluorescent proteins and thus not advantageous. Cryo-STED with organic dyes was also not performed widely but was demonstrated by Giske (2007) for slowly frozen samples. Giske reports further that performing STED at low temperatures allows the use of STED beams of shorter wavelengths which increases their depletion efficiencies, allowing an enhancement of the spatial resolution. This is explained by the observation that at CT less molecules populate higher translational states of the S_0 state, which results in narrower absorption and emission spectra and thus a smaller overlap between them.

Yang et al. (2015) developed another approach, which is based on excited state saturation of individual fluorophores at liquid helium temperature and reach resolutions below 10 nm. They use a donut-shaped excitation beam with powers comparable to those used in RT RESOLFT with fluorescent proteins. In their approach single-molecules are turned to resonance such that their intensity distribution reproduces the donut shaped excitation beam. They apply an additional Gaussian beam, modulate its intensity and measure the response of the sample, which will be only linear at molecule positions. In contrast to SMLM, with their approach it is possible to resolve molecules which do not blink.

2.6. Conclusion

Taken together, sample-freezing as a fixation strategy in nanoscopy has several advantages, like high biological sample preservation and the possibility to perform cryo-correlative studies with cryo-EM or cryo-ET. Hence, there is a high demand for suitable fluorescent markers. The advances in the development of fluorescent markers for CT have been addressed in section 1.6. Many fluorescent proteins have been shown to be photoswitchable at CT, but the switching efficiency remains to be improved. To get closer to this goal, the switching mechanisms of fluorescent proteins at CT is investigated in this work. According to the work of Tuijtel et al. (2019), rsEGFP2 appears to be a promising fluorescent marker with a faster switching than other investigated variants. Moreover, they observed similar switching kinetics for the variants which they investigated. This could suggest that there might be a switching mechanism at CT which is general to these and similar fluorescent proteins, which would be of great interest. Considering the studies of Hoffman et al. (2020), also mEmerald is a promising candidate for applications based on photoswitching at CT.

II. Materials and Methods

Painting by the author illustrating diffraction

Note on the organization of this chapter

The materials and methods which are already described in the publications in the appendix are not re-described here for the most part. However, the parts to which additional details are given are summarized again here to provide context.

Note on protein expression and purification

Mutagenesis, transformation, expression, and purification of rsEGFP2, EGFP, mEmerald, rsEGFP2-V151A, rsEGFP2-V151L, rsFolder2-V151A and rsFolder2-V151L was performed by Dr. Virgile Adam and Ninon Zala, as described in El Khatib et al. (2016), Coquelle et al. (2018) and (Adam et al., 2022, see appendix).

3. Crystallography

X-ray crystallography is a method to determine the 3-dimensional structure of a molecule at atomic resolution by measuring the diffraction of X-rays by a crystal of that molecule. Even complex protein structures can be determined by this method if it is possible to get crystals of that protein.

3.1. Protein crystal growth and harvesting

The fact that proteins are large, mobile, have only little interaction with each other and have to be in aqueous solution to retain their structure, makes it difficult to grow protein crystals. However, several strategies have been developed to still make it possible. One common method is the hanging drop

vapor diffusion, which was utilized in this work. This is done by preparing a protein drop and a reservoir solution with higher precipitant concentration than the protein drop and putting them into a closed system, such that the water molecules of the protein drop will slowly diffuse through the air towards the reservoir solution until equal precipitant concentrations are reached.

For rsEGFP2 crystals, the protocol of Dr. Tadeo Moreno Chicano was used: the reservoir solution was prepared by mixing 100 mM HEPES buffer (pH 8.1) with 1.9 M ammonium sulfate. Each reservoir was filled with 1 ml solution. The protein drops were prepared by mixing 2 µl of a protein solution of 13 mg/ml concentration (containing HEPES at pH 7.5) with 2 µl of the reservoir solution. It was placed on a cover glass, which was put on a reservoir each (Figure 20). Crystals were grown at RT.

For rsEGFP2-V151A the protein concentration had to be adjusted to 60 mg/ml to obtain crystals and the reservoir solution with HEPES of pH 7.5 and 1.85M ammonium sulfate led to the best results.

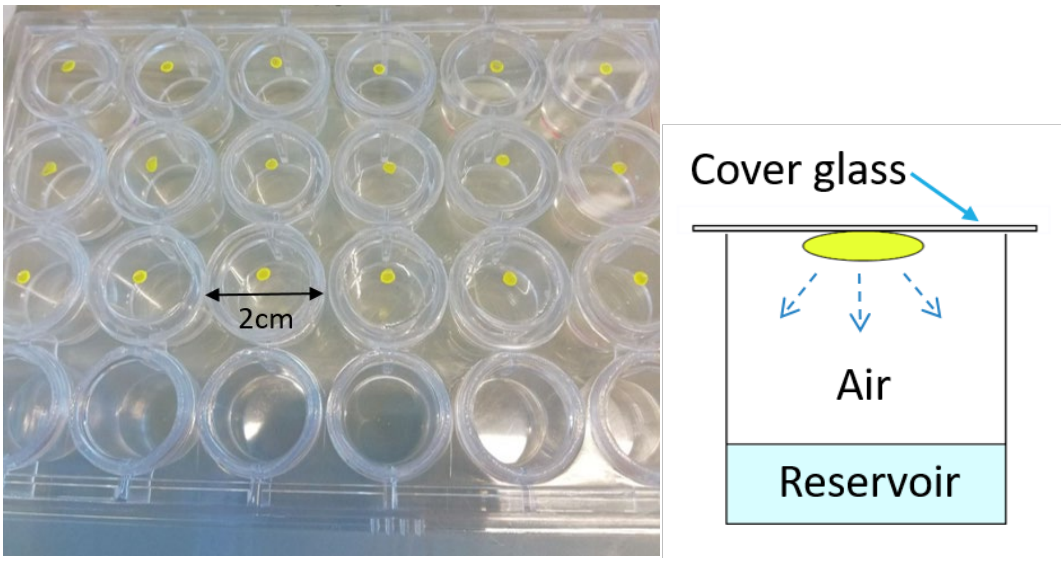

Figure 20: Photograph of a well-plate with reservoirs containing the reservoir solution closed with cover glasses with hanging protein drops and a corresponding scheme on the right.

After two days, crystals were observed in the protein drops on the cover glass (Figure 21). Crystal dimensions were in average ~50 × 40 × 200 µm³ for rsEGFP2 and ~150 × 200 × 800 µm³ for rsEGFP2-V151A.

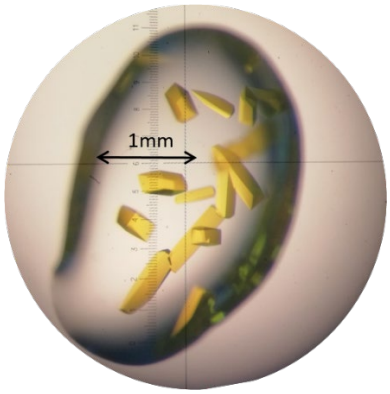

Figure 21: Photograph of rsEGFP2-V151A crystals grown in a drop by the Hanging drop vapor diffusion method.

3.2. X-ray diffraction

For measuring molecule structures with atomic resolution of 1-2 Å by diffraction, the wavelength of the light irradiation must be in the same order of magnitude, to fulfill the Bragg-equation

$$n\lambda = 2d_{hkl}\sin(\theta), \qquad (1)$$

with the diffraction order n, the irradiation wavelength λ, the lattice spacing d_{hkl} and the scattering angle θ, for a successful diffraction. X-rays are electromagnetic waves with wavelengths between 0.1 and 25 Å and are therefore used for solving the structures of proteins in an Angstrom range. The X-rays are scattered by the electrons of the molecules in the crystal and produce a diffraction pattern, which is the Fourier transform of the molecule structure. By collecting the diffraction patterns for different irradiation angles, 3-dimensional information of the molecule structure can be extracted.

The scattered waves of each molecule interfere and contribute to the intensity of each diffraction spot. The sum of the scattering of all *N* atoms of one unit cell (repeating unit in a crystal lattice) is defined as the structure factor

$$F(hkl) = \sum_{j=1}^{N} f_j \cdot \exp\left(2\pi i\left(hx_j + ky_j + lz_j\right)\right) \tag{2}$$

with the atomic scattering factor f_j of the j^{th} atom and the miller indices h, k, l which are assigned to each diffraction spot resulting from scattering at the atom positions x_j, y_j, z_j of the crystal lattice. It contains the information about the arrangement of the atoms in the unit cell.

As X-rays are scattered almost only by the electrons, one can integrate over the electron density $\rho(xyz)$ with the coordinates x, y, z of a unit cell with the volume V, instead of summing over the atoms, and express eq. (2) as

$$F(hkl) = V \int_{x=0}^{1} \int_{y=0}^{1} \int_{z=0}^{1} \rho(xyz) \exp\big(2\pi i(hx + ky + lz)\big)\, dx\, dy\, dz. \tag{3}$$

The integration can be transformed into a summation, as diffraction only occurs at discrete directions. As $F(hkl)$ is the Fourier transform of $\rho(xyz)$ and vice versa, one can write

$$\rho(xyz) = \frac{1}{V} \sum_{h} \sum_{k} \sum_{l} F(hkl) \exp\big(-2\pi i(hx + ky + lz)\big), \tag{4}$$

which is the relation between the diffraction data and the electron density distribution in the crystal structure. $F(hkl)$ contains the information about the amplitude $|F(hkl)|$ and the phase φ_{hkl} of the diffracted beam

$$F(hkl) = |F(hkl)| \exp(i\varphi_{hkl}). \tag{5}$$

From the diffraction spot intensity only the amplitude can be measured. The phase information is not given and has to be obtained by other methods as for example molecular replacement, discussed in section 3.5.

3.3. Data collection and processing

We collected X-ray diffraction data sets (Figure 22) at 100 K at the European Synchrotron Radiation Facility (ESRF, Grenoble, France) on the beamline ID30A-3/MASSIF-3 with an Eiger_4M (Dectris) detector (Crystal 1 and 3) and on the beamline ID30B of the ESRF with a Pilatus3_6M (Dectris) detector (Crystal 2).

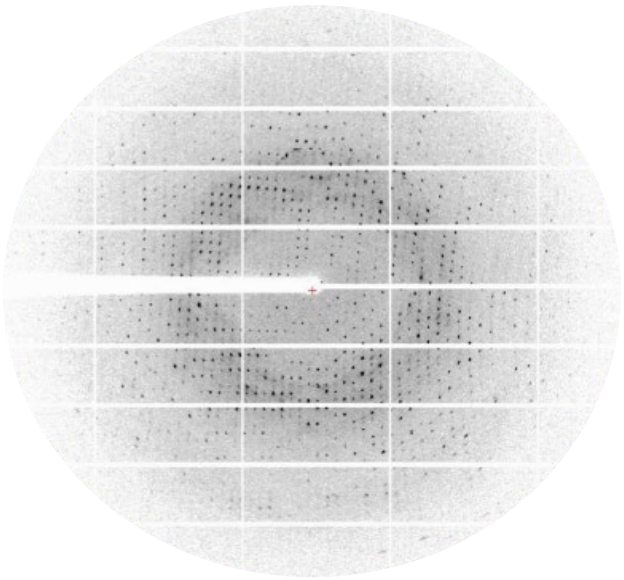

Figure 22: Diffraction pattern collected at the ESRF. The thick white line in the middle is caused by the shadow of the beam blocker, which protects the detector from too intensive light of the central spot.

We collected crystal data on the full range of 360° to improve the completeness of our datasets, after we collected data on a smaller range in previous experiments and did not obtain sufficient completeness. For this we estimated the recommended irradiation power for a recommended collection range by an automated characterization procedure and reduced that power according to the factor by which we increased the collection range.

The first step of processing is indexing, where the spots are numbered with the miller indices followed by integrating the data to estimate the intensities

of the spots and to assign values. From the relative distances of the reflection spot positions the space group can be determined. Space group determination with XDS (Kabsch, 2001) suggested that the space group of our rsEGFP2 crystals is $P2_12_12_1$, which is the primitive orthorhombic unit cell system with a two-fold screw axis 2_1 in all three directions. Further, the high-resolution cutoff needs to be determined according to the data quality, which is not trivial. There are several quality factor as for example the R_{merge}-factor which compares each individual reflection to a weighted average of all symmetry related repetitions of this reflection (Evans & Murshudov, 2013). However, as it depends on the multiplicity of the data, it is not the best option and other quality indicators were developed, as for example the correlation coefficient $CC_{1/2}$ (Evans & Murshudov, 2013). This is a measure of linear correlation between two randomly chosen halves of the data.

We compared manual processing using XDS (Kabsch, 2001) with several auto-processing software. Auto-processing with AutoProc (Vonrhein et al., 2011) and XDSAPP (Krug et al., 2012) appeared to be the best choice, as it led to comparable results as with manual processing, but took less amount of time.

3.4. Molecular replacement

After the intensities are worked out, the next step is the phase determination. As the phase information is not given by the measured diffraction patterns, it has to be determined separately. The most common approach is molecular replacement, in which the phases of structure factors of a similar structure are used to reconstruct the phases of the structure factors obtained by the experiment. The known structure of the similar protein is set as the starting model of the protein structure that has to be worked out. For this, it is necessary to determine the orientation of the two

protein structures and to match them by a proper rotation. Then a translation is required to superimpose the two structures.

We used MOLREP (Vagin & Teplyakov, 2010) within the CCP4i2 suite (Potterton et al., 2018) for molecular replacement. The rsEGFP2 on-state structure (PDB entry 5DTX, Kathib et al. 2016) was used as a starting model for Crystal 1 and the on-state of Crystal 3. The rsEGFP2 off-state (PDB entry 5DTY, Kathib et al. 2016) was used as a starting model for Crystal 2 and the off-state of Crystal 3.

3.5. Refinement

In the next step, the model is refined until it best matches the real data. The structure factors calculated by the model (F_{calc}) need to be adjusted to match the observed ones (F_{obs}). The correlation between those two is given by the R-factor (with the scaling factor b), which has to be minimized:

$$R = \frac{\sum_{hkl} \| F_{\mathrm{obs}} | - b | F_{\mathrm{calc}} \|}{\sum_{hkl} | F_{\mathrm{obs}} |} \tag{6}$$

A risk is to overinterpret the diffraction data without improving the model or even worsening it. To examine the quality of the fit, the additional R-factor R_{free} was introduced by Brünger (1992), which takes into account an independent, randomly chosen set of data, which is excluded from the refinement process (5-10% of the total data) and thus is not biased by overfitting of the data. R_{free} is calculated by the same equation as the R-factor. The two R-factors should decrease by a comparable percentage during refinement if the data is not overfitted.

For refining fluorescent protein structures also the chromophore needs to be considered. The geometrical restraints of the chromophore are defined in a separate Crystallographic Information File (CIF). It lists all present

atoms and defines several restrains such as angles and types of chemical bonds or the planarity.

In this work, refinement was mainly performed with REFMAC5 (Murshudov et al., 2011) within the CCP4i2 suite and cycles of manual model building in between with Coot (Emsley et al., 2010). The electron density and the atomic model can be visualized in Coot (Figure 23). The rsEGFP2 chromophore CIF file was also downloaded from the PDB. The chromophore structure was then manually linked to the protein structure in Coot.

In validation steps within Coot or additional programs such as Molprobity (Williams et al., 2018), it is examined if bond lengths and angles of the resulting model match typical values of known structures. Refinement and validation were performed as described in the appendix (publication Mantovanelli et al., p. S4).

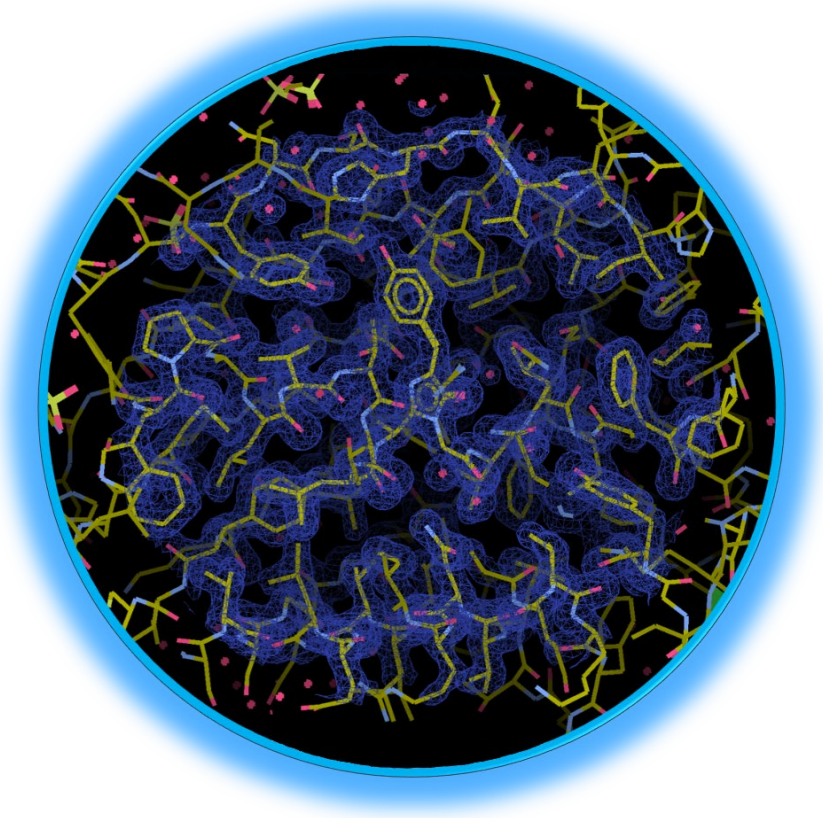

Figure 23: Electron density of the observed structure of an rsEGFP2 crystal in blue and the model, which is fitted to the data in yellow, displayed in Coot.

A helpful tool for refinement is to display F_{obs}-F_{calc} difference maps, which indicate differences between the calculated model and the observed data. It highlights regions where electron density is present, but no model was built or vice versa. These maps are typically displayed with a root mean square deviation of ±3σ.

Furthermore, F_{obs}-F_{obs} difference maps between different datasets can be created to observe small differences between those datasets. As demonstrated by Ursby & Bourgeois (1997), the signal-to-noise ratio of these difference maps can be improved by including weighting factors for each structure factor. In their approach they assume a Gaussian error distribution for each structure factor and that the average difference between two structure factors corresponding to the same reflection is zero. They also estimate the real error for each difference amplitude from the measurements. Depending on how high these errors are, each difference amplitude is weighted with a factor, to give less weight to measurements with a high error, such that they get closer to the assumed structure factor difference.

3.6. Q-weighted difference map calculation trial

We tried to calculate Q-weighted $2F_{obs}$(on)-F_{obs}(off) maps using a CNS (Brunger, 2007; Brunger et al., 1998) based script developed by Ursby & Bourgeois (1997), modified by Dr. Jacques-Philippe Colletier, to compare the on- and off-state structures of rsEGFP2. We could only apply it successfully on other test datasets but no meaningful $2F_{obs}$(on)-F_{obs}(off) difference maps could be obtained with our crystallography data shown in Figure 35, as indicated by the presence of arbitrary noise in the Q-weighted map (Figure 24).

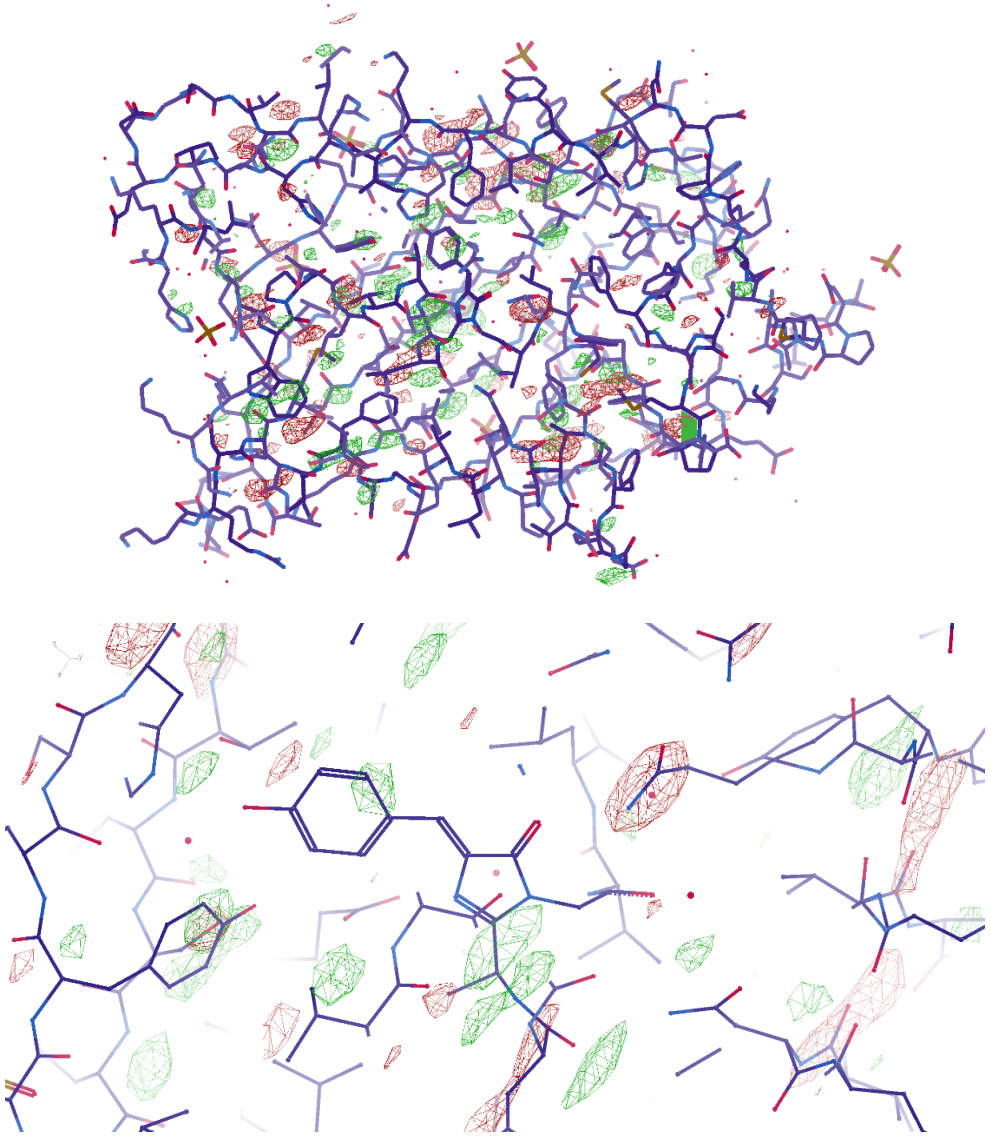

Figure 24: Q-weighted difference map of rsEGFP2 on- and cryo-switched off-states shown at ±3σ and zoom of the chromophore region. Arbitrary noise indicates that the difference map is not meaningful.

To get a meaningful comparison between two datasets typically R_{iso}-values (isomorphism factor) lower than 0.1 are recommended, indicating the fraction of global differences between the datasets. For our data the overall value was $R_{iso} = 0.141$ and the value for the highest resolution shell was $R_{iso} = 0.236$ (Table 3: R_{iso}-factors for each resolution shell indicating the isomorphism between two X-ray diffraction data sets, which correspond to rsEGFP2 in the on-state and in the cryo-switched off-state. One possible reason for this is that global illumination damage on the crystal caused too

strong differences between the datasets and thus made them incomparable. However, in that case a unit cell dimension change would be likely but only a minor change from A = 52.46 Å, B = 60.77 Å and C = 71.75 Å (on-state) to A = 52.40 Å, B = 60.75 Å and C = 71.58 Å (off-state) was observed for this data (Figure 35). Thus, the reason for the non-isomorphism between the datasets remains unclear. Further, the low resolution of the datasets does not allow to reveal slight structural changes. We reasoned that it would be beneficial to obtain higher quality data. Attempts to increase the completeness of the data by collecting data on a larger range (360°) as compared to previous data collections to improve the quality of the Q-weighted difference maps, were successful but still did not allow to obtain a meaningful Q-weighted difference map.

Resolution (Å)	**R_{iso}-factor**
10	0.103
7.07	0.114
5.77	0.099
5	0.107
4.47	0.106
4.08	0.119
3.78	0.127
3.54	0.141
3.33	0.143
3.16	0.162
3.02	0.175
2.89	0.193
2.77	0.205
2.67	0.2
2.58	0.221
2.5	0.227
2.43	0.226
2.31	0.236
Overall R_{iso}-factor :	0.141

Table 3: R_{iso}-factors for each resolution shell indicating the isomorphism between two X-ray diffraction data sets, which correspond to rsEGFP2 in the on-state and in the cryo-switched off-state.

4. Absorption and Fluorescence Spectroscopy

Absorption spectroscopy is a technique to record absorption of light by a sample as a function of wavelength. It can be used to measure the presence of substances in a sample or to determine states of a molecule. Typically, a polychromatic light beam is directed on a sample and the intensity of the light which goes through the sample is measured for each wavelength. The intensities of the entering light beam and the light which goes through the sample are compared to determine the optical density of the sample depending on the wavelength. With fluorescence spectroscopy the fluorescence emitted by a sample after excitation with light can be studied.

4.1. Microspectrophotometry on fluorescent proteins

With microspectrophotometers the spectra of microscopic samples can be measured. With UV-Vis spectroscopy the spectral range of 200 - 800 nm is studied. Typically, microspectrophotometers convert light into electric current using photodiodes or photomultipliers. Either the incoming radiation intensity or individual photons can be measured by this.

For integrative intensity measurements often charge coupled devices (CCD) are used. They consist of several photodiods, which can transform light into electric current due to the photoelectrical effect. The electric charge is accumulated in a capacitor and passes then, controlled by a circuit, the neighbored capacitors till it finally is converted into a detectable voltage.

Individual photon detection is limited to experiments where the number of incoming photons per surface and per time unit is low enough, so that they can be distinguished. Accordingly, for individual photon counting the

detector readout time and pixel size are key parameters which determine the time resolution and the maximum signal that can be detected.

By measuring absorption of protein solutions at 280 nm, the concentration of the protein can be determined, as the amino acid tryptophan has a strong absorption at this wavelength. Moreover, in fluorescent proteins different fluorescent states can be identified from the absorption spectra because the chromophore absorbs different wavelengths in the fluorescent and in the non-fluorescent state. Further, their emission spectra can be monitored by microspectrophotometry. The spectra can also be recorded for different time points to observe spectral evolutions, such as photoswitching between different states upon excitation with laser light, requiring a dedicated setup.

Typically, protein solutions are used as a sample but also protein crystals can be utilized if the setup allows it. However, applying absorption microspectrophotometry on crystals is not straightforward. They have a high optical density and therefore too thick crystals absorb all incoming light such that it cannot reach the detector and thus no spectral information can be collected. This problem can be avoided by using thin crystals. Another challenge of using crystals is that due to the periodic repetitive orientation of molecules in the crystal different amount of light passes the crystal depending on its orientation in the light path. This thus has to be adjusted for each crystal till sufficient signal can be obtained at the detector. Fluorescence microspectrophotometry on crystals faces less challenges but the light emitted by the crystal molecules can be reabsorbed by the dense crystal, which can lead to artifacts.

4.2. Microspectrophotometer setup

To investigate the photoswitching between different states in fluorescent proteins it is very helpful to simultaneously collect absorption and fluorescence spectra time-series. Our home-built microspectrophotometer

(Figure 25), developed by Byrdin & Bourgeois (2016), allows us to simultaneously record time series of absorption and fluorescence spectra of crystals or solution samples at CT or RT upon modulated illumination with laser light. To achieve this, laser illumination, absorption light, and fluorescence signal pass the same light path through a common objective.

Figure 25: Photograph of our home-build microspectrophotometer, which was developped by (Byrdin & Bourgeois, 2016).

The sample is aligned between two objectives onto a magnetized goniometer and can be cooled by a cryo-stream (Oxford Cryosystems) (Figure 26). The upper objective is exchangeable. 2-fold, 10-fold or 15-fold magnification can be chosen. The objectives are mirror objectives, which have the advantage to reduce chromatic aberration and thus are more appropriate for spectrophotometer detection. The lasers, absorbance light, and two CCD spectrometers are connected to the setup by optical fibers. The optical fiber collimation is achieved by parabolic mirrors, as they also

induce less chromatic aberration as compared to conventional collimation lenses. Further, optical filters in polka dot design are used as beam splitters, as they are not sensitive to the angle of the incoming illumination and thus do not produce artifacts when splitting beams of polychromatic light. The setup allows the positioning of different dichroic beam splitters at each stage, depending on the requirements of the experiment. A CCD camera allows the sample observation during alignment and sample illumination.

To avoid that absorbance and fluorescence measurements disturb each other, their detection is alternated. With mechanical shutters, controlled by a pulse generator, the lasers, spectrometers, and lamp are synchronized. The time which is needed to open the shutters (~1 ms) limits the maximum temporal resolution but the necessary integration time to obtain enough signal (~10 ms) is usually an even more limiting factor.

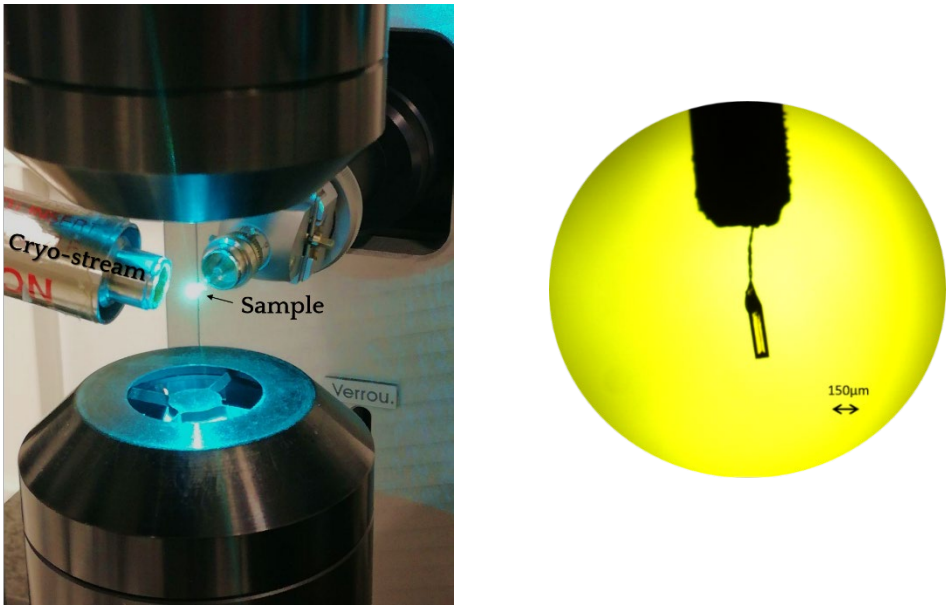

Figure 26: An rsEGFP2 crystal in a silicon loop (zoomed in on the right) is placed between two objectives at the microspectrophotometer and is cooled by a cryo-stream. It fluoresces green upon illumination with 488 nm laser light.

4.3. Protocols

4.3.1 Microspectrophotometer setup in this work

In this work a 15-fold magnification was utilized. The sample was illuminated by fiber coupled (200 or 600 µm diameter, Avantes) lasers of 488, 405 or 355 nm wavelength (LBX-488-200 and LBX-405-200, Oxxius and MPL-F-355, CNI) and a white lamp (Deuterium-halogen lamp, AvaLight-DH-S-BAL, Avantes), connected by an optical fiber (100 µm, Avantes), as shown in Figure 27. Fluorescence and absorbance of the sample were recorded by spectrometers. The fluorescence spectrometer (AvaSpec ULS 2048L-USB2, Avantes) was protected by a dichroic mirror (Di02-R488, Semrock) of the 488 nm laser illumination and is connected to the setup by an optical fiber of 100 µm diameter (Avantes). In addition, a notch filter (NF03-488E-25, Semrock) was mounted in the light path directly before the fluorescence spectrometer to filter out the remaining laser light, together with a 10-fold optical density filter to avoid signal saturation. A (400-700 nm) beam-splitter was put in the main light path to allow the detection of fluorescence with the spectrometer and with a visible light CCD camera after sample illumination. A Polka Dot beam-splitter allowed the sample illumination with the white lamp and detection of the light at the camera and the fluorescence spectrometer afterwards. The absorption spectrometer (AvaSpec ULS 2048L-USB2, Avantes) detected the lamp light during the laser dark times and was connected to the setup with an optical fiber of 200 µm diameter (Avantes). A digital delay-pulse generator (9518, Quantum Composer) was used to control the exposure times and the spectrometer readouts. The spectrometers, the laser and the camera were connected to a computer to control their settings, as for example the laser power, and to save the recorded data. The sample was visualized by a CCD camera before data acquisition in order to align it and to choose the illumination area. Beam splitters, mirrors and optical fibers are exchangeable in this setup. A split fiber of 200 µm diameter was used to connect the two Oxxius lasers of the

same laser box together with the 355 nm laser to the setup for to allow subsequent illumination of the three lasers. For crystals a fiber of 600 µm was used to maximize the illumination area at the crystal. The absorption spectrometer was coupled with a 200 µm diameter fiber to maximize the signal.

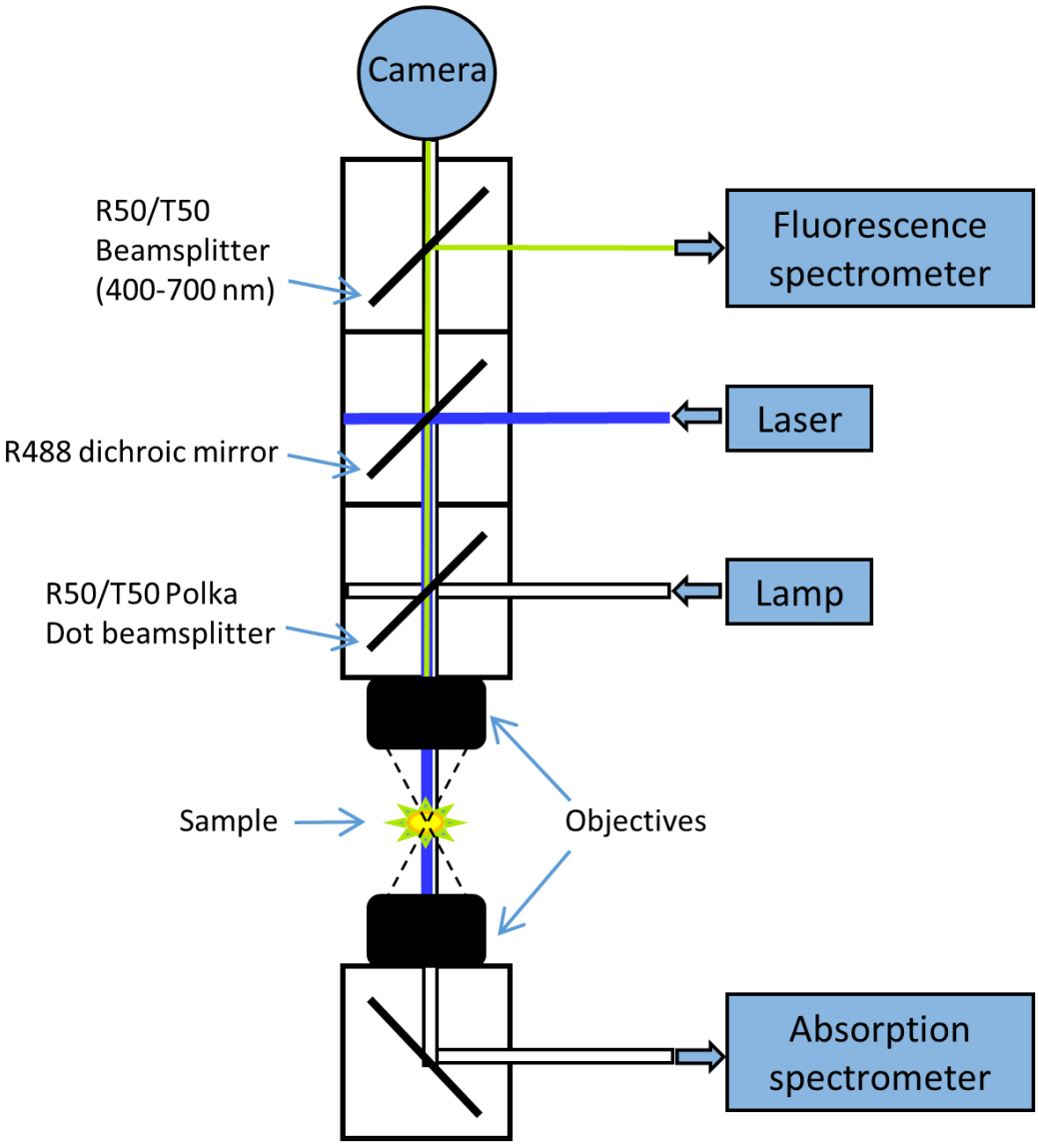

Figure 27: Microspectrophotometer setup used for this work.

The laser illumination scheme was set as described in Mantovanelli et al. (see appendix). Briefly, in each measurement period a white lamp was switched on and absorbance was measured in this time, starting with a short time delay of 10 ms (Figure 28). Further, 10 ms after the lamp was switched

off, the laser was switched on and the fluorescence measurement was initiated 5 ms after turning on the laser (Figure 28). These time delays are necessary to avoid synchronization errors as for example the data collection starting before illumination. However, these time delays could have caused another error instead. As we observed a fast fluorescence decay in the first few milliseconds of laser illumination due to the formation of a short-lived dark state (see section 7.7), the maximum fluorescence intensity might be systematically underestimated. This is because the data collection then would only start after the fluorescence already decayed to some part. Apart from this systematic error, a further non-systematic synchronization error might arise, if the starting time of the fluorescence detection is fluctuating due to software or hardware. This might in particular cause artifacts in the relative fluorescence recovery levels. Especially, the first time point of fluorescence data acquisition is prone to errors, as the fluorescence decay starts with a fast off-switching phase in the first seconds.

For this reason, the fluorescence data should be considered together with the absorbance data, which are more reliable in terms of relative recovery levels. However, it was observed that the fluorescence data is probably more reproducible in the decay phase, whereas the absorbance data was sometimes affected by baseline drifts (see section 4.3.3).

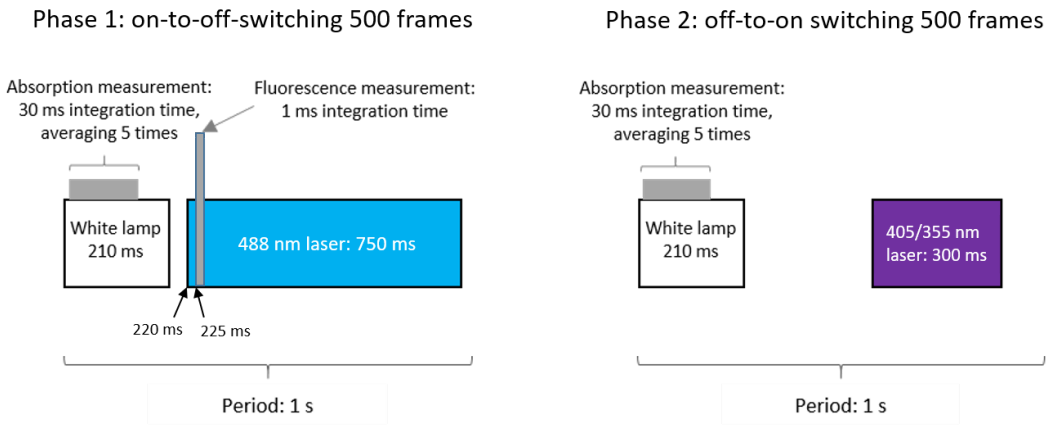

Figure 28: Laser scheme applied in this work.

4.3.2 Solution sample preparation

Purified protein was mixed with 50mM HEPES buffer solution (pH 7.5), 50mM NaCl and 20% glycerol of the final solution. The best signal was obtained with final protein concentrations of 20mg/ml. The glycerol concentration should not be lowered to avoid ice formation.

To measure the pH-dependence of rsEGFP2, it was mixed with different buffer solutions and also 20% glycerol. 1M MES was used for obtaining buffer solutions with a pH between 5 and 6. 1M Hepes was used for pH7. The final protein concentration was 7mg/ml.

4.3.3 Solution sample illumination

For measurements at CT or RT, the final protein solutions were sucked into capillaries of 50 µm x 100 µm section which were put onto a goniometer base. These were mounted on our microspectrophotometer, where in the case of CT measurements, a 110 K gaseous cryo-stream (Oxford Cryosystems) was used to continuously cool the sample. It is crucial to orient the capillary precisely parallel to the objectives and put the focus in the exact middle of the sample. The reference spectra of the lamp should be measured in an empty capillary if the absorption spectra of the protein are measured in a capillary, as the spectrum of the capillary glass affects the baseline. Further, baseline drifts due to ice crystal formation were sometimes observed during experiments at CT. Measurements at RT were affected by diffusion. Thus the RT switching kinetics obtained with this setup should only be considered qualitatively.

The illumination scheme with the 488 nm, the 405 nm and the 355 nm lasers are described in detail in the appendix (publication Mantovanelli et al., pp. S2-S3).

Relatively high laser powers, as compared to typical laser powers used in SMLM were chosen, to accelerate the switching kinetics in order to observe complete switching phases without extending the acquisition time to several hours per switching cycle, which also would lead to more ice formation. However, if these experiments were to be repeated, the same laser powers should be used for each experiment for a better comparability. Since we generally worked with the full possible laser power, and this maximum power varied greatly from one use to the next for our lasers, the laser power often varies from experiment to experiment. Further, for a few experiments a different optical fiber was used to connect the laser, leading to a two-fold higher power.

4.3.4 Crystal preparation

Crystals were harvested from a crystal drop (as shown in Figure 20) with cryo-loops. They were soaked for a few seconds in a cryo-protectant solution consisting of the reservoir solution mixed with 20% glycerol to avoid ice formation. The crystals were flash-cooled immediately in the cryo-stream (110K) on the microspectrophotometer, where they were pre-illuminated and subjected to fluorescence and absorption micro-spectrophotometry as described in the appendix (publication Mantovanelli et al., pp. S2-S4).

4.3.5 Crystal pre-illumination

The first goal was to observe the off-state of rsEGFP2 and rsEGFP2-V151A after cryo-switching and to compare it to the initial on-state. To obtain the on-state structure, the protein crystals were left non-illuminated on one part (Position 1) and were illuminated on the other (Position 2) with the 488 nm laser to obtain the off-state structure.

We noticed that it is important to use crystals of small dimensions, as crystals with too high optical density absorb too much light and thus the absorption spectrum signal is saturated. Further, the laser power should be low enough to avoid heating or partial disordering of the crystal. The rsEGFP2-V151A crystal (Crystal 3) for which the data was shown in Figure 38 was too big (150 × 200 × 800 µm³), hence the optical density was too high to obtain good absorption data. The applied illumination power of 300 W/cm² combined with the high optical density of the crystal most likely led to heating it close to RT (estimation see section 4.4.1).

Following crystals were irradiated with a low laser power of 46 W/cm² for 700 s. In this work data of one representative rsEGFP2 crystal (Crystal 1) is shown (Figure 35 and appendix, publication Mantovanelli et al., Suppl. Table 2).

The second goal was to reproduce the RT switched off-state, which should be in trans-conformation, and to examine if subsequent back-on switching at CT changes the conformation. To achieve this, rsEGFP2 crystals were switched off at RT over their whole volume with 488 nm laser light (~100 mW/cm²) for 30 s in the crystallization drop. Crystals were then harvested immediately, and flash cooled at the microspectrophotometer. One part of the crystals was not illuminated a second time to keep the RT off-state (data of representative Crystal 2 shown in Suppl. Table 3, Position 1) and the other part was illuminated with the 405 nm laser (14 W/cm²) for 180 s at 110 K, to obtain the cryo-recovered state (Suppl. Table 3, Position 2).

The relatively high power of 488 nm light, which was used at RT to guarantee complete off-switching of the crystal, eventually led to partial photo-bleaching.

The on-state structure obtained from Crystal 1 (Position 1) and the RT off-state structure obtained from Crystal 2 (Position 1) are displayed together in Figure 36 and show the expected cis-trans isomerization.

4.3.6 Spectroscopy data analysis

The detailed analysis of the spectral data is described in the appendix (publication Mantovanelli et al., pp. S4-S5).

The absorbance data baseline was corrected with an offset based on the average baseline between 550 and 650 nm. For some samples ice crystal formation caused a baseline drift, which was especially visible at the 280 nm tryptophan absorbance peak. Attempts to correct this baseline drift resulted in data biases and thus were not applied.

Fluorescence spectra were integrated in the full range between 495 and 630 nm to account for the whole signal. Absorbance data was integrated between 470 and 500 nm to follow the on-state of rsEGFP2. As for mEmerald and EGFP broader on-state peaks were observed, the integration range was adjusted for these variants to broader integration ranges, as indicated in the corresponding figure captions.

To calculate the recovery levels, the difference between the maximum and minimum value of the recovery phase was dived by the difference between the maximum and minimum value of the first decay phase.

4.3.7 Triplet state quencher attachement

Dr. Virgile Adam produced a double cysteine mutant of rsEGFP2 (rsEGFP2-2cys) by replacing the residues K207 and L222 by cysteins, to obtain an analogue to the double cysteine mutant of alpha-GFP developed by Henrikus et al. (2021).

Azobenzene maleimide derivative was attached to rsEGFP2-2cys according to the protocol of Henrikus et al., with some modifications.

First the necessary buffers were produced:

Standard buffer: 50mM potassium phosphate buffer, 50mM KCl, 5% glycerol

DTT-buffer: 50 mM potassium phosphate, 50 mM KCl, 5% glycerol, 5 mM DTT (Dithiothreitol)

DMSO+AB solution: 1ml DMSO + 2,7mg Azobenzene maleimide (100 nmol)

The attachment protocol was the following:

3 ml nickel beads were loaded on a nickel resin and washed with 20 ml water and equilibrated with 20 ml standard buffer. After incubating 100 µl of 5mg/ml protein solution for 40 minutes with 2 ml of the buffer containing the reducing agent DTT, 20 ml of standard buffer were added to it and the resulting solution was loaded on the nickel resin. DTT was washed off with 20 ml standard buffer. The resin was closed and 20 ml of standard buffer containing 200 µl of DMSO+AB solution was added to it to carry out maleimide-cysteine coupling in the resin. The solution was left in the resin for two days at 4°C upon continuous mixing by rotation around the short axis of the resin to facilitate the reaction. The mixture was then washed off with 20 ml standard buffer till only the protein remained. The protein was eluted with 20 ml of imidazole buffer and loaded into two Amicon-Ultra-4 (10 kDalton) filters, which were put into a centrifuge to wash off the imidazole and unbound ABD. In the next step 4 ml of HEPES buffer was added into both tubes for a second washing cycle in the centrifuge and 1 ml HEPES (pH 7.5) buffer for a third washing cycle. Finally, 70 µl of 20 mg/ml protein was obtained.

4.3.8 Triplet state lifetime measurement

For the measurement of the triplet state lifetime only fluorescence was recorded and thus the white lamp was not used. The objective with 15-fold magnification was used. Fluorescence was detected with a Si Switchable Gain Detector (PDA36A2, Thorlabs) and a LeCroy Wavejet 334A oscilloscope (DC – 300 MHz bandpass). An Oxxius laser (LBX-488-200) with 300 µs switching time was used. It was coupled to the setup by a 600 µm optical fiber (Avantes). For each measurement 64 illumination sequences of 40 ms laser exposition followed by 960 ms dark time were averaged. The measurements were conducted while the sample was cooled to 110K with the cryo-stream.

The obtained data was fitted with a free bi-exponential model with an offset. The error bars result from measurement errors of three independent measurements.

Laser powers were measured with a sensor (S121C) connected to a calibrated power meter (PM100D, Thorlabs).

4.4. Calculations

4.4.1 Temperature elevation in a rsEGFP2-V151A crystal of big dimensions

The rsEGFP2-V151A crystal for which unexpected fast switching kinetics were observed had big dimensions was possibly affected by a temperature rise. It was cooled by a 100K nitrogen stream and irradiated by laser light. The possible temperature rise is estimated in the following:

To get a temperature rise dT_C in the crystal C with the mass m and the heat capacity C_p, the heat δQ is necessary:

$$\delta Q = -mC_p\, dT_{C.} \tag{1}$$

δQ can be expressed as the sum of all heat contributions, here this is the power source with the contribution δQ_P and the nitrogen bath with the contribution δQ_N:

$$\delta Q = \delta Q_N + \delta Q_P. \tag{2}$$

The heat δQ_P, which is absorbed by the sample in the time window dt, is the power $-P$:

$$\frac{\delta Q_P}{dt} = -P. \tag{3}$$

The heat δQ_N that can be taken off from the crystal at the exchange surface S, with the distance D between the sample surface and the nitrogen layer, in the time dt, can be expressed by

$$\frac{\delta Q_N}{dt} = k_B S \frac{T_C(t) - T_N}{D}, \tag{4}$$

with the thermal conductivity k_B of the nitrogen.

Inserting equations (1), (3) and (4) into equation (2) gives:

$$-mC_p dT_C = \left(\frac{k_B S}{D}(T_C(t) - T_N) - P\right) dt. \tag{5}$$

This can be solved by:

$$T_C(t) = A \cdot exp\left(-\frac{k_B S}{DmC_P} \cdot t\right) + T_N + P\frac{D}{k_B S}. \tag{6}$$

At $\rightarrow \infty$, when the equilibrium is reached, the following equation is obtained:

$$\lim_{t\to\infty}(T_C(t)) = T_N + P\frac{D}{k_B S}. \tag{7}$$

The temperature change which is caused by a certain power can be calculated then by

$$\Delta T = \frac{PD}{k_B S}. \tag{8}$$

With the optical density OD and the laser power P_L we can calculate the power absorbed by the crystal, assuming that the laser size is smaller than the crystal surface, which was the case in our experiments:

$$P = P_L\,(1 - 10^{-OD}). \tag{9}$$

The big crystals for which an unexpected fast switching was observed, had an optical density of $OD = 3.5$. Further, for these big crystals an exchange surface of the crystals with the nitrogen bath of $S = 800\,\mu m \cdot 150\,\mu m = 1.2 \cdot 10^{-7} m^2$ is assumed, according to the dimensions of the crystals and the orientation to the nitrogen stream. The distance to the nitrogen bath was approximated to be $D \approx 10^{-5}\,m$. With the laser power of $P = 15\,mW$ (which was used in the experiments which led to an unexpected behavior) and the Boltzmann factor $k_B = 10\,\frac{\mathrm{mW}}{\mathrm{m \cdot K}}$, this leads to a temperature rise of:

$$\Delta T = \frac{P_L\,(1 - 10^{-OD})D}{k_B S} = \frac{15\,mW \cdot (1 - 10^{-3.5}) \cdot 10^{-5}\,m}{10\,\frac{mW}{m \cdot K} \cdot 1.2 \cdot 10^{-7}\,m^2} \approx 125K.$$

4.4.2 Quantum yield calculation of rsEGFP2 on-to-off cryo-switching

We consider the values, corresponding to the data shown in Figure 46 F. We used a laser with the wavelength $\lambda = 488 \cdot 10^{-9} m$ and the power density $\rho = 325\,\frac{W}{cm^2} = 3250000\,\frac{W}{m^2}$ (calculated by considering the laser spot size $S = \pi r^2 = \pi \cdot (12{,}5\,\mu m)^2 = 4{,}9 \cdot 10^{-10}\,m^2$) and obtained the fluorescence decay rate $k = 0.03969\,s^{-1}$. Considering the extinction coefficient

$\varepsilon_{488\,on-state} = 4858\frac{m^2}{mol}$ of rsEGFP2 in the on-state, the avogadro number $N_A = 6 \cdot 10^{23}\,mol^{-1}$ and the planck constant multiplied with the light constant $h \cdot c = 1.986 \cdot 10^{-25} Jm$ we obtain the quantum yield Φ of on-to-off switching using the same equation as Regis Faro et al. (2010):

$$\Phi = \frac{h \cdot c \cdot S \cdot N_A \cdot k}{P \cdot \lambda \cdot \varepsilon \cdot \ln(10)} = 6.1 \cdot 10^{-7}$$

5. PALM-Microscope

Photo-activated localization microscopy is a stochastic super-resolution wide-field fluorescence microscopy technique, which is typically used to perform single-molecule imaging. We used the PALM-microscope available in our lab to measure switching kinetics of fluorescent proteins at the ensemble level. Further, Dr. Oleksandr Glushonkov performed measurements at the ensemble and single-molecule level on a cryo-PALM setup.

5.1. RT switching at the ensemble level

Details of sample preparation, data acquisition and data processing are described in the appendix (publication Adam et al.: Supporting information p. 9-12).

Briefly, the sample was prepared by mixing the protein solution into a polyacrylamide gel and spreading it between two cover slides, separated with a spacer. Its fluorescence emission evolution at the ensemble level upon 488 and 405 nm laser illumination was measured with a home-built PALM microscope. Switching kinetics were extracted from a small region,

which was exposed to the maximum laser intensity to make sure that the illumination was homogenous.

The sample can also be prepared without the spacer and put directly between the cover slides, but the spacer increases the sample thickness, which improves the signal significantly. This improvement comes with the cost that fluorescent proteins from other layers than the focused one contribute to the fluorescence signal. Thus the signal that we measured had to be corrected for these contributions by estimating the depth dependent point spread function of the objective, which was done by Dr. Dominique Bourgeois. For each x_0 y_0 position of the recorded signal the contributions of all defocused molecules at other x y positions were estimated. The laser power density with which the molecules were illuminated was obtained from a separately measured two dimensional beam profile, which was considered to be constant in the third dimension. From this information the switching kinetics of the illuminated molecules could be modelled. The overall switching kinetics are the sum of the contribution of all molecules in the sample weighted by the fraction of their signals arriving at the considered detector region. A small region in the center of the recorded signal was selected for modelling the switching kinetics because the highest laser intensity was obtained in this region. Thus, the out-of-focus molecules would exhibit slower switching, as they would be exposed to lower laser power and thus the overall switching brightness would be underestimated without the corrections.

The signal was fitted with a kinetic model, which was developed and incorporated into a Matlab routine by Dr. Dominique Bourgeois. In addition to one on- and one off-state it includes a short-lived reversible dark state which can be reached from the on-state (Figure S15, in Adam et al.). The routine considers the rates between these states to calculate the emitted fluorescence as a function of time.

5.2. Cryo-switching at the single-molecule level

In collaboration with the team of Prof. Dr. Jörg Enderlein (Georg August University Göttingen), Dr. Oleksandr Glushonkov developed a cryo-PALM setup in our lab to perform single-molecule localization microscopy also at CT. This instrument allows testing fluorescent proteins and new illumination strategies in real single-molecule localization microscopy applications and enables potential biological applications.

The cryostat was developed by Li et al. (2015) to be combined with epi-fluorescence microscopes for single-molecule fluorescence imaging and spectroscopy with air objectives. It allows cooling with liquid nitrogen down to 89K. Thermal isolation is reached with a vacuum layer between an outer and an inner tank. The sample is decoupled from unstable setup parts to ensure high mechanical stability. Further, the sample is connected to a copper disc which transfers heat from the sample to the liquid nitrogen tank, to ensure thermal stability.

The cryo-PALM microscope setup and data collection protocols of Dr. Oleksandr Glushonkov are described in the appendix (publication Mantovanelli et al., pp. S6-S7). Briefly, wide-field epi-fluorescence illumination is reached by focusing the laser beams through an air objective with 60-fold magnification. The 488 nm, 405 nm and 355 nm lasers are combined using a dichroic mirror and a set of lenses and mirrors. Further, a dichroic mirror and a band-pass filter are used to separate excitation and emission signal. The final image is focused onto a EMCCD (Electron multiplying charge-coupled device) camera.

III. Results

Painting by the author showing the rsEGFP2 chromophore upon room- (left) and cryo-temperature switching (right) with corresponding absorption spectra

Introduction

To make single-molecule localization microscopy possible at CT, fluorescent proteins which photo-switch efficiently at CT are needed. For this goal, one possible approach is to mutate fluorescent proteins in order to improve their photo-switching. Another approach is to test already existing fluorescent proteins for their switching properties and optimize the environmental conditions, as for example the illumination scheme. For both cases, it is crucial to understand the underlying switching mechanism, to optimally improve it.

We conducted spectroscopic and structural investigations mainly on the fluorescent protein rsEGFP2, and also on rsEGFP2-V151A, rsEGFP2-V151L, mEmerald and EGFP at CT and RT to understand their switching mechanisms and we developed an illumination strategy to enhance their off-to-on recovery at CT.

We initially focused our investigations on rsEGFP2, which is known to be a fast switcher at RT (Grotjohann et al., 2012), as we anticipated that the switching at CT would also be relatively fast for this protein. Also Tuijtel et al. (2019) suggested that rsEGFP2 is the fastest switching fluorescent protein from the ones they have tested.

In this chapter, our observations of the differences of the RT and CT switching mechanisms of rsEGFP2 are described. Our data suggest the rise of two off-states upon on-to-off switching at CT with the same isomeric state as the initial on-state and blue-shifted absorption spectra as compared to the off-states at RT. We observed that by using a 355 nm laser instead of a 405 nm laser, the CT off-state recovery is substantially enhanced. This result was confirmed at the single-molecule level. Our investigations of EGFP and mEmerald at CT and RT, indicate that their switching mechanisms are very similar to the rsEGFP2 switching at CT, which together with previously published observations (see section 1.6) hints that this mechanism could be quite general amongst GFP like proteins.

In another project of our group, the switching contrast of rsEGFP2 and rsFolder2 at RT was improved by applying point mutations at the V151 sidechain. In that work, also two off-states were reported. We discuss the hypothesis that two initial on-state populations might be the cause of the two off-states at RT and CT.

6. Switching contrast of rsEGFP2 and mutants at RT

Our group (Adam et al., 2022, see appendix) observed with serial femtosecond crystallography studies that rsEGFP2 and rsFolder2 can switch into two different trans-conformations (*trans1* and *trans2*), upon off-switching at RT, with a ratio depending on environmental conditions and / or on a possible heterogeneity of the on-state chromophore. It was observed that the trans2 conformation is similar to the trans-conformation of rsFolder, which has a lower switching contrast as rsEGFP2 and rsFolder2. Thus, the hypothesis was that if the presence of *trans2* could be decreased in rsEGFP2 and rsFolder2, the switching contrast (see section 2.2), which is an important property for nanoscopy applications, could be enhanced.

To control the off-state heterogeneity, two mutants were developed for each wild-type (rsEGFP2 and rsFolder2) by Adam et al. The V151 sidechain was shortened (rsEGFP2-V151A / rsFolder2-V151A) or lengthened (rsEGFP2-V151L / rsFolder2-V151L) with a point mutation to facilitate or hinder switching to *trans1*. The data of Adam et al. showed that the V151A mutants switched mainly into *trans1* and the V151L mutants mainly into *trans2*, while the wildtypes switched to both trans-conformations.

To investigate if the switching contrast was enhanced as expected, we switched off and back on rsEGFP2, rsFolder2 and their V151A and V151L mutants at the ensemble level on our PALM microscope, while measuring fluorescence. The data was processed with a Matlab routine, developed by

Dr. Dominique Bourgeois, which includes a kinetic model (see Adam et al. 2022, Supporting Information).

Our data (Figure 29) showed that indeed, the on-to-off switching contrast was enhanced for the V151A mutants (119±21 for rsEGFP2-V151A and 125±11 for rsFolder2-V151A) and, in the control experiment, decreased for the V151L mutants (15±1 for rsEGFP2-V151L and 15±1 for rsFolder2-V151L) as compared to the wild-type (43±5 for rsEGFP2 and 46±3 for rsFolder2). It was observed that the V151L mutants recover more efficiently to the on-state.

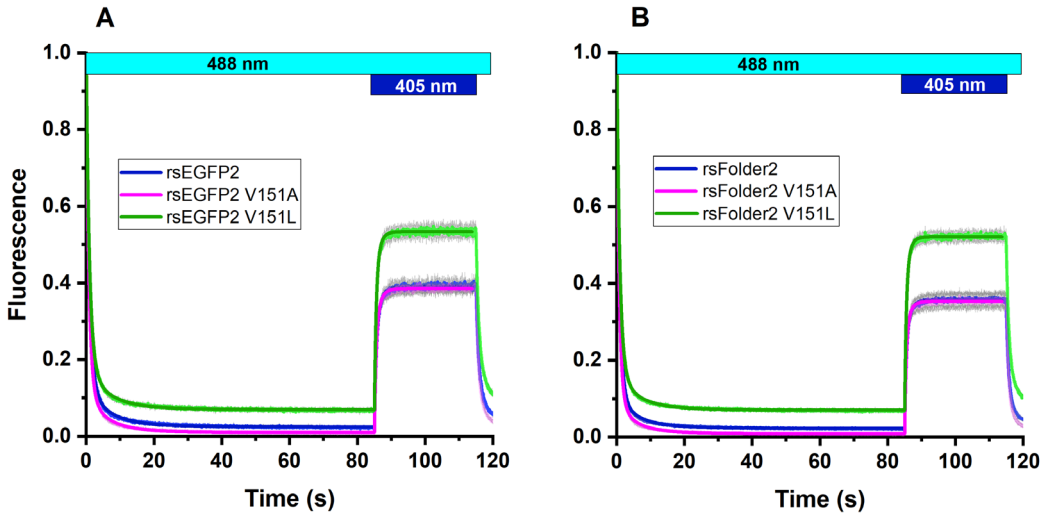

Figure 29: Switching kinetics of (A) rsEGFP2, rsEGFP2-V151A and rsEGFP2-V151L and (B) rsFolder2, rsFolder2-V151A and rsFolder2-V151L monitored by epifluorescence microscopy. Purified proteins embedded in polyacrylamide gel (pH 8) were illuminated with 488 nm laser light (0.27 W/cm²) for on-to-off switching and with additional 405 nm laser light (0.03 W/cm²) for off-to-on recovery. Mean (pale colors) and standard deviation (grey) are shown for 6 independent measurements. Fits from the kinetic model are represented with dark solid lines. Fluorescence was normalized to 1 at the start of acquisition.

The absorption spectra of the V151A mutants are blue-shifted compared to the V151L spectra (Figure 4, Adam et al., 2022, appendix) and thus have less overlap with the on-state spectra. Accordingly, a lower extinction coefficient of the off-state of the A-mutant (27±3 M^{-1} cm^{-1} for rsEGFP2-

V151A and 34±2 M^{-1} cm^{-1} for rsFolder2-V151A) at 488 nm as compared to the L-mutant (122±2 M^{-1} cm^{-1} and 145±5 M^{-1} cm^{-1}) was measured (Adam et al., 2022). This can explain why for the V151A-mutants the 488 nm laser leads to lower residual off-to-on switching and thus to an enhanced on-to-off switching contrast and a lower off-to-on recovery.

This off-to-on switching contrast enhancement of more than two times can be useful for improving nanoscopy applications with fluorescent proteins at RT (see section 2.2).

7. rsEGFP2 switching mechanism at CT

7.1. Spectroscopic investigations: RT vs. CT

It is well known that rsEGFP2 undergoes cis-trans isomerization and protonation at RT upon illumination with 488 nm laser light (El Khatib et al., 2016). In contrast, the cryo-switching mechanism of rsEGFP2 remains to be investigated. Our hypothesis was that rsEGFP2 could undergo the same switching mechanism at CT as at RT but with less efficiency, as protein dynamics are hampered below the glass transition temperature. In previous studies, Dr. Oleksandr Glushonkov measured absorption spectra time series of rsEGFP2 solution samples at RT (Figure 30, RT and Figure 31 A, B) and CT during off switching with 488 nm laser light and on switching with 405 nm laser light with our microspectrophotometer (Byrdin & Bourgeois, 2016). In this work, we continued the investigations at CT and obtained the results shown in Figure 30 (CT) and Figure 31 C, D.

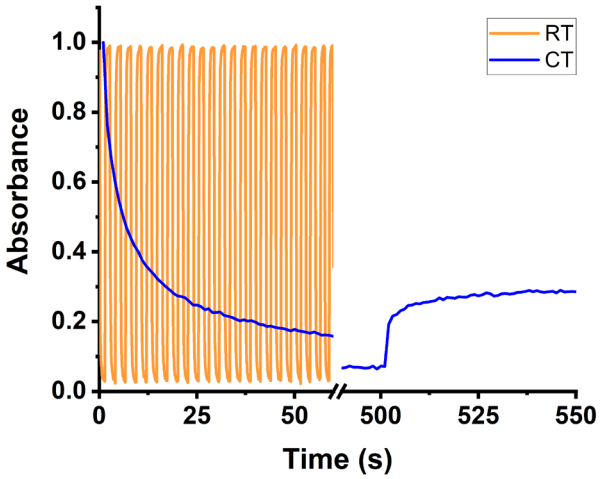

Figure 30: Comparison of rsEGFP2 photoswitching at RT (measured by Dr. O. Glushonkov) and CT of one representative measurement. Absorption spectra were recorded by microspectrophotometry and integrated in the spectral range of 470-500 nm. For data at RT (orange), samples were illuminated with 488 nm light (1.4 s, 490 W/cm²) and 405 nm light (1.4 s, 100 W/cm²) 23 times. For data at CT (blue), 488 nm illumination (5.7 kW/cm²) was performed for 500 seconds and 405 nm illumination (0.95 kW/cm²) for 50 seconds. Data was normalized to 1 at the start of acquisition.

One observation was the strongly reduced rate of switching at CT (Figure 30), even if much higher laser powers were used, which is expected due to limited dynamics below the glass transition temperature. The other remarkable observation was the blue shift of the off-state absorption peak at CT from 411 to 385 nm (Figure 31) which indicates different properties of the cryo-switched off-state and thus a different switching mechanism. Furthermore, the fluorescence (Figure 32) and absorbance (Figure 31) spectra at CT are more structured. Similar effects were observed for the wildtype GFP at 77K (Chattoraj et al., 1996). The structured shape could be explained by less exchange between different translational or rotational states at lower temperature due to the reduced thermal energy of the molecules. A molecule at RT has a higher thermal energy thus in average a higher speed and therefore should be more affected by the Doppler Effect than a molecule at CT (p. 704, Chang, 2000). Thus a molecule at RT would

be exposed to more different wavelengths of incoming illumination which would lead to transitions to other translational and rotational states, causing broader absorption spectra (p. 704, Chang, 2000).

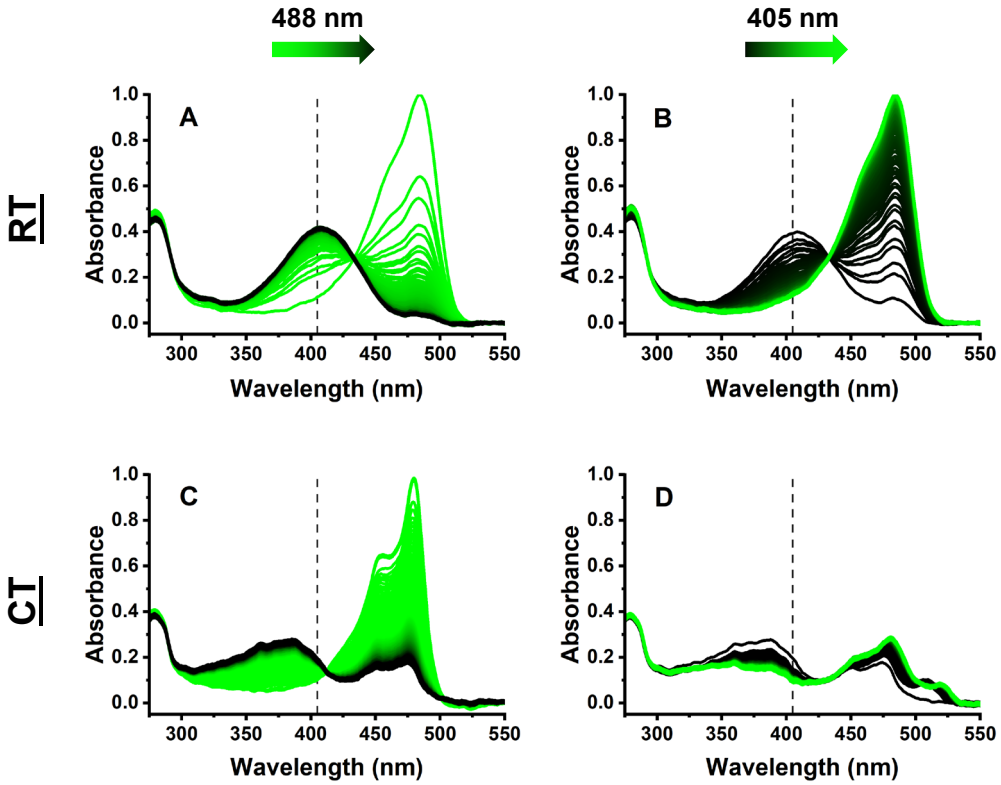

Figure 31: Representative spectral series of rsEGFP2 photoswitching measured with absorption microspectrophotometry. (A) on-to-off switching at RT with 488 nm laser light (80 W/cm²) (data obtained by Dr. O. Glushonkov). (B) off-to-on switching at RT with 405 nm laser light (4 W/cm²) (data obtained by Dr. O. Glushonkov). (C) on-to-off switching at CT with 488 nm laser light (400 W/cm²). (D) off-to-on switching at CT with 405 nm laser light (200 W/cm²). Absorption spectra during on-to-off switching are shown from green to black (A, C) and from black to green during off-to-on switching (B, D). Absorption spectra were normalized at the on-state peak of the first spectrum of each series in A and C. For better visibility of the peak shifts, dashed vertical lines are placed at 405 nm.

Moreover, the overall spectra are slightly blue-shifted at CT. For absorption, this could also be explained by the reduced thermal energy of molecules at CT. As the molecules at CT are less favored to get excited to higher

translational and rotational states, the energy gap from the ground state to the first excited state is higher and shorter wavelengths of the illumination become necessary for excitation. To explain the fluorescence spectra, the S_1 state needs to be considered. At higher temperatures solvent relaxation can cause a lowering of the S_1 state energy. As a result, the emitted wavelength upon transition to the ground state S_0 is shorter at CT.

The shape of the recovered fluorescence spectrum remained the same as the one of the initial on-state at CT (Figure 32), suggesting that the same on-state is present before and after photoswitching at CT.

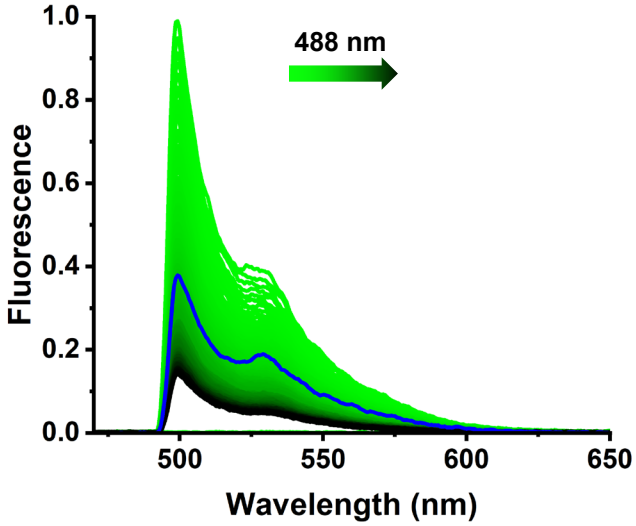

Figure 32: Representative rsEGFP2 fluorescence spectra during on-to-off switching (green-to-black) at CT upon illumination with 488 nm laser light (400 W/cm²) and recovered fluorescence after 405 nm laser illumination (200 W/cm², blue).

Another important result was that upon illumination with 405 nm light, much less on-state recovery was obtained at CT. While at RT up to 100% could be recovered, at CT only 25% could be switched back to the fluorescent state (Figure 30). Our aim was then to find a way to improve this recovery level.

To exclude that the off-state absorption peak shift arises only due to freezing, we measured the absorption after RT off-switching by 488 nm illumination followed by flash freezing and found an only minor shift to 406 nm (Figure 33). After flash freezing, off-to-on switching was performed by 405 nm illumination in order to investigate to which extent it is possible to recover the on-state at CT from the frozen RT switched off-state (Figure 33).

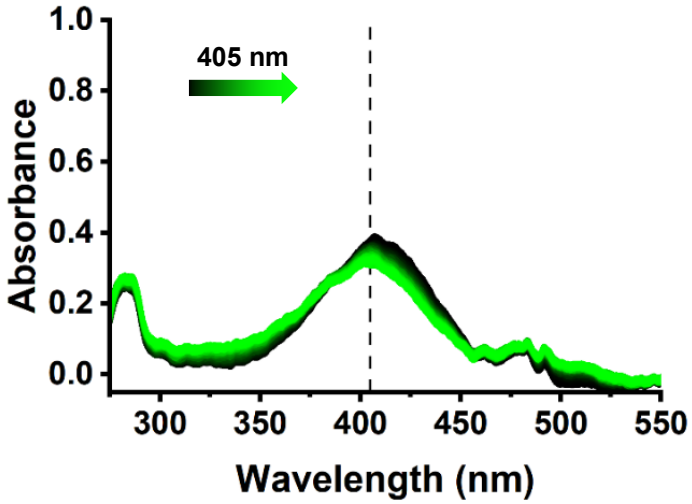

Figure 33: Absorption microspectrophotometry measurements of rsEGFP2 photoswitching. Off-state spectrum after on-to-off switching at RT and flash cooling followed by off-to-on switching (black-to-green) with 405 nm illumination (0.1 kW/cm²). The first spectrum was normalized to match the height of the protonated peak of the first spectrum in Figure 31A.

An only minor rise at around 520 nm and almost no rise at the usual on-state peak at 480 nm could be observed (see discussion chapter).

To further study the cryo-switching mechanism, structural data was collected by X-ray Crystallography. The on-to-off switching kinetics observed in solution were reproduced with crystals (Figure 34), before structural data collection.

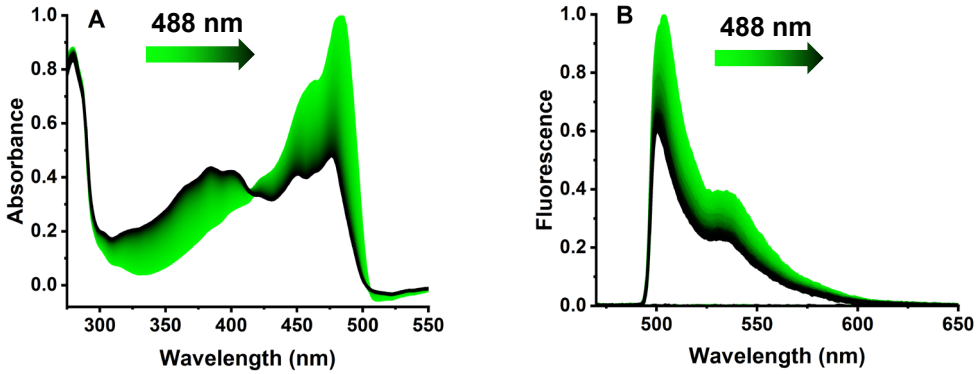

Figure 34: *On-to-off photoswitching (green-to-black) of an rsEGFP2 crystal at 110 K upon illumination with 488 nm laser light (50 W/cm²) for 700 s monitored by (A) absorption and (B) fluorescence emission microspectrophotometry. Spectra were normalized to 1 at the on-state peak of the first spectrum.*

The solution and in-cristallo measurements look similar besides some minor differences as for example the tryptophan absorbance peak at 280 nm which is more pronounced in the crystal measurements. As the crystals were irradiated with lower laser illumination power to avoid irradiation damage, the off-switching is less complete. The next step was the structural analysis of the off-switched state in order to reveal its nature.

7.2. Structural investigations

The crystallography data suggests that at CT no cis-trans-isomerization occurs, but the off-state remains in the cis-conformation (Figure 35). This observation is the same as Regis Faro et al. (2011) reported for Dronpa. The result confirms the hypothesis that there is a different switching mechanism at CT. The fact that the on-state structure does not show decarboxylation of Glu223 and the off-state structure does (see red density

in Figure 35 B) is a good control that the off-state structure was correctly collected from a crystal region which was illuminated with 488 nm light to induce off-switching and most likely also induced the decarboxylation. To observe slight differences between the on- and off-state higher resolution data would be necessary and Q-weighted difference maps could then be beneficial to see these differences (see section 3.5 and 3.6).

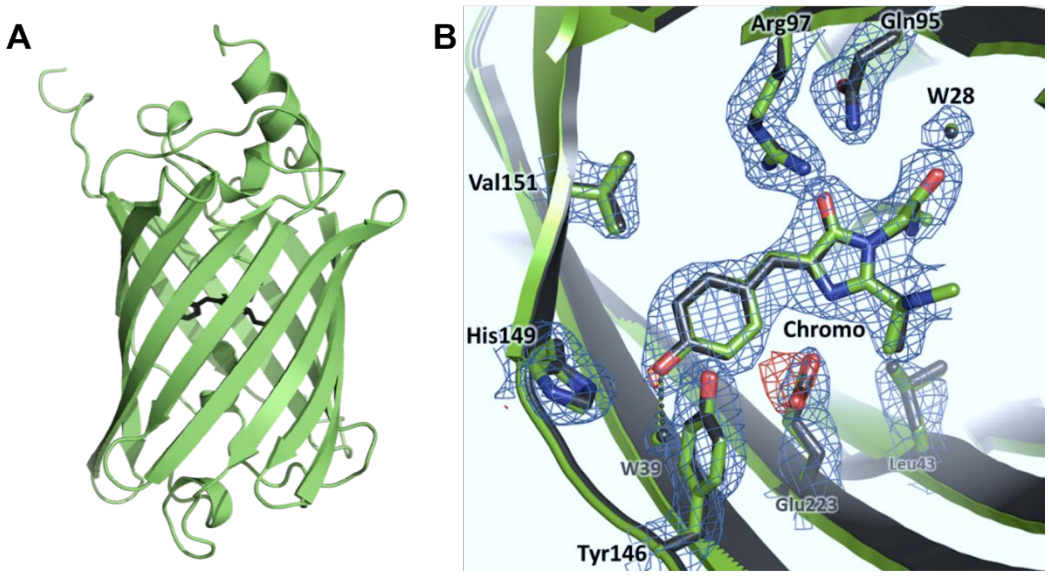

Figure 35: Structural view of rsEGFP2 switching at CT. (A) Overall view of rsEGFP2 in the cryo-off-switched state. The β-barrel structure is shown in green and the chromophore in dark grey. (B) Refined models of the chromophore and surrounding residues of rsEGFP2 in the on-state in cis-conformation (green carbons and water molecules, resolution 2.3 Å) and in the cryo-switched off-state in cis-conformation (dark grey carbons and water molecules, PDB code 8AHA, resolution 2.4 Å), which was switched with 488 nm laser light for 700 s (50 W/cm²). The $2F_{obs}$-F_{calc} electron density map of the cryo-switched off-state is shown at 1σ (blue) and the F_{obs}-F_{calc} difference electron density map (red: negative, green: positive) at ±3 σ. W: water molecules. The data which is shown in panel B was displayed in Pymol (Schrödinger & DeLano, 2020) by Dr. Virgile Adam.

Control experiments with crystals switched at RT showed a cis-trans-isomerization (Figure 36). Again, decarboxylation can be observed at the Glu223. Moreover, a red density can be seen on the hydroxybenzylidene

moiety, most likely due to photobleaching of many molecules upon pre-illumination with too high 488 nm laser power at RT.

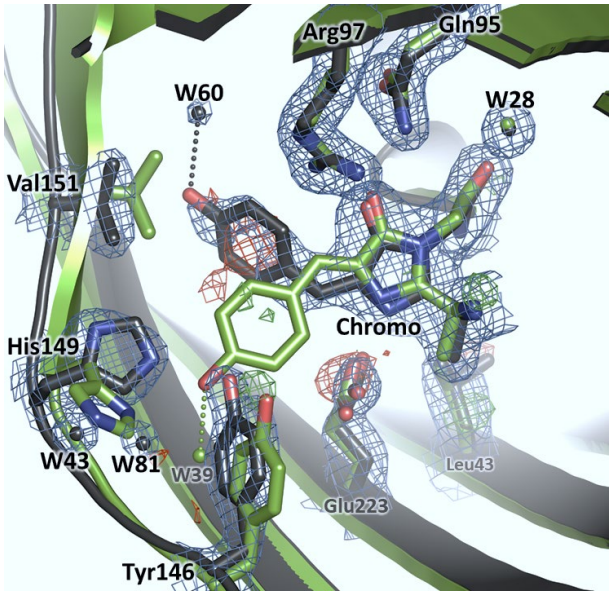

Figure 36: Structural view of rsEGFP2 RT switching (control experiment). Refined models of the chromophore and surrounding residues of rsEGFP2 of the on-state in cis-conformation (green carbons and water molecules) and the off-state in trans-conformation (dark grey carbons and water molecules), which was switched with 488 nm laser light for 30 s (100 mW/cm²). The $2F_{obs}$-F_{calc} electron density map of the cryo-switched off-state is shown at 1σ (blue) and the F_{obs}-F_{calc} difference electron density map (red: negative, green: positive) at ±3 σ. W: water molecules. The data shown in this figure was displayed in Pymol by Dr. Virgile Adam.

Crystals first switched off at RT and subsequently switched on at CT appeared to stay in the trans-conformation (Figure 37). From this it can be concluded that major conformational changes in rsEGFP2 are hampered at CT. The chromophore structure which is in the state which was switched off at RT and back on at CT also shows the red density which is observable for the chromophore in the state only switched off at RT because the data was collected on the same crystal. That the red density is larger for the back-switched chromophore might be because it was illuminated also with a 405 nm laser.

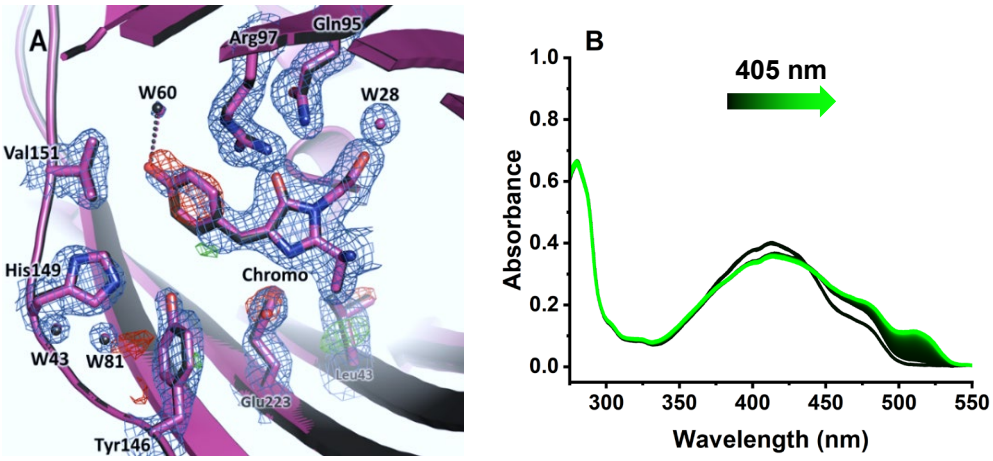

Figure 37: (A) Refined models of the chromophore and surrounding residues of rsEGFP2 in the trans off-state (dark grey carbons and water molecules) after RT on-to-off-switching with 488 nm illumination (100 mW/cm²) and in the same conformation (purple carbons and water molecules, PDB model 8AHB) after the same illumination followed by 405 nm illumination (14 W/cm² for 180 s) at CT. As the structures overlap the first one is mainly not visible. The $2F_{obs}$-F_{calc} electron density map of the second structure is shown at 1σ (blue) and the corresponding F_{obs}-F_{calc} difference electron density map (red: negative, green: positive) at ±3 σ. W: water molecules. (B) The off-to-on switching (black-to-green) during 405 nm illumination of the crystal used in (A) was monitored by absorption microspectrophotometry. The absorbance spectra were normalized at the protonated peak as in Figure 33. The data which is shown in panel A was displayed in Pymol by Dr. Virgile Adam.

The observations (Figure 37) are in line with the solution measurements (Figure 33), which suggest that the RT off-switched state is not significantly recoverable to the on-state at CT, except of a minor rise of a red-shifted on-state peak. The data would be consistent with this state being a fluorescent state in trans-conformation (On_{trans}).

7.3. Laser power dependent heating in crystals

In parallel, rsEGFP2-V151A crystals were analyzed, as with this variant a better switching contrast was achieved at RT as compared to the wild-type

(see section 6) and thus studying the differences between the two variants at CT appeared to be a subject of interest. The variants were also compared by performing solution measurements, as described in section 8.1.

For rsEGFP2-V151A crystals with optimized pre-illumination no successful diffraction was obtained but another interesting observation was a laser power dependent heating of the crystals. A fast switching mechanism was noticed when rsEGFP2-V151A crystals were switched with 488 nm light of high power (300 W/cm²), which started with a fast phase with the speed of the RT switching mechanism, followed by a slower phase, resembling the CT switching (Figure 38 A). The structural data of this crystal shows that 38% of the chromophores stayed in the cis-conformation while the other fraction underwent cis-trans-isomerization (Figure 38 B). Dr. Virgile Adam contributed to the occupancy refinement steps.

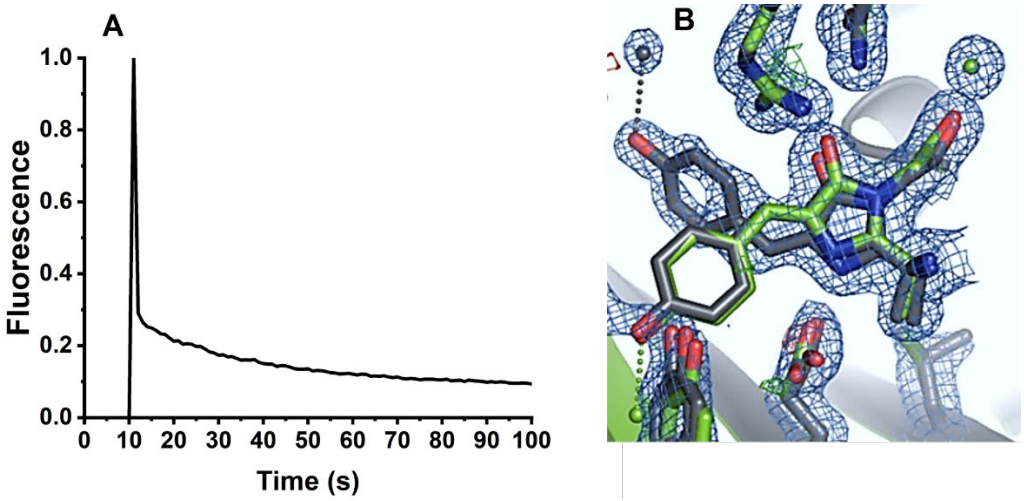

Figure 38: (A) Fluorescence kinetics upon off-switching with 488 nm laser light of 300 W/cm² power density. (B) Structural view of rsEGFP2 switching at CT with high laser power which caused a temperature rise. Refined models of the chromophore and surrounding residues of rsEGFP2-V151A in the on-state in cis-confirmation (green carbons and water molecules) and in the off-switched state in cis- (38% occupancy) and trans-conformation (62% occupancy) (dark grey carbons and water molecules), which was switched with 488 nm laser light (300 W/cm²). The $2F_{obs}$-F_{calc} electron density map of the off-state is shown at 1σ (blue) and the F_{obs}-F_{calc} difference electron density map (red: negative, green: positive) at ±3 σ. W: water molecules. The data which is shown in panel B was displayed in Pymol by Dr. Virgile Adam.

By an estimation of the temperature rise as a function of laser power, temperatures of near RT were calculated for the applied laser power density of 300 W/cm² (see section 4.4.1). The rsEGFP2-V151A crystals had very big dimensions (0.15 mm × 0.2 mm × 0.8 mm), which also contributes to the temperature rise, as thicker samples absorb more light. Taken together, this data suggests that in the first phase of off-switching the crystal was heated close to RT due to strong photon absorption by the crystal at 488 nm, such that the typical RT switching involving a cis-trans isomerization took place. In a second phase the crystal was mainly switched to the off-state and thus absorbed less light and reached temperatures below the glass transition temperature again. By consequence, the remaining proteins in the on-state switched to the cryo-off-state in cis-conformation.

Besides, because of the crystal size, the optical density was too high to obtain good absorption spectra. After this observation we started to use smaller crystals and lower laser power.

7.4. Enhancing switching efficiency: 405 nm laser vs. 355 nm laser

7.4.1 Experiments at the ensemble level

Typically, off-to-on switching of rsEGFP2 at RT is performed with continuous 405 nm laser light. Because of the blue shifted absorption peak of the cryo-switched off-state at CT, Dr. Daniel Thédié and Dr. Oleksandr Glushonkov decided in previous studies to try a 355 nm laser, which was pulsed, for back on-switching at CT, which indeed increased the on-state recovery. In this work, we performed quantitative repetitions of these measurements. The absorbance recovery level increased from ~25%, obtained with 405 nm laser light, to ~50% by using the 355 nm laser (Figure

39). It should be noted that the fluorescence recovery level only improved from ~32% to ~51% (Figure 39) but as the fluorescence might be affected by synchronization errors (see section 4.3.1), the fluorescence recovery level is probably more prone to errors than the absorbance data. In addition, less fluorescence recovery is recorded, when the sample already has bleached in the moment of fluorescence recording, as it was the case here for the data with the 355 nm laser recovery. Hence, for the recovery phase the absorbance data is probably more reliable than the fluorescence data. However, for the decay phase we observed that the fluorescence data is more reproducible because it is not impacted by baseline drifts.

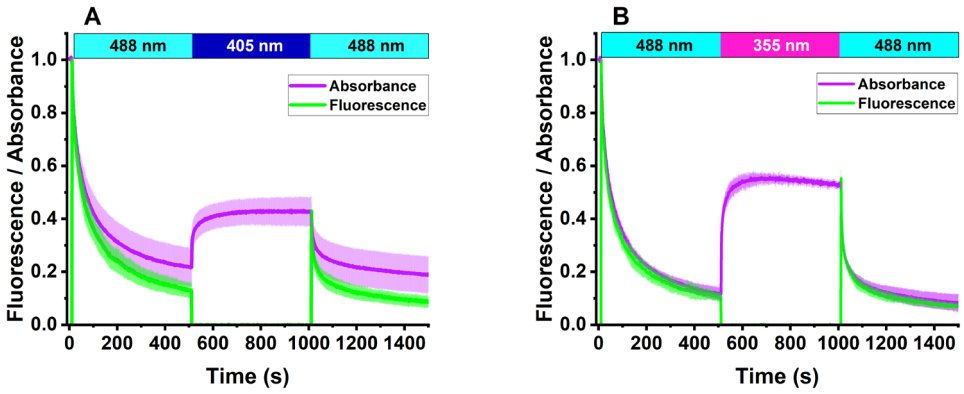

Figure 39: Integrated absorbance (470-500 nm spectral range) and integrated fluorescence (495-630 nm spectral range) of on-to-off switching followed by off-to-on recovery of rsEGFP2 at CT. (A) Recovery by 405 nm illumination and (B) recovery by 355 nm illumination. Absorbance (purple) and fluorescence (green) switching kinetics were obtained by alternate illumination at 488 nm (400 W/cm²) and either 405 nm (200 W/cm²) or 355 nm (30 W/cm²) at CT and are normalized to 1 at the start of acquisition. Fluorescence was only recorded in the presence of 488 nm illumination. The mean and standard deviation of 3 measurements are shown.

The question remained whether the improvement of the recovery was due to the different wavelength or the pulsing of the laser. We had two hypotheses. One possibility was that the pulsing could lead to less bleaching because the pulse duration is in the nanosecond range and the

pulses are alternated by gaps without illumination with a duration in the millisecond range. As the life-time of the excited state is in the nanosecond range and the life-time of the triplet state is in the millisecond range, the triplet state is typically more prone to bleaching. With the pulsed laser the triplet state could be protected from bleaching because the pulse would act only on the singlet state and lead to its excitation but during the subsequent formation of the triplet state the laser would be already in the non-illumination phase.

The other hypothesis was that the switching contrast (definition see section 2.2) could be higher using 355 nm laser light, as it can be absorbed much less by the on-state than 405 nm light, and thus leads to less undesired off-switching during on-state recovery.

In the end, neither option proved correct but a third one did. A second off-state (Off_2) was found which only can be recovered by UV light and is blue shifted compared to the first off-state (Off_1) which can be recovered by both lasers. This finally explained the difference in the recovery levels depending on the laser.

First, to examine the switching contrast- or bleaching-hypothesis, rsEGFP2 solution samples were illuminated with 488 nm light, followed by 405 nm light and then 355 nm light. If the 405 nm laser would irreversibly bleach the protein, such that the subsequent 355 nm laser would not be able to recover more than the 405 nm laser, one could conclude that the use of only 355 nm laser would lead to less bleaching and thus lead to a higher on-state recovery. In contrast, if the 355 nm laser would still increase the recovery after 405 nm illumination, we initially assumed that it could be concluded that the 355 nm laser leads to a much better switching contrast and for this reason more recovery could be reached. The result was indeed a further increase of the recovery by 355 nm light (Figure 40).

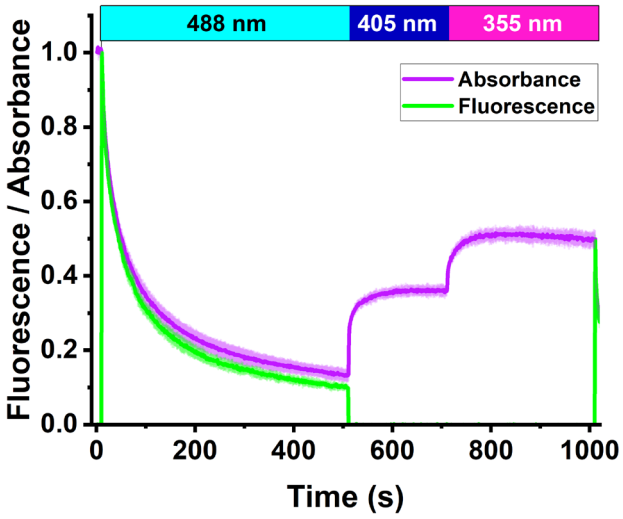

Figure 40: Integrated absorbance (470-500 nm spectral range) and fluorescence (495-630 nm spectral range) of on-to-off switching by 488 nm laser light (400 W/cm²) followed by off-to-on recovery of rsEGFP2 by illumination with 405 nm (300 W/cm²) and subsequent illumination with 355 nm (25 W/cm²) light at CT. Absorbance and fluorescence are normalized to 1 at the first point of acquisition. Fluorescence was only recorded in the presence of 488 nm illumination. The mean and standard deviation of 3 measurements are shown.

However, estimations of the switching contrast based on the ratio of the measured off- and on-switching rates upon 405 nm laser illumination suggested that the switching contrast is ~900 (see appendix, Supplementary Information of Mantovanelli et al.). This indicates that the switching contrast obtained by 405 nm light illumination does not affect the recovery level.

Also the bleaching hypothesis could be further excluded by as we observed only linear bleaching effects (see section 7.5) and bleaching of the triplet state would require a second photon, leading to a non-linear effect.

Interestingly, we noticed that the evolution of the left side of the off-state absorption spectrum differed depending on which laser (the 355 nm laser or the 405 nm laser) was used for the recovery phase. To investigate this,

the absorption spectra, which were previously collected to compare the recovery obtained by 405 nm and 355 nm light, were integrated from 315 to 325 nm to analyze the apparently different evolution (Figure 41).

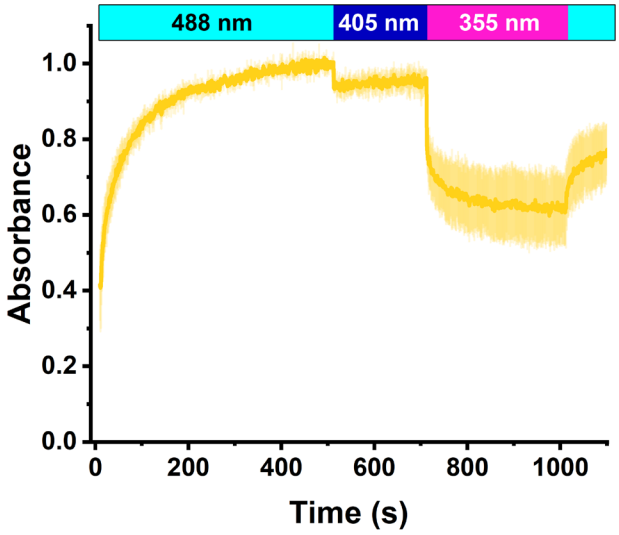

Figure 41: Integrated absorbance between 315 and 325 nm, during switching at CT with 488 nm illumination (400 W/cm²), followed by illumination with 405 nm (300 W/cm²) and 355 nm light (30 W/cm²). Absorbance was normalized to 1 at the highest point. The mean and standard deviation of 3 measurements are shown.

Strikingly, the evolution was very different depending on the laser which was used for the recovery phase. This led us to the hypothesis that not only one off-state (Off_1), with a main absorbance at the maximum peak of the total off-state absorption spectrum but a second off-state (Off_2), with a blue-shifted absorbance spectrum as compared to the maximum peak of the total CT off-state spectrum, could be present. This second off-state raised upon illumination with 488 nm light, and it was only recoverable to the on-state upon illumination with 355 nm light, whereas the other part of the off-state spectrum (Off_1) was recoverable with both, the 405 nm and 355 nm laser, which would explain why the 355 nm laser leads to more total recovery.

If one compares the shape of the absorption after recovery with the different lasers one can also see that after back-on-switching with the 405 nm laser there is a bigger fraction remaining on the left side of the off-state spectrum (Figure 42). In contrast, the 355 nm laser depopulates all off-states almost completely. It is not excluded that more than two off-states are present, which are also recovered by the presented illumination schemes, or that for example the minor fraction which was not recovered by the 355 nm laser would be the signature of a not recoverable off-state.

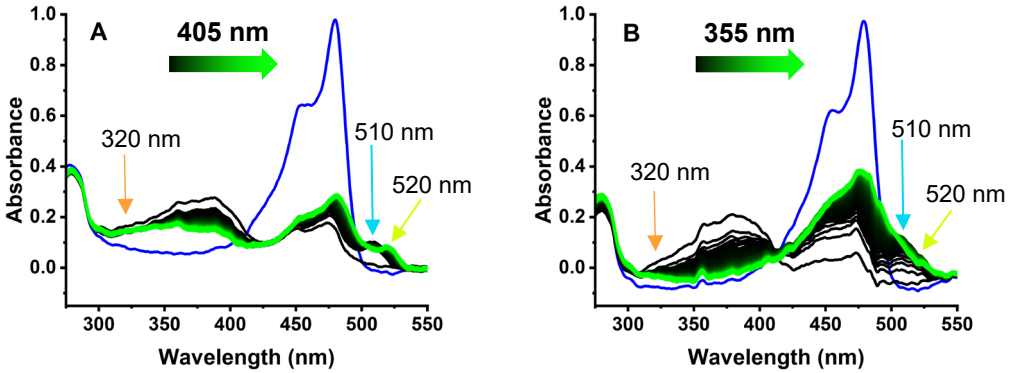

Figure 42: Representative absorption spectra series of rsEGFP2 CT photoswitching, recovered by 405 or 355 nm laser light after previous off-switching with 488 nm light (see Figure 31 C). (A) Off-to-on switching with 405 nm laser light (200 W/cm²) displayed in black to green and (B) off-to-on switching with 355 nm laser light (15 W/cm²) displayed in black to green. The initial on-states are shown in blue.

To confirm the new hypothesis, again three lasers were applied, but this time the 355 nm laser was followed by the 405 nm laser (Figure 43). The data suggests that the 405 nm laser even populates more of $Off_{2,}$ instead of recovering it to the on-state, which is reasonable, as the on-state still absorbs at 405 nm and thus can be switched off by the 405 nm laser.

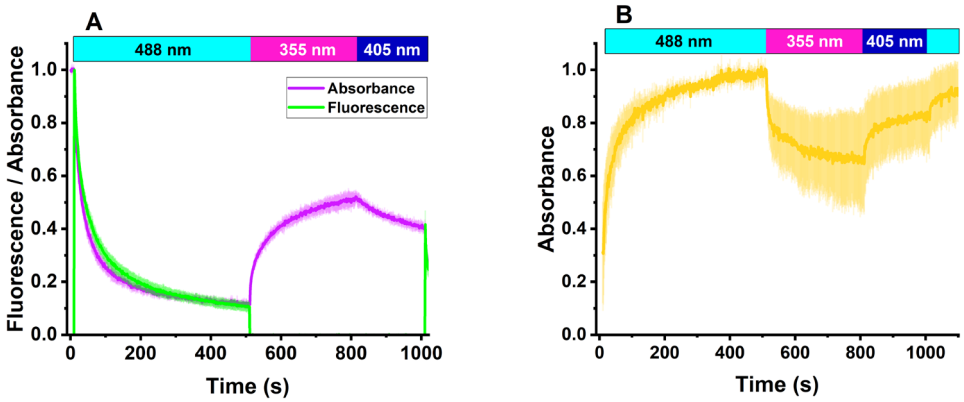

Figure 43: (A) Absorbance integrated in the 470-500 nm spectral range and fluorescence (495-630 nm spectral range) and (B) absorbance integrated in the 315-325 nm spectral range of on-to off switching by 488 nm laser light (400 W/cm²) followed by off-to-on recovery of rsEGFP2 by illumination with 355 nm (20 W/cm²) and subsequent illumination with 405 nm light (300 W/cm²) at CT. Absorbance and fluorescence are normalized to 1 at the highest value. Fluorescence was only recorded in the presence of 488 nm illumination. The mean and standard deviation of 3 measurements are shown.

By computation of difference-spectra, individual spectra of the two off-states were extracted with peak maxima of ~385 nm for *Off₁* and ~365 nm for *Off₂* (Figure 44).

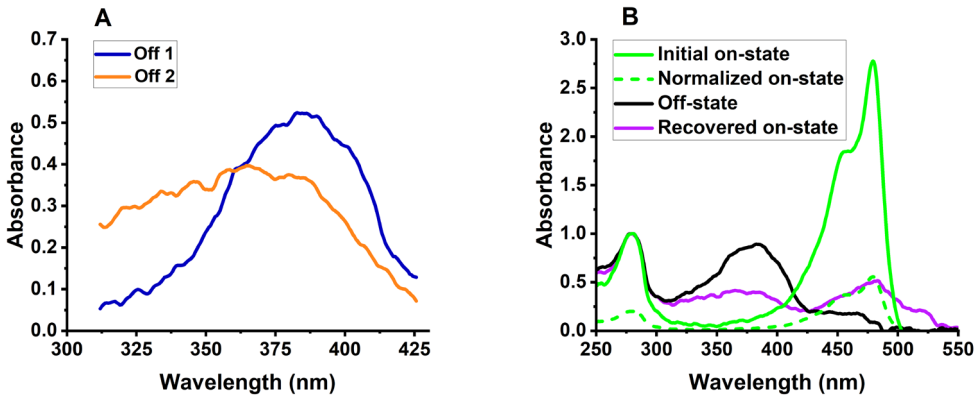

Figure 44: (A) Off₁ (blue) and Off₂ (orange) absorption spectra estimated by difference-spectra computation. (B) Absorption spectrum of rsEGFP2 in the initial on-state (green, and normalized version with dashed line), in the off-state (black) and in the by 405 nm light recovered on-state (purple).

To obtain the *Off*$_2$ absorption spectrum, a scaled version of the original on-state spectrum was subtracted from the on-state spectrum which was recovered with 405 nm light after previous off-switching with 488 nm light. This *Off*$_2$ spectrum was then subtracted from the off-state spectrum after 488 nm light illumination, which should contain both off-states, to obtain the *Off*$_1$ spectrum.

Furthermore, a rise of the absorption spectra around 520 nm was observed upon illumination with 405 nm laser light which was not as pronounced upon 355 nm illumination (Figure 42). A possible explanation would be that the trans-off-state, which usually appears upon RT off-switching, might appear also at CT to a small extent. Then it could be switched by 405 nm light to a fluorescent on-state in trans-conformation. As the trans-off-state does not significantly absorb 355 nm light, it cannot be switched efficiently by it to the trans-on-state. However, the trans-off-state population is only minor and for this reason does not contribute to a more efficient switching upon 405 nm light illumination. In Figure 37 the trans-on-state signature is strongly visible, as the preliminary RT off-switching upon 488 nm light produced a high amount of the trans-off-state and thus can be switched to the trans-on-state by 405 nm light.

Besides, another minor peak at ~510 nm was visible in some conditions upon recovery with the 355 or 405 nm laser (Figure 42). This state appears to be not very pronounced in rsEGFP2, but it should be noted that it is present, as it may play a major role in other samples (see discussion, *On*$_3$ state).

7.4.2 Experiments at the single-molecule level

Very recently, Dr. Oleksandr Glushonkov performed single molecule experiments on rsEGFP2 upon illumination with 405 nm and 355 nm light (Figure 45). To test whether the recovery level improvement by the 355 nm laser can be also achieved at the single molecule level, he applied a similar illumination scheme as shown in Figure 40. The normalized number of localizations per frame as a function of time, displayed in Figure 45 A, shows that the 405 nm illumination recovers a fraction of molecules, which were switched off by the 488 nm light and the subsequently applied 355 nm light recovers a larger fraction. Grouping the molecules and calculating the cumulative number of recovered molecules confirms this result (Figure 45 B). His data suggests that also at the single-molecule level 355 nm illumination improves the off-to-on recovery level as compared to 405 nm illumination. This confirms that our new illumination scheme can be advantageous for cryo-PALM applications by improving the effective labelling efficiency.

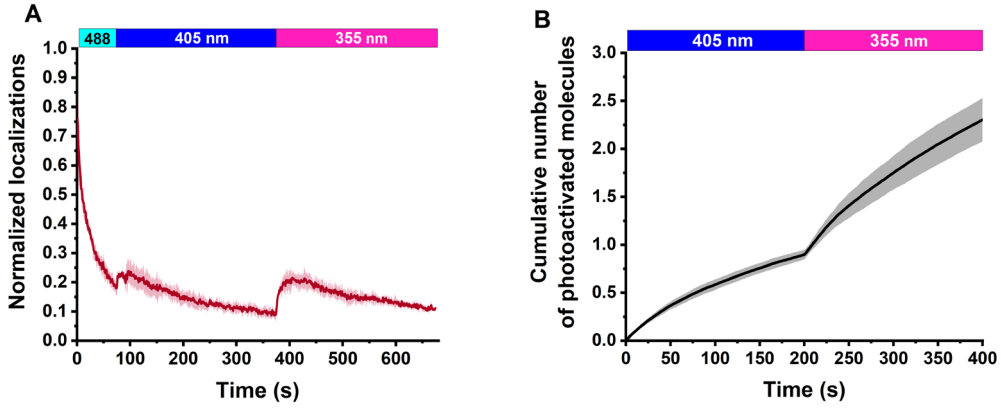

Figure 45 (data obtained by Dr. O. Glushonkov): Single molecule experiments with rsEGFP2 at CT. under 488 nm, 405 nm and 355 nm illumination. (A) Number of localizations per frame. (B) Cumulative number of photoactivated molecules after grouping localizations. Data and standard deviation of 3 measurements are shown.

7.5. Power dependent switching kinetics

In the photo-convertible fluorescent protein mEos4b a non-linear dependence of the photoconversion efficiency on the laser power was observed, which is caused by non-linear photobleaching of the green state upon 405 nm light illumination (Wulffele et al., 2022). They suggest that upon absorption of a 405 nm photon by the green state, an intermediate state is formed which can further react to the bleached state by absorbing a second 405 nm photon. We examined whether a similar non-linear bleaching behavior could be observed for rsEGFP2 photoswitching.

rsEGFP2 off-switching with 488 nm light followed by on-switching with 405 nm or 355 nm light was repeatedly measured for different powers of the three lasers. The comparison of the on-state recovery levels showed that there is no significant difference depending on the laser power (Figure 46 A, C, E). The off- and on-switching rates increased linearly with the laser power (Figure 46 B, D, F). Thus, non-linear effects were not observed.

We calculated an off-to-on switching quantum yield of $\Phi = 6.1 \cdot 10^{-7}$ for a power of 325 W/cm² (see section 4.4.2) which is in the same order of magnitude as the quantum yields reported by Regis Faro et al. (2010) for EYFP, Dronpa and IrisFP.

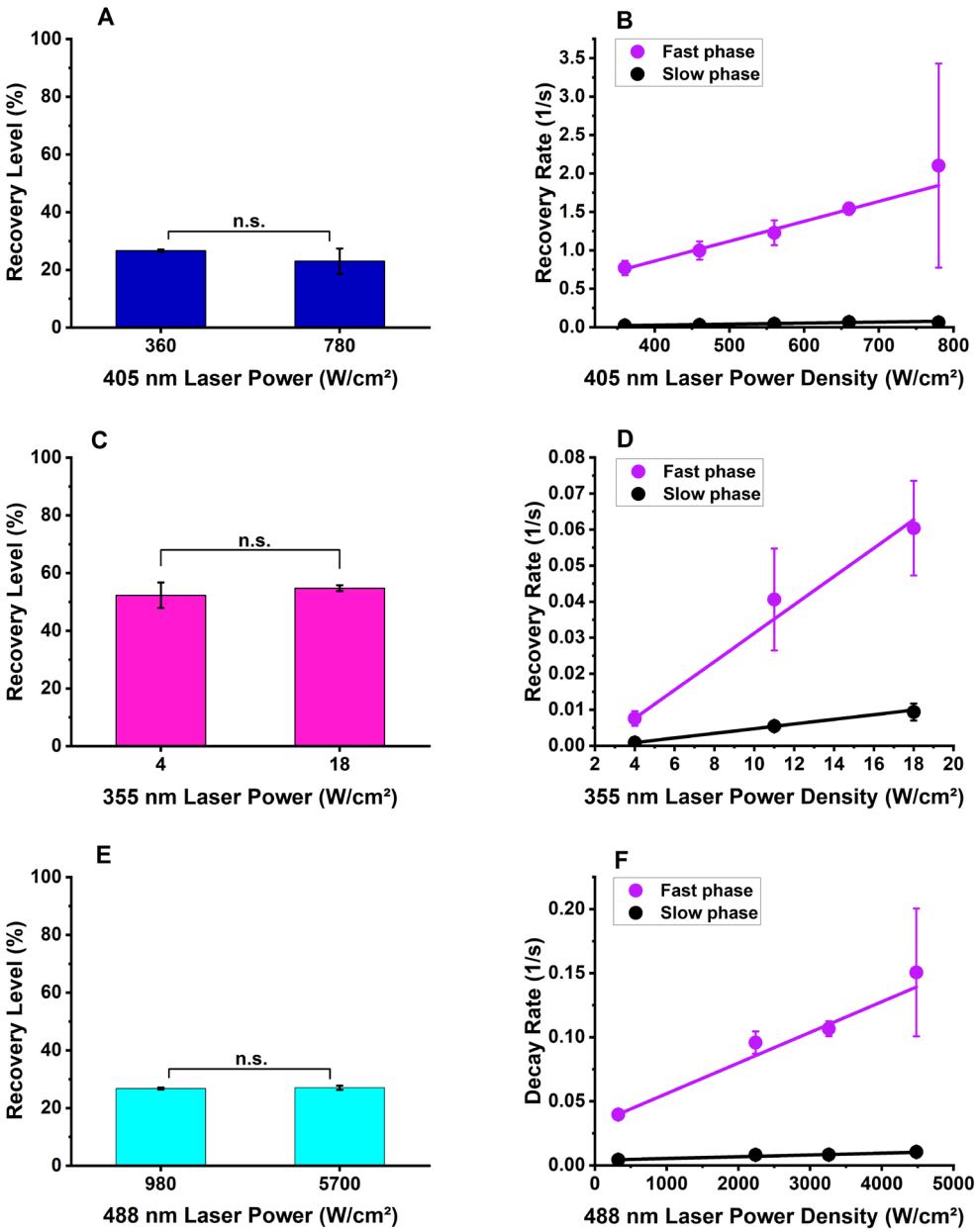

Figure 46: rsEGFP2 on-state recovery levels after (A) on-to-off switching with constant power of 488 nm laser light (1.0 kW/cm²) and off-to-on switching with different powers of 405 nm laser light (360 W/cm² and 780 W/cm²) or (C) different powers of 355 nm laser light (4 W/cm² and 18 W/cm²) and (E) on-to-off switching with different powers of 488 nm laser light (980 W/cm² and 5700 W/cm²) and constant power of 405 nm laser light (500 W/cm²). (B) rsEGFP2 off-to-on switching rates at CT as a function of 405 nm laser power density, (D) as a function of 355 nm laser power density and (F) on-to-off switching rates as a function of 488 nm laser power density. Mean rates and standard deviations were extracted from bi-exponential fits of 3 independent measurements. Resulting data points were fitted with a linear model. n.s: not significant.

Bleaching was more pronounced for higher laser powers without significantly decreasing the recovery level, as indicated by the absorbance decay (Figure 47).

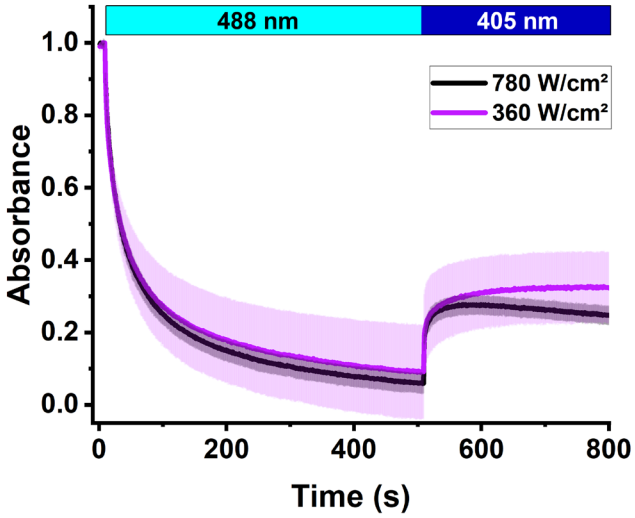

Figure 47: Comparison of rsEGFP2 recovery upon illumination with different 405 nm laser powers. Absorbance decay observed at 780 W/cm² suggests the start of photobleaching. Absorption spectra were integrated in the 470-500 nm spectral range to calculate absorbance. On-to-off switching was performed at CT with 488 nm laser light (1.0 kW/cm²) and off-to-on switching with 405 nm laser light with lower (360 W/cm²) or higher power density (780 W/cm²). Absorbance is normalized to 1 at the start of acquisition. The mean and standard deviation of 3 measurements are shown.

Taken together, non-linear effects, as they were observed for mEos4b, could not be observed in rsEGFP2.

It was also investigated which effects bleaching could cause after many switching cycles. Applying the illumination scheme for several cycles showed that the recovery enhancement by the 355 nm laser as compared to the 405 nm laser decreases after long illumination time, such that in the 5th switching cycle the same recovery is obtained by both lasers (Figure 48). Laser powers for the 405 nm and the 355 nm laser were chosen such that

a comparable recovery rate was reached. However, to achieve this a 20 times higher power was used for the 405 nm laser. That means that even with a much lower power the 355 nm laser leads to more recovery but also to faster bleaching. Nevertheless, the 355 nm laser could be more advantageous, as for SMLM experiments the first switching cycle might in principle be enough to localize the single molecules. SMLM simulations performed by Jip Wulffelé suggest that the 355 nm laser would be more advantageous despite the stronger bleaching (see appendix, publication Mantovanelli et al.).

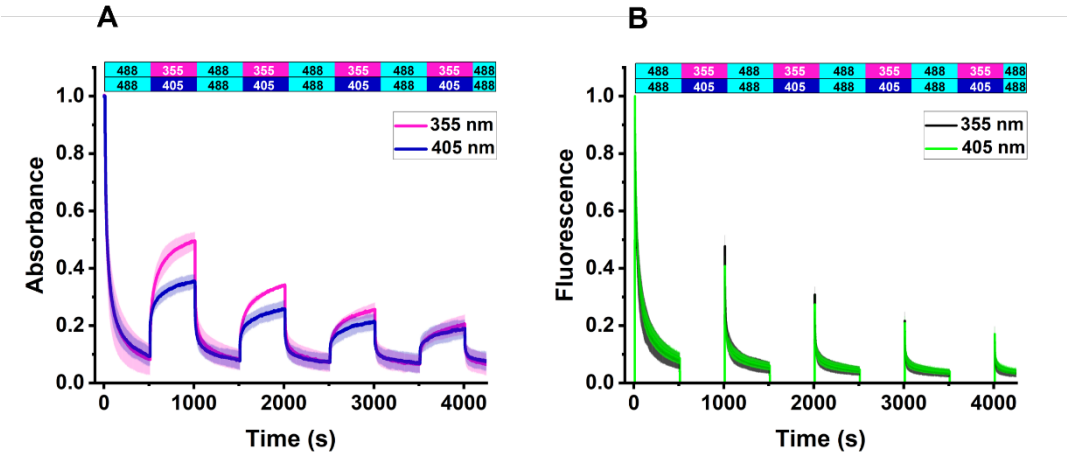

Figure 48: Comparison of multiple switching cycles of rsEGFP2 at CT with 405 nm or 355 nm light recovery. The absorbance signal was calculated by integration of the absorption spectra in the range between 470-500 nm. rsEGFP2 was switched back and forth with 488 nm (1000 W/cm²) and either 405 nm (200 W/cm², blue) or 355 nm (10 W/cm², magenta) laser light. The mean and standard deviation of 3 measurements are shown, of which 2 were performed by Dr. O. Glushonkov.

7.6. pH dependent switching kinetics

After revealing that the switching mechanism at CT differs from the known RT switching mechanism, our goal was to investigate the nature of the CT mechanism in detail. As the chromophore does not appear to undergo major

conformational changes upon switching at CT, protonation or formation of radicals could be the underlying mechanisms in the cryo-off-state formation.

To study if protonation is involved, we measured switching kinetics of rsEGFP2 in buffers of different pH values (Figure 49)

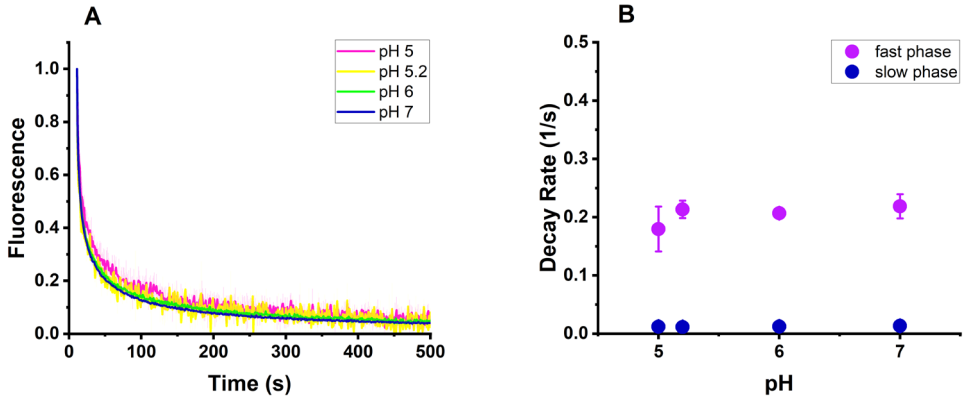

Figure 49: pH dependent switching kinetics of rsEGFP2. (A) Mean fluorescence decay during off-to-on switching of rsEGFP2 embedded in buffers of different pH value upon illumination with 488 nm laser light of 900 W/cm² power density. Fluorescence is normalized to 1 at the start of acquisition. (B) Fluorescence decay rates were calculated by bi-exponential fitting of each individual data set. Mean and standard deviation are shown for 2 independent measurements for pH 5.2 and 3 independent measurements per pH for the other measurements.

No dependence of the rsEGFP2 on-to-off switching kinetics on the pH of the buffer solution could be observed. For lower pH (5 and 5.2) the data is noisier, because only a minor fraction of the molecules is initially in the on-state upon high proton concentration in the buffer, as most of the molecules are in a protonated state (Chattoraj et al., 1996) absorbing at ~400 nm (Figure 49 A, C). Hence, only a small number of molecules can undergo on-to-off switching upon 488 nm illumination, which results in a low signal-to-noise ratio and thus in a bigger error bar for the pH 5 measurements shown in Figure 49 B. Hence, we concluded that the lower mean value of the pH 5 measurements is only a result of this low signal-to-noise ratio but does not come from a real effect. A repetition of this measurement recently performed

by Dr. Virgile Adam confirmed that no pH dependence can be observed between pH 5 and pH 9 (revised version Mantovanelli et al., 2022, in preparation). Taken together, the data suggests that no protonation event is involved in the formation of the cryo-off-states.

Moreover, we compared the absorption spectra of rsEGFP2 in a pH 5 buffer using 405 nm or 355 nm light for off-to-on recovery to gain more insights into the influence of the protonated state on the switching mechanism (Figure 50). Interestingly, the shape of the initial absorption spectrum shown in Figure 50 A/C reminds on the GFP spectrum at CT shown by Creemers et al. (1999) (see Figure 16), who observed a red-shifted protonated peak and a blue shifted anionic peak.

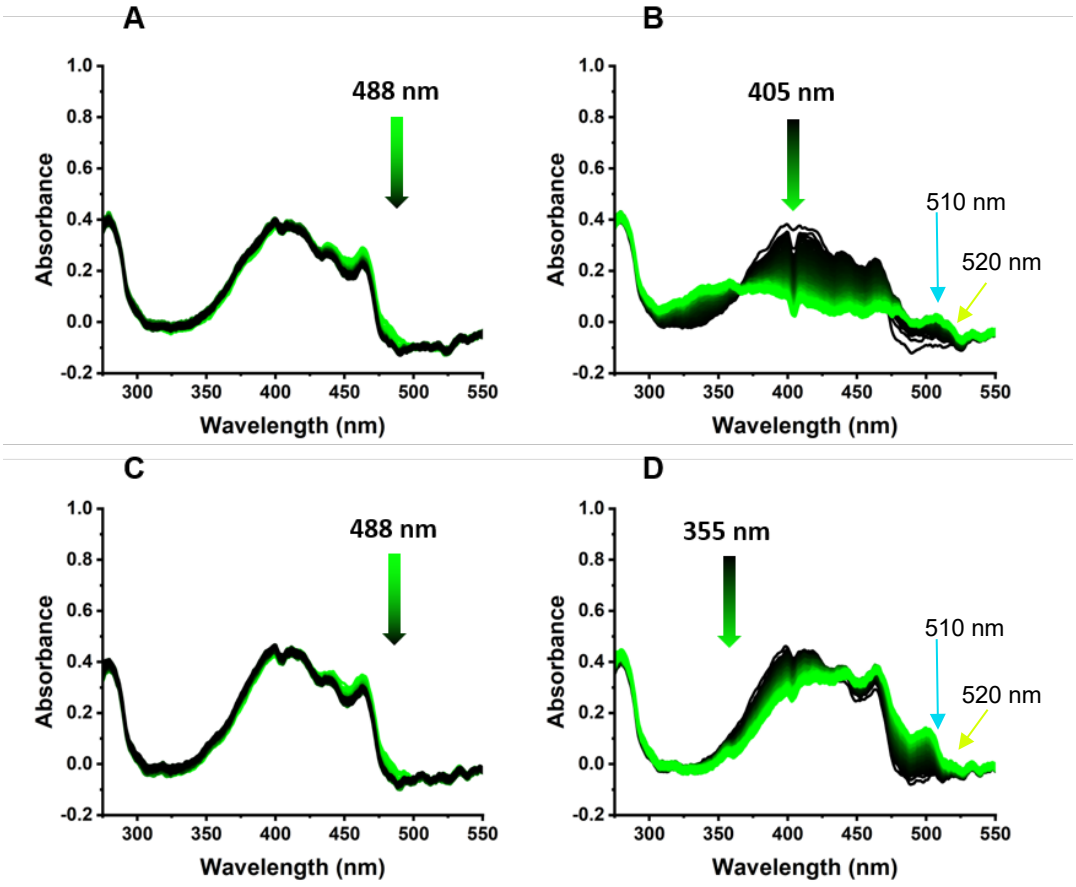

Figure 50: rsEGFP2 absorption spectra at pH 5 upon illumination with different lasers. (A) Application of 488 nm light (900 W/cm²) for 500 s and (B) subsequently applied 405 nm light (450 W/cm²) for 500 s. (C) 488 nm light illumination for 500 s (D) followed by illumination with 355 nm light (8 W/cm²) for 500 s. Data is normalized at 280 nm as the data of Figure 31.

Application of a 405 nm laser after 488 nm illumination shows a substantial reduction of the protonated state and a strong increase of a state with the maximum absorbance at ~365 nm, which likely can be assigned to the *Off*$_2$ state. Further, a rise at 510 nm occurs upon illumination with the 405 nm or the 355 nm laser and can probably be assigned to the fluorescent state which also arose in other experiments (see discussion chapter, *On*$_3$ state). Also the initial 480 nm on-state is populated to some extent in the recovery phase, but more with the 355 nm laser. Probably, the 405 nm laser switches the protonated state to the on-states and back to *Off*$_2$, similar to the experiment presented in Figure 43 A, where 405 nm illumination was applied after 488 and 355 nm illumination. In the emission spectrum (Figure 51) a red-shift of the main peak is observed after the recovery, indicating that another on-state is present to more extent after the recovery phase as at the start of the illumination. Application of the 355 nm laser (Figure 50 D) only leads to a rise of the on-states but not of the *Off*$_2$ state, as it can recover the *Off*$_2$ state to the on-state. This data is a further argument in favor of the presence of the two off-states.

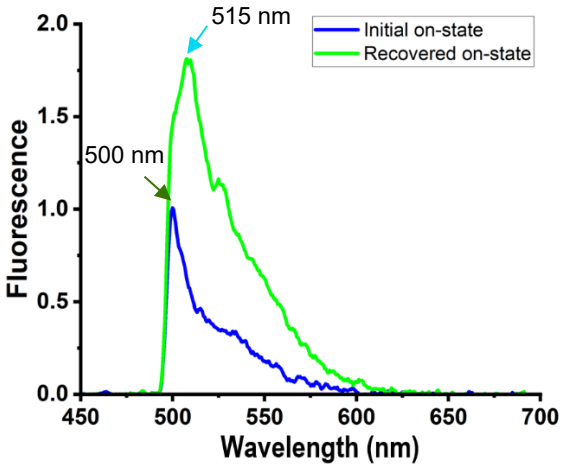

Figure 51: Fluorescence spectra of rsEGFP2 in a pH5 buffer in the initial on-state (blue) and the recovered on-state (green) after 488 nm laser illumination and subsequent 405 nm laser illumination corresponding to the absorbance data shown in Figure 50.

Another observation is the ability of the 405 nm laser to substantially depopulate the protonated state. As reported by Regis Faro et al. (2010),

for the fluorescent protein EYFP at CT only a very minor change in the absorption spectrum was observed upon 405 nm illumination. Probably a high laser power, as used in our experiments, is needed to achieve switching of the protonated state to other states. It is also likely that it is bleached by the strong illumination.

We also studied the effect of populating the on-state before on-to-off switching, applying 405 nm laser light before 488 nm laser light (Figure 52).

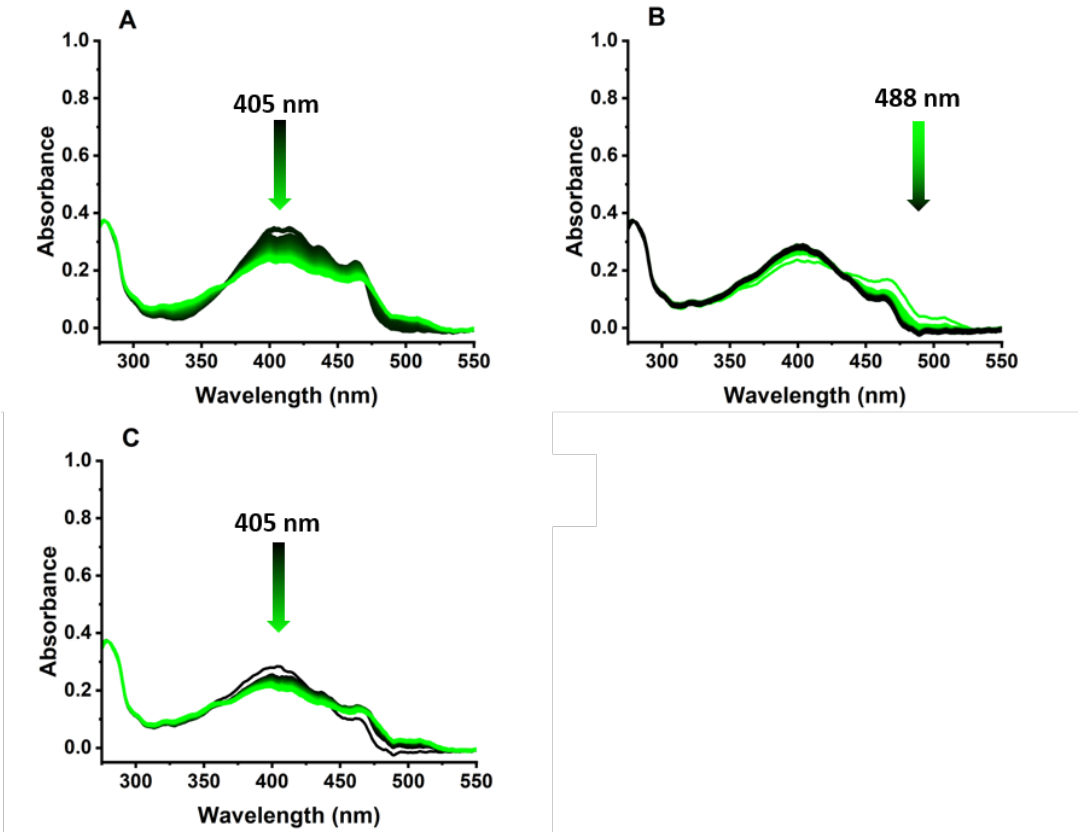

Figure 52: Absorption spectra series of rsEGFP2 photoswitching at pH 5 at CT. (A) Off-to-on switching with 405 nm laser light (900 W/cm²) for 100 s, (B) on-to-off switching with 488 nm laser light (1000 W/cm²) for 3000 s and again (C) off-to-on switching with 405 nm laser light (900 W/cm²) for 100 s. Data is normalized at the 280 nm peak as the spectra of Figure 31 C.

Illumination of 405 nm before 488 nm illumination (Figure 52 A) gives a similar result as if it is applied after (Figure 50 B). The next phase, application of 488 nm after 405 nm looks differently than in Figure 50. It is

not surprising that more molecules are in the on-state after pre-illumination with the 405 nm laser and thus more molecules can be switched off with the 488 nm laser. However, it is interesting that the on-to-off-switching starts with a faster phase. The switching from the protonated off-state to the on-states also occurs immediately in the first second of acquisition. The evolving on-state spectrum with the rise at ~520 nm is reminiscent of the spectrum obtained after RT off-switching followed by on-switching at CT (see Figure 37 B), which we assigned to a fluorescent trans-state. As this rise at 520 nm is also visible after cryo-switching at pH 7 without preliminary RT switching (Figure 42), we expressed the hypothesis, that a small fraction of molecules still undergoes cis-trans isomerization at CT. This would also be the case at low pH and this fraction of molecules in the trans-state would switch upon deprotonation to the trans-on-state we see at low pH.

Due to the shorter illumination with 405 nm light, the protonated peak is switched off less than in Figure 50 which could explain why less of the ~510 nm peak arises here which makes the 520 nm peak more visible. In the discussion chapter we address the hypothesis that the ~510 nm peak corresponds to a third on-state in cis-conformation (On_3) which can be reached from the protonated cis-state.

7.7. Triplet state lifetime

The triplet state is known to be an intermediate state in several photochemical reaction pathways in green fluorescent proteins as e. g. radical formation (Byrdin et al., 2018). To examine if the triplet state might be an intermediate state in rsEGFP2 cryo-switching, we wanted to estimate the triplet state lifetime at CT, as a long lifetime allows more reactions from this state. To estimate the triplet state lifetime at CT, we measured the first 40 ms of the fluorescence decay of rsEGFP2 upon illumination with different powers of 488 nm light. According to our estimations the lifetime of the triplet

state is ~8ms (see below). Our group (Rane et al., 2023) states that the fluorescence decay on these short time scales corresponds to a short-lived dark state formation. Rane et al. assign this dark state to the triplet state as they measured the absorption spectrum of this state and found it to correspond to the triplet state absorption spectrum. However, to prove this hypothesis further experiments to observe phosphorescence with the same lifetime would need to be carried out, which is challenging because the phosphorescence signal is only weak.

Our measurements of the fluorescence time trace showed a decay phase, almost reaching a plateau (Figure 53 A). The fluorescence decay might consist of a fast phase, corresponding to the triplet state formation, and a slow phase corresponding to reversible or irreversible switching to other dark states. The fast and slow phase decay rates were determined for different 488 nm illumination powers by a free bi-exponential fit with an offset (Figure 53 B).

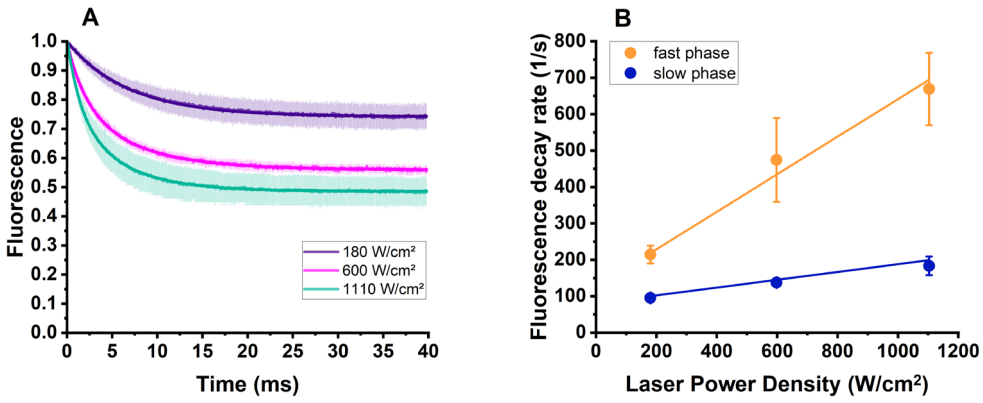

Figure 53: (A) Normalized fluorescence decay (to 1 at start of acquisition) upon illumination with 488 nm laser light at different power densities. (B) Fitted decay rates as a function of excitation power with corresponding linear fits. Mean and standard deviation of 3 measurements are shown. Each measurement was averaged over 64 illumination sequences of 40 ms laser irradiation and 960 ms dark time in order to obtain data which is smooth enough to be fitted.

To explain the results, a model of three states is proposed by Rane et al., containing the ground state S_0, the first excited state S_1 and the triplet state T_1 (for further explanation see Jablonski diagram in Figure 1). Both the initial

amplitude and decay rate of the fluorescence increased with power. This is expected because with increasing power the molecules are excited with a higher rate to undergo the transition from the ground state S_0 to the first excited state S_1 from which they can relax by emitting a photon or reach the triplet state by intersystem crossing. However, the transition rate from T_1 to S_0 does not strongly depend on the power in the used power range and therefore a faster relative fluorescence decay is observed for higher powers.

By extrapolating the fitted fast phase decay values linearly, the decay rate in presence of zero illumination power was estimated (Figure 53 B), which corresponds to the recovery rate from the short-lived dark state to the fluorescent states and thus can be assigned to the triplet state lifetime, according to Rane et al. The fluorescence decay rates are determined by the sum of the rate of direct intersystem crossing from the singlet to the triplet state and the rate of returning to the singlet state. If no power is applied, the rate for direct intersystem crossing is zero and thus the rate corresponding to the time for the triplet state to return to the singlet state, can be determined. From the linear fit of the data of Figure 53 B we obtain the triplet state lifetime of ~8ms at CT. Repetitions of these measurements by Rane et al. with an additional photomultiplier for achieving higher resolution of the fluorescence data and a new strategy for laser power determination led to values of 14.4 ± 4.0 ms for rsEGFP2 and 15.6 ± 2.7 for EGFP at CT. These results can be compared to the triplet state lifetime of 10 ms at RT reported by Byrdin et al. (2018) for EGFP in an argon saturated buffer. Shorter lifetimes were observed in buffers with oxygen (Byrdin et al., 2018).

The similar lifetime at CT and RT suggests that also at CT the triplet state might be an intermediate state of photo-physical reactions. Further, due to the lack of oxygen quenching at CT, longer lifetimes can be reached than at RT. As the lifetime of the triplet state appears to be relatively long at CT we concluded that the triplet state could be an intermediate state of rsEGFP2 cryo-switching despite a relatively low reactivity at CT due to the absence of oxygen.

7.8. Triplet state quencher attachment

To study the role of the triplet state in the cryo-switching mechanism, we wanted to quench the triplet state in rsEGFP2 and analyze resulting changes in the switching kinetics. As the diffusion of buffer molecules is hampered at CT, simple mixing of triplet state quenchers into the protein buffer did not appear to be promising. As our attempts did not show an effect, we were searching for a solution how to attach the quenchers and found the approach of Henrikus et al. (2021), which we applied on rsEGFP2. They covalently attached different triplet state quenchers to α-GFP, such as Trolox, Nitrophenyl, Cyclooctatetraene, and azobenzene derivative (ABD), of which only ABD increased the photostability of α-GFP, whereas the other quenchers did not show an effect. They express the hypothesis that due to the relatively high energy of the ABD triplet-state it might quench triplet-states of fluorophores more efficiently.

We attached ABD to a double cysteine mutant (K207/L222) of rsEGFP2, recombinantly produced by Dr. Virgile Adam according to the protocol of Henrikus et al. Absorption and fluorescence spectra and kinetics were measured for the rsEGFP2-double-cystein-mutant (rsEGFP2-2cys) with and without attached quenchers and compared measurements of the wild-type in the same conditions (Figure 54).

The wildtype and double-cysteine-mutant show similar decays, but rsEGFP2-2cys recovers less. Overall, it is comparable to the wildtype and was therefore used for the studies with ABD. rsEGFP2-2cys-ABD shows exactly the same switching kinetics as rsEGFP2-2cys, which means that no effect was obtained by our quencher attachment. This can have three reasons. Either the attachment of ABD was not successful, or ABD does not quench the triplet state in the given conditions, or it quenches the triplet state, but this does not affect the switching kinetics of rsEGFP2 because the triplet state is not involved in the switching mechanism.

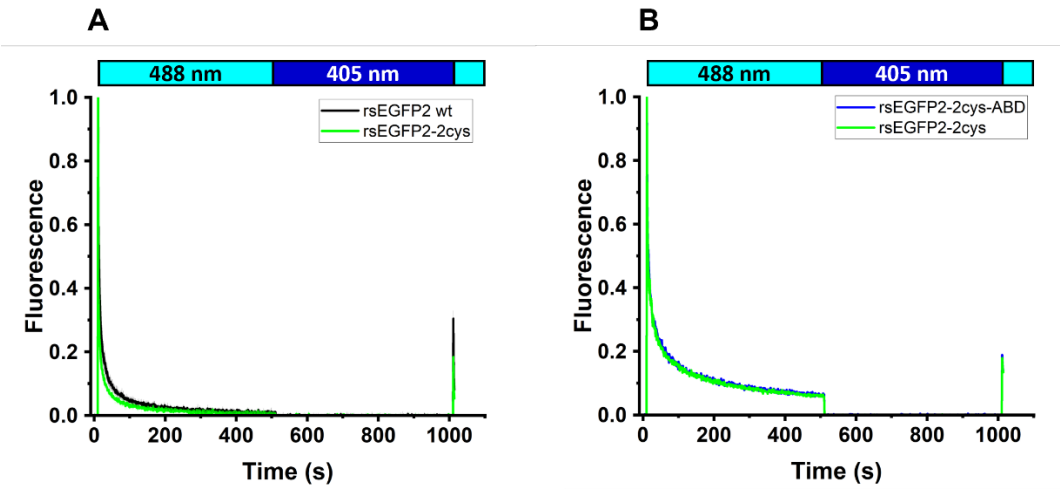

Figure 54: Integrated fluorescence (495-630 nm spectral range) of rsEGFP2-2cys (green) in comparison to (A) the wildtype (black) during on-to-off switching by 488 nm laser light (5900 W/cm²) and off-to-on switching upon 405 nm laser light illumination (290 W/cm²) or (B) the wildtype and rsEGFP2 with attached ABD (blue) during on-to-off switching by 488 nm laser light (4500 W/cm²) and off-to-on switching upon 405 nm laser light illumination (2100 W/cm²). Fluorescence was only recorded in the presence of 488 nm illumination and was normalized to 1 at the first point of the acquisition. In (A), the mean and standard deviation of 3 measurements are shown, in (B) one measurement of each variant is shown.

To check if ABD was bound successfully, the absorption spectra of the double-cysteine-mutant with and without ABD were considered (Figure 55).

The absorption spectra of the rsEGFP2-2cys resemble the rsEGFP2-wt spectra. The absorption spectrum of the rsEGFP2-2-cystein mutant with attached ABD shows a rise at around 320 nm as compared to the original spectra, which indicates a successful binding of ABD, as it has a maximum absorption peak at 320 nm. This rise in our 320 nm absorption spectrum was larger than in that shown by Henrikus et al. (2021), indicating that we should have at least a similar labelling efficiency. The absorption spectrum of alpha-GFP with successfully bound ABD, shown by Henrikus et al. (2021) shows a similar increase of the 280 nm peak as our data.

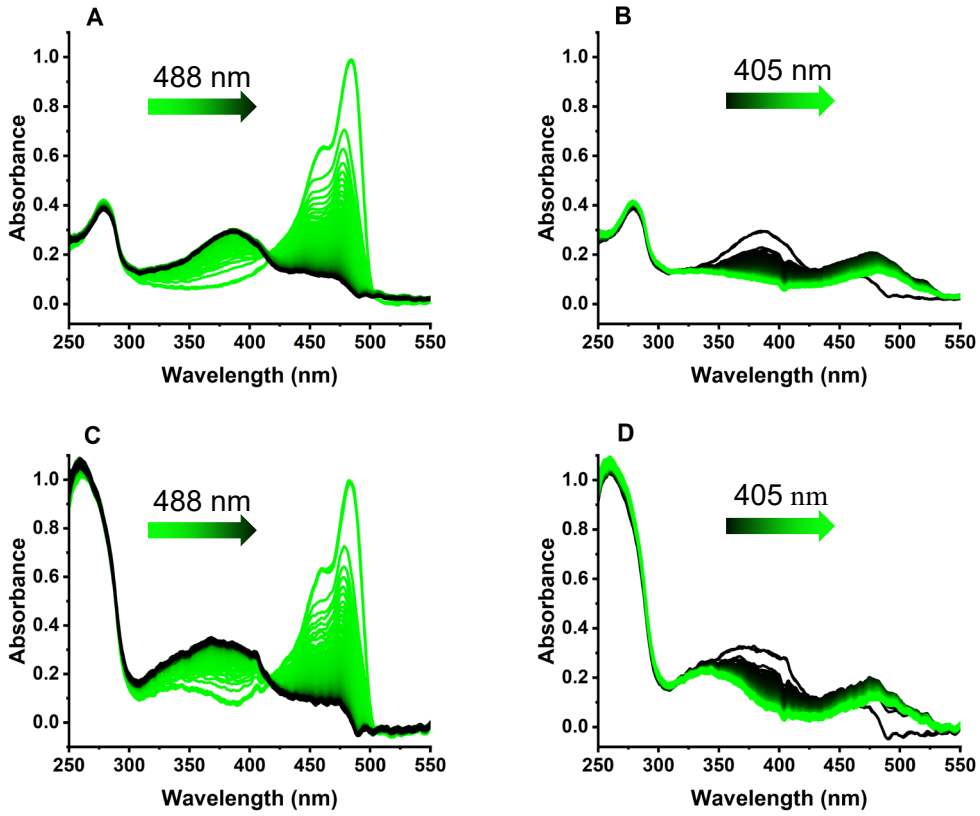

Figure 55: Representative absorption spectra of rsEGFP2-2cys (A, B) and rsEGFP2-2cys-ABD (C, D) upon on-to-off switching by 488 nm laser light (4500 W/cm²) (A, C) and off-to-on recovery by 405 nm laser light (2100 W/cm²) (B, D), monitored by micro-spectrophotometry at CT. Absorbance was normalized to 1 at the maximum of the on-state peak.

Estimating the molar concentration of ABD in the sample by considering the molar extinction coefficient of 22219 $cm^{-1}M^{-1}$ of azobenzene at 320 nm, the sample sickness of 50 µm, and the rise of the absorbance peak at 320 nm of the initial spectrum in Figure 55 C as compared to the initial spectrum in Figure 55 A, which has an optical density of 0.21 at the not normalized anionic peak, led to c = 0.097 mol/m^3. Comparing this to the molar concentration of rsEGFP2-2cys of c = 0.71 mol/m^3 suggests a labeling efficiency of ~14% for the binding of one ABD per molecule or ~7% for the binding of two, which is maybe not enough to observe an effect. It would further be possible that in our case the ABD was not bound but is present in the protein solution in an unbound manner and thus produces the rise at

320 nm. However, this is unlikely because unbound ABD was washed off extensively (see methods section 4.3.7).

It was expressed by Henrikus et al. that it is not confirmed if triplet state quenching is the reason of the photostability increase by ABD. Thus, it would be possible that the reason why we do not observe a difference in the kinetics is that ABD does not quench the triplet state.

In case the labelling would be successful, and in case ABD indeed quenches the triplet state, we would expect to observe a difference in the cryo-switching kinetics if the triplet state is involved. As the quenching is based on electron transitions it should also be possible at CT.

To confirm if the triplet state is involved in rsEGFP2 photoswitching, the labeling efficiency should be improved and also other triplet state quenchers could be attached to rsEGFP2-2cys. Further, the triplet-state lifetime measurements of rsEGFP2-2cys with attached quenchers would be helpful for investigating if they indeed quench the triplet state.

8. Switching mechanism of other proteins

8.1. rsEGFP2-V151A and rsEGFP2-V151L

To get a better understanding of the rsEGFP2 switching mechanism, we decided to test other GFP variants, starting with the mutants rsEGFP2-V151A and -V151L. The presence of two off-states after cryo-off-switching reminds on the two off-states after RT off-switching described by Adam et al. (2022). Adam et al. mention the hypothesis that also the on-state at RT might consist of two on-state populations. It would be interesting to

investigate if this hypothesis would be consistent with the observations made at CT.

To investigate if the rsEGFP2-V151A and -L mutants would also influence the cryo-switching mechanism, we illuminated the mutants with the same illumination scheme as used in Figure 39 for rsEGFP2 and measured the fluorescence during switching (Figure 56).

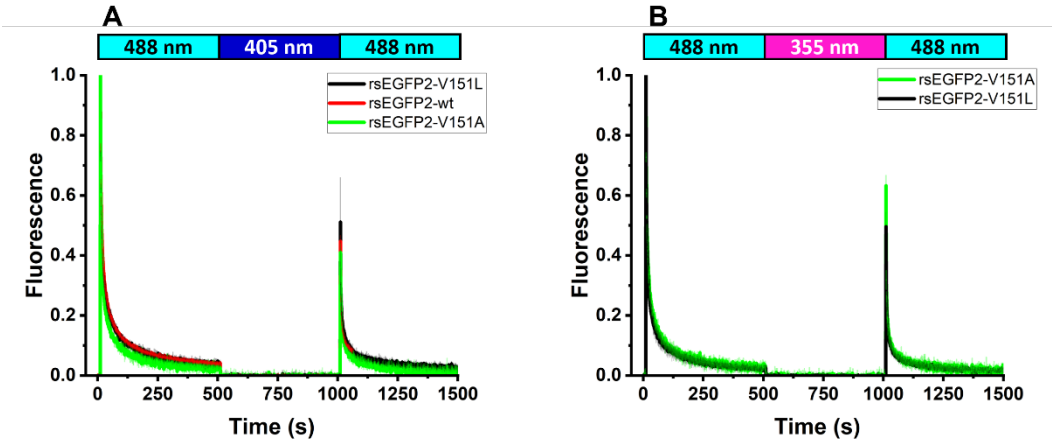

Figure 56: Integrated Fluorescence (495-630 nm spectral range) of (A) rsEGFP2-V151A (green), rsEGFP2 wt (red) and rsEGFP2-V151L (black) upon on-to-off switching by 488 nm laser light (950 W/cm²) and off-to-on switching by 405 nm (510 W/cm²) or (B) rsEGFP2-V151A (green) and rsEGFP2-V151L (black) upon on-to-off switching by 488 nm laser light (950 W/cm²) and off-to-on switching by 355 nm laser light (14 W/cm²). Fluorescence was only recorded in the presence of 488 nm illumination. Spectra are normalized to the first point of acquisition. The mean and standard deviation of 3 measurements are shown.

The data indicates that the rsEGFP2-V151A mutant recovers more efficiently upon 355 nm illumination (62% recovery) and less efficiently upon 405 nm illumination (39% recovery). It further suggests that rsEGFP2-V151L recovers to an intermediate amount with both lasers (49% recovery with 405 nm light and 48% recovery with 355 nm light). The recovery of the rsEGFP2 wild-type is in between those of the mutants (42% with 405 nm illumination). Recovery measurements of the wildtype with 355 nm light

were not measured on the same day, ensuring exactly the same conditions of the instrument, but the recovery ratio obtained in other experiments can be considered. In the experiment displayed in Figure 39, the 355 nm laser improves the fluorescence recovery obtained by the 405 nm laser by a factor of ~1.24. In the first cycle of the data shown in Figure 48 the factor is about 1.5. Taking the mean value of these factors, the expected recovery of the wildtype using 355 nm laser light would be about 58%, which is also in between the recovery levels obtained with the mutants.

If this data can be confirmed by absorbance measurements a conclusion could be that by the V151 mutation either the formation of Off_1 or Off_2 is favored (absorbance data collection for this experiment was not successful). Possible hypotheses how to interpret the results are explained in the discussion chapter.

8.2. mEmerald

8.2.1 mEmerald at CT

To examine if and to which extent other proteins of the GFP family are switchable at CT, we measured switching kinetics for mEmerald with the same illumination scheme as for rsEGFP2 (Figure 57). mEmerald was shown to switch efficiently at CT by Hoffman et al. (2020).

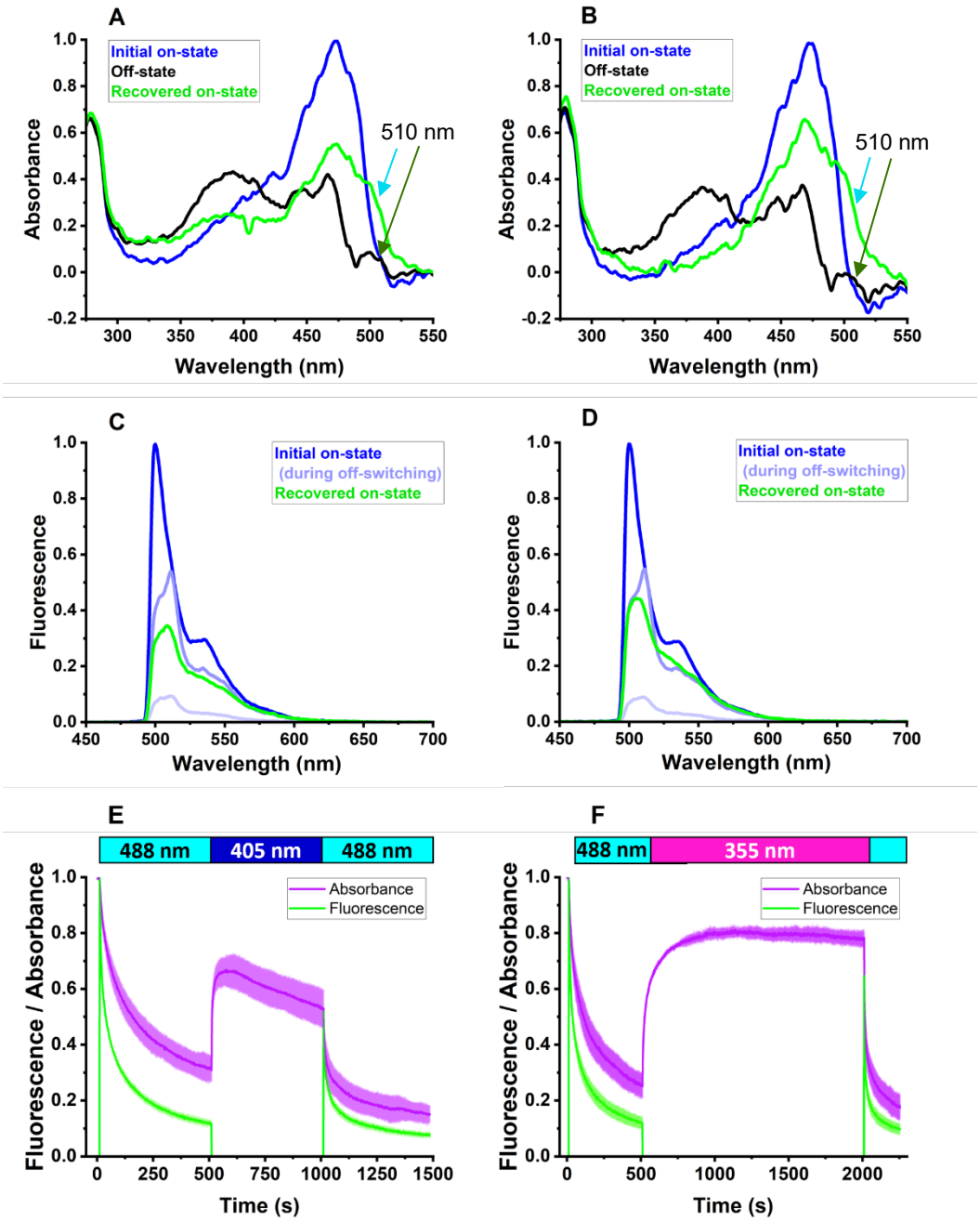

Figure 57: Absorption spectra of mEmerald at CT before (blue) and after (black) on-to-off switching with 488 nm laser light (780 W/cm²) and after off-to-on recovery (green) upon (A) 405 nm illumination (700 W/cm²) or (B) upon 355 nm illumination (12 W/cm²). Fluorescence spectra of the initial on-state (blue, and light blue during off-switching) and the ones recovered upon (C) 405 nm or (D) 355 nm illumination (green). Fluorescence (green), integrated in the spectral range of 495-630 nm, and absorbance (purple), integrated in the range of 450-510 nm, upon off-switching with 488 nm illumination and recovery with (E) 405 nm illumination and (F) or 355 nm illumination is shown with mean and standard deviation of 3 independent measurements.

The absorption and fluorescence spectra and switching kinetics of mEmerald are comparable to those of rsEGFP2. The peak maxima of the on- and off-states are at similar positions but the on-state peak of mEmerald appears to be slightly broader. To account for the broader absorbance spectrum a larger integration range was chosen to display the on-state evolution kinetics than for rsEGFP2. A difference as compared to rsEGFP2 is that upon off-switching of mEmerald a small shoulder of the absorbance peak around 490-510 nm remains (Figure 57 black arrows) and that in the emission spectrum a clear peak at 515 nm becomes visible in the off-switching phase, as observed in Figure 51. One possible interpretation could be that that the On_3 state, discussed in section 7.6, could be present here, which might rise from a fraction of protonated molecules in cis-conformation (Off_3) (see discussion chapter). The on-state recovery of mEmerald is in principle similar to the rsEGFP2 recovery as well but the additional shoulder at 510 nm in the absorbance spectrum is rising even more (Figure 57 cyan arrows), which is consistent with the idea that this could be the On_3 state, which rises upon illumination with 355 or 405 nm light.

Interestingly, the 355 nm laser also improves the recovery as compared to the use of the 405 nm laser. Again, after recovery with the 405 nm laser a larger fraction of the off-state is remaining, indicating that also in mEmerald two off-states are present. Upon 355 nm illumination mEmerald reaches 73% absorbance and 60% fluorescence recovery, upon 405 nm illumination only 51% absorbance and 45% fluorescence recovery. For both lasers this appears to be an improvement as compared to rsEGFP2 (25% recovery with the 405 nm laser and 50% recovery with the 355 nm laser). However, the On_3 and Off_3 states affect the fraction of mEmerald molecules which are initially in the anionic on-state absorbing at 480 nm, might influence the relative recovery levels in mEmerald and thus this protein would not necessarily be a more efficient switcher (see discussion chapter). Further,

more experiments should be carried out to exclude artifacts caused by a baseline drift. Due to strong illumination power of the 405 nm laser a strong bleaching phase is observed in the recovery phase, which also influences the fluorescence recovery.

In the recovered emission spectrum, the 515 nm peak is more pronounced after back-switching with the 405 nm laser than with the 355 nm laser. Possibly, the 355 nm recovers more of the other on-state (absorbing at ~480 nm and emitting at ~500 nm), such that the 515 nm on-state emission spectrum becomes less visible.

Taken together, the observations concerning the different off-states suggest that mEmerald undergoes a switching mechanism similar to the one of rsEGFP2 and that the findings for rsEGFP2 could possibly be generalized to other GFP like proteins. Furthermore, the apparently more efficient recovery of mEmerald and the influence of artifacts caused by samples which were not fully in the on-state at the beginning should be investigated.

8.2.2 mEmerald at RT

mEmerald was reported to not be efficiently switchable at RT (Shaner et al., 2007, 2013). We wanted to examine if and to which extent switching is possible upon strong illumination power as used at cryo-temperature and observed a similar behavior as at CT (Figure 58).

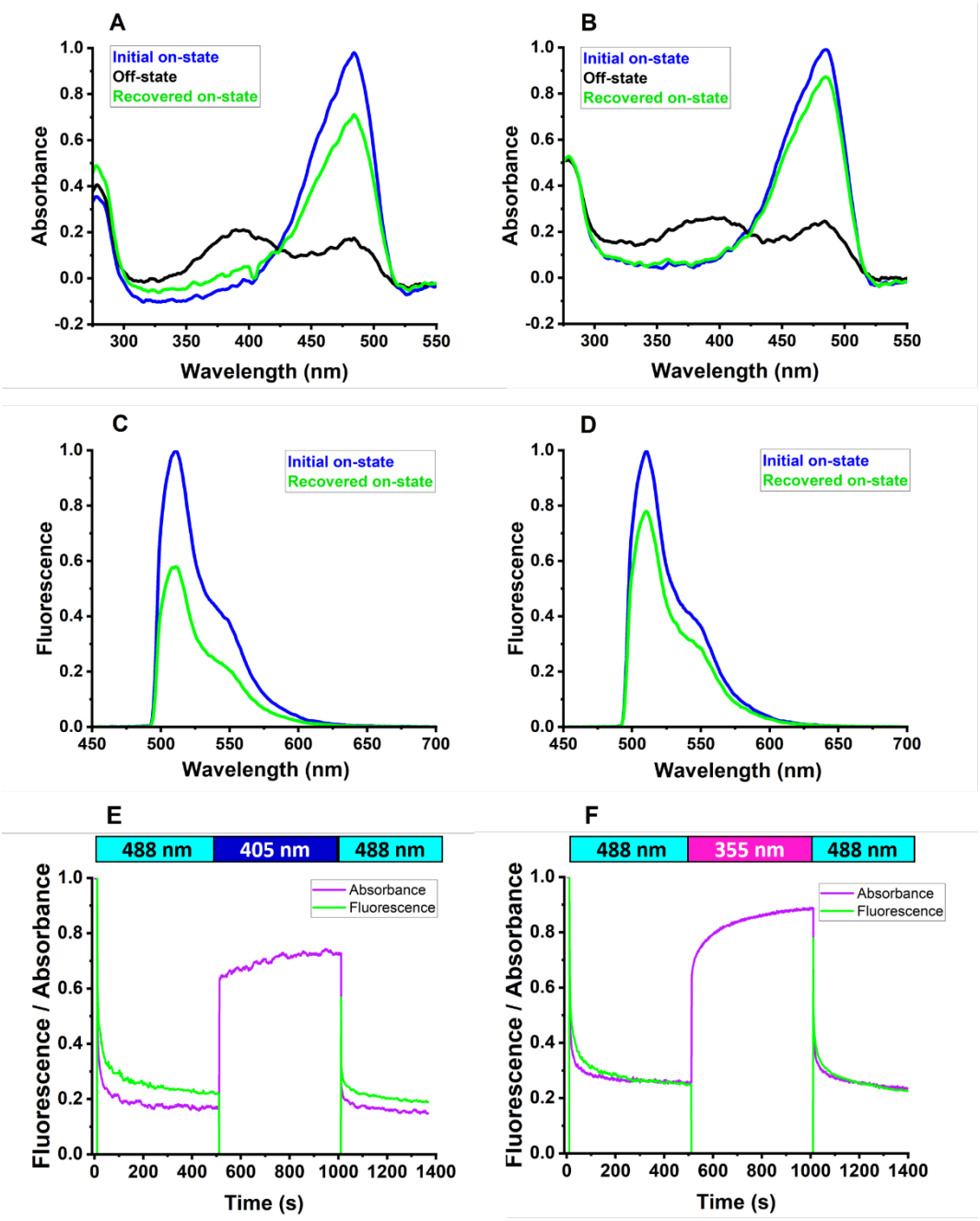

Figure 58: RT switching of mEmerald. Absorption spectra of the initial on-state in blue, the off-switched state after on-to-off switching with 488 nm illumination (900 W/cm²) in black and the recovered on-state in green, after recovery with (A) 405 nm illumination (450 W/cm²) and with (B) 355 nm illumination (8 W/cm²). Fluorescence spectra of the initial on-state (blue) and the recovered spectra upon (C) 455 nm or (D) 355 nm illumination (green). Integrated fluorescence (495-630 nm spectral range, green) and integrated absorbance (450-510 nm spectral range, purple) for one measurement is shown for on-to-off-switching with 488 nm illumination and off-to-on switching with (E) 405 nm illumination and (F) with 355 nm illumination.

The on-to-off-switching contrast seems to be lower as compared to the CT switching, whereas the recovery appears to be higher. However, it must be considered, that the switching kinetics are very likely affected by diffusion artifacts and thus no quantitative conclusions can be made. On the other hand, the recovery levels can be compared relatively to each other. The spectra are not concerned by diffusion artifacts and thus can inform about the present states. Interestingly, also at RT the 355 nm laser improves the on-state recovery, as compared to the 405 nm laser. The absorption peak maximum of the off-state has a similar position as at CT. Further, a larger fraction of the off-state is remaining after recovery with the 405 nm laser than with the 355 nm laser, which might be due to the presence of two off-states of which one is not recoverable with 405 nm light, as it is the case for rsEGFP2 at CT. However, it cannot be excluded that here this is only an artifact of the unstable baseline, regarding the rise at 280 nm after recovery with 405 nm illumination. Taken together, more experiments have to be performed with mEmerald at RT to make conclusions but our observations would be consistent with the hypothesis that mEmerald undergoes the same switching mechanism at CT and RT. Possibly, the cryo-switching mechanism, found in rsEGFP2, takes place for other proteins of the GFP family and is also present at RT, but for efficiently switchable proteins at RT, like rsEGFP2, this mechanism has to compete with the more efficient ones and thus is not observable. However, it remains to be investigated how it is possible that the same off-states as found at CT are stable enough at RT to show a similar behavior as at CT (see discussion chapter).

8.3. EGFP

8.3.1 EGFP at CT

To investigate how far the cryo-switching mechanism of rsEGFP2 might be generalizable to proteins of the GFP family, we studied the switching kinetics of EGFP at CT (Figure 59) and compared it to the observations obtained with rsEGFP2 and mEmerald.

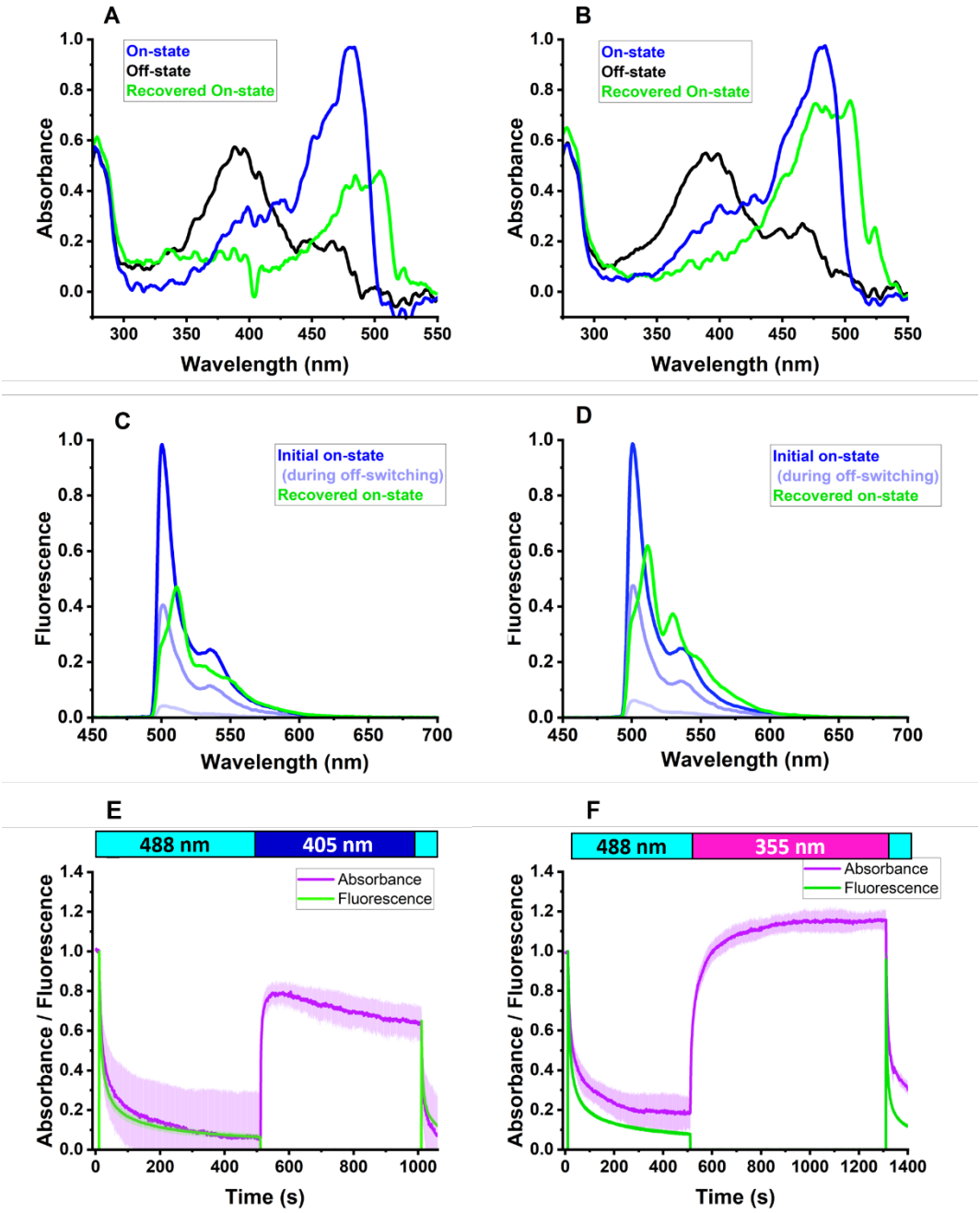

Figure 59: Absorption spectra of EGFP at CT of the initial on-state (blue), the off-switched state (black) after on-to-off switching with 488 nm laser light (900 W/cm²) and the recovered state (green) after (A) off-to-on recovery upon 405 nm illumination (450 W/cm²) or (B) off-to-on recovery upon 355 nm illumination (8 W/cm²). Fluorescence spectra of the initial on-state (blue), the ones recovered by (C) 455 nm and (D) 355 nm illumination (green). Integrated fluorescence (495-630 nm spectral range, green) and integrated absorbance (440-540 nm spectral range, purple) for 3 independent measurements are shown in (E) for off-switching with 488 nm illumination and recovery with 405 nm illumination and (F) for off-switching with 488 nm illumination and recovery with 355 nm illumination.

Interestingly, the switching efficiency of EGFP at CT is comparable to the one of rsEGFP2 and mEmerald. The off-state and initial on-state spectra resemble as well in terms of shape and peak maxima. Also, the effect of the 405 nm and 355 nm lasers are comparable. Upon recovery with 405 nm illumination a larger fraction remains in the off-state than with the 355 nm laser. This supports the hypothesis that the rsEGFP2 cryo-switching mechanism is also present in EGFP and thus maybe also in other proteins of the GFP family. It is also in line with the observation of Tuijtel et al. (2019), that the fluorescent proteins they tested, including EGFP, were able to switch at CT, regardless of their switching mechanism at RT and showed resembling switching kinetics.

The fully complete recovery of EGFP after the first switching cycle upon illumination with 355 nm laser light is likely biased by the fact that the sample appeared to be partly in a protonated state at the beginning (Figure 59 A), which possibly arose upon acidification after being stored at 280 K for 4 years. Therefore, it remains unclear how efficient the recovery of the first cycle would be for a fresh sample. The second switching cycle shows a less efficient recovery (73% for absorbance and 60% for fluorescence) (Figure 60), comparable to the recovery of mEmerald. This recovery is still substantial, and it would be of high interest to repeat the EGFP measurements with fresh samples to reinvestigate the recovery of the first switching cycle.

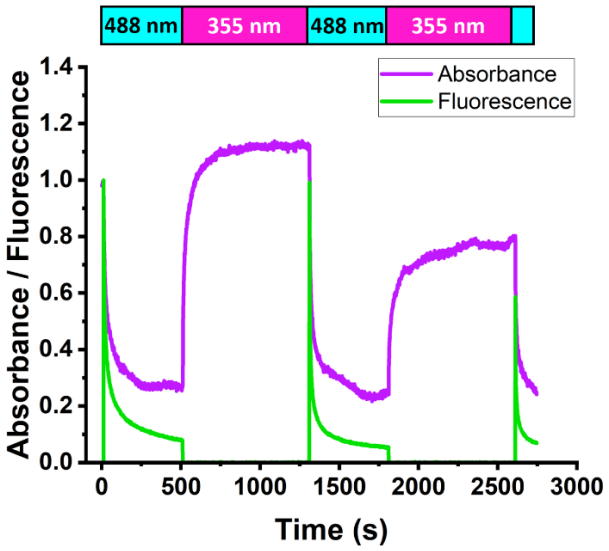

Figure 60: Integrated fluorescence (green, 495 nm-630 nm spectral range) and absorbance (purple, 440-540 nm spectral range) of one measurement of EGFP cryo-switching. The protein was switched off upon illumination with 488 nm laser light (900 W/cm²) and back on upon illumination with 355 nm laser light (8 W/cm²). Fluorescence and absorbance data were normalized to 1 at the start of acquisition.

Another interesting observation is that upon recovery of the on-state, a second absorbance peak at 510 nm arises (Figure 59 A and B), which seems to be fluorescent as well, regarding the change in the fluorescence spectra. This absorbance peak was also observed for rsEGFP2 and mEmerald, but to a minor extent (On_3). A broad integration range was chosen to follow the absorbance kinetics of EGFP due to the high amount of the arising red-shifted on-state. In the emission spectrum of EGFP a clear peak arises at 515 nm (Figure 59 C, D), which we assume to correspond to On_3 (see discussion chapter). This peak was also observed in mEmerald but was more pronounced in the off-switching phase than after recovery, which seems to be the opposite for EGFP. Further, the initial 530 nm shoulder of the main emission peak is replaced by two shoulders in EGFP in the spectrum of the recovered on-state. The main one is slightly blueshifted and the minor one is slightly redshifted as compared to the initial shoulder. This might be for example the emission signature of the state with

520 nm absorption which is also rising here, which we suggested to be a fluorescent trans-state (see discussion chapter).

8.3.2 EGFP at RT

Regarding the improvement of the recovery of mEmerald with 355 nm instead of 405 nm illumination at RT, we wondered if it generally could apply for non-switchable proteins at RT and we thus repeated the same measurements with EGFP (Figure 61). The data shows that the recovery level does not appear to differ much depending on the laser. It should be noted that only one measurement was performed per condition, which should be repeated to get quantitative data. However, it is interesting that the shape and peak maxima of the absorption spectra, as well as the off-switching rate and switching contrast resemble the RT mEmerald data. A slightly better recovery with the 355 nm laser as compared to the 405 nm laser can be observed as well but more data is necessary to confirm this. Whether a different fraction of the off-state is remaining depending on the laser used for recovery, cannot be concluded from this data due to a large baseline shift during the recovery with the 405 nm laser. Overall, the observations do not contradict the hypothesis that the switching mechanism we found could also be present at RT.

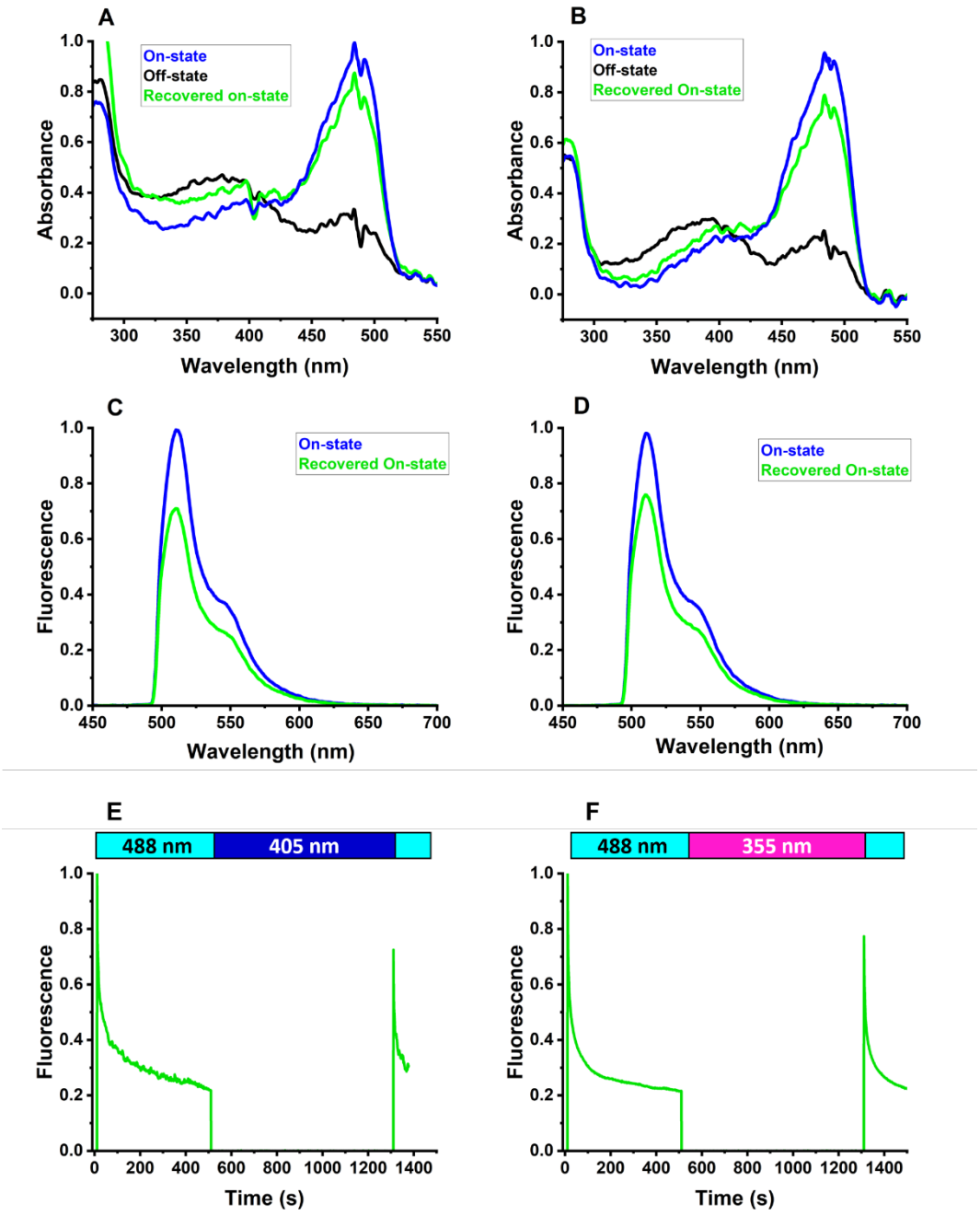

Figure 61: RT switching of EGFP. Absorption spectra of the initial on-state (blue), the off-switched state after 488 nm illumination (940 W/cm², black) and the recovered on-state (green), after recovery with (A) 405 nm illumination (800 W/cm²) and with (B) 355 nm illumination (15 W/cm²). Fluorescence spectra of the initial on-state are shown in blue and the recovered spectra by (C) 405 nm or (D) 355 nm laser light, in green. Integrated fluorescence (495-630 spectral range, green) and for one measurement is shown upon off-switching with 488 nm laser light and off-to-on switching upon (E) 405 nm and (F) 355 nm illumination.

Taken together, EGFP appears to be a good candidate for future investigations for possible improvement of cryo-nanoscopy applications, as it might be switching as efficient as rsEGFP2 or even more efficient. Further, it can provide insights in the possibly similar switching mechanisms and moreover allow to study this mechanism at RT, in case it can be shown that for EGFP the same mechanism is present as at CT.

9. Discussion and Outlook

9.1. Two off-states at CT (*Off$_1$* and *Off$_2$*)

Taken the results together, it can be concluded that at CT, rsEGFP2 undergoes a different switching mechanism than at RT. Instead of changing its conformation from cis to trans, the on-state transforms into two different off-states (*Off$_1$* and *Off$_2$*) with different absorption spectra, both blue-shifted as compared to the RT off-state (Figure 44). *Off$_1$* is recoverable with 405 nm and 355 nm light and *Off$_2$* only with 355 nm light. Consequently, a better total recovery is achieved by the latter laser. Hence, the use of a 355 nm laser might improve the labelling efficiency in SMLM applications at CT.

Our structural data suggests that these off-states are in cis-conformation like the on-state. As no difference in the on-to-off switching speed was observed depending on the pH (Figure 49), we deem unlikely that the switching mechanism leading to these off-states is based on protonation of the chromophore. We rather assume that electron transfer plays a role. This assumption is supported by recent experiments carried out by Dr. Oleksandr Glushonkov, which show that rsEGFP2 on-to-off and off-to-on switching is accelerated if it is embedded in poly vinyl alcohol (PVA) instead of glycerol (revised version Mantovanelli et al., 2022, in preparation). It was shown that PVA favors electron transfer in fluorescent proteins (Zondervan et al.,

2003). Further, we observed that the off-states partially relax in the absence of light. Quantitative investigations recently carried out by Dr. Virgile Adam showed that 25% of the recoverable on-state by 405 nm light can recover thermally (revised version Mantovanelli et al., 2022, in preparation).

This cryo-switching mechanism might be general for many proteins of the GFP family, as the behavior observed in spectroscopic investigations of rsEGFP2 was also observed for the other tested proteins - mEmerald and EGFP. Moreover, Tuijtel et al. (2019) observed similar kinetics at CT for many different fluorescent proteins, notably for Padron and PA-GFP, which show a different mechanism at RT (see section 1.6). Further, the switching of EYFP, Dronpa and IrisFP demonstrated by Regis Faro et al. (2010) is in line with these results. The absorption spectra of the off-states in EYFP (Regis Faro et al., 2010) remind on the spectra we observed for rsEGFP2. This indicates that a similar off-switching mechanism takes place for these proteins. Regis Faro et al. (2010) expressed the hypothesis that protonation of the chromophore might be the underlying mechanism of cryo-switching of EYFP, Dronpa and IrisFP but our data rather suggests that our proposed mechanism also occurs for these proteins. Of note, most tested fluorescent proteins were reported to exhibit a negative reversible switching mechanism at CT, regardless of their RT switching mechanism and if they were of anthozoan or hydrozoan origin. This is also an argument in favor of the hypothesis that these proteins could have a similar cryo-switching-mechanism.

9.2. Two major on-states at CT (*On$_1$* and *On$_2$*)

It is possible that either off-state is reached from a different on-state (*Off$_1$* from *On$_1$* and *Off$_2$* from *On$_2$*) or that there is only one initial on-state from which both off-states are reached. An indication for the existence of two initial on-states is given by the data displayed in Figure 46, where the switching kinetics of rsEGFP2 upon subsequent application of 488 nm, 355 nm and 405 nm laser light are shown. It was observed that in this case

the 405 nm illumination leads to depopulation of the on-state, as it only recovers back Off_1 but continuously populates Off_2. If this would happen starting from only one on-state or two exchangeable on-states, the whole on-state population would be converted to Off_2 after a certain time. However, the data suggests that a plateau value is reached in the 405 nm illumination phase, indicating that a significant fraction of the on-state remains. Simulations of switching kinetics at the ensemble level performed by Jip Wulffelé (see appendix, publication Mantovanelli et al., Supplementary Information) confirmed that in the presence of only one initial on-state, it would decay to zero, but if two not exchangeable on-states are present, a plateau value would be reached, indicating that one of the on-states is not switched off.

If this hypothesis is correct, one way to explain why the rsEGFP2-V151A and -V151L mutants reach different recovery levels (Figure 56), would be the following scenario: if two on-state populations are present, the mutation of the V151 residue could change the equilibrium between those populations and if they are switched to the off-states, also the equilibrium between Off_1 and Off_2 would be different. As Off_1 is recoverable with both the 405 nm and 355 nm lasers, and Off_2 only with the 355 nm laser, the recovery would then differ for the V151A and V151L mutant depending on which laser was used. According to this hypothesis, the V151A mutation would favor the presence of On_2 which switches to Off_2 and can only be recovered by 355 nm illumination, whereas the V151L mutation would favor On_1 and thus Off_1, which is recoverable with both lasers and thus its recovery would be independent on which of the two lasers is used. By consequence, rsEGFP2-V151A would recover more efficiently with the 355 nm laser than with the 405 nm laser, whereas the recovery of the V151L mutant should be similar with both lasers. The data is consistent with this hypothesis. As the recovery of rsEGFP2-V151A by 355 nm light is enhanced as compared to the recovery of rsEGFP2-V151L with the same illumination, this would also mean that the Off_2 state is better recoverable than the Off_1 state, for example because Off_1 is bleached more by the 355 nm laser than Off_2. To obtain more information about the present states,

absorption spectra time series of the mutants should be measured as well, and synchronization errors of the fluorescence data, resulting from fluctuations of the data collection start caused by the instrument (see section 4.3.1), need to be excluded to confirm that the differences between the mutants result from a real effect. As discussed in section 4.3.1 the synchronization errors of the fluorescence data might bias the observed recovery levels and should better be considered together with absorption data to make reliable conclusions.

In case the hypothesis that the suggested two on-states are present could be confirmed, it would be also interesting to investigate with the V151A and -L mutants if the on-states are related to the heterogeneity found at RT.

9.3. Two minor on-states at CT (*On$_3$* and *On$_{trans}$*)

Upon protonation of the chromophore of the fluorescent proteins achieved by adding a buffer of low pH a fraction of molecules switches into a protonated off-state in cis conformation (Figure 50 A). Samples which were stored for a long time at 280 K showed a not fully anionic peak at the beginning, before any illumination, thus we expressed the hypothesis that the fluorescent proteins were also partly in a protonated state, due to sample acidification over time. This behavior was observed for rsEGFP2 in long stored crystals and especially in solution measurements of EGFP (Figure 59 A/B, blue spectrum). Interestingly, for protonated samples due to low pH, as well as for long stored samples, a higher absorbance rise at ~510 nm was observed after recovery with 355 or 405 nm light. This rise was especially pronounced for EGFP (Figure 59 A/B green spectrum) and relatively pronounced in mEmerald (Figure 57 A/B green spectrum). The rise at ~510 nm was also slightly visible in rsEGFP2 for which no partly protonated state was observable from the absorption spectra (Figure 42 see cyan arrows).

It would be possible that from the protonated cis-off-state a third on-state On_3, corresponding to the absorbance rising at 510 nm, can be formed. It was observed that in correlation to the rise of the 510 nm On_3 absorbance peak, a rise of a ~515 nm emission peak occurred and thus it seems likely this is related. For example, for the EGFP data a strong rise of the 515 nm emission is observable, together a reduced rise in the initial emission peak at ~500 nm (Figure 59 C/D green spectrum). Interestingly, the fluorescence spectra obtained after recovery at low pH (Figure 51) resemble these fluorescence spectra of EGFP, which suggests that indeed protonation at low pH and after long storage have a comparable effect. Also, mEmerald appears to behave as a protein which was stored for a long time, although it was freshly prepared. If this effect is reproducible, it could be that initial protonation in mEmerald is more favored. The small fraction of absorbance rise at 510 nm in not acidified samples suggests that in these ones a minor fraction of protonated state is present.

These observations indicate that it is important to control the protonation conditions of the sample, as this can influence the switching kinetics. A reduced initial on-state could lead to biased switching kinetics, as the relative recovery in the second cycle will be increased by this effect.

Moreover, a putative fourth on-state was observed. After preliminary off-switching at RT, leading to cis-trans-isomerization, followed by on-switching at CT, an absorbance rise around 520 nm was observed instead of a rise of the 480 nm on-state (Figure 37 B and Figure 33), and we suggested that it could be a fluorescent trans-state. A small rise in absorbance at 520 nm is also visible after on-switching at CT without preliminary off-switching at RT (Figure 42 see yellow arrows). It appears upon recovery with 405 nm or 355 nm laser light, but it is more pronounced if the 405 nm laser is applied. This is consistent regarding that the trans-off-state has a main absorbance peak around 405 nm. One possible explanation for the absorbance rise at 520 nm upon off-to-on switching would be that a small fraction of molecules still undergoes cis-trans isomerization at CT and that this trans-state Off_{trans}

would switch then to a fluorescent trans-state On_{trans} upon photoinduced deprotonation upon 405 nm or 355 nm laser light.

9.4. Competitive switching mechanisms at CT and RT

Qualitative experiments with mEmerald and EGFP further hinted on possible similarities of the CT and RT switching mechanism in not efficiently switchable fluorescent proteins at RT, as similar maxima in the off-state spectra and the improved recovery with the 355 nm laser as compared to 405 nm laser illumination (see mEmerald at RT in Figure 58, and EGFP at RT in Figure 61). It would be conceivable that the discussed cryo-switching mechanism including the two off-states is also present at RT but competes with other mechanisms, such that it is not observed for RSFPs but might be observed in non-switchable fluorescent proteins. The hypothesis, that a fraction of molecules is able to undergo cis-trans isomerization at CT is in line with the idea of competing mechanisms.

However, due to the higher thermal energy at RT, it is surprising that the two off-states would not be exchangeable at RT, as suggested by the difference in the recovery levels depending on the illumination wavelength. Further, if the off-states are radical states, one would expect them to be unstable at RT as electron transfer occurs much faster at RT. It might be possible that at RT stabilization of these states could be reached by the protein matrix. However, it remains to be investigated if the RT and CT switching mechanisms are indeed comparable or if different mechanisms take place, leading to similar effects.

9.5. Kinetic model of the cryo-switching mechanism

We propose the model shown in Figure 62, with the main mechanism displayed in the inner circle, showing the switching between two on-states

On$_1$ and *On*$_2$, which do not exchange, and which might switch to *Off*$_1$ and *Off*$_2$ by electron transfer. The off-states could switch back by the same mechanism, mainly induced by light and partly by thermal relaxation.

Our data would further be consistent with the lower part of the model (outer circle). If enough protons are present in the buffer, also a fraction of protonated molecules in cis-conformation might be formed, which subsequently might switch to a third on-state *On*$_3$. Upon illumination with 488 nm laser light a minor fraction of molecules might be able to undergo cis-trans isomerization as at RT and then be switched upon deprotonation to the fluorescent *On*$_{trans}$.

All proposed states could undergo photobleaching upon illumination.

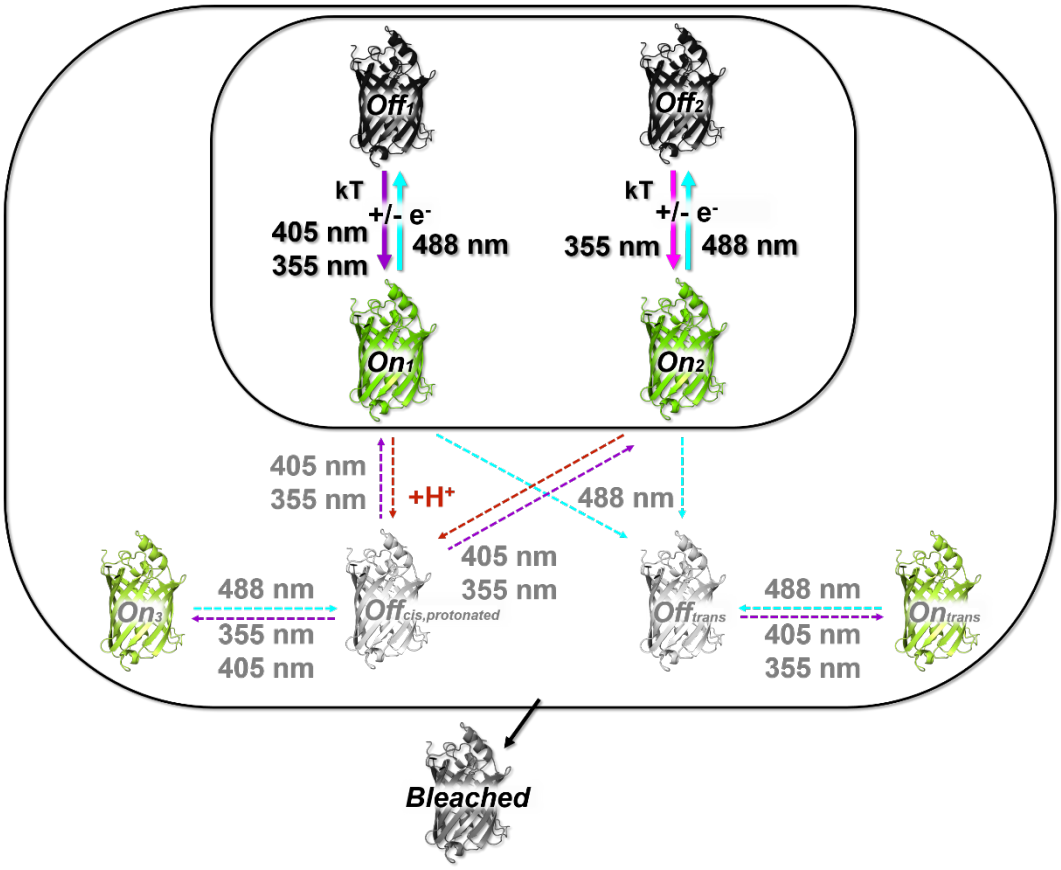

Figure 62: Model for rsEGFP2 photoswitching at CT between different fluorescent and non-fluorescent states. Main model shown in bright colors and possible competing mechanisms are shown in light colors.

9.6. Prospects

It would be of high interest to confirm that EGFP and mEmerald undergo the same cryo-switching mechanism as rsEGFP2, as suggested by our spectroscopic data. For this, more data is required to confirm the reproducibility of our results, especially for the RT data on EGFP and mEmerald which only could give preliminary hints. Moreover, crystallographic investigations should be performed to compare with our observations for rsEGFP2. Further, other fluorescent proteins should be studied to investigate how general the rsEGFP2 cryo-switching mechanism is.

For revealing more details about the present on- and off- states, also for rsEGFP2, it might be beneficial to obtain high-resolution crystallography data of these states to identify slight differences in the electron density of the on- and off-states or between the off-states. Further, more investigations should be carried out on the involvement of the triplet state in the switching mechanism by attaching different triplet state quenchers and confirming by triplet state lifetime measurements that they indeed quench the triplet state. As proposed above, it might be that upon cryo-off-switching radical dark states are formed with the triplet state being the intermediate state.

Electron paramagnetic resonance studies could be used to investigate if radical states are formed. If it can be confirmed that EGFP and mEmerald exhibit the same switching mechanism at RT and CT, Nuclear magnetic resonance studies could be performed, which is only feasible on samples at RT and thus it could be studied if the triplet state is involved. However, it would be challenging to sufficiently populate the triplet state.

We observed that the recovery level of rsEGFP2 upon on-switching depends on the ability of the illumination to recover all present off-states. It might be beneficial to engineer a GFP variant which switches to only one of the described off-states and combine this with the use of the appropriate laser for recovery to reach an even better recovery. If this would be possible

for the Off_1 state, this would have the advantage that the 405 nm laser could be used, which causes less bleaching than the 355 nm laser. A challenge of applying the 355 nm laser could also be that the microscope setup needs to be adapted. A starting point could be the investigation of the recovery levels of the V151 mutants. Concerning this, our data hints on possible differences between rsEGFP2-V151A and rsEGFP2-V151L, which however remain to be confirmed by absorbance measurements.

In SMLM simulations performed by Jip Wulffelé using the model described in Figure 62 (inner circle), it was suggested that by using the 355 nm laser instead of the 405 nm laser, images of the nuclear pore complex of Nup96 nucleoporin could be obtained with a higher labeling efficiency despite higher bleaching of the 355 nm laser (see appendix, publication Mantovanelli et al., Figure 8). It would be of high interest to show this also with a real sample on the cryo-PALM setup of our group.

Traduction des sections résumées

État de l'art :

La protéine fluorescente verte (GFP) a été découverte chez la méduse *Aequorea victoria* en 1962 par Osamu Shimomura, qui a reçu le prix Nobel en 2008 avec Martin Chalfie et Roger Tsien "pour la découverte et le développement de la protéine fluorescente verte" (Zimmer, 2009). Le principal avantage de la GFP par rapport aux autres marqueurs fluorescents est qu'elle est entièrement codée génétiquement. Il est donc possible de fusionner l'ADN de la GFP à celui d'autres protéines, qui peuvent ainsi être suivies par détection de fluorescence.

La luminosité de la fluorescence de la GFP a été améliorée et de nouvaux variants, comme par exemple la protéine fluorescente verte améliorée (EGFP), ont été développés en incluant des mutations, ce qui a été le point de départ de nombreux variants différents. Grâce à des approches permettant de contrôler la transition entre les deux états de protonation du chromophore présents dans la GFP et d'optimiser leurs propriétés, des protéines phototransformables ont été développées. Les protéines fluorescentes photoactivables (PAFP) peuvent être activées d'un état non fluorescent à un état fluorescent lors de l'illumination par une lumière laser d'une certaine longueur d'onde (généralement 405 nm). Cela permet des applications importantes telles que la microscopie de localisation photoactivée PALM. Des protéines fluorescentes commutables de manière réversible (RSFP) ont été conçues, car elles sont utiles pour de nombreuses applications importantes, comme RESOLFT. Elles peuvent passer d'un état fluorescent à un état non fluorescent par illumination avec certaines longueurs d'onde de lumière laser (généralement 405 nm et 488 nm). Il a été observé que dans de nombreuse RSFPs, le mécanisme sous-jacent de la photocommutation est une isomérisation cis-trans du chromophore (Andresen et al., 2005). À partir de ces connaissances, d'autres RSFP ont pu être développées, comme rsEGFP (Grotjohann et al., 2011) et rsEGFP2

(Grotjohann et al., 2012). En outre, des protéines fluorescentes photoconvertibles (PCFP), qui peuvent passer d'un état à un autre avec des longueurs d'onde d'émission différentes, ont été découvertes chez les coraux. Par exemple, les protéines de la famille Eos peuvent passer d'un état vert à un état rouge (Wiedenmann et al., 2004).

Les protéines fluorescentes sont largement utilisées comme marqueurs fluorescents en microscopie à fluorescence. En 2014, le prix Nobel de chimie a été attribué aux Dr. Eric Betzig, Dr. Stefan Hell et Dr. William E. Moerner pour avoir surmonté la limite de diffraction en développant la microscopie de fluorescence à super-résolution (nanoscopie) (Möckl et al., 2014). Ils ont développé deux approches différentes, indépendamment l'une de l'autre. Betzig et Moerner ont élaboré la microscopie à localisation photo-activée (PALM) (Betzig et al., 2006), qui est basée sur la localisation de protéines fluorescentes uniques et constitue une technique de nanoscopie stochastique. L'autre approche, basée sur la déplétion par émission stimulée (STED) (Hell & Wichmann, 1994), a été développée par Stefan Hell et est basée sur le contrôle de l'émission de colorants fluorescents excités par la désexcitation induite par l'émission stimulée et est une méthode de nanoscopie déterministe. STED et d'autres techniques similaires basées sur différents fluorophores et transitions optiques sont résumées sous le terme de "transitions optiques (fluorescentes) saturables réversibles" (RESOLFT) (Hell et al., 2004). Hofmann et al. (2005) décrivent l'utilisation de protéines à commutation réversible pour RESOLFT. La vitesse des enregistrements RESOLFT avec des protéines fluorescentes a été considérablement améliorée par le développement de la protéine à commutation rapide rsEGFP2 par Grotjohann et al. (2012).

De plus, il existe une forte demande pour réaliser la microscopie de localisation de molécules uniques (SMLM) à température cryogénique afin d'éviter la fixation chimique des cellules, qui crée des artefacts à haute résolution (Whelan & Bell, 2015). La congélation des échantillons comme stratégie de fixation en nanoscopie présente plusieurs avantages, comme la préservation élevée des échantillons biologiques et la possibilité

d'effectuer des études de cryocorrélation avec la microscopie cryo-électronique ou la tomographie cryo-électronique.

Pour la SMLM à température cryogénique, des fluorophores efficacement commutables, subissant une commutation très complète, sont nécessaires, mais la dynamique est entravée à température cryogénique et il est donc difficile de trouver des fluorophores appropriés. Les protéines fluorescentes présentent un avantage par rapport aux fluorophores dont la commutation repose sur la diffusion de molécules tampons, car la diffusion est entravée en dessous de la température de transition vitreuse. Cependant, la dynamique des protéines fluorescentes est également entravée à température cryogénique et il est difficile de trouver une protéine efficacement commutable.

De nombreuses protéines fluorescentes se sont révélées photosensibles à température cryogénique, mais l'efficacité de la commutation doit encore être améliorée. Pour se rapprocher de cet objectif, les mécanismes de commutation des protéines fluorescentes à température cryogénique sont étudiés dans ce travail. Selon les travaux de Tuijtel et al. (2019), rsEGFP2 semble être un marqueur fluorescent prometteur avec une vitesse de commutation plus élevée que les autres variants étudiés. En outre, ils ont observé une cinétique de commutation similaire pour les variants qu'ils ont étudiés. Cela pourrait suggérer qu'il pourrait y avoir un mécanisme de commutation à température cryogénique qui est général à ces protéines fluorescentes et à d'autres similaires, ce qui serait d'un grand intérêt. Compte tenu des études de Hoffman et al. (2020), mEmerald est également un candidat prometteur pour les applications basées sur la photocommutation à température cryogénique.

Une approche possible pour obtenir des protéines fluorescentes qui photo-commutent efficacement à température cryogénique consiste à les muter afin d'améliorer leur photocommutation. Une autre approche consiste à tester les propriétés de commutation de protéines fluorescentes déjà existantes et à optimiser des conditions, comme par exemple le schéma d'illumination. Dans les deux cas, il est essentiel de comprendre le

mécanisme de commutation sous-jacent pour l'améliorer de manière optimale.

Résultats et discussion :

Nous avons mené des études spectroscopiques et structurales principalement sur la protéine fluorescente rsEGFP2, mais aussi sur rsEGFP2-V151A, rsEGFP2-V151L, mEmerald et EGFP à température cryogénique et à température ambiante afin de comprendre leurs mécanismes de commutation et nous avons développé une stratégie d'illumination pour améliorer l'efficacité du retour de l'état photocommuté à l'état fluorescent à température cryogénique. Nous avons d'abord concentré nos recherches sur rsEGFP2, qui est connu pour être un commutateur rapide à température ambiante (Grotjohann et al., 2012), car nous avons anticipé que la commutation à température cryogénique serait également relativement rapide pour cette protéine.

Nous avons mesuré des séries temporelles de spectres d'absorption UV-vis et de fluorescence sur des échantillons de rsEGFP2 en solution à température ambiante et à température cryogénique pendant la commutation vers l'état non fluorescent avec un laser de 488 nm sur un microspectrophotomètre. Une observation a été la vitesse fortement réduite de commutation à température cryogénique, même si des puissances laser beaucoup plus élevées ont été utilisées, ce qui est attendu en raison de la dynamique limitée en dessous de la température de transition vitreuse. L'autre observation remarquable a été le décalage vers le bleu du pic d'absorption de l'état non fluorescent à température cryogénique. Nos données de cristallographie aux rayons X recueillies à partir de cristaux de rsEGFP2, suggèrent qu'à température cryogénique, aucune isomérisation cis-trans ne se produit lors de l'illumination de 488 nm, mais que l'état off reste dans la conformation cis.

Les séries temporelles de spectres d'absorption et de fluorescence recueillies lors de l'illumination avec une lumière de 405 nm, ont montré que la récupération de l'état fluorescent était fortement réduite à température cryogénique. Alors que l'on peut récupérer jusqu'à 100 % à température ambiante, à température cryogénique seuls 25 % pouvent être ramenés à l'état fluorescent. Le niveau de récupération de l'absorbance est passé de ~25 %, obtenu avec une lumière laser de 405 nm, à ~50 % en utilisant le laser de 355 nm. Nous avons constaté la présence de deux états non fluorescents dont l'un ne peut être récupéré que par la lumière UV et est décalé vers le bleu (Off_2) par rapport à l'autre état non fluorescent (Off_1) qui peut être récupéré par les deux lasers.

Si l'on considère l'ensemble des résultats, on peut conclure qu'à température cryogénique, rsEGFP2 adopte un mécanisme de commutation différent de celui à température ambiante. Au lieu de changer sa conformation de cis à trans, l'état fluorescent se transforme en deux états non fluorescents différents (Off_1 et Off_2) en conformation cis avec des spectres d'absorption différents, tous deux décalés vers le bleu par rapport à l'état off à température ambiante. Off_1 est récupérable avec une lumière de 405 nm et 355 nm et Off_2 seulement avec une lumière de 355 nm. Par conséquent, une meilleure récupération totale est obtenue avec ce dernier laser. Ce résultat a été confirmé au niveau de la molécule unique. Il se peut que l'état triplet soit un état intermédiaire des états radicaux qui peuvent se former lors de la cryo-commutation. L'utilisation d'un laser de 355 nm pourrait améliorer l'efficacité du marquage dans les applications SMLM à température cryogénique.

Comme aucune différence dans la vitesse de commutation de l'état on à l'état off n'a été observée en fonction du pH, nous estimons peu probable que le mécanisme de commutation conduisant à ces états non fluorescents soit basé sur la protonation du chromophore. Nous supposons plutôt que le transfert d'électrons joue un rôle. Cette hypothèse est soutenue par des expériences récentes menées par Dr. Oleksandr Glushonkov, qui montrent

que la commutation de rsEGFP2 de l'état fluorescent à l'état off et vice versa est accélérée si la protéine est intégrée dans de l'alcool polyvinylique (PVA) au lieu de glycérol (version révisée Mantovanelli et al., 2022, en préparation).

Ce mécanisme de cryo-commutation pourrait être général pour de nombreuses protéines de la famille GFP, car le comportement observé dans les investigations spectroscopiques de rsEGFP2 a également été observé pour les autres protéines testées - mEmerald et EGFP. De plus, Tuijtel et al. (2019) ont observé une cinétique similaire à température cryogénique pour de nombreuses protéines fluorescentes différentes, notamment pour Padron et PA-GFP, qui présentent un mécanisme de commutation différent à température ambiante.

Dans un autre projet de notre groupe, le contraste de commutation de rsEGFP2 et rsFolder2 à température ambiante a été amélioré par l'application de mutations ponctuelles au niveau du résidu V151. Dans ce travail, deux états non fluorescents différents ont également été identifiés. Nous discutons de l'hypothèse selon laquelle deux populations initiales à l'état fluorescent pourraient être à l'origine des deux états non fluorescents à température ambiante et température cryogénique.

Nous proposons le modèle illustré à la Figure 62, le mécanisme principal étant représenté dans le cercle intérieur, montrant la commutation entre deux états fluorescents On_1 et On_2, qui ne s'échangent pas, et qui pourraient passer à Off_1 et Off_2 par transfert d'électrons. Les états non fluorescents pourraient revenir par le même mécanisme. Ils pourraient se relaxer partiellement par voie thermique.

Nos données seraient en outre cohérentes avec la partie inférieure du modèle (Figure 62, cercle extérieur). Si suffisamment de protons sont présents dans le tampon, une fraction de molécules protonées en conformation cis pourrait également être formée, qui pourrait ensuite passer à un troisième état fluorescent On_3. Lors de l'illumination avec une lumière laser de 488 nm, une fraction mineure de molécules pourrait être capable de subir une isomérisation cis-trans comme à température ambiante et

ensuite être commutée lors de la déprotonation vers l'état fluorescent On_{trans}.

Il serait très intéressant de confirmer que EGFP et mEmerald subissent le même mécanisme de cryocommutation que rsEGFP2, comme le suggèrent nos données spectroscopiques. En outre, d'autres protéines fluorescentes devraient être étudiées afin de déterminer dans quelle mesure le mécanisme de cryocommutation de rsEGFP2 est général.

Pour révéler plus de détails sur les états fluorescents et non fluorescents, également pour rsEGFP2, il pourrait être utile d'obtenir des données cristallographiques à haute résolution de ces états afin d'identifier de légères différences dans la densité électronique des états fluorescents et non fluorescents ou entre les états non fluorescents. En outre, des recherches supplémentaires devraient être menées sur l'implication de l'état triplet dans le mécanisme de commutation en attachant différents extincteurs d'état triplet et en confirmant par des mesures de durée de vie qu'ils éteignent effectivement l'état triplet.

Bibliography

Adam, V., Berardozzi, R., Byrdin, M., & Bourgeois, D. (2014). Phototransformable fluorescent proteins: Future challenges. *Current Opinion in Chemical Biology*, *20*, 92–102. https://doi.org/10.1016/j.cbpa.2014.05.016

Adam, V., Hadjidemetriou, K., Jensen, N., Shoeman, R. L., Woodhouse, J., Aquila, A., Banneville, A., Barends, T. R. M., Bezchastnov, V., Boutet, S., Byrdin, M., Cammarata, M., Carbajo, S., Eleni Christou, N., Coquelle, N., de la Mora, E., el Khatib, M., Moreno Chicano, T., Bruce Doak, R., … Weik, M. (2022). Rational Control of Off-State Heterogeneity in a Photoswitchable Fluorescent Protein Provides Switching Contrast Enhancement**. *ChemPhysChem*, *23*(19). https://doi.org/10.1002/cphc.202200192

Adam, V., Lelimousin, M., Boehme, S., Desfonds, G., Nienhaus, K., Field, M. J., Wiedenmann, J., McSweeney, S., Nienhaus, G. U., & Bourgeois, D. (2008). Structural characterization of IrisFP, an optical highlighter undergoing multiple photo-induced transformations. *Proceedings of the National Academy of Sciences*, *105*(47), 18343–18348. https://doi.org/10.1073/pnas.0805949105

Afzelius, B. A., & Maunsbach, A. B. (2004). Biological untrastructure research; the first 50 years. In *Tissue and Cell* (Vol. 36, Issue 2, pp. 83–94). Elsevier Ltd. https://doi.org/10.1016/j.tice.2003.11.001

Ando, R., Mizuno, H., & Miyawaki, A. (2004). Regulated Fast Nucleocytoplasmic Shuttling Observed by Reversible Protein Highlighting. *Science*, *306*(5700), 1370–1373. https://doi.org/10.1126/science.1102506

Andresen, M., Stiel, A. C., Fölling, J., Wenzel, D., Schönle, A., Egner, A., Eggeling, C., Hell, S. W., & Jakobs, S. (2008). Photoswitchable fluorescent proteins enable monochromatic multilabel imaging and dual color fluorescence nanoscopy. *Nature Biotechnology*, *26*(9), 1035–1040. https://doi.org/10.1038/nbt.1493

Andresen, M., Stiel, A. C., Trowitzsch, S., Weber, G., Eggeling, C., Wahl, M. C., Hell, S. W., & Jakobs, S. (2007). Structural basis for reversible photoswitching in Dronpa. *Proceedings of the National Academy of Sciences*, *104*(32), 13005–13009. https://doi.org/10.1073/pnas.0700629104

Andresen, M., Wahl, M. C., Stiel, A. C., Schäfer, L. v, Trowitzsch, S., Weber, G., Eggeling, C., Grubmüller, H., Hell, S. W., & Jakobs, S. (2005). *Structure and mechanism of the reversible photoswitch of a fluorescent protein*. www.pnas.orgcgidoi10.1073pnas.0502772102

Betzig, E., Patterson, G. H., Sougrat, R., Lindwasser, O. W., Olenych, S., Bonifacino, J. S., Davidson, M. W., Lippincott-Schwartz, J., & Hess, H. F. (2006). Imaging Intracellular Fluorescent Proteins at Nanometer Resolution. *Science*, *313*(5793), 1642–1645. https://doi.org/10.1126/science.1127344

Bizzarri, R., Nifosì, R., Abbruzzetti, S., Rocchia, W., Guidi, S., Arosio, D., Garau, G., Campanini, B., Grandi, E., Ricci, F., Viappiani, C., & Beltram, F. (2007).

Green Fluorescent Protein Ground States: The Influence of a Second Protonation Site near the Chromophore. *Biochemistry*, *46*(18), 5494–5504. https://doi.org/10.1021/bi602646r

Bizzarri, R., Serresi, M., Cardarelli, F., Abbruzzetti, S., Campanini, B., Viappiani, C., & Beltram, F. (2010). Single Amino Acid Replacement Makes Aequorea victoria Fluorescent Proteins Reversibly Photoswitchable. *Journal of the American Chemical Society*, *132*(1), 85–95. https://doi.org/10.1021/ja9014953

Bourgeois, D., & Adam, V. (2012). Reversible photoswitching in fluorescent proteins: A mechanistic view. In *IUBMB Life* (Vol. 64, Issue 6, pp. 482–491). https://doi.org/10.1002/iub.1023

Brakemann, T., Stiel, A. C., Weber, G., Andresen, M., Testa, I., Grotjohann, T., Leutenegger, M., Plessmann, U., Urlaub, H., Eggeling, C., Wahl, M. C., Hell, S. W., & Jakobs, S. (2011). A reversibly photoswitchable GFP-like protein with fluorescence excitation decoupled from switching. *Nature Biotechnology*, *29*(10), 942–947. https://doi.org/10.1038/nbt.1952

Brakemann, T., Weber, G., Andresen, M., Groenhof, G., Stiel, A. C., Trowitzsch, S., Eggeling, C., Grubmüller, H., Hell, S. W., Wahl, M. C., & Jakobs, S. (2010). Molecular Basis of the Light-driven Switching of the Photochromic Fluorescent Protein Padron. *Journal of Biological Chemistry*, *285*(19), 14603–14609. https://doi.org/10.1074/jbc.M109.086314

Brejc, K., Sixma, T. K., Kitts, P. A., Kain, S. R., Tsien, R. Y., Ormo, M., & James Remington, S. (1997). *Structural Basis for Dual Excitation and Photoisomerization of the Aequorea victoria Green Fluorescent Protein. PNAS* (Vol. 94, Issue 6).

Brünger, A. T. (1992). Free R value: a novel statistical quantity for assessing the accuracy of crystal structures. *Nature*, *355*(6359), 472–475. https://doi.org/10.1038/355472a0

Brunger, A. T. (2007). Version 1.2 of the crystallography and nmr system. *Nature Protocols*, *2*(11), 2728–2733. https://doi.org/10.1038/nprot.2007.406

Brunger, A. T., Adams, P. D., Marius Clore, G., Delano, W. L., Gros, P., Grosse-kunstleve, R. W., Jiang, J., Kuszewski, fJOHN, Nilges, M., Pannu, N. S., Read, R. J., Rice, L. M., Simonson, T., & Warren, G. L. (1998). Crystallography & NMR System: A New Software Suite for Macromolecular Structure Determination. In *Acta Cryst* (Vol. 54, pp. 905-921).

Byrdin, M., & Bourgeois, D. (2016). The CAL(AI)2DOSCOPE: A Microspectrophotometer for Accurate Recording of Correlated Absorbance and Fluorescence Emission Spectra. *Spectroscopy Europe*, 14–17.

Byrdin, M., Duan, C., Bourgeois, D., & Brettel, K. (2018). A Long-Lived Triplet State Is the Entrance Gateway to Oxidative Photochemistry in Green Fluorescent Proteins. *Journal of the American Chemical Society*, *140*(8), 2897–2905. https://doi.org/10.1021/jacs.7b12755

Chalfie, M., Tu, Y., Euskirchen, G., Ward, W. W., & Prasher, D. C. (1994). Green Fluorescent Protein as a Marker for Gene Expression. *Science*, *263*(5148), 802–805. https://doi.org/10.1126/science.8303295

Chang, Y.-W., Chen, S., Tocheva, E. I., Treuner-Lange, A., Löbach, S., Søgaard-Andersen, L., & Jensen, G. J. (2014). Correlated cryogenic photoactivated localization microscopy and cryo-electron tomography. *Nature Methods*, *11*(7), 737–739. https://doi.org/10.1038/nmeth.2961

Chang, R. (2000), Physical chemistry for the chemical and biological sciences. *University Science Books* (Vol. 1).

Chattoraj, M., King, B. A., Bublitz, G. U., & Boxer, S. G. (1996). *Ultra-Fast Excited State Dynamics in Green Fluorescent Protein: Multiple States and Proton Transfer* (Vol. 93, Issue 16).

Cody, C. W., Prasherj1·4, D. C., Westler, W. M., Prendergast, F. G., & Ward, W. W. (1993). Chemical Structure of the Hexapeptide Chromophore of the Aequorea Green-Fluorescent Protein^. In *Biochemistry* (Vol. 32). https://pubs.acs.org/sharingguidelines

Coquelle, N., Sliwa, M., Woodhouse, J., Schirò, G., Adam, V., Aquila, A., Barends, T. R. M., Boutet, S., Byrdin, M., Carbajo, S., de la Mora, E., Doak, R. B., Feliks, M., Fieschi, F., Foucar, L., Guillon, V., Hilpert, M., Hunter, M. S., Jakobs, S., … Weik, M. (2018). Chromophore twisting in the excited state of a photoswitchable fluorescent protein captured by time-resolved serial femtosecond crystallography. *Nature Chemistry*, *10*(1), 31–37. https://doi.org/10.1038/nchem.2853

Cormack, B. P., Valdivia, R. H., & Falkow, S. (1996). FACS-optimized mutants of the green fluorescent protein (GFP) (GFP mutation; FITC; fluorescence-activated cell sorter; fluorescence intensity). In *Gene* (Vol. 173).

Crameri, A., Whitehorn, E. A., Tate, E., & Stemmer, W. P. C. (1996). Improved Green Fluorescent Protein by Molecular Evolution Using DNA Shuffling. *Nature Biotechnology*, *14*(3), 315–319. https://doi.org/10.1038/nbt0396-315

Creemers, T. M. H., Lock, A. J., Subramaniam, V., Jovin, T. M., & Völker, S. (1999). Three photoconvertible forms of green fluorescent protein identified by spectral hole-burning. *Nature Structural Biology*, *6*(6), 557–560. https://doi.org/10.1038/9335

Creemers, T. M. H., Lock, A. J., Subramaniam, V., Jovin, T. M., & Völker, S. (2000). Photophysics and optical switching in green fluorescent protein mutants. *Proceedings of the National Academy of Sciences*, *97*(7), 2974–2978. https://doi.org/10.1073/pnas.050365997

Cubitt, A. B., Woollenweber, L. A., & Heim, R. (1999). *Understandmg S tructure-Function Relationsbps in the Aequorea victoria Green Fluorescent Protein*.

Dahlberg, P. D., & Moerner, W. E. (2021). Cryogenic Super-Resolution Fluorescence and Electron Microscopy Correlated at the Nanoscale. *Annual Review of Physical Chemistry*, *72*(1), 253–278. https://doi.org/10.1146/annurev-physchem-090319-051546

Dahlberg, P. D., Sartor, A. M., Wang, J., Saurabh, S., Shapiro, L., & Moerner, W. E. (2018). Identification of PAmKate as a Red Photoactivatable Fluorescent Protein for Cryogenic Super-Resolution Imaging. *Journal of the American Chemical Society*, *140*(39), 12310–12313. https://doi.org/10.1021/jacs.8b05960

Dahlberg, P. D., Saurabh, S., Sartor, A. M., Wang, J., Mitchell, P. G., Chiu, W., Shapiro, L., & Moerner, W. E. (2020). Cryogenic single-molecule fluorescence annotations for electron tomography reveal in situ organization of key proteins in *Caulobacter*. *Proceedings of the National Academy of Sciences*, *117*(25), 13937–13944. https://doi.org/10.1073/pnas.2001849117

Day, R. N., & Davidson, M. W. (2009). The fluorescent protein palette: Tools for cellular imaging. *Chemical Society Reviews*, *38*(10), 2887–2921. https://doi.org/10.1039/b901966a

Delagrave, S., Hawtin, R. E., Silva, C. M., Yang, M. M., & Youvan, D. C. (1995). Red-Shifted Excitation Mutants of the Green Fluorescent Protein. *Nature Biotechnology*, *13*(2), 151–154. https://doi.org/10.1038/nbt0295-151

Dertinger, T., Colyer, R., Iyer, G., Weiss, S., & Enderlein, J. (2009). Fast, background-free, 3D super-resolution optical fluctuation imaging (SOFI). *Proceedings of the National Academy of Sciences*, *106*(52), 22287–22292. https://doi.org/10.1073/pnas.0907866106

De Zitter, E., Thédié, D., Mönkemöller, V., Hugelier, S., Beaudouin, J., Adam, V., Byrdin, M., van Meervelt, L., Dedecker, P., & Bourgeois, D. (2019). Mechanistic investigation of mEos4b reveals a strategy to reduce track interruptions in sptPALM. *Nature Methods*, *16*(8), 707–710. https://doi.org/10.1038/s41592-019-0462-3

Dickson, R. M., Cubitt, A. B., Tsien, R. Y., & Moerner, W. E. (1997). On/off blinking and switching behaviour of single molecules of green fluorescent protein. *Nature*, *388*(6640), 355–358. https://doi.org/10.1038/41048

Dubochet, J., Adrian, M., Chang, J.-J., Homo, J.-C., Lepault, J., McDowall, A. W., & Schultz, P. (1988). Cryo-electron microscopy of vitrified specimens. *Quarterly Reviews of Biophysics*, *21*(2), 129–228. https://doi.org/10.1017/S0033583500004297

Dubochet, J., Lepault, J., Freeman, R., Berriman, J. A., & Homo, J.-C. (1982). Electron microscopy of frozen water and aqueous solutions. *Journal of Microscopy*, *128*(3), 219–237. https://doi.org/10.1111/j.1365-2818.1982.tb04625.x

El Khatib, M., Martins, A., Bourgeois, D., Colletier, J. P., & Adam, V. (2016). Rational design of ultrastable and reversibly photoswitchable fluorescent proteins for super-resolution imaging of the bacterial periplasm. *Scientific Reports*, *6*. https://doi.org/10.1038/srep18459

Elowitz, M. B., Surette, M. G., Wolf, P.-E., Stock, J., & Leibler, S. (1997). Photoactivation turns green fluorescent protein red. *Current Biology*, *7*(10), 809–812. https://doi.org/10.1016/S0960-9822(06)00342-3

Emsley, P., Lohkamp, B., Scott, W. G., & Cowtan, K. (2010). Features and development of *Coot*. *Acta Crystallographica Section D Biological Crystallography*, *66*(4), 486–501. https://doi.org/10.1107/S0907444910007493

Evans, P. R., & Murshudov, G. N. (2013). How good are my data and what is the resolution? *Acta Crystallographica Section D Biological Crystallography*, *69*(7), 1204–1214. https://doi.org/10.1107/S0907444913000061

Gehenio, M. P., & Luyet, B. J. (1940). *Life and death at low temperatures, by B. J. Luyet ... and P. M. Gehenio ...* Biodynamica,. https://doi.org/10.5962/bhl.title.6570

Giske, A. (2007). *CryoSTED microscopy A new spectroscopic approach for improving the resolution of STED microscopy using low temperature*.

Grotjohann, T., Testa, I., Leutenegger, M., Bock, H., Urban, N. T., Lavoie-Cardinal, F., Willig, K. I., Eggeling, C., Jakobs, S., & Hell, S. W. (2011). Diffraction-unlimited all-optical imaging and writing with a photochromic GFP. *Nature*, *478*(7368), 204–208. https://doi.org/10.1038/nature10497

Grotjohann, T., Testa, I., Reuss, M., Brakemann, T., Eggeling, C., Hell, S. W., & Jakobs, S. (2012). rsEGFP2 enables fast RESOLFT nanoscopy of living cells. *ELife*, *1*. https://doi.org/10.7554/eLife.00248

Gunewardene, M. S., Subach, F. V., Gould, T. J., Penoncello, G. P., Gudheti, M. V., Verkhusha, V. V., & Hess, S. T. (2011). Superresolution Imaging of Multiple Fluorescent Proteins with Highly Overlapping Emission Spectra in Living Cells. *Biophysical Journal*, *101*(6), 1522–1528. https://doi.org/10.1016/j.bpj.2011.07.049

Ha, T., & Tinnefeld, P. (2012). Photophysics of fluorescent probes for single-molecule biophysics and super-resolution imaging. In *Annual Review of Physical Chemistry* (Vol. 63, pp. 595–617). https://doi.org/10.1146/annurev-physchem-032210-103340

Heim, R., & Tsien, R. Y. (1996). Engineering green fluorescent protein for improved brightness, longer wavelengths and fluorescence resonance energy transfer. *Current Biology*, *6*(2), 178–182. https://doi.org/10.1016/S0960-9822(02)00450-5

Hell, S. W., Dyba, M., & Jakobs, S. (2004). Concepts for nanoscale resolution in fluorescence microscopy. *Current Opinion in Neurobiology*, *14*(5), 599–609. https://doi.org/10.1016/j.conb.2004.08.015

Hell, S. W., & Wichmann, J. (1994). Breaking the diffraction resolution limit by stimulated emission: stimulated-emission-depletion fluorescence microscopy. *Optics Letters*, *19*(11), 780. https://doi.org/10.1364/OL.19.000780

Henderson, J. N., Ai, H., Campbell, R. E., & Remington, S. J. (2007). Structural basis for reversible photobleaching of a green fluorescent protein homologue. *Proceedings of the National Academy of Sciences*, *104*(16), 6672–6677. https://doi.org/10.1073/pnas.0700059104

Henrikus, S. S., Tassis, K., Zhang, L., Velde, J. H. M., Gebhardt, C., Herrmann, A., Jung, G., & Cordes, T. (2021). Characterization of Fluorescent Proteins with Intramolecular Photostabilization**. *ChemBioChem*, *22*(23), 3283–3291. https://doi.org/10.1002/cbic.202100276

Hoffman, D. P., Shtengel, G., Xu, C. S., Campbell, K. R., Freeman, M., Wang, L., Milkie, D. E., Pasolli, H. A., Iyer, N., Bogovic, J. A., Stabley, D. R., Shirinifard, A., Pang, S., Peale, D., Schaefer, K., Pomp, W., Chang, C. L., Lippincott-Schwartz, J., Kirchhausen, T., … Hess, H. F. (2020). Correlative three-dimensional super-resolution and block-face electron microscopy of whole vitreously frozen cells. *Science*, *367*(6475). https://doi.org/10.1126/science.aaz5357

Hofmann, M., Eggeling, C., Jakobs, S., & Hell, S. W. (2005). Breaking the diffraction barrier in fluorescence microscopy at low light intensities by using reversibly photoswitchable proteins. *Proceedings of the National Academy of Sciences*, *102*(49), 17565–17569. https://doi.org/10.1073/pnas.0506010102

Hulleman, C. N., Li, W., Gregor, I., Rieger, B., & Enderlein, J. (2018). Photon Yield Enhancement of Red Fluorophores at Cryogenic Temperatures. *ChemPhysChem*, *19*(14), 1774–1780. https://doi.org/10.1002/cphc.201800131

Kabsch, W. (2001) Chapter 11.3. *Integration, scaling, space-group assignment and post refinement* in *International Tables for Crystallography*, Volume F. Crystallography of Biological Macromolecules, Rossmann, M.G. and Arnold, E. (2001). Editors. Dordrecht: Kluwer Academic Publishers.

Kaufmann, R., Schellenberger, P., Seiradake, E., Dobbie, I. M., Jones, E. Y., Davis, I., Hagen, C., & Grünewald, K. (2014). Super-Resolution Microscopy Using Standard Fluorescent Proteins in Intact Cells under Cryo-Conditions. *Nano Letters*, *14*(7), 4171–4175. https://doi.org/10.1021/nl501870p

Klar, T. A., & Hell, S. W. (1999). Subdiffraction resolution in far-field fluorescence microscopy. *Optics Letters*, *24*(14), 954. https://doi.org/10.1364/OL.24.000954

Kneen, M., Farinas, J., Li, Y., & Verkman, A. S. (1998). Green Fluorescent Protein as a Noninvasive Intracellular pH Indicator. *Biophysical Journal*, *74*(3), 1591–1599. https://doi.org/10.1016/S0006-3495(98)77870-1

Kremers, G.-J., Goedhart, J., van Munster, E. B., & Gadella, T. W. J. (2006). Cyan and Yellow Super Fluorescent Proteins with Improved Brightness, Protein Folding, and FRET Förster Radius ˈ. *Biochemistry*, *45*(21), 6570–6580. https://doi.org/10.1021/bi0516273

Krug, M., Weiss, M. S., Heinemann, U., & Mueller, U. (2012). XDSAPP: a graphical user interface for the convenient processing of diffraction data using XDS. *Journal of Applied Crystallography*, *45*(3), 568–572. https://doi.org/10.1107/S0021889812011715

Laptenok, S. P., Gil, A. A., Hall, C. R., Lukacs, A., Iuliano, J. N., Jones, G. A., Greetham, G. M., Donaldson, P., Miyawaki, A., Tonge, P. J., & Meech, S. R. (2018). Infrared spectroscopy reveals multi-step multi-timescale

photoactivation in the photoconvertible protein archetype dronpa. *Nature Chemistry*, *10*(8), 845–852. https://doi.org/10.1038/s41557-018-0073-0

Liu, B., Xue, Y., Zhao, W., Chen, Y., Fan, C., Gu, L., Zhang, Y., Zhang, X., Sun, L., Huang, X., Ding, W., Sun, F., Ji, W., & Xu, T. (2015). Three-dimensional super-resolution protein localization correlated with vitrified cellular context. *Scientific Reports*, *5*(1), 13017. https://doi.org/10.1038/srep13017

Liu, R. S., & Asato, A. E. (1985). The primary process of vision and the structure of bathorhodopsin: a mechanism for photoisomerization of polyenes. *Proceedings of the National Academy of Sciences*, *82*(2), 259–263. https://doi.org/10.1073/pnas.82.2.259

Li, W., Stein, S. C., Gregor, I., & Enderlein, J. (2015). Ultra-stable and versatile widefield cryo-fluorescence microscope for single-molecule localization with sub-nanometer accuracy. *Optics Express*, *23*(3), 3770. https://doi.org/10.1364/OE.23.003770

Lukyanov, K. A., Fradkov, A. F., Gurskaya, N. G., Matz, M. v., Labas, Y. A., Savitsky, A. P., Markelov, M. L., Zaraisky, A. G., Zhao, X., Fang, Y., Tan, W., & Lukyanov, S. A. (2000). Natural Animal Coloration Can Be Determined by a Nonfluorescent Green Fluorescent Protein Homolog. *Journal of Biological Chemistry*, *275*(34), 25879–25882. https://doi.org/10.1074/jbc.C000338200

Marchant, J. S., Stutzmann, G. E., Leissring, M. A., LaFerla, F. M., & Parker, I. (2001). Multiphoton-evoked color change of DsRed as an optical highlighter for cellular and subcellular labeling. *Nature Biotechnology*, *19*(7), 645–649. https://doi.org/10.1038/90249

Matz, M. v., Fradkov, A. F., Labas, Y. A., Savitsky, A. P., Zaraisky, A. G., Markelov, M. L., & Lukyanov, S. A. (1999). Fluorescent proteins from nonbioluminescent Anthozoa species. *Nature Biotechnology*, *17*(10), 969–973. https://doi.org/10.1038/13657

Mazal, H., Wieser, F.-F., & Sandoghdar, V. (2022). Deciphering a hexameric protein complex with Angstrom optical resolution. *ELife*, *11*. https://doi.org/10.7554/eLife.76308

McAnaney, T. B., Zeng, W., Doe, C. F. E., Bhanji, N., Wakelin, S., Pearson, D. S., Abbyad, P., Shi, X., Boxer, S. G., & Bagshaw, C. R. (2005). Protonation, Photobleaching, and Photoactivation of Yellow Fluorescent Protein (YFP 10C): A Unifying Mechanism. *Biochemistry*, *44*(14), 5510–5524. https://doi.org/10.1021/bi047581f

McKinney, S. A., Murphy, C. S., Hazelwood, K. L., Davidson, M. W., & Looger, L. L. (2009). A bright and photostable photoconvertible fluorescent protein. *Nature Methods*, *6*(2), 131–133. https://doi.org/10.1038/nmeth.1296

Merzlyak, E. M., Goedhart, J., Shcherbo, D., Bulina, M. E., Shcheglov, A. S., Fradkov, A. F., Gaintzeva, A., Lukyanov, K. A., Lukyanov, S., Gadella, T. W. J., & Chudakov, D. M. (2007). Bright monomeric red fluorescent protein with an extended fluorescence lifetime. *Nature Methods*, *4*(7), 555–557. https://doi.org/10.1038/nmeth1062

Mizuno, H., Mal, T. K., Wälchli, M., Kikuchi, A., Fukano, T., Ando, R., Jeyakanthan, J., Taka, J., Shiro, Y., Ikura, M., & Miyawaki, A. (2008). Light-dependent regulation of structural flexibility in a photochromic fluorescent protein. *Proceedings of the National Academy of Sciences*, *105*(27), 9227–9232. https://doi.org/10.1073/pnas.0709599105

Möckl, L., Lamb, D. C., & Bräuchle, C. (2014). Super-resolved Fluorescence Microscopy: Nobel Prize in Chemistry 2014 for Eric Betzig, Stefan Hell, and William E. Moerner. *Angewandte Chemie International Edition*, *53*(51), 13972–13977. https://doi.org/10.1002/anie.201410265

Moser, F., Pražák, V., Mordhorst, V., Andrade, D. M., Baker, L. A., Hagen, C., Grünewald, K., & Kaufmann, R. (2019). Cryo-SOFI enabling low-dose super-resolution correlative light and electron cryo-microscopy. *Proceedings of the National Academy of Sciences*, *116*(11), 4804–4809. https://doi.org/10.1073/pnas.1810690116

Nahmani, M., Lanahan, C., DeRosier, D., & Turrigiano, G. G. (2017). High-numerical-aperture cryogenic light microscopy for increased precision of superresolution reconstructions. *Proceedings of the National Academy of Sciences*, *114*(15), 3832–3836. https://doi.org/10.1073/pnas.1618206114

Ormö, M., Cubitt, A. B., Kallio, K., Gross, L. A., Tsien, R. Y., & Remington, S. J. (1996). Crystal Structure of the Aequorea victoria Green Fluorescent Protein. *Science*, *273*(5280), 1392–1395. https://doi.org/10.1126/science.273.5280.1392

Paez-Segala, M. G., Sun, M. G., Shtengel, G., Viswanathan, S., Baird, M. A., Macklin, J. J., Patel, R., Allen, J. R., Howe, E. S., Piszczek, G., Hess, H. F., Davidson, M. W., Wang, Y., & Looger, L. L. (2015). Fixation-resistant photoactivatable fluorescent proteins for CLEM. *Nature Methods*, *12*(3), 215–218. https://doi.org/10.1038/nmeth.3225

Patterson, G. H., & Lippincott-Schwartz, J. (2002). A Photoactivatable GFP for Selective Photolabeling of Proteins and Cells. *Science*, *297*(5588), 1873–1877. https://doi.org/10.1126/science.1074952

Pédelacq, J. D., Cabantous, S., Tran, T., Terwilliger, T. C., & Waldo, G. S. (2006). Engineering and characterization of a superfolder green fluorescent protein. *Nature Biotechnology*, *24*(1), 79–88. https://doi.org/10.1038/nbt1172

Potterton, L., Agirre, J., Ballard, C., Cowtan, K., Dodson, E., Evans, P. R., Jenkins, H. T., Keegan, R., Krissinel, E., Stevenson, K., Lebedev, A., McNicholas, S. J., Nicholls, R. A., Noble, M., Pannu, N. S., Roth, C., Sheldrick, G., Skubak, P., Turkenburg, J., … Wojdyr, M. (2018). CCP4i2: the new graphical user interface to the CCP4 program suite. *Acta Crystallographica Section D Structural Biology*, *74*(2), 68–84. https://doi.org/10.1107/S2059798317016035

Prasher, D. C., Eckenrode, V. K., Ward, W. W., Prendergast, F. G., & Cormier, M. J. (1992). Primary structure of the Aequorea victoria green-fluorescent protein. *Gene*, *111*(2), 229–233. https://doi.org/10.1016/0378-1119(92)90691-H

Rane, L., Wulffele, J., Bourgeois, D., Glushonkov, O., Mantovanelli, A. M. R., Zala, N., Byrdin, M. (2023). Light-Induced Forward and Reverse Intersystem Crossing in Green Fluorescent Proteins at Cryogenic Temperatures. *J. Phys. Chem. B*. https://doi.org/10.1021/acs.jpcb.3c02971

Regis Faro, A., Adam, V., Carpentier, P., Darnault, C., Bourgeois, D., & de Rosny, E. (2010). Low-temperature switching by photoinduced protonation in photochromic fluorescent proteins. *Photochemical and Photobiological Sciences*, *9*(2), 254–262. https://doi.org/10.1039/b9pp00121b

Regis Faro, A., Carpentier, P., Jonasson, G., Pompidor, G., Arcizet, D., Demachy, I., & Bourgeois, D. (2011). Low-Temperature Chromophore Isomerization Reveals the Photoswitching Mechanism of the Fluorescent Protein Padron. *Journal of the American Chemical Society*, *133*(41), 16362–16365. https://doi.org/10.1021/ja207001y

Rust, M. J., Bates, M., & Zhuang, X. (2006). Sub-diffraction-limit imaging by stochastic optical reconstruction microscopy (STORM). *Nature Methods*, *3*(10), 793–796. https://doi.org/10.1038/nmeth929

Sartori, A., Gatz, R., Beck, F., Rigort, A., Baumeister, W., & Plitzko, J. M. (2007). Correlative microscopy: Bridging the gap between fluorescence light microscopy and cryo-electron tomography. *Journal of Structural Biology*, *160*(2), 135–145. https://doi.org/10.1016/j.jsb.2007.07.011

Sawin, K. E., & Nurse, P. (1997). Photoactivation of green fluorescent protein. *Current Biology*, *7*(10), R606–R607.

Schrödinger, L., & DeLano, W. (2020). *PyMOL*. Retrieved from http://www.pymol.org/pymol

Schwartz, C. L., Sarabash, V. I., Ataullakhanov, F. I., McIntosh, J. R., & Nicastro, D. (2007). Cryo-fluorescence microscopy facilitates correlations between light and cryo-electron microscopy and reduces the rate of photobleaching. *Journal of Microscopy*, *227*(2), 98–109. https://doi.org/10.1111/j.1365-2818.2007.01794.x

Shaner, N. C., Lambert, G. G., Chammas, A., Ni, Y., Cranfill, P. J., Baird, M. A., Sell, B. R., Allen, J. R., Day, R. N., Israelsson, M., Davidson, M. W., & Wang, J. (2013). A bright monomeric green fluorescent protein derived from Branchiostoma lanceolatum. *Nature Methods*, *10*(5), 407–409. https://doi.org/10.1038/nmeth.2413

Shaner, N. C., Patterson, G. H., & Davidson, M. W. (2007). Advances in fluorescent protein technology. In *Journal of Cell Science* (Vol. 120, Issue 24, pp. 4247–4260). https://doi.org/10.1242/jcs.005801

Subach, O. M., Patterson, G. H., Ting, L.-M., Wang, Y., Condeelis, J. S., & Verkhusha, V. v. (2011). A photoswitchable orange-to-far-red fluorescent protein, PSmOrange. *Nature Methods*, *8*(9), 771–777. https://doi.org/10.1038/nmeth.1664

Subach, F. v, Patterson, G. H., Manley, S., Gillette, J. M., Lippincott-Schwartz, J., & Verkhusha, V. v. (2009). Photoactivatable mCherry for high-resolution

two-color fluorescence microscopy. *Nature Methods*, *6*(2), 153–159. https://doi.org/10.1038/nmeth.1298

Tanaka, K. A. K., Suzuki, K. G. N., Shirai, Y. M., Shibutani, S. T., Miyahara, M. S. H., Tsuboi, H., Yahara, M., Yoshimura, A., Mayor, S., Fujiwara, T. K., & Kusumi, A. (2010). Membrane molecules mobile even after chemical fixation. *Nature Methods*, *7*(11), 865–866. https://doi.org/10.1038/nmeth.f.314

Tsien, R. Y. (1998). THE GREEN FLUORESCENT PROTEIN. In *Annu. Rev. Biochem* (Vol. 67).

Tuijtel, M. W., Koster, A. J., Jakobs, S., Faas, F. G. A., & Sharp, T. H. (2019). Correlative cryo super-resolution light and electron microscopy on mammalian cells using fluorescent proteins. *Scientific Reports*, *9*(1), 1369. https://doi.org/10.1038/s41598-018-37728-8

Ursby, T., & Bourgeois, D. (1997). Improved Estimation of Structure-Factor Difference Amplitudesfrom Poorly Accurate Data. *Acta Crystallographica Section A Foundations of Crystallography*, *53*(5), 564–575. https://doi.org/10.1107/S0108767397004522

Vagin, A., & Teplyakov, A. (2010). Molecular replacement with MOLREP. *Acta Crystallographica Section D Biological Crystallography*, *66*(1), 22–25. https://doi.org/10.1107/S0907444909042589

Vonrhein, C., Flensburg, C., Keller, P., Sharff, A., Smart, O., Paciorek, W., Womack, T., & Bricogne, G. (2011). Data processing and analysis with the autoPROC toolbox. *Acta Crystallographica Section D: Biological Crystallography*, *67*(4), 293–302. https://doi.org/10.1107/S0907444911007773

Waldo, G. S., Standish, B. M., Berendzen, J., & Terwilliger, T. C. (1999). Rapid protein-folding assay using green fluorescent protein. *Nature Biotechnology*, *17*(7), 691–695. https://doi.org/10.1038/10904

Weisenburger, S., Boening, D., Schomburg, B., Giller, K., Becker, S., Griesinger, C., & Sandoghdar, V. (2017). Cryogenic optical localization provides 3D protein structure data with Angstrom resolution. *Nature Methods*, *14*(2), 141–144. https://doi.org/10.1038/nmeth.4141

Weisenburger, S., Jing, B., Renn, A., & Sandoghdar, V. (2013). *Cryogenic localization of single molecules with angstrom precision* (P. Verma & A. Egner, Eds.; p. 88150D). https://doi.org/10.1117/12.2025373

Whelan, D. R., & Bell, T. D. M. (2015). Image artifacts in Single Molecule Localization Microscopy: why optimization of sample preparation protocols matters. *Scientific Reports*, *5*(1), 7924. https://doi.org/10.1038/srep07924

Wiedenmann, J., Gayda, S., Adam, V., Oswald, F., Nienhaus, K., Bourgeois, D., & Nienhaus, G. U. (2011). From EosFP to mIrisFP: structure-based development of advanced photoactivatable marker proteins of the GFP-family. *Journal of Biophotonics*, *4*(6), 377–390. https://doi.org/10.1002/jbio.201000122

Wiedenmann, J., Ivanchenko, S., Oswald, F., Schmitt, F., Röcker, C., Salih, A., Spindler, K.-D., & Nienhaus, G. U. (2004). EosFP, a fluorescent marker protein with UV-inducible green-to-red fluorescence conversion. *Proceedings of the National Academy of Sciences*, *101*(45), 15905–15910. https://doi.org/10.1073/pnas.0403668101

Williams, C. J., Headd, J. J., Moriarty, N. W., Prisant, M. G., Videau, L. L., Deis, L. N., Verma, V., Keedy, D. A., Hintze, B. J., Chen, V. B., Jain, S., Lewis, S. M., Arendall, W. B., Snoeyink, J., Adams, P. D., Lovell, S. C., Richardson, J. S., & Richardson, D. C. (2018). MolProbity: More and better reference data for improved all-atom structure validation. *Protein Science*, *27*(1), 293–315. https://doi.org/10.1002/pro.3330

Wolff, G., Hagen, C., Grünewald, K., & Kaufmann, R. (2016). Towards correlative super-resolution fluorescence and electron cryo-microscopy. *Biology of the Cell*, *108*(9), 245–258. https://doi.org/10.1111/boc.201600008

Woodhouse, J., Nass Kovacs, G., Coquelle, N., Uriarte, L. M., Adam, V., Barends, T. R. M., Byrdin, M., de la Mora, E., Bruce Doak, R., Feliks, M., Field, M., Fieschi, F., Guillon, V., Jakobs, S., Joti, Y., Macheboeuf, P., Motomura, K., Nass, K., Owada, S., … Weik, M. (2020). Photoswitching mechanism of a fluorescent protein revealed by time-resolved crystallography and transient absorption spectroscopy. *Nature Communications*, *11*(1), 741. https://doi.org/10.1038/s41467-020-14537-0

Wulffele, J., Thédié, D., Glushonkov, O., & Bourgeois, D. (2022). mEos4b Photoconversion Efficiency Depends on Laser Illumination Conditions Used in PALM. *The Journal of Physical Chemistry Letters*, *13*(22), 5075–5080. https://doi.org/10.1021/acs.jpclett.2c00933

Xu, X., Xue, Y., Tian, B., Feng, F., Gu, L., Li, W., Ji, W., & Xu, T. (2018). Ultra-stable super-resolution fluorescence cryo-microscopy for correlative light and electron cryo-microscopy. *Science China Life Sciences*, *61*(11), 1312–1319. https://doi.org/10.1007/s11427-018-9380-3

Yang, B., Trebbia, J.-B., Baby, R., Tamarat, Ph., & Lounis, B. (2015). Optical nanoscopy with excited state saturation at liquid helium temperatures. *Nature Photonics*, *9*(10), 658–662. https://doi.org/10.1038/nphoton.2015.152

Yokoe, H., & Meyer, T. (1996). Spatial dynamics of GFP-tagged proteins investigated by local fluorescence enhancement. *Nature Biotechnology*, *14*(10), 1252–1256. https://doi.org/10.1038/nbt1096-1252

Zhang, G., Gurtu, V., & Kain, S. R. (1996). *An Enhanced Green Fluorescent Protein Allows Sensitive Detection of Gene Transfer in Mammalian Cells* (Vol. 227).

Zhang, L., Patel, H. N., Lappe, J. W., & Wachter, R. M. (2006). Reaction progress of chromophore biogenesis in green fluorescent protein. *Journal of the American Chemical Society*, *128*(14), 4766–4772. https://doi.org/10.1021/ja0580439

Zhang, M., Chang, H., Zhang, Y., Yu, J., Wu, L., Ji, W., Chen, J., Liu, B., Lu, J., Liu, Y., Zhang, J., Xu, P., & Xu, T. (2012). Rational design of true

monomeric and bright photoactivatable fluorescent proteins. *Nature Methods*, *9*(7), 727–729. https://doi.org/10.1038/nmeth.2021

Zimmer, M. (2009). GFP: from jellyfish to the Nobel prize and beyond. *Chemical Society Reviews*, *38*(10), 2823. https://doi.org/10.1039/b904023d

Zondervan, R., Kulzer, F., Orlinskii, S. B., & Orrit, M. (2003). Photoblinking of Rhodamine 6G in Poly(vinyl alcohol): Radical Dark State Formed through the Triplet. *The Journal of Physical Chemistry A*, *107*(35), 6770–6776. https://doi.org/10.1021/jp034723r

Acknowledgements

Photograph by the author showing the *Institut de Biologie Structurale Grenoble,* where this thesis was written.

This thesis work would not have been possible without a number of people.

First of all, I thank my supervisor Dr. Dominique Bourgeois for the dedicated guidance and very useful feedback throughout this thesis work. I was very lucky to have a supervisor who always had a helpful advice for me for any situation. Thanks to you I learned a lot during the last years.

I would like to thank my thesis jury members, Dr. Agathe Espagne, Pr. Brahim Lounis, Pr. Eve de Rosny, Pr. Marie Erard and Dr. Antoine Royant for accepting to be part of the jury and for reading my thesis.

I thank Pr. Marie Erard, Dr. Bernhard Brutscher and Dr. Hélène Malet for being part of my CSI committee and for the helpful discussions concerning my work progress.

I thank the Pixel team and those who have been in the team during the years of my thesis: Dr. Oleksandr Glushonkov, Dr. Virgile Adam, Dr. Martin Byrdin, Jip Wulffelé, Dr. Arijit Maity, Mrinalini Lianne Rao, Dr. Pascale Tacnet, Dr. Philippe Frachet, Lukas Rane, Dr. Daniel Thédié, Dr. Nina Christou, Dr. Samy Dufour and all I2SR group members for always making me feel welcome in the team and that I could ask for advice at any time. Especially, I thank Sasha, Virgile and Martin, who always did their best to answer my questions, helped me with any issues and introduced me into new work fields.

Further, I would like to thank Dr. Martin Weik and the Dynamop group for including me in the interesting work about the rsEGFP2 mutants, for welcoming me in the team and for helpful advice. Thank you, Dr. Elke de Zitter, for your help with the crystallography difference maps, Ninon Zala, for producing proteins and helping me with issues in the lab and Dr. Tadeo Moreno Chicano, for teaching me how to grow crystals.

I thank the group of Pr. Jörg Enderlein for the collaboration in the cryo-PALM project.

I would like to thank the ESRF Grenoble for providing their beamline facilities and for making the efforts to provide a remote mode during the pandemics.

Merci, Olivia Mazzilli, d'avoir résolu tout problème administratif.

Ich bedanke mich herzlich bei meiner Familie und meinen Freunden für die moralische Unterstützung während der letzten Jahre und für die Hilfe beim Korrekturlesen und Formatieren der Doktorarbeit, insbesondere für die Hilfe von Illya.

Appendix

1. Main text and Supplementary Information of the publication:

Photophysical studies at cryogenic temperature reveal a novel photo-switching mechanism of rsEGFP2

2022, *bioRxiv* preprint server for biology

(https://doi.org/10.1101/2022.08.22.504779)

Angela M. R. Mantovanelli, Oleksandr Glushonkov, Virgile Adam, Jip Wulffele, Daniel Thédié, Martin Byrdin, Ingo Gregor, Oleksii Nevskyi, Jörg Enderlein, Dominique Bourgeois

2. Main text and Supplementary Information of the publication:

Rational Control of Off-State Heterogeneity in a Photoswitchable Fluorescent Protein Provides Switching Contrast Enhancement

2022, *ChemPhysChem*, *23*(19)

(https://doi.org/10.1002/cphc.202200192)

Dr. Virgile Adam, Dr. Kyprianos Hadjidemetriou, Dr. Nickels Jensen, Dr. Robert L. Shoeman, Dr. Joyce Woodhouse, Dr. Andrew Aquila, Dr. Anne-Sophie Banneville, Dr. Thomas R. M. Barends, Dr. Victor Bezchastnov, Dr. Sébastien Boutet, Dr. Martin Byrdin, Dr. Marco Cammarata, Prof. Dr. Sergio Carbajo, Dr. Nina Eleni Christou, Dr. Nicolas Coquelle, Dr. Eugenio De la Mora, Dr. Mariam El Khatib, Dr. Tadeo Moreno Chicano, Prof. Dr. R. Bruce Doak, Prof. Dr. Franck Fieschi, Dr. Lutz Foucar, Dr. Oleksandr Glushonkov, Alexander Gorel, Dr. Marie Luise Grünbein, Mario Hilpert, Dr. Mark Hunter, Dr. Marco Kloos, Dr. Jason E. Koglin, Dr. Thomas J. Lane, Dr. Mengning Liang, Angela Mantovanelli, Dr. Karol Nass, Dr. Gabriela Nass Kovacs, Dr. Shigeki Owada, Christopher M. Roome, Dr. Giorgio Schirò, Dr. Matthew Seaberg, Miriam Stricker, Michel Thépaut, Dr. Kensuke Tono, Prof. Dr. Kiyoshi Ueda, Dr. Lucas M. Uriarte, Dr. Daehyun You, Ninon Zala, Dr. Tatiana Domratcheva, Prof. Dr. Stefan Jakobs, Dr. Michel Sliwa, Prof. Dr. Ilme Schlichting, Dr. Jacques-Philippe Colletier, Dr. Dominique Bourgeois, Dr. Martin Weik

Photophysical studies at cryogenic temperature reveal a novel photoswitching mechanism of rsEGFP2.

Angela M. R. Mantovanelli†, Oleksandr Glushonkov†, Virgile Adam†, Jip Wulffele†, Daniel Thédié†£, Martin Byrdin†, Ingo Gregor‡, Oleksii Nevskyi‡, Jörg Enderlein‡ & Dominique Bourgeois†*

† Institut de Biologie Structurale, CNRS, Université Grenoble Alpes, CEA, IBS, 38044 Grenoble, France

‡ Institute of Physics–Biophysics, Georg August University, 37077 Göttingen, Germany

ABSTRACT: Single-molecule-localization-microscopy (SMLM) at cryogenic temperature opens new avenues to investigate intact biological samples at the nanoscale and perform cryo-correlative studies. Genetically encoded fluorescent proteins (FPs) are markers of choice for cryo-SMLM, but their reduced conformational flexibility below the glass transition temperature hampers efficient photoswitching at low temperature. We investigated cryo-switching of rsEGFP2, one of the most efficient reversibly switchable fluorescent protein at ambient temperature due to facile *cis-trans* isomerization of the chromophore. UV-visible microspectrophotometry and X-ray crystallography revealed a completely different switching mechanism at ~110 K. At this cryogenic temperature, on-off photoswitching involves the formation of 2 dark states with blue shifted absorption relative to that of the *trans* protonated chromophore populated at ambient temperature. Only one of these dark states can be switched back to the fluorescent state by 405 nm light, while both of them are sensitive to UV light at 355 nm. The rsEGFP2 photoswitching mechanism discovered in this work adds to the panoply of known switching mechanisms in fluorescent proteins. It suggests that employing 355 nm light in cryo-SMLM experiments using rsEGFP2 or possibly other FPs could improve the achievable effective labeling efficiency in this technique.

INTRODUCTION

Super-resolution fluorescence microscopy has revolutionized our ability to investigate life at the nanoscale [1]. Yet, to prevent motion artifacts and facilitate labeling, many nanoscopy studies are still based on chemically fixed cells. Chemical fixation of membrane proteins remains challenging, and a number of artifacts may result from fixation that become even more detrimental as the quest for high-resolution increases [2–4]. One strategy to better preserve the fine morphological details of biological samples is to image flash-frozen cells at cryogenic temperature (CT) [5–14]. Furthermore, performing super-resolution microscopy at CT opens the door to cryo-correlative (CLEM) studies with cryo-electron microscopy [6,10,15]. In addition, CT-fluorescence imaging offers additional benefits such as improved quantum yield and reduced photobleaching of the fluorescence markers, as well as narrowing of fluorescence emission bands, potentially facilitating multicolor data acquisition schemes [6,11,16–18]. Yet, although impressive progresses have been achieved recently [14,19,20], cryo-nanoscopy faces significant challenges. One of those concerns the development of user-friendly instrumentation compatible with high numerical-aperture objectives and long data acquisition time with low sample drift [11,21–24]. A more fundamental issue concerns the development of fluorescent markers with efficient photoswitching properties at CT [7,13,17,25–27].

Fluorescent proteins (FPs) are arguably the most appropriate markers for super-resolution microscopy at CT, as they are genetically encoded and thus do not require fixation or permeabilization for efficient labeling. In contrast, many organic dyes do not cross membranes naturally. Furthermore, organic dyes typically used in single-molecule localization techniques such as stochastic optical reconstruction microscopy ((d)STORM) or point accumulation in nanoscale topography (PAINT) cannot be used at CT because their efficient blinking relies on the diffusion of buffer molecules or of the fluorophores themselves, which is arrested in a frozen solvent. A number of fluorescent proteins have been tested for their ability to switch at CT [7–9,11,13,14,25,27]. While phototransformable FPs [28,29] have been mostly investigated [7,8,11,25–27], other more standard FPs have also been shown to undergo cryo-switching [8,9,14,26]. Conflicting results have sometimes been reported, notably concerning reversibly switchable FPs (RSFPs). For example Dronpa has

been shown to not switch at CT, due to restricted structural dynamics [7,30], to cryo-switch moderately [26] or quite efficiently [8,13]. While the positively photoswitchable FP Padron was reported to maintain *trans* to *cis* isomerization at 100 K [27], negative photoswitching at 77 K was also observed [13]. Overall, mechanistic knowledge about the photoswitching mechanisms adopted by FPs at CT remains scarce, although some hypotheses have been put forward such as the possible involvement of the triplet state in the case of mEmerald [14] or of Kolbe-driven photo-decarboxylation of the conserved Glu222 (GFP amino-acid numbering) in PA-GFP or PA-mKate [25,31]. In this work, employing a combination of UV-visible microspectrophotometry, X-ray crystallography and single-molecule studies, we focused on the cryo-switching mechanism of rsEGFP2, a well-known RSFP [32] for which extended knowledge has been gathered in the case of switching at room temperature (RT) [33–37]. We show that switching of rsEGFP2 at ~110 K proceeds via a completely different pathway than at RT, which does not involve chromophore isomerization but instead populates 2 dark states in the *cis* conformation of the chromophore. Based on ensemble data and advanced single-molecule simulations, we show that the use of 355 nm laser light is expected to enhance the effective rsEGFP2 labeling efficiency in cryo-PALM experiments.

RESULTS

Stimulated by our recent structural investigations of rsEGFP2 at RT [33–36], and by the fact that this RSFP was recently shown to maintain efficient switching at 77 K [13], we were interested to know whether cryo-switching proceeds by the same *cis trans* isomerization mechanism as observed at RT. In view of the very efficient switching of rsEGFP2 observed at 300 K, we initially assumed that sufficient conformational flexibility could be maintained at CT to enable isomerization. UV-visible microspectrophotometry experiments using a dedicated instrument [38] were first performed on flash-cooled samples of purified rsEGFP2 mixed with glycerol which were held in micro capillaries (Supplementary Methods).

In comparison with RT switching, a considerably reduced rate of switching upon illumination with 488 nm laser light was observed at ~110 K (Supplementary Fig. 1, Supplementary Fig. 2). Furthermore, in contrast with the off-state reached at RT (absorption peak maximum at 411 nm) (Fig. 1A), the absorption peak for the cryo-switched off-state (Fig. 1C) was largely blue shifted (peak maximum at 385 nm) and more structured. The blueshift was not an effect of the temperature at which spectra were recorded, as the absorption of a sample switched at RT followed by flash cooling was only blue shifted to a minor extent (peak maximum at 406 nm) (Fig. 1E). Whereas back switching by typical 405 nm laser light was nearly complete at RT (Fig. 1B), only partial recovery was obtained at CT after extensive illumination (Fig. 1D, Supplementary Fig. 1). A significant fraction of rsEGFP2 molecules appeared to be trapped in the off-state, and a minor red-shifted absorbance peak was also observed to grow at 520 nm. Interestingly, if rsEGFP2 was off-switched at RT and then flash cooled to CT (Fig. 1E), little back switching could be observed by 405 nm illumination, populating mostly the red shifted absorbance peak (Fig. 1F). This suggests that below the glass transition temperature the protonated *trans* chromophore (the off-switched state at RT) is unable to efficiently undergo *trans* to *cis* back-isomerization followed by deprotonation to the canonical anionic fluorescent state absorbing at 479 nm. Taken together, these data suggest that the off-state reached upon 488 nm illumination at CT differs from that populated at RT.

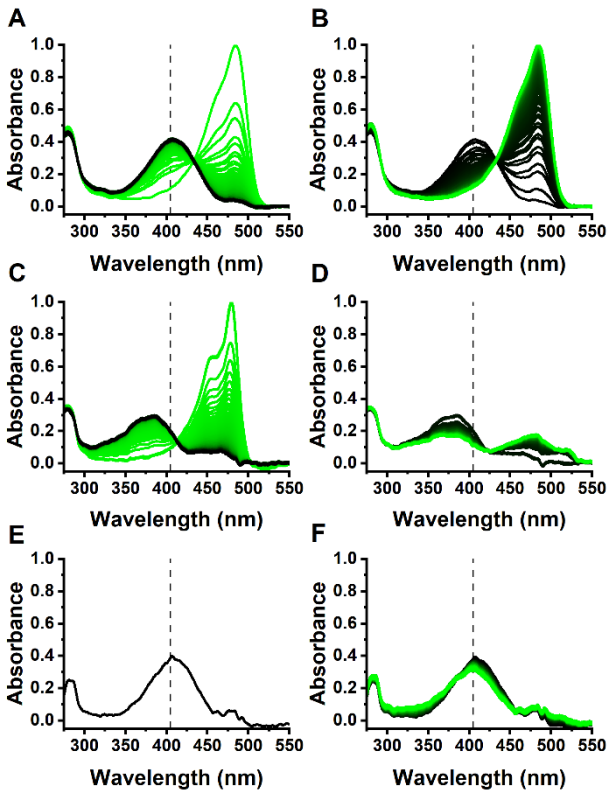

Figure 1: Photoswitching of rsEGFP2 monitored by absorption microspectrophotometry. (A) on-to-off switching at RT with 488 nm laser light (80 W/cm²). (B) off-to-on switching at RT with 405 nm laser light (4 W/cm²). (C) on-to-off switching at 110 K with 488 nm laser light (5.8 kW/cm²). (D) off-to-on swiching at CT with 405 nm laser light (0.7 kW/cm²). (E) on-to-off switching at RT followed by flash cooling. (F) on-to-off switching at RT followed by flash cooling and illumination with 405 nm laser light (0.1 kW/cm²). Spectral series evolve from green to black during off-switching (A, C) or from black to green during on-switching (B, D, F). Absorbance spectra in (A, B) and (C, D) were normalized at the anionic chromophore peak of the first spectrum of each series in A and C, respectively. Spectra in E and F were normalized to match the height of the protonated peak of the first spectrum in A. Representative spectral series are shown from n ≥ 3 measurements. Dashed vertical lines are positioned at 405 nm to guide the eye.

Titration experiments as a function of the employed laser power and fitting of the observed cryo-switching rates indicate that off-switching by 488 nm light as well as on-switching by 405 nm light are (at least) biphasic (Supplementary Fig. 3). The multiphasic nature of photoswitching curves in rsEGFP2 has been observed at RT [36] and could result from heterogeneous FP populations. It also follows from the fact that at CT the protein molecules cannot tumble in the vitreous solvent and thus switch at different rates depending on their dipole orientation. The fitted rates varied linearly as a function of the applied laser power, suggesting that both off-switching and on-switching at 110 K proceed via single-photon absorption mechanisms (Supplementary Fig. 3).

In line with the absorbance data, off-switching at CT of rsEGFP2 by 488 nm light and subsequent on-switching by 405 nm light only allowed the recovery of ~25 % of the fluorescence (Fig. 2A). Such a low recovery level is problematic for cryo-PALM applications, as only a minor fraction of the fluorescently labeled biological targets would then be detectable, giving rise to a low effective labeling efficiency. In comparison, in standard RT PALM using green-to-red photoconvertible FPs, typically 60 to 70% of the labels can be imaged under favorable illumination conditions [39,40].

Photobleaching during off-switching by 488 nm light or on switching by 405 nm light at CT can be invoked to explain the low recovery level to the fluorescent state. In particular, increasing the 405 nm light power density resulted in faster recovery that was nevertheless followed by a progressive decay of the on-state absorbance (Supplementary Fig. 4A), suggesting a balance between back switching and photobleaching mechanisms. Yet, the fraction of recovered on-state absorbance was independent of the applied 488 nm or 405 nm power density, suggesting that nonlinear bleaching mechanisms are not predominant (Supplementary Fig. 4B).

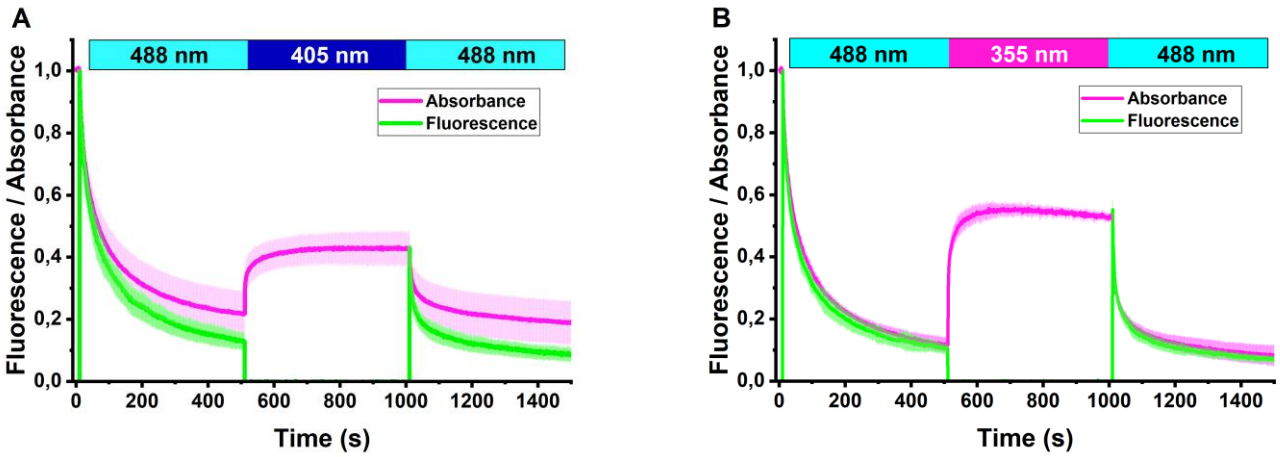

Figure 2: On-state recovery of switched off rsEGFP2 at cryogenic temperature. Absorbance and fluorescence levels are calculated by integration of the absorption and fluorescence emission spectra in 470-500 nm and 495-630 nm spectral ranges, respectively. (A) recovery by 405 nm light. (B) recovery by 355 nm light. Absorbance (magenta) and fluorescence (green) switching kinetics are measured at 110 K by alternate illumination at 488 nm (0.4 kW/cm²) and either 405 nm (0.2 kW/cm²) or 355 nm (0.03 kW/cm²), as indicated in the upper bars. Absorbance and fluorescence are normalized to 1 at start of acquisition. Fluorescence is only measured in the presence of 488 nm light. The mean ± s.d. of n = 3 measurements is shown.

In addition to photobleaching, two other mechanisms may contribute to the limited recovery of the fluorescent on state. The first mechanism is similar to that limiting the photoswitching contrast in e.g. RESOLFT experiments at RT [36] and involves residual off-switching by 405 nm light. Calculations that assume a wavelength independent off-switching quantum yield (Supplementary Methods) suggest that the ratio of on-switching and off-switching rates by the 405 nm light amounts to ~900. Therefore, off-switching by 405 nm light is not expected to contribute to the limited recovery level.

The second mechanism involves dark state trapping and would be in line with the residual off-state absorption observed in the spectra of Fig. 1D. In fact, although 405 nm light is nearly centered on the absorption band of the off-switched rsEGFP2 chromophore at RT, it sits on the red edge of the CT off-switched absorption band, possibly limiting on-state recovery. Thus, we replaced the 405 nm laser by a 355 nm laser. This wavelength sits on the blue edge of the absorption band, and the higher energy photons may thus interact more efficiently with the CT off-switched chromophore. 355 nm light effectively enhanced the rsEGFP2 recovery level to ~50 % (Fig. 2B), in line with near-

complete disappearance of the off-state absorption band after illumination (Supplementary Fig. 5).

To further confirm the different on-switching efficiencies of 405 nm and 355 nm light, we sequentially applied both lasers (Fig. 3). Application of 355 nm light after 405 nm light increased the recovery level to ~45 %, close to the level observed with 355 nm light only (Fig. 3A). Application of 405 nm light after 355 nm light substantially decreased the recovery level (Fig. 3B). Those data suggest that 355 nm light is able to pump back to the on-state a fraction of rsEGFP2 molecules residing in an off-state that does not respond to 405 nm light (Off_1), while another fraction of molecules appears to reside in a second off-state (Off_2) sensitive to both 405 nm and 355 nm light. Upon off-switching at CT by 488 nm light, Off_1 and Off_2 are populated and do not exchange significantly. Application of 405 nm light after 355 nm light repopulates Off_1 due to residual off-switching at this wavelength while the Off_2 steady state level is maintained. This mechanism is clearly visible upon monitoring the absorbance at 320 nm (Supplementary Fig. 6). The observation of Off_1 and Off_2 is reminiscent of the 2 off states recently observed spectroscopically and structurally in rsEGFP2 at RT [35,36].

The 355 nm laser we used was a nanosecond YAG laser pulsed at 3.3 kHz, so that we wondered whether pulsing played a role in the improved recovery level. The temporal profile of laser illumination would be expected to act on the switching kinetics in case of a mechanism involving 2 photons or more. Yet, titration of the on-switching rate as a function of the employed 355 nm laser power density suggested, as for 488 nm and 405 nm lasers, a single-photon mechanism (Supplementary Fig. 7A). In addition, varying the intensity of the 355 nm illumination also did not have a significant effect on the recovery level (Supplementary Fig. 7B). These data indicate that the enhanced recovery of

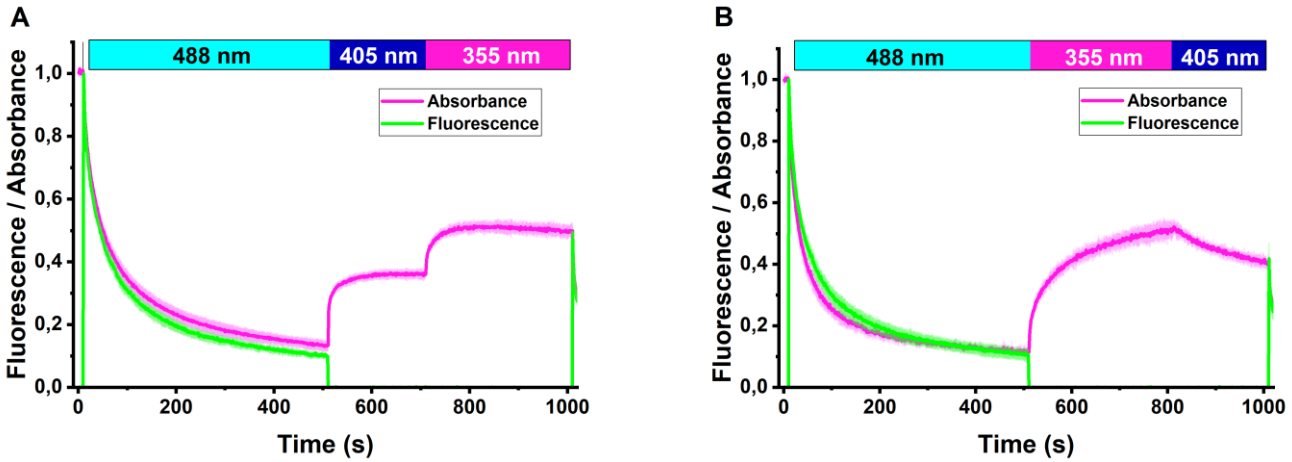

Figure 3: Recovery of rsEGFP2 on state by subsequent illumination with 405 nm and 355 nm light. Absorbance and fluorescence levels are calculated by integration of the absorption and fluorescence emission spectra in 470-500 nm and 495-630 nm spectral ranges, respectively. (A) recovery by 405 nm light followed by 355 nm light. (B) recovery by 355 nm light followed by 405 nm light. Absorbance (magenta) and fluorescence (green) evolutions are measured at 110 K by illumination at 488 nm (0.4 kW/cm²), 405 nm (0.3 kW/cm²) and 355 nm (0.025 kW/cm²), according to the schemes indicated in the upper bars. Absorbance and fluorescence are normalized to 1 at start of acquisition. Fluorescence was only measured in the presence of 488 nm light. The mean ± s.d. of n = 3 measurements is shown.

the rsEGFP2 on-state relative to that observed by 405 nm illumination is mostly due to the blue shifted wavelength and not to the pulsed pattern of the employed 355 nm laser.

Strikingly, we also observed that to achieve on-switching at similar rates, the needed 355 nm average power density was ~20 times lower than that required using 405 nm light. Photoswitching efficiency depends on the product of the extinction coefficient by the switching quantum yield at the used wavelength. Attempts to obtain pure absorption spectra of Off_1 and Off_2 by computing difference spectra (Supplementary Fig. 8) suggested that, for both off states, differences in extinction coefficients at the 2 illumination wavelengths are unlikely to explain the drastic changes in switching efficiency. This suggests that, at CT, the on-switching quantum yield at the lower-energy 405 nm wavelength is significantly lower than at 355 nm for Off_2, and practically zero for Off_1.

Off-switching of RSFPs at RT typically involves protonation of the chromophore at the hydroxybenzylidene ring. To evaluate the possible involvement of proton transfer during off-switching at CT, we measured the pH-dependence of the switching rate in flash-cooled solution samples (Supplementary Fig. 9). The results reveal a faster switching rate at low pH, consistent with a Henderson-Hasselbalch response yielding an apparent pKa of 4.9. In view of

the effective pH increase upon flash cooling, such value appears consistent with the known pKa=5.8 of the rsEGFP2 chromophore at RT.

Finally, we recorded multi-switching absorbance and fluorescence curves with on-switching either induced by 405 nm or 355 nm light (Fig. 4, Supplementary Fig. 10). Photofatigue at CT was much higher than that measured at RT [32]. This observation is in line with the incomplete recovery observed in Fig. 2A and 2B attributed in part to photobleaching by 488 nm, 405 nm and 355 nm light. Of note, photofatigue developed faster when 355 nm light was employed. Thus, the advantage of a higher on-state recovery using 355-nm light is progressively offset by faster photobleaching upon repeated switching. This finding suggests that the *Off*$_1$ dark state is more prone to photobleaching than *Off*$_2$, but may also relate to enhanced photodamage by UV light as compared to 405 nm light on biological material, including at CT [41].

In order to investigate the structural signature of the rsEGFP2 cryo off-switched states, we illuminated rsEGFP2 crystals maintained in the ~110 K nitrogen gas stream of our microspectrophotometer with 488 nm light.

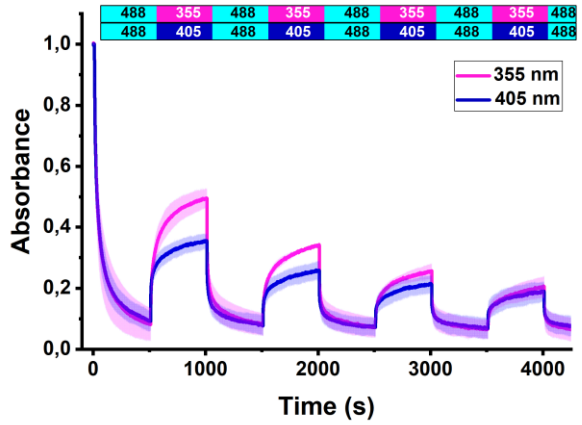

Figure 4: Absorbance photofatigue switching curves of rsEGFP2 at CT. The absorbance signal was calculated by integration of the absorption spectra in the 470-500 nm spectral range. rsEGFP2 was switched back and forth with 488 nm (1.0 kW/cm²) and either 405 nm (0.2 kW/cm², blue) or 355 nm (0.01 kW/cm², magenta) laser light, according to the illumination schemes shown in the upper bars. The mean ± s.d. of n = 3 measurements is shown.

We verified by absorption microspectrophotometry that the same off-states were produced as in solution samples (Supplementary Fig. 11), and collected cryo-crystallographic data after transfer to an ESRF synchrotron beamline. No significant *cis-trans* isomerization could be observed (Fig. 5), as opposed to control measurements where crystals were illuminated at RT (Supplementary Fig. 12).

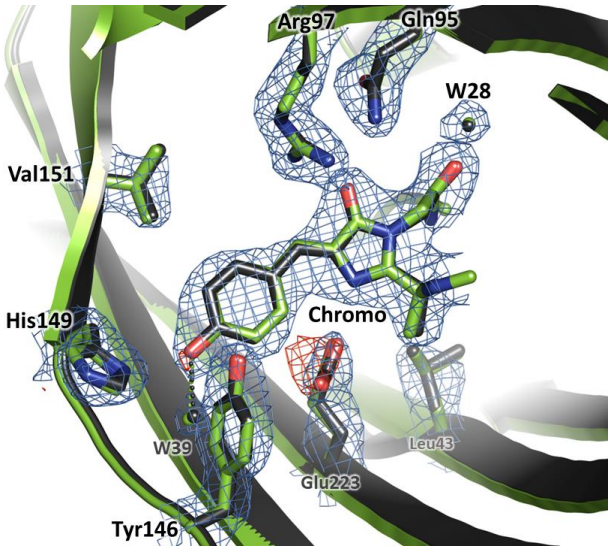

Figure 5. Crystallographic views of rsEGFP2 switching at CT. Refined models of the chromophore and surrounding residues of rsEGFP2 are shown in the *cis* on state (green carbons and water molecules) and in the cryo-switched off state (dark grey carbons and water molecules, PDB code 8AHA), switched with 488 nm laser light for 700 s (0.05 kW/cm²). The $2F_{obs}$-F_{calc} electron density map contoured at 1σ (blue) and the F_{obs}-F_{calc} difference electron density maps contoured at ±3 σ (red: negative, green: positive) of the cryo-switched off state are shown. W: water molecules

Furthermore, at the resolution of our data (2.4 Å), difference electron density maps did not allow to identify any significant conformational change between the off-switched and on-switched states, nor, consequently, between *Off*$_1$ and *Off*$_2$. Residual negative electron density at the level of the conserved Glu223 (rsEGFP2 amino-acid numbering) suggested partial decarboxylation of this residue. Decarboxylation through electron transfer via a Kolbe mechanism has previously been observed in fluorescent proteins to induce photoactivation [31] or photobleaching [42]. We tentatively assign the decarboxylation observed here to photobleaching. Overall, the crystallographic data are consistent with the notion that the rsEGFP2 cryo off-states are predominantly *cis* states.

We also observed that chromophores switched off at RT by 488 nm laser light and then irradiated at CT with 405 nm laser light essentially stayed in the *trans*-conformation (Supplementary Fig. 13. This is in line with the observation by spectroscopy that on-switching at CT of the RT-off-switched chromophore is limited to weak recovery of a red-shifted on-state (Fig. 1D). The data are in fact consistent with a scenario in which this residual red shifted on-state would originate from anionic chromophores in the *trans* configuration. Of note, significant negative difference electron density is visible on Glu223 as well as on the hy-

droxybenzylidene moiety of the chromophore. Decarboxylation of Glu223 in the *trans* isomer form of the chromophore might induce chromophore destabilization, a signature for photobleaching that might have resulted from the extensive 405 nm illumination employed in this experiment.

To complement our results at the ensemble level, we collected single-molecule fluorescence traces from purified rsEGFP2 molecules flash frozen on coverslips, using a PALM microscope operating at CT (110 K) (Supplementary Methods) [21]. The flash-frozen samples were initially off-switched by 488 nm light, and 405 nm light was then turned on to elicit single-molecule activation. A representative single-molecule pattern and a single-molecule trace are shown in Supplementary Fig. 14. Analysis of the data allowed generating histograms revealing the rsEGFP2 single-molecule photophysical behaviour at CT (Fig. 6, Supplementary Fig. 14).

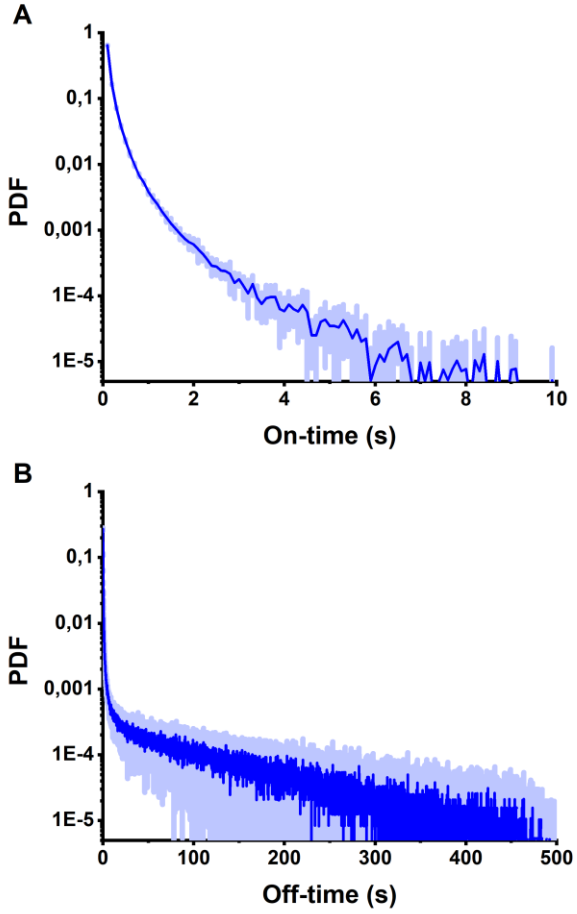

Figure 6. Single molecule behavior of rsEGFP2 at CT. (A) on-times and (B) off-times histograms. The mean ± s.d. of n = 7 measurements is shown. PDF: probability density function.

The on-time and off-time histograms are clearly multiphasic. The fast phases in both histograms suggest that the rsEGFP2 molecules rapidly toggle between an on-state (half on time = 36.5 ms) and a short-lived dark state (half off-time = 63 ms), that we refer as Off_{sl}. Due to its short duration, Off_{sl} is not apparent in the ensemble data but plays a central role in the observed blinking pattern at the single-molecule level. The slow phase of the on-time histogram is mostly attributed to the fixed dipole orientation of the fluorescent proteins at CT, generating an anisotropic response to illumination (as for the kinetic traces measured at the ensemble level). The slow phase of the off-time histogram is, at least in part, attributed to the long-lived Off_2 dark state. Molecules in Off_1 do not contribute to the off-time histogram in the absence of 355 nm light. Of note, the median number of detected photons per merged localization (370±16 ph, Supplementary Fig. 15 is similar to typical values recorded from SMLM datasets collected at RT with green-to-red photoconvertible fluorescent proteins (PCFPs) such as mEos4b (397±42 ph, Supplementary Methods). This can be explained by the strongly increased fluorescence quantum yield of FPs at CT, which compensates for the lower numerical aperture (NA) of the air-objective used in our cryo-microscope, while in both cases, short-lived blinking interrupts photon emission by single molecules. Yet, due to the larger point spread function of the cryo-microscope, the median localization precision achieved at CT (38±0.5 nm) is lower than that at RT with PCFPs (24±3.5 nm) (Supplementary Fig. 15). Thus, with current state-of-the-art methodology, and in view of the relatively limited number of switching cycles achievable by single molecules (Fig 4), FP-based CT-SMLM data may not provide nanoscale images of superior quality as compared to RT-SMLM data.

DISCUSSION

Combining the ensemble and single-molecule data presented above allows drawing a consistent model of the cryo-photophysical behavior of rsEGFP2 (Fig. 7). We propose that rsEGFP2 in its thermally relaxed on-state adopts two conformations (On_1 and On_2) that are in rapid exchange at RT, but that do not exchange significantly anymore at CT. These two populations may differ by e.g. different H-bonding patterns around the chromophore. On_1, upon illumination by 488 nm light at CT, produces the non-fluorescent state Off_1, while On_2 switches to Off_2. Upon illumination with 405 nm light, Off_2 is able to switch back to On_2, while Off_1 remains essentially unresponsive. Upon illumination with 355 nm light, both Off_1 and Off_2 are able to switch back to their respective fluorescent on-states, causing more extensive recovery than with 405 nm illumination. The two populations of rsEGFP2 molecules do not photobleach at the same rate, with On_1/Off_1 being more prone to photodestruction. Finally, the single-molecule data revealed that On_2, in addition to switching to Off_2, efficiently switch to one (or several) additional short-lived dark state(s), Off_{sl}, upon illumination with 488 nm

light at CT. Although On_1 was essentially unobserved in our single-molecule data (collected in the absence of 355 nm light), Off_{sl} might also be reached from this state.

We propose that, in addition, a residual fraction of the on-state rsEGFP2 molecules is still able to photo-isomerize to a *trans* configuration, producing a protonated off-state similar to that populated at RT. This RT-like off-state is able to deprotonate upon absorption of a 405 nm photon, producing a fluorescent *trans* state with red-shifted absorption and fluorescence-emission. This mechanism likely explains why, in cryo-PALM imaging, prior illumination of the sample at RT followed by flash cooling and single-molecule data collection at CT still elicits single-molecule blinking [13]. However, in view of the low signal recovered in such case (Fig. 1E), this procedure likely results in very unfavorable effective labeling efficiency and should not be recommended. The RT-like off-state, with its absorption band peaking at around 400 nm, is only weakly sensitive to 355 nm light, in contrast to 405 nm light. Thus less red-shifted fluorescent molecules are produced upon 355 nm light illumination.

Radical species are known to form in FPs and are typically short-lived [43]. We propose that Off_{sl} be an anionic or cationic short-lived radical formed via photoinduced electron transfer. We deem unlikely that Off_{sl} be the triplet state, in view of its duration (~60 ms) that largely exceeds the triplet state lifetime (~1 ms) measured in fluorescent proteins, albeit at RT [44].

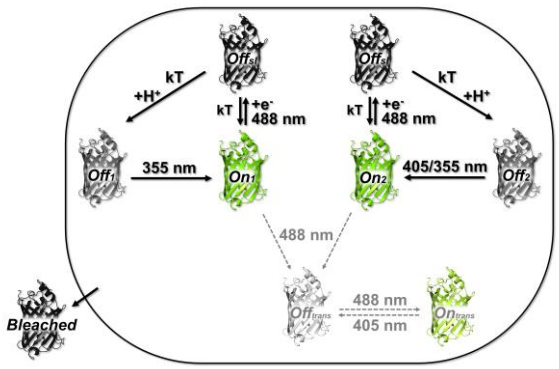

Figure 7. Proposed model of rsEGFP2 photophysics at CT. Sensitivity to light at defined wavelengths is indicated. kT: thermal activation. Dashed lines indicate residual involvement of *trans* chromophore states in CT-photoswitching.

The exact natures of Off_1 and Off_2 remain to be determined. Whether they are also radicals and reached through the triplet state would be important to know, to elucidate the main mechanism of cryo-off switching. The formation of long-lived radical species could be investigated by electron paramagnetic resonance (EPR), if sufficient sample quantities could be produced. The dependence of Off_1 and/or Off_2 formation on addition of triplet state quenchers, oxidizing or reducing agents would unfortunately be difficult to study due to the lack of diffusion of such molecules at CT. However, attaching quenchers such as azobenzene directly to rsEGFP2 could be an exciting alternative strategy [45]. The pH-dependence of the rsEGFP2 cryo off-switching rate, on the other hand, indicates that conversion to Off_1 and/or Off_2 is facilitated at acidic pH lower than the chromophore pKa. This suggests a possible role of H-bonding patterns surrounding the chromophore and proton transfer during off-switching at CT, despite reduced H^+ diffusion below the glass transition temperature [46]. Overall, an appealing scenario is that Off_1 and/or Off_2 would form upon rare protonation of Off_{sl} and thus be protonated radical species. Such species might be similar to the radical state previously identified in the bi-photochromic fluorescent protein IrisFP [47,48].

The existence of two rsEGFP2 on states that would exchange at RT but not at CT, although consistent with all our data, is not fully demonstrated by our study. Yet, it is interesting to relate this hypothesis with the fact that multiple switching pathways have also been identified at RT [36,37]. In the future, it could be interesting to investigate the cryo-switching mechanisms of the rsEGFP2 V151A and V151L mutants, which have been shown to abrogate off-state heterogeneity at RT [36].

Another finding of the present study is the much higher back switching quantum yield of Off_1 by 355 nm light (× ~20) as compared to 405 nm light. Whereas species-specific quantum yields are generally assumed to be wavelength independent, a wavelength-dependence of some reaction yields has been measured in organic molecules [49]. However, to our knowledge, such a strong wavelength-dependence of a phototransformation quantum yield in a fluorescent protein has not been reported to date. This dependence is likely a function of temperature, exacerbated at CT. We propose that at CT, vibrational relaxation may be slowed down to a point where phototransformation pathways efficiently compete with relaxation. Thus, if photoswitching is promoted from a vibrationally excited state preferentially reached by 355 nm excitation, the corresponding quantum yield may effectively be greatly enhanced.

To evaluate the potential gain in using 355 nm rather than 405 nm light in cryo-SMLM experiments, we performed simulations using the recently developed SMIS software [50]. Our main goal was to evaluate whether the more efficient on switching provided by 355 nm illumination could improve the effective labeling efficiency of rsEGFP2 despite more pronounced photobleaching. First the ensemble switching behaviour was reproduced by implementing the rsEGFP2 photophysical model described above (neglecting the residual formation of *trans* chromophores). The spectroscopic signatures of all photoactive states were included and phototransformation quantum yields (Supplementary

Table 1) were adjusted to match the observed photoswitching rates as well as the differential photofatigue behavior measured with 405 nm and 355 nm light (Supplementary Fig. 16. The refined photophysical model was then used in virtual cryo-SMLM experiments aimed at quantitative imaging of the Nup96 nucleoporin within nuclear pore complexes (NPCs) [51]. The results, presented in Fig. 8, show that the effective labeling efficiency can be raised from ~32% to ~54%. Thus, based on our rsEGFP2 photophysical model, we conclude that the more efficient recovery level offered by the 355 nm laser prevails over the more stringent photobleaching induced by this laser. This finding will now need to be confirmed in genuine experimental conditions.

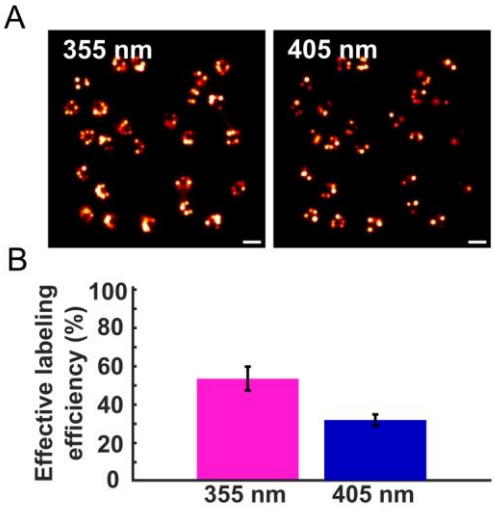

Figure 8. Simulated cryo-SMLM experiments of quantitative imaging of NPCs. (A) Reconstructed images using 355 nm or 405 nm illumination. (B) Effective labeling efficiency using 355 nm or 405 nm illumination. The mean ± s.d. of n = 4 simulations is shown. Scale bar: 200 nm

CONCLUSION

This work presents the first in-depth investigation of the cryo-switching mechanism of a fluorescent protein. We have shown that rsEGFP2, an efficient RSFP that switches at ambient temperature through coupled *cis-trans* isomerization and protonation of its chromophore, adopts a different switching mechanism at cryogenic temperature. Because of the lack of conformational freedom below the glass transition temperature (~ 180 K), isomerization of the rsEGFP2 chromophore is largely hindered at ~110 K. In contrast, this FP populates two off-switched states adopting *cis* configurations and displaying absorption bands largely blue shifted relative to that of the *trans* protonated off-state reached at RT. A 405 nm laser classically used in RT-SMLM switches back only one of the off-states. In contrast, a 355 nm laser applied at very low power is able to efficiently reactivate both off states and thus a larger fraction of the molecules. Cryo-SMLM simulations on the Nuclear Pore Complex suggest that indeed there would be a net gain in using such a laser for real studies thanks to an increase of effective labeling efficiency. Yet, cellular damage induced by 355 nm light, although likely limited at cryogenic temperature, would need to be evaluated. It will also be interesting in the future to evaluate whether the results reported here can be generalized to other FPs such as mEmerald [14]. As the cryo switching mechanism of rsEGFP2 does not seem to relate to the switching mechanism adopted at RT, we anticipate that FPs that are not necessarily phototransformable at RT may share the described behaviour and be sensitive to reactivation by 355 nm light. In fact, the various FPs studied by Tuijtel et al [13] appear to show relatively similar behaviors, including EGFP. Of note, in the case of Padron, it is remarkable that both negative and positive cryo switching have been described [13,27]. It is likely that this protein, while it can sustain *trans* to *cis* isomerization at CT (positive switching) can also undergo the same cryo-switching mechanism as rsEGFP2 (negative switching). The present study highlights that population heterogeneity is a major hallmark of fluorescent protein photophysical behavior. Removing this heterogeneity in favor of only the On_2 population would be an even more attractive option than using 355 nm light for efficient activation of rsEGFP2 at CT. In conclusion, the present study opens the door to FP engineering and optimization of illumination conditions to improve cryo-photoswitching in cryo-SMLM.

ASSOCIATED CONTENT

Supporting Information. Supplementary Methods, Supplementary Figures and Supplementary Tables. This material is available free of charge via the Internet at http://pubs.acs.org.

AUTHOR INFORMATION

Corresponding Author

* dominique.bourgeois@ibs.fr

Author Contributions

D.B. conceived and supervised the project. A.M., O.G. and D.T. performed microspectrophotometry experiments. O.G. performed single-molecule experiments. A.M. and V.A. performed crystallography experiments. J.W. performed simulations. A.M., V.A., J.W. and O.G. processed the data. D.T. discovered the advantage of using a 355 nm laser. M.B. and O.G. developed and optimized the microspectrophotomer instrument. I.G., O.N. and J.E. designed the cryogenic super-resolution microscope. D.B., O.G., V.A. J.W. and A.M. wrote the manuscript with input from all authors.

Present Addresses

£ Institute of Cell Biology and SynthSys, University of Edinburgh, EH9 3FF, Edinburgh, UK.

Funding Sources

This work was supported by the Agence Nationale de la Recherche (grant no. ANR-17-CE11-0047-01 and ANR-20-CE11-

0013-01) and used the M4D imaging platform of the Grenoble Instruct-ERIC Center (ISBG: UMS 3518 CNRS-CEA-UGA-EMBL) with support from FRISBI (grant no. ANR-10-INBS-05-02) and GRAL, a project of the Université Grenoble Alpes graduate school (Ecoles Universitaires de Recherche) CBH-EUR-GS (ANR-17-EURE-0003) within the Grenoble Partnership for Structural Biology (PSB). A.M. acknowledges funding by the CEA. J.W. Acknowledges funding by the GRAL Labex.

ACKNOWLEDGMENT

We thank Antoine Royant for the loan of the 355 nm laser and Ninon Zala for rsEGFP2 protein production. Michel Sliwa is acknowledged for providing insight on wavelength-dependent phototransformation quantum yields.

ABBREVIATIONS

SMLM, single molecule localization microscopy ; (d)STORM, stochastic optical reconstruction microscopy ; PAINT, point accumulation in nanoscale topography ; PALM, photoactivation localization microscopy ; RT, room temperature ; CT, cryogenic temperature ; FPs, fluorescent proteins ; RSFPs, reversibly switchable fluorescent proteins ; PCFPs, photoconvertible fluorescent proteins ; CLEM, correlative light and electron microscopy ; EPR, electron paramagnetic resonance ; ESRF, European Synchrotron Radiation Facility ; NPC, nuclear pore complex.

REFERENCES

(1) Liu, S.; Hoess, P.; Ries, J. Super-Resolution Microscopy for Structural Cell Biology. ***Annual*** *Review of Biophysics* **2022**, *51* (1), 301–326. https://doi.org/10.1146/annurev-biophys-102521-112912.

(2) Schnell, U.; Dijk, F.; Sjollema, K. A.; Giepmans, B. N. G. Immunolabeling Artifacts and the Need for Live-Cell Imaging. *Nat. Methods* **2012**, *9* (2), 152–158. https://doi.org/10.1038/nmeth.1855.

(3) Whelan, D. R.; Bell, T. D. M. Image Artifacts in Single Molecule Localization Microscopy: Why Optimization of Sample Preparation Protocols Matters. *Sci Rep* **2015**, *5*, 7924. https://doi.org/10.1038/srep07924.

(4) Tanaka, K. A. K.; Suzuki, K. G. N.; Shirai, Y. M.; Shibutani, S. T.; Miyahara, M. S. H.; Tsuboi, H.; Yahara, M.; Yoshimura, A.; Mayor, S.; Fujiwara, T. K.; Kusumi, A. Membrane Molecules Mobile Even after Chemical Fixation. *Nat. Methods* **2010**, *7* (11), 865–866. https://doi.org/10.1038/nmeth.f.314.

(5) Sartori, A.; Gatz, R.; Beck, F.; Rigort, A.; Baumeister, W.; Plitzko, J. M. Correlative Microscopy: Bridging the Gap between Fluorescence Light Microscopy and Cryo-Electron Tomography. *Journal of structural biology* **2007**, *160* (2), 135–145.

(6) Schwartz, C. L.; Sarbash, V. I.; Ataullakhanov, F. I.; McIntosh, J. R.; Nicastro, D. Cryo-Fluorescence Microscopy Facilitates Correlations between Light and Cryo-Electron Microscopy and Reduces the Rate of Photobleaching. *Journal of microscopy* **2007**, *227* (Pt 2), 98–109.

(7) Chang, Y.-W.; Chen, S.; Tocheva, E. I.; Treuner-Lange, A.; Löbach, S.; Søgaard-Andersen, L.; Jensen, G. J. Correlated Cryogenic Photoactivated Localization Microscopy and Cryo-Electron Tomography. *Nature Methods* **2014**, *11* (7), 737–739. https://doi.org/10.1038/nmeth.2961.

(8) Liu, B.; Xue, Y.; Zhao, W.; Chen, Y.; Fan, C.; Gu, L.; Zhang, Y.; Zhang, X.; Sun, L.; Huang, X.; Ding, W.; Sun, F.; Ji, W.; Xu, T. Three-Dimensional Super-Resolution Protein Localization Correlated with Vitrified Cellular Context. *Scientific Reports* **2015**, *5*, 13017–13028.

(9) Kaufmann, R.; Schellenberger, P.; Seiradake, E.; Dobbie, I. M.; Jones, E. Y.; Davis, I.; Hagen, C.; Grünewald, K. Super-Resolution Microscopy Using Standard Fluorescent Proteins in Intact Cells under Cryo-Conditions. *Nano Letters* **2014**, *14* (7), 4171–4175. https://doi.org/10.1021/nl501870p.

(10) Wolff, G.; Hagen, C.; Grünewald, K.; Kaufmann, R. Towards Correlative Super-Resolution Fluorescence and Electron Cryo-Microscopy. *Biol Cell* **2016**, *108* (9), 245–258. https://doi.org/10.1111/boc.201600008.

(11) Nahmani, M.; Lanahan, C.; DeRosier, D.; Turrigiano, G. G. High-Numerical-Aperture Cryogenic Light Microscopy for Increased Precision of Superresolution Reconstructions. *Proceedings of the National Academy of Sciences* **2017**, *114* (15), 3832–3836. https://doi.org/10.1073/pnas.1618206114.

(12) Dahlberg, P. D.; Saurabh, S.; Sartor, A. M.; Wang, J.; Mitchell, P. G.; Chiu, W.; Shapiro, L.; Moerner, W. E. Cryogenic Single-Molecule Fluorescence Annotations for Electron Tomography Reveal in Situ Organization of Key Proteins in Caulobacter. *Proceedings of the National Academy of Sciences* **2020**, *117* (25), 13937–13944. https://doi.org/10.1073/pnas.2001849117.

(13) Tuijtel, M. W.; Koster, A. J.; Jakobs, S.; Faas, F. G. A.; Sharp, T. H. Correlative Cryo Super-Resolution Light and Electron Microscopy on Mammalian Cells Using Fluorescent Proteins. *Sci Rep* **2019**, *9* (1), 1369. https://doi.org/10.1038/s41598-018-37728-8.

(14) Hoffman, D. P.; Shtengel, G.; Xu, C. S.; Campbell, K. R.; Freeman, M.; Wang, L.; Milkie, D. E.; Pasolli, H. A.; Iyer, N.; Bogovic, J. A.; Stabley, D. R.; Shirinifard, A.; Pang, S.; Peale, D.; Schaefer, K.; Pomp, W.; Chang, C.-L.; Lippincott-Schwartz, J.; Kirchhausen, T.; Solecki, D. J.; Betzig, E.; Hess, H. F. Correlative Three-Dimensional Super-Resolution and Block-Face Electron Microscopy of Whole Vitreously Frozen Cells. *Science* **2020**, *367* (6475), eaaz5357. https://doi.org/10.1126/science.aaz5357.

(15) Dahlberg, P. D.; Moerner, W. E. Cryogenic Super-Resolution Fluorescence and Electron Microscopy Correlated at the Nanoscale. *Annu Rev Phys Chem* **2021**, *72*, 253–278. https://doi.org/10.1146/annurev-physchem-090319-051546.

(16) Moerner, W. E.; Orrit, M. Illuminating Single Molecules in Condensed Matter. *Science* **1999**, *283* (5408), 1670–1676. https://doi.org/10.1126/science.283.5408.1670.

(17) Hulleman, C. N.; Li, W.; Gregor, I.; Rieger, B.; Enderlein, J. Photon Yield Enhancement of Red Fluorophores at Cryogenic Temperatures. *Chemphyschem* **2018**, *19* (14), 1774–1780. https://doi.org/10.1002/cphc.201800131.

(18) Weisenburger, S.; Jing, B.; Hänni, D.; Reymond, L.; Schuler, B.; Renn, A.; Sandoghdar, V. Cryogenic Colocalization Microscopy for Nanometer-Distance Measurements. *ChemPhysChem* **2014**, *15* (4), 763–770. https://doi.org/10.1002/cphc.201301080.

(19) Weisenburger, S.; Boening, D.; Schomburg, B.; Giller, K.; Becker, S.; Griesinger, C.; Sandoghdar, V. Cryogenic Optical Localization Provides 3D Protein Structure Data with Angstrom Resolution. *Nat. Methods* **2017**, *14* (2), 141–144. https://doi.org/10.1038/nmeth.4141.

(20) Mazal, H.; Wieser, F.-F.; Sandoghdar, V. Deciphering a Hexameric Protein Complex with Angstrom Optical Resolution. *eLife* **2022**, *11*, e76308. https://doi.org/10.7554/eLife.76308.

(21) Li, W.; Stein, S. C.; Gregor, I.; Enderlein, J. Ultra-Stable and Versatile Widefield Cryo-Fluorescence Microscope for Single-Molecule Localization with Sub-Nanometer Accuracy. *Optics Express* **2015**, *23* (3), 3770–3783. https://doi.org/10.1364/OE.23.003770.

(22) Faoro, R.; Bassu, M.; Mejia, Y. X.; Stephan, T.; Dudani, N.; Boeker, C.; Jakobs, S.; Burg, T. P. Aberration-Corrected Cryoimmersion Light Microscopy. *Proceedings of the National Academy of Sciences* **2018**, *115* (6), 1204–1209. https://doi.org/10.1073/pnas.1717282115.

(23) Xu, X.; Xue, Y.; Tian, B.; Feng, F.; Gu, L.; Li, W.; Ji, W.; Xu, T. Ultra-Stable Super-Resolution Fluorescence Cryo-Microscopy for Correlative Light and Electron Cryo-Microscopy. *Sci China Life Sci* **2018**, *61* (11), 1312–1319. https://doi.org/10.1007/s11427-018-9380-3.

(24) Wang, L.; Bateman, B.; Zanetti-Domingues, L. C.; Moores, A. N.; Astbury, S.; Spindloe, C.; Darrow, M. C.; Romano, M.; Needham, S. R.; Beis, K.; Rolfe, D. J.; Clarke, D. T.; Martin-Fernandez, M. L. Solid Immersion Microscopy Images Cells under Cryogenic Conditions with 12 Nm Resolution. *Commun Biol* **2019**, *2* (1), 74. https://doi.org/10.1038/s42003-019-0317-6.

(25) Dahlberg, P. D.; Sartor, A. M.; Wang, J.; Saurabh, S.; Shapiro, L.; Moerner, W. E. Identification of PAmKate as a Red Photoactivatable Fluorescent Protein for Cryogenic Super-Resolution Imaging. *J. Am. Chem. Soc.* **2018**, *140* (39), 12310–12313. https://doi.org/10.1021/jacs.8b05960.

(26) Faro, A. R.; Adam, V.; Carpentier, P.; Darnault, C.; Bourgeois, D.; Rosny, E. de. Low-Temperature Switching by Photoinduced Protonation in Photochromic Fluorescent Proteins. *Photochem. Photobiol. Sci.* **2010**, *9* (2), 254–262. https://doi.org/10.1039/B9PP00121B.

(27) Faro, A. R.; Carpentier, P.; Jonasson, G.; Pompidor, G.; Arcizet, D.; Demachy, I.; Bourgeois, D. Low-Temperature Chromophore Isomerization Reveals the Photoswitching Mechanism of the Fluorescent Protein Padron. *Journal of the American Chemical Society* **2011**, *133* (41), 16362–16365.

(28) Shcherbakova, D. M.; Sengupta, P.; Lippincott-Schwartz, J.; Verkhusha, V. V. Photocontrollable Fluorescent Proteins for Superresolution Imaging. *Annual Review of Biophysics* **2014**, *43* (1), 303–329. https://doi.org/10.1146/annurev-biophys-051013-022836.

(29) Adam, V.; Berardozzi, R.; Byrdin, M.; Bourgeois, D. Phototransformable Fluorescent Proteins: Future Challenges. *Curr Opin Chem Biol* **2014**, *20*, 92–102. https://doi.org/10.1016/j.cbpa.2014.05.016.

(30) Mizuno, H.; Mal, T. K.; Wälchli, M.; Kikuchi, A.; Fukano, T.; Ando, R.; Jeyakanthan, J.; Taka, J.; Shiro, Y.; Ikura, M.; Miyawaki, A. Light-Dependent Regulation of Structural Flexibility in a Photochromic Fluorescent Protein. *PNAS* **2008**, *105* (27), 9227–9232. https://doi.org/10.1073/pnas.0709599105.

(31) van Thor, J. J.; Gensch, T.; Hellingwerf, K. J.; Johnson, L. N. Phototransformation of Green Fluorescent Protein with UV and Visible Light Leads to Decarboxylation of Glutamate 222. *Nature structural biology* **2002**, *9* (1), 37–41.

(32) Grotjohann, T.; Testa, I.; Reuss, M.; Brakemann, T.; Eggeling, C.; Hell, S. W.; Jakobs, S. RsEGFP2 Enables Fast RESOLFT Nanoscopy of Living Cells. *eLIFE* **2012**, *1*, e00248. https://doi.org/10.7554/eLife.00248.

(33) El Khatib, M.; Martins, A.; Bourgeois, D.; Colletier, J.-P.; Adam, V. Rational Design of Ultrastable and Reversibly Photoswitchable Fluorescent Proteins for Super-Resolution Imaging of the Bacterial Periplasm. *Sci Rep* **2016**, *6*, 18459. https://doi.org/10.1038/srep18459.

(34) Coquelle, N.; Sliwa, M.; Woodhouse, J.; Schirò, G.; Adam, V.; Aquila, A.; Barends, T. R. M.; Boutet, S.; Byrdin, M.; Carbajo, S.; De la Mora, E.; Doak, R. B.; Feliks, M.; Fieschi, F.; Foucar, L.; Guillon, V.; Hilpert, M.; Hunter, M. S.; Jakobs, S.; Koglin, J. E.; Kovacsova, G.; Lane, T. J.; Lévy, B.; Liang, M.; Nass, K.; Ridard, J.; Robinson, J. S.; Roome, C. M.; Ruckebusch, C.; Seaberg, M.; Thepaut, M.; Cammarata, M.; Demachy, I.; Field, M.; Shoeman, R. L.; Bourgeois, D.; Colletier, J.-P.; Schlichting, I.; Weik, M. Chromophore Twisting in the Excited State of a Photoswitchable Fluorescent Protein Captured by Time-Resolved Serial Femtosecond Crystallography. *Nature Chemistry* **2017**, *10*, 31.

(35) Woodhouse, J.; Nass Kovacs, G.; Coquelle, N.; Uriarte, L. M.; Adam, V.; Barends, T. R. M.; Byrdin, M.; de la Mora, E.; Bruce Doak, R.; Feliks, M.; Field, M.; Fieschi, F.; Guillon, V.; Jakobs, S.; Joti, Y.; Macheboeuf, P.; Motomura, K.; Nass, K.; Owada, S.; Roome, C. M.; Ruckebusch, C.; Schirò, G.; Shoeman, R. L.; Thepaut, M.; Togashi, T.; Tono, K.; Yabashi, M.; Cammarata, M.; Foucar, L.; Bourgeois, D.; Sliwa, M.; Colletier, J.-P.; Schlichting, I.; Weik, M. Photoswitching Mechanism of a Fluorescent Protein Revealed by Time-Resolved Crystallography and Transient Absorption Spectroscopy. *Nature Communications* **2020**, *11* (1), 1–11. https://doi.org/10.1038/s41467-020-14537-0.

(36) Adam, V.; Hadjidemetriou, K.; Jensen, N.; Shoeman, R.; Woodhouse, J.; Aquila, A.; Banneville, A.-S.; Barends, T.; Bezchastnov, V.; Boutet, S.; Byrdin, M.; Cammarata, M.; Carbajo, S.; Christou, N.-E.; Coquelle, N.; de la Mora, E.; El Khatib, M.; Moreno Chicano, T.; Doak, R.; Bourgeois, D.; Weik, M. Rational Control of Structural Off-State Heterogeneity in a Photoswitchable Fluorescent Protein Provides Switching Contrast Enhancement. *BioRXiv*. November 5, 2021. https://doi.org/10.1101/2021.11.05.462999.

(37) Chang, J.; Romei, M. G.; Boxer, S. G. Structural Evidence of Photoisomerization Pathways in Fluorescent Proteins. *J. Am. Chem. Soc.* **2019**, *141* (39), 15504–15508. https://doi.org/10.1021/jacs.9b08356.

(38) Byrdin, M.; Bourgeois, D. The CAL(AI)2DOSCOPE: A Microspectrophotometer for Accurate Recording of Correlated Absorbance and Fluorescence Emission Spectra. *Spectroscopy Europe*. 2016, pp 14–17.

(39) Durisic, N.; Laparra-Cuervo, L.; Sandoval-Álvarez, Á.; Borbely, J. S.; Lakadamyali, M. Single-Molecule Evaluation of Fluorescent Protein Photoactivation Efficiency Using an in Vivo Nanotemplate. *Nat Methods* **2014**, *11* (2), 156–162. https://doi.org/10.1038/nmeth.2784.

(40) Wulffele, J.; Thédié, D.; Glushonkov, O.; Bourgeois, D. MEos4b Photoconversion Efficiency Depends on Laser Illumination Conditions Used in PALM. *J. Phys. Chem. Lett.* **2022**, *13* (22), 5075–5080. https://doi.org/10.1021/acs.jpclett.2c00933.

(41) Vernede, X.; Lavault, B.; Ohana, J.; Nurizzo, D.; Joly, J.; Jacquamet, L.; Felisaz, F.; Cipriani, F.; Bourgeois, D. UV Laser-Excited Fluorescence as a Tool for the Visualization of Protein Crystals Mounted in Loops. *Acta Crystallogr D Biol Crystallogr* **2006**, *62* (Pt 3), 253–261.

(42) Duan, C.; Adam, V.; Byrdin, M.; Ridard, J.; Kieffer-Jaquinod, S.; Morlot, C.; Arcizet, D.; Demachy, I.; Bourgeois, D. Structural Evidence for a Two-Regime Photobleaching Mechanism in a Reversibly Switchable Fluorescent Protein. *J. Am. Chem. Soc.* **2013**, *135* (42), 15841–15850. https://doi.org/10.1021/ja406860e.

(43) Vegh, R. B.; Bravaya, K. B.; Bloch, D. A.; Bommarius, A. S.; Tolbert, L. M.; Verkhovsky, M.; Krylov, A. I.; Solntsev, K. M. Chromophore Photoreduction in Red Fluorescent Proteins Is Responsible for Bleaching and Phototoxicity. *J. Phys. Chem. B* **2014**, *118* (17), 4527–4534. https://doi.org/10.1021/jp500919a.

(44) Byrdin, M.; Duan, C.; Bourgeois, D.; Brettel, K. A Long-Lived Triplet State Is the Entrance Gateway to Oxidative Photochemistry in Green Fluorescent Proteins. *J. Am. Chem. Soc.* **2018**, *140* (8), 2897–2905. https://doi.org/10.1021/jacs.7b12755.

(45) Henrikus, S. S.; Tassis, K.; Zhang, L.; van der Velde, J. H. M.; Gebhardt, C.; Herrmann, A.; Jung, G.; Cordes, T. Characterization of Fluorescent Proteins with Intramolecular Photostabilization**. *ChemBioChem* **2021**, *22* (23), 3283–3291. https://doi.org/10.1002/cbic.202100276.

(46) Fisher, M.; Devlin, J. P. Defect Activity in Amorphous Ice from Isotopic Exchange Data: Insight into the Glass Transition. *J. Phys. Chem.* **1995**, *99*, 11584–11590.

(47) Adam, V.; Carpentier, P.; Violot, S.; Lelimousin, M.; Darnault, C.; Nienhaus, G. U.; Bourgeois, D. Structural Basis of X-Ray-Induced Transient Photobleaching in a Photoactivatable Green Fluorescent Protein. *J. Am. Chem. Soc.* **2009**, *131* (50), 18063–18065. https://doi.org/10.1021/ja907296v.

(48) Roy, A.; Field, M. J.; Adam, V.; Bourgeois, D. The Nature of Transient Dark States in a Photoactivatable Fluorescent Protein. *J Am Chem Soc* **2011**, *133* (46), 18586–18589. https://doi.org/10.1021/ja2085355.

(49) Sotome, H.; Une, K.; Nagasaka, T.; Kobatake, S.; Irie, M.; Miyasaka, H. A Dominant Factor of the Cycloreversion Reactivity of Diarylethene Derivatives as Revealed by Femtosecond Time-Resolved Absorption Spectroscopy. *J. Chem. Phys.* **2020**, *152* (3), 034301. https://doi.org/10.1063/1.5134552.

(50) Bourgeois, D. Single Molecule Imaging Simulations with Full Fluorophore Photophysics. *bioRxiv*. June 17, 2022, p https://doi.org/10.1101/2022.06.14.496133.

(51) Thevathasan, J. V.; Kahnwald, M.; Cieśliński, K.; Hoess, P.; Peneti, S. K.; Reitberger, M.; Heid, D.; Kasuba, K. C.; Hoerner, S. J.; Li, Y.; Wu, Y.-L.; Mund, M.; Matti, U.; Pereira, P. M.; Henriques, R.; Nijmeijer, B.; Kueblbeck, M.; Sabinina, V. J.; Ellenberg, J.; Ries, J. Nuclear Pores as Versatile Reference Standards for Quantitative Super-resolution Microscopy. *Nat. Methods* **2019**, *16* (10), 1045–1053. https://doi.org/10.1038/s41592-019-0574-9.

Table of Contents artwork

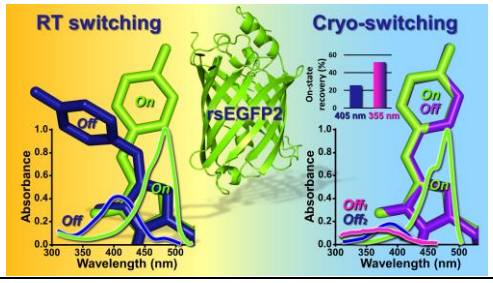

Supplementary information

Photophysical studies at cryogenic temperature reveal a novel photoswitching mechanism of rsEGFP2.

Angela M. R. Mantovanelli[1], Oleksandr Glushonkov[1], Virgile Adam[1], Jip Wulffele[1], Daniel Thédié[1], Martin Byrdin[1], Ingo Gregor[2], Oleksii Nevskyi[2], Jörg Enderlein[2] & Dominique Bourgeois[1]*

1 – Institut de Biologie Structurale, CNRS, Université Grenoble Alpes, CEA, IBS, 38044 Grenoble, France
2 – Institute of Physics−Biophysics, Georg August University, 37077 Göttingen, Germany

Supplementary Methods

Protein expression and purification

rsEGFP2 was expressed and purified as described earlier.[1] Briefly, expressing cells were lysed and 6xHis-tagged rsEGFP2 was purified by gravity flow immobilized metal affinity chromatography (IMAC) using 100 ml of Ni-NTA resin, followed by size exclusion chromatography on a HiLoad 16/600 Superdex 75 prep grade column.

Solution sample preparation

For microspectrophotometry experiments at pH 7.5, purified rsEGFP2 was mixed with a buffer solution containing 50 mM HEPES pH 7.5, 20% glycerol and 50 mM NaCl, providing a final protein concentration of 20 mg/ml. For pH-dependent experiments, purified rsEGFP2 was mixed with buffer solutions containing 20% glycerol and 1M MES (pH5 and 6), 1M HEPES (pH7) or 1M Tris (pH9), providing a final protein concentration of 7 mg/ml.

Solution sample illumination

For microspectrophotometry experiments at RT, rsEGFP2 solution samples were sucked into capillaries of 0.5 mm x 1 mm section attached to a goniometer base. The capillaries were then mounted to our home-built microspectrophotometer.[2]

For microspectrophotometry experiments at CT, solution samples were prepared in the same way, but flash-cooled in a 110 K nitrogen gaseous cryo-stream (Oxford Cryosystems) connected to the microspectrophotometer.

Samples were illuminated with alternating 488 nm and 405 nm or 355 nm lasers for on-to-off and off-to-on protein switching, respectively, according to the scheme shown in Supplementary Fig. 17. During on-to-off switching phases, absorption and fluorescence spectra were recorded in an interleaved manner. During off-to-on switching phases, only absorption spectra were collected to avoid unwanted off-switching by 488 nm excitation light.

The cycle time was 1 second. Laser illumination, white-light illumination and spectroscopic data collection were synchronized using a digital delay-pulse generator (9518, Quantum Composer). For on-to-off switching, the pulse sequence started with triggering of a Deuterium-Halogen lamp (AvaLight-DH-S-BAL, Avantes) and one of two CCD-based spectrometers (AvaSpec ULS 2048L-USB2, Avantes) to record absorption spectra (integration time of 30 ms with averaging of 5 spectra). Then a fiber coupled 488 nm laser (LBX-488-200, Oxxius) was used to induce rsEGFP2 off-switching for 750 ms (75% of the cycle time). Fluorescence spectra were collected by recording fluorescence emission excited by the 488 nm laser in an epifluorescence mode for 1 ms, 5 ms after the start of laser illumination. Emitted light passed through a 488 nm dichroic mirror (Di02-R488, Semrock) and a notch filter (NF03-488E-25, Semrock), and was detected by the second AvaSpec spectrometer, using an integration time of 1 ms. For off-to-on switching, absorption spectra were collected using the same protocol except that a fiber coupled 405 nm laser (LBX-405-200, Oxxius) or a 355 nm laser (MPL-F-355, CNI) were used with a reduced duty cycle (30% of the cycle time), starting after 600 ms. Pulsing frequency of the YAG-based 355 nm laser was measured to be 3.3 kHz, with pulse durations of ~10 ns.

Laser powers were measured at sample position using a calibrated power meter (PM100D, Thorlabs) with a 355 nm light sensitive sensor (S170C, Thorlabs) and another sensor sensitive to 488 nm and 405 nm light (S121C). Laser beam profiles (circular top flat) were recorded from images collected through the objective of the microspectrophotometer onto a CCD camera. Laser power densities were calculated by dividing the measured powers by the beam profile surface areas.

At CT, using input optical fibers of 200 µm diameter (25 µm spot size at sample position) laser power densities were adjusted in the range 430-5700 W/cm² (488 nm), 120-780 W/cm² (405 nm) and 4-33 W/cm² (355 nm). At RT, laser power densities of 81 W/cm² (488 nm) and 4 W/cm² (405 nm) were used, except for Supplementary Fig. 1, where similar laser power densities as used at CT were employed (0.5 kW/cm² and 0.1 kW/cm² for 488 nm and 405 nm lasers, respectively).

Crystal preparation

rsEGFP2 crystals were grown at 20°C by the hanging drop vapor diffusion method with a drop of 2 µl of rsEGFP2 solution at 13 mg/ml mixed with 2 µl mother liquor against a 1 ml mother liquor solution containing 100 mM HEPES buffer, pH 8.1 mixed with 1.9 M ammonium sulfate. Crystal dimensions were ~$50 \times 40 \times 200$ µm³. Crystals were harvested with cryo-loops, soaked for a few seconds in a cryo-protectant solution containing the mother liquor mixed with 20% glycerol, and immediately flash cooled.

Crystal pre-illumination

Crystals were illuminated under continuous cooling (110K) on our home-built micro-spectrometer, as described in the *Solution sample illumination* section.

Crystal 1 (off-switching at CT, Supplementary Table 2) was left non-illuminated on ~half of its volume to allow collecting the structure of the on state as a control (Position 1). The other half was illuminated with the 488 nm laser (600 µm fiber diameter, ~80 µm spot size) for 700 s to allow collecting the structure of the cryo-switched off state (Table 2, Position 2). The laser power density was kept at low level (46 W/cm²), to preserve the crystal from heating and partial disordering, considering the very high optical density of rsEGFP2 crystals in the on-state at 488 nm. Progression of off-switching was monitored by fluorescence and absorption microspectrophotometry (Supplementary Fig. 12) using the same acquisition scheme described in the *Solution sample illumination* section.

Crystal 2 (off-switching at RT, back on-switching at CT, Supplementary Table 3) was switched off at RT over its whole volume with 488 nm laser light (3.4 W/cm², 600µm fiber) for 30 s directly in its crystallization drop. The crystal was then flash cooled and mounted on the microspectrophotometer, and illuminated at 110K on ~half of its volume with the 405 nm laser (14W/cm², 600 µm fiber diameter, ~80 µm spot size) for 180 s. Progression of residual on-switching was monitored by absorption microspectrophotometry (Supplementary Fig. 13B) using the same acquisition scheme described in the *Solution sample illumination* section. The non-405 nm illuminated part of the crystal was used to obtain the structure of the RT-

switched off state (Table 3, Position 1) and the illuminated part was used to obtain the RT-off-switched and then cryo-back-switched state (Table 3, Position 2). The extensive exposure to 488 nm light at RT, used to ensure complete off switching of the crystal, possibly led to partial photobleaching.

The on-state structure obtained from Crystal 1 (Position 1) and the RT-switched off-state structure obtained from Crystal 2 (Position 1) are shown together in Supplementary Fig. 12 to confirm the observation of a *cis-trans* isomerization at RT with our setup.

Crystallographic data collection

X-ray diffraction data sets were collected at 100 K at the European Synchrotron Radiation Facility (ESRF, Grenoble, France) on the beamline ID30A-3/MASSIF-3 (Crystal 1) equipped with an Eiger_4M (Dectris) detector and on the beamline ID30B of the ESRF (Crystal 2) equipped with a Pilatus3_6M (Dectris).

Structure Refinement

Data was processed with AutoProc[3] (Crystal 1) and XDSAPP[4] (Crystal 2), and merged data were phased by molecular replacement with MOLREP,[5] within the CCP4i2 suite,[6] using the rsEGFP2 on-state structure (PDB entry 5DTX) as starting model for Crystal 1 and the rsEGFP2 off-state (PDB entry 5DTY) as a search model for Crystal 2. To obtain the final models, refinement was performed with Refmac5[7] in consecutive cycles (with isotropic B-factors) and finalised with Phenix[8] and manual model building in-between cycles with Coot.[9] As expected, the on-state structure of Crystal 1 was successfully fitted with the model in cis-conformation (PDB entry 5DTX). As for the off-state of Crystal 1 refinement with the chromophore in trans-conformation was not successful and the chromophore appeared to be in the *cis*-conformation as well, we used the cis-conformation model also for the off-state which turned out to be successful. For Crystal 2 both states, the off-state and the off-to-on switched state, could be only fitted successfully with the *trans*-conformational model (PDB entry 5DTY).
The structures were validated using Molprobity[10] and Coot validation tools.

Analysis of kinetic evolution of spectral data

Absorbance spectra were individually baseline corrected with a constant offset calculated based on the average optical density in the 550-650 nm range, eventually corrected to avoid negative optical densities in the 480-540 nm of the spectra. Spectra were smoothed with a moving average filter (smoothing factor of 10) using Matlab 2021a (The MathWorks). On-state populations were monitored by integrating absorbance spectra between 470 and 500 nm, or fluorescence spectra between 495 and 630 nm. To extract decay and recovery rates, off-switching and on-switching curves were fitted with bi-exponential models (ExpGro2 and ExpDec2, respectively) in Origin 2021b (OriginLab Corporation). The rates were calculated taking into account the whole measurement period of 1 s (instead of actual laser illumination times) for each data point.

For calculation of the rsEGFP2 on-state recovery levels, the difference between the maximum and minimum value of the recovery (on-switching) phase was dived by the difference between the maximum and minimum value of the initial off-switching phase.

Extraction of Off1 and Off2 absorption spectra

The absorbance spectrum of the protein in the initial on-state (Supplementary Fig. 8B, green), the spectrum after off-switching with 488 nm laser light (black), and the spectrum of the sample after back on-switching with 405 nm laser light (magenta) were analysed to extract the spectra of each off-state. The on-state spectrum (green) was first scaled to match the shape of the on-state spectrum back-switched with 405 nm light (magenta) to provide the light green spectrum in Supplementary Fig. 8B. Then this scaled spectrum (light green) was subtracted from the back-switched spectrum (magenta), providing the Off_2 spectrum (Supplementary Fig. 8A, blue). Finally, the Off_2 spectrum was subtracted from the experimental off-state spectrum (black), which contains the signatures of both off-states together, to provide the Off_1 spectrum (Supplementary Fig. 8A, magenta).

Estimation of residual off-switching by the 405 nm laser

Residual off-switching by the 405 nm laser was estimated using the ensemble fluorescence on- and off-switching data. First, the off and on-switching rates were estimated using the half-life and half rise time of the fluorescent intensity under 488 nm and 405 nm illumination respectively. The off and on-switching quantum yields were then calculated by dividing the rates by the respective excitation rates (off-switching QY = 5.4e-8, on-switching QY = 2.8e-5). Finally, the switching contrast was estimated by calculating the on- and off-switching rates under 100W/cm^2 405-nm illumination, which gave an off-switching rate of 4.8e-4 s^{-1} and an on-switching rate of 0.43 s^{-1}, resulting in an off:on ratio of ~900.

Ensemble and single-molecule simulations

Simulations were performed using the recently developed SMIS software (ref). A simplified photophysical model of rsEGFP2 was used consisting of two on-state populations (On_1 and On_2) with corresponding off and dark states. The photo switching quantum yields were estimated using the rates extracted from the experimental ensemble and single-molecule data. The photoswitching fatigue experiments were used to estimate the relative populations of On_1 and On_2 (70% and 30% respectively) and the photobleaching quantum yields. It should be noted that different combinations of photobleaching quantum yields from the *On* and *Off* states provide the same ensemble behavior (Supplementary Table 1 and Supplementary Fig. 16).

Single-molecule simulations were performed in 2D using nuclear pore complexes (NPCs) virtually labeled with rsEGFP2 (8 corners, 4 molecules per corner). Off-switching was achieved by 1200 W/cm^2 488 illumination and on-switching by 0.01 W/cm^2 355 nm or 0.2 W/cm^2 405 nm light illumination. Molecules were localized using Thunderstorm,[11] after which the effective labeling efficiency was determined using SMAP.[12] Four simulations of 1 million frames with 25 NPCs each were run.

Single-molecule measurements at cryogenic temperature

Single-molecule measurements were performed on a home-built setup (Supplementary Fig. 18). The microscope body and the cryostat were kindly provided to us by Joerg Enderlein et al and are thoroughly described in a dedicated publication.[13]

Samples were prepared by mixing 1 µl of purified rsEGFP2 fluorescent protein and 1 µl of 1/100 stock dilution of TetraSpek beads (T7279, Thermo Fisher Scientific) in 100 µl of 0.3% w/v PVA (363138-25G, Sigma-Aldrich) in 50 mM HEPES, 300 mM NaCl buffer at pH7.5, to obtain a final protein concentration of 100 nM. Then, round fused silica cover glasses, 12 mm in diameter (Shanghai Wechance Industrial Co., Ltd), were cleaned in a UV-ozone cleaner (UVOCS) for 20 min and spin-coated with a protein/polymer mixture (7.5 µl drop) in two steps: 30 s at 1000 rpm followed by 60s at 3000 rpm.[14] The cover glass was next plunge frozen in LN2, mounted on the sample holder and transferred to the cryostat. A vacuum of ~10^{-3}-10^{-4} Pa was regenerated with a turbo pump (HiCube, Pfeiffer Vaccum). A temperature sensor installed at the level of the sample-mount chamber gave a value of 110 K. A flexible tube delivering dry gaseous N_2 was taped to the bottom of the cryostat to prevent residual condensation/ ice formation during experiments.

To excite rsEGFP2, the sample was illuminated with a 488 nm laser (LBX-488-200, Oxxius) at 275 W/cm². This power density was shown in previous studies to be sufficiently low to not induce sample devitrification.[15] As an additional control, we compared the rsEGFP2 emission spectrum on the single-molecule cryo-microscope with that measured on the microspectrophotometer (Supplementary Fig. 19). Both spectra showed similar band narrowing when compared to a spectrum collected at RT.

A UV laser at 405 nm (06-MLD 405 nm, Cobolt), set to 1 mW/cm², was used for protein activation. This very small power density was used to account for the rather high protein concentration of our samples.

Fluorescence was collected by a long working distance Olympus air objective (0.7 NA) and detected by an EMCCD camera (Evolve 512, Photometrics). The pixel size measured with a Thorlabs ruler (R1L3S2P) was 276 nm/px.

The integration of a fiber-coupled 355 nm laser to the cryo-microscope is currently in progress.

Single molecule data were acquired with Micro-Manager 2.0. The camera exposure time was set to 100 ms and EM Gain to 200. The acquisition sequence was programmed in Labview, which sends trigger pulses to camera and lasers (Supplementary Fig. 20).

Single molecules were localized using the ThunderSTORM plugin of ImageJ and data was further analyzed with in-house Matlab code.[16] Active times were calculated as the sum of on- and off-times (as most molecules were not irreversibly photobleached at the end of the acquisitions). Number of photons and localization precision were exported from ThunderSTORM after merging localizations belonging to the same molecule (maximum

distance between two localizations: 20 nm; blinking gap: 1). To compare the photon budget and localization uncertainty of rsEGPF2 with a standard PCFP, single-molecule data of mEos4b from previous work[16] was used. These data were processed in the same manner as the rsEGFP2 data presented in this work to extract the median photon budget per merged localization and the median localization uncertainty.

References

(1) El Khatib, M.; Martins, A.; Bourgeois, D.; Colletier, J.-P.; Adam, V. Rational Design of Ultrastable and Reversibly Photoswitchable Fluorescent Proteins for Super-Resolution Imaging of the Bacterial Periplasm. *Sci Rep* **2016**, *6*, 18459. https://doi.org/10.1038/srep18459.

(2) Byrdin, M.; Bourgeois, D. The CAL(AI)2DOSCOPE: A Microspectrophotometer for Accurate Recording of Correlated Absorbance and Fluorescence Emission Spectra. *Spectroscopy Europe*. 2016, pp 14–17.

(3) Vonrhein, C.; Flensburg, C.; Keller, P.; Sharff, A.; Smart, O.; Paciorek, W.; Womack, T.; Bricogne, G. Data Processing and Analysis with the AutoPROC Toolbox. *Acta Crystallogr D Biol Crystallogr* **2011**, *67* (Pt 4), 293–302. https://doi.org/10.1107/S0907444911007773.

(4) Krug, M.; Weiss, M. S.; Heinemann, U.; Mueller, U. XDSAPP: A Graphical User Interface for the Convenient Processing of Diffraction Data Using XDS. *J Appl Cryst* **2012**, *45* (3), 568–572. https://doi.org/10.1107/S0021889812011715.

(5) Vagin, A.; Teplyakov, A. Molecular Replacement with MOLREP. *Acta crystallographica. Section D, Biological crystallography* **2010**, *66* (Pt 1), 22–25. https://doi.org/10.1107/S0907444909042589.

(6) Potterton, L.; Agirre, J.; Ballard, C.; Cowtan, K.; Dodson, E.; Evans, P. R.; Jenkins, H. T.; Keegan, R.; Krissinel, E.; Stevenson, K.; Lebedev, A.; McNicholas, S. J.; Nicholls, R. A.; Noble, M.; Pannu, N. S.; Roth, C.; Sheldrick, G.; Skubak, P.; Turkenburg, J.; Uski, V.; von Delft, F.; Waterman, D.; Wilson, K.; Winn, M.; Wojdyr, M. CCP4i2: The New Graphical User Interface to the CCP4 Program Suite. *Acta Crystallogr D Struct Biol* **2018**, *74* (Pt 2), 68–84. https://doi.org/10.1107/S2059798317016035.

(7) Murshudov, G. N.; Vagin, A. A.; Dodson, E. J. Refinement of Macromolecular Structures by the Maximum-Likelihood Method. *Acta Crystallogr. D* **1997**, *53*, 240–255.

(8) Adams, P. D.; Afonine, P. V.; Bunkoczi, G.; Chen, V. B.; Davis, I. W.; Echols, N.; Headd, J. J.; Hung, L.-W.; Kapral, G. J.; Grosse-Kunstleve, R. W.; McCoy, A. J.; Moriarty, N. W.; Oeffner, R.; Read, R. J.; Richardson, D. C.; Richardson, J. S.; Terwilliger, T. C.; Zwart, P. H. PHENIX: A Comprehensive Python-Based System for Macromolecular Structure Solution. *Acta Crystallographica Section D* **2010**, *66* (2), 213–221. https://doi.org/10.1107/S0907444909052925.

(9) Emsley, P.; Lohkamp, B.; Scott, W. G.; Cowtan, K. Features and Development of Coot. *Acta Crystallogr D Biol Crystallogr* **2010**, *66* (Pt 4), 486–501. https://doi.org/10.1107/S0907444910007493.

(10) Williams, C. J.; Headd, J. J.; Moriarty, N. W.; Prisant, M. G.; Videau, L. L.; Deis, L. N.; Verma, V.; Keedy, D. A.; Hintze, B. J.; Chen, V. B.; Jain, S.; Lewis, S. M.; Arendall, W. B.; Snoeyink, J.; Adams, P. D.; Lovell, S. C.; Richardson, J. S.; Richardson, D. C. MolProbity: More and Better

Reference Data for Improved All-Atom Structure Validation. *Protein Sci* **2018**, *27* (1), 293–315. https://doi.org/10.1002/pro.3330.

(11) Ovesný, M.; Křížek, P.; Borkovec, J.; Švindrych, Z.; Hagen, G. M. ThunderSTORM: A Comprehensive ImageJ Plug-in for PALM and STORM Data Analysis and Super-Resolution Imaging. *Bioinformatics* **2014**, *30* (16), 2389–2390. https://doi.org/10.1093/bioinformatics/btu202.

(12) Ries, J. SMAP: A Modular Super-Resolution Microscopy Analysis Platform for SMLM Data. *Nat Methods* **2020**, *17* (9), 870–872. https://doi.org/10.1038/s41592-020-0938-1.

(13) Li, W.; Stein, S. C.; Gregor, I.; Enderlein, J. Ultra-Stable and Versatile Widefield Cryo-Fluorescence Microscope for Single-Molecule Localization with Sub-Nanometer Accuracy. *Optics Express* **2015**, *23* (3), 3770–3783. https://doi.org/10.1364/OE.23.003770.

(14) Mazal, H.; Wieser, F.-F.; Sandoghdar, V. Deciphering a Hexameric Protein Complex with Angstrom Optical Resolution. *eLife* **2022**, *11*, e76308. https://doi.org/10.7554/eLife.76308.

(15) Tuijtel, M. W.; Koster, A. J.; Jakobs, S.; Faas, F. G. A.; Sharp, T. H. Correlative Cryo Super-Resolution Light and Electron Microscopy on Mammalian Cells Using Fluorescent Proteins. *Sci Rep* **2019**, *9* (1), 1369. https://doi.org/10.1038/s41598-018-37728-8.

(16) Wulffele, J.; Thédié, D.; Glushonkov, O.; Bourgeois, D. MEos4b Photoconversion Efficiency Depends on Laser Illumination Conditions Used in PALM. *J. Phys. Chem. Lett.* **2022**, *13* (22), 5075–5080. https://doi.org/10.1021/acs.jpclett.2c00933.

Supplementary figures

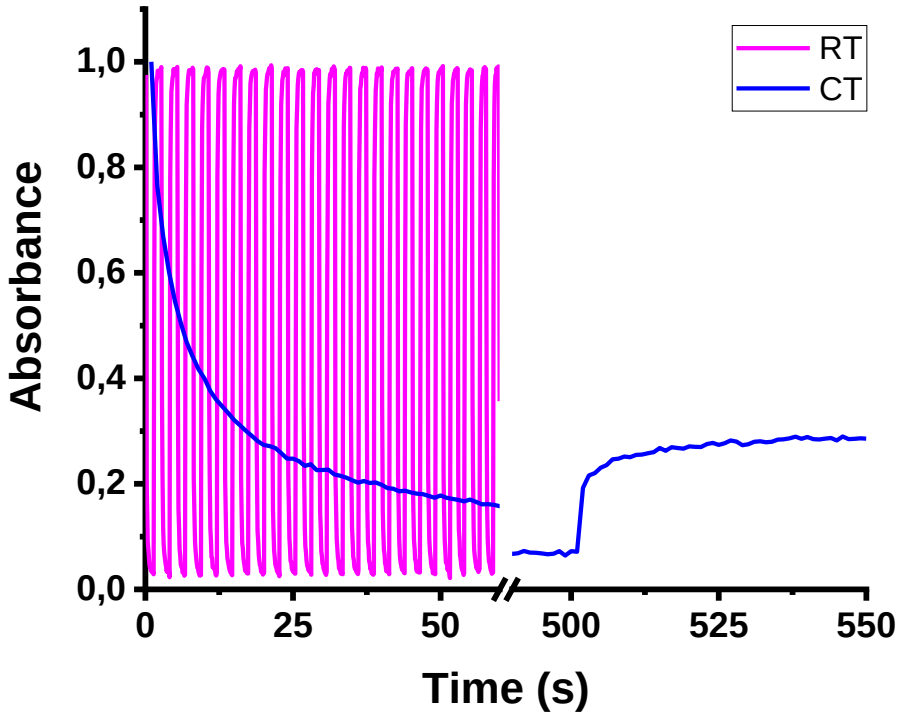

Figure S1: Comparison of rsEGFP2 photoswitching at room and cryogenic temperature. Absorbance is measured by integration of the absorbance spectra in the 470-500 nm spectral range. For data at RT (magenta), alternative illumination at 488 nm (1.4 s, 490 W/cm²) and 405 nm (1.4 s, 100 W/cm²) was carried out 23 times. For data at CT (blue), illumination at 488 nm (5.7 kW/cm²) was performed for 500 seconds followed by illumination at 405 nm (0.95 kW/cm²) for 50 seconds. Data normalized to 1 at the start of acquisition.

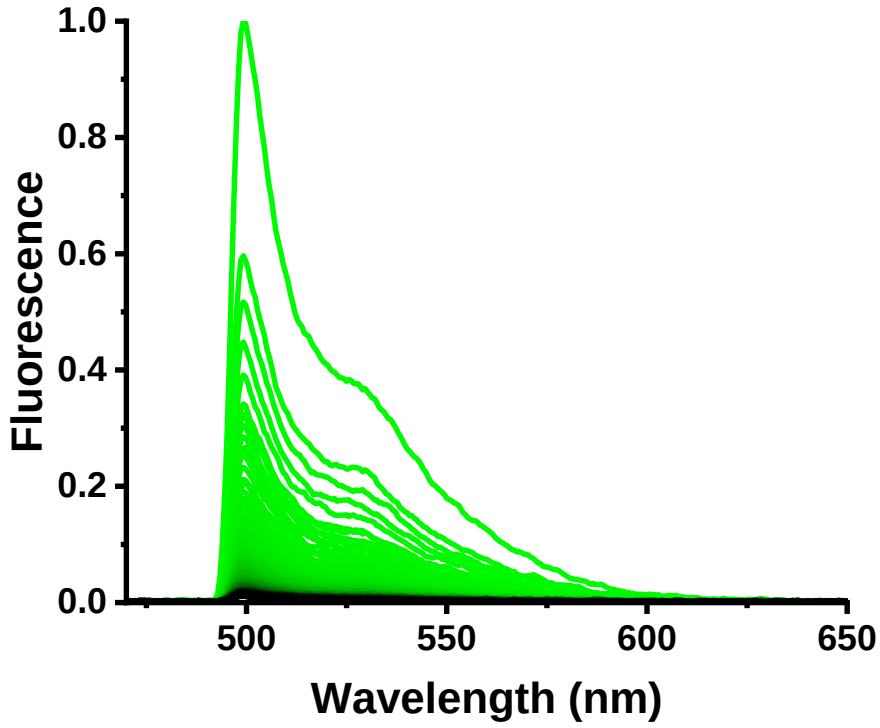

Figure S2: On-to-off photoswitching (green-to-black) of rsEGFP2 at 110 K with 488 nm laser light (5.8 kW/cm²) applied for 500 s, monitored by fluorescence microspectrophotometry. Fluorescence emission spectra were normalized to 1 at the maximum value of the first spectrum.

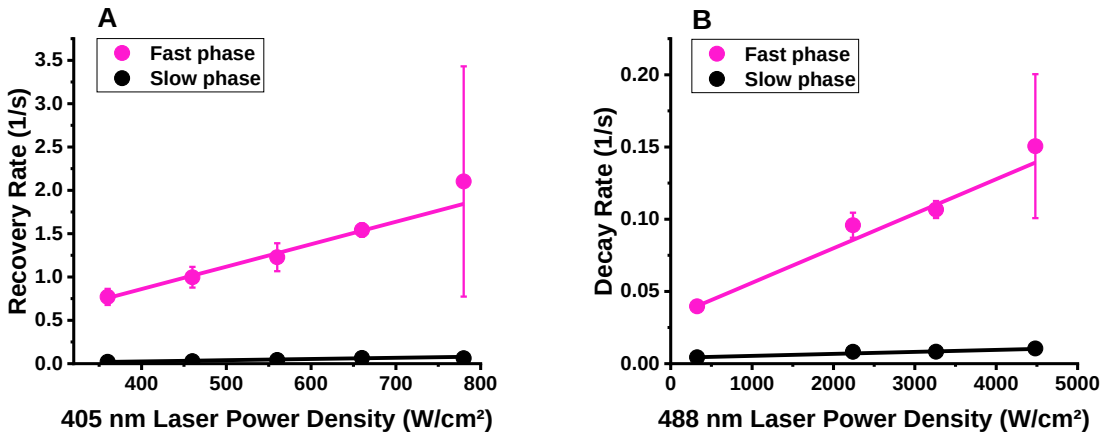

Figure S3: Rates of rsEGFP2 off-to-on switching at CT as a function of 405 nm laser power density (A) and on-to-off switching as a function of 488 nm laser power density (B). Mean rates and standard deviations were extracted from bi-exponential fits of 3 independent switching measurements. Straight lines show linear fits to experimental rates as a function of laser power densities.

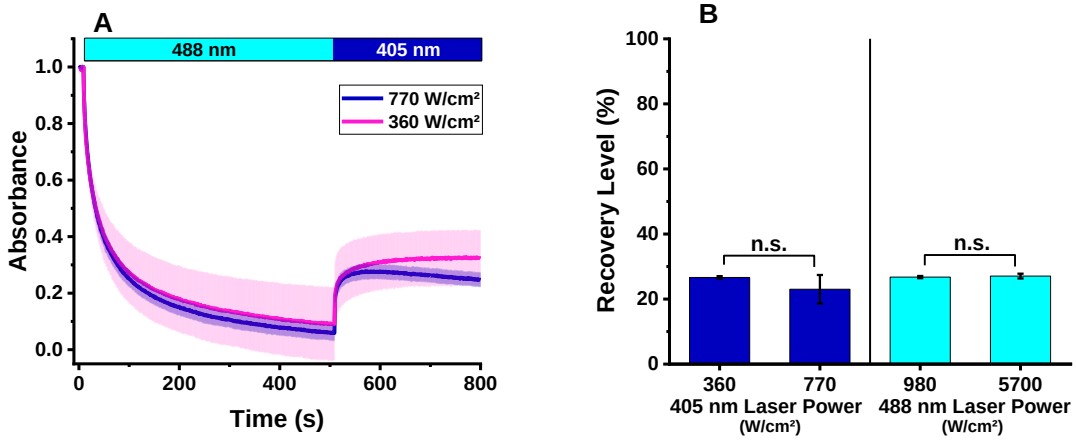

Figure S4: (A) Evolution of rsEGFP2 recovered on-state absorbance upon illumination with medium or strong 405 nm laser light. The decay of absorbance observed at 0.8 kW/cm² suggests the onset of photobleaching. Absorbance is calculated by integration of the absorption spectra in the 470-500 nm spectral range. Absorbance switching kinetics was measured at 110 K by alternate illumination (indicated in the upper bar) with 488 nm (1.0 kW/cm²) and 405 nm laser light with lower (0.36 kW/cm²) or higher power density (0.77 kW/cm²). Absorbance is normalized to 1 at start of acquisition. The mean ± s.d. of n ≥ 3 measurements is shown. (B) Off-to-on recovery levels compared for two different 405 nm laser power densities, using 488 nm laser light at 1.0 kW/cm² for initial off switching, or two different 488 nm laser power densities, using 405 nm laser light at 0.5 kW/cm² for recovery. n.s: not significant.

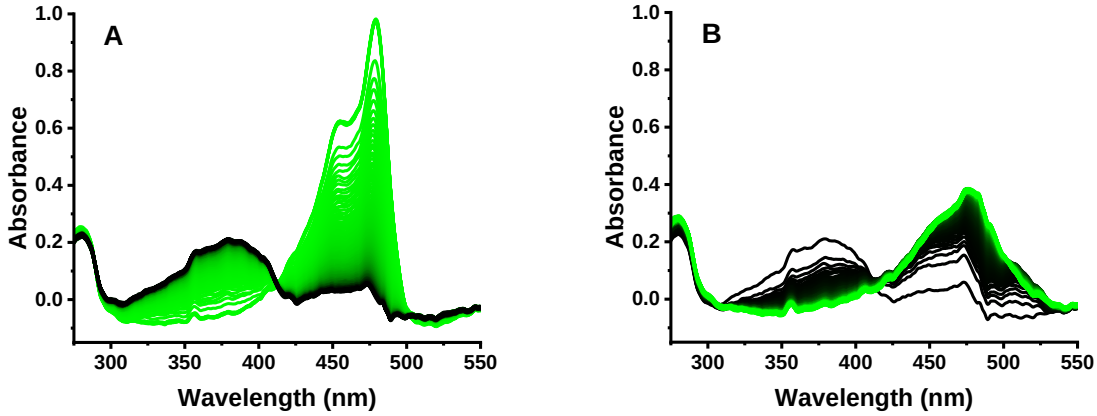

Figure S5: On-to-off photoswitching (green-to-black) of rsEGFP2 at 110 K with 488 nm laser light (0.9 kW/cm²) for 500 s (A) and off-to-on photoswitching (black-to-green) with 355 nm laser light (0.015 kW/cm²) for 500 s (B) monitored by absorption microspectrophotometry. Spectra were normalized at the anionic chromophore peak of the first spectrum in A.

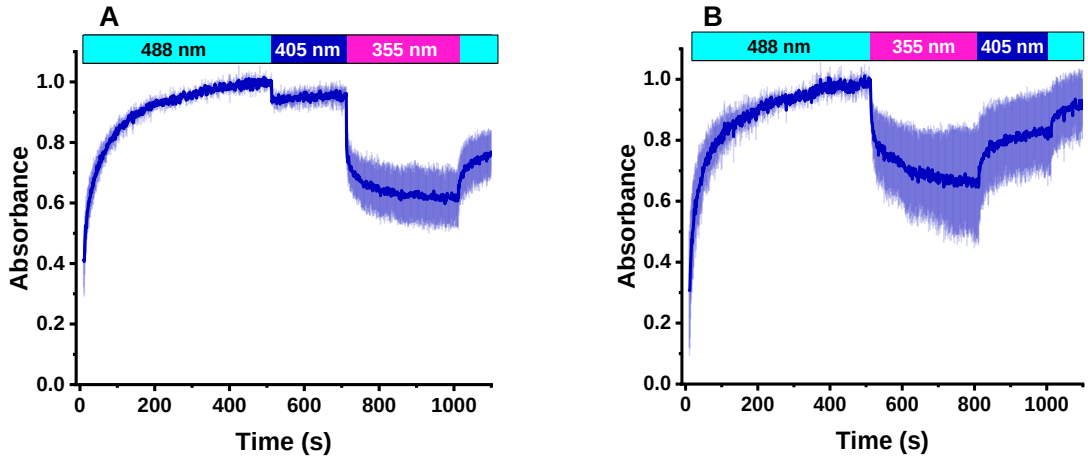

Figure S6: Evolution of absorbance at 320 nm, representative of the Off_1 population, during rsEGFP2 switching at CT with 488 nm (0.4 kW/cm²), and subsequent illumination with 405 nm (0.3 kW/cm²) followed by 355 nm laser illumination (0.03 kW/cm²) (A), or 355 nm (0.02 kW/cm²) followed by 405 nm laser illumination (0.3 kW/cm²) (B), according to the schemes indicated in the upper bars. Integrated absorbance between 315 and 325 nm was measured. Absorbance was normalized to 1 at the highest value of the first phase (488 nm illumination). The mean ± s.d. of n = 3 measurements is shown.

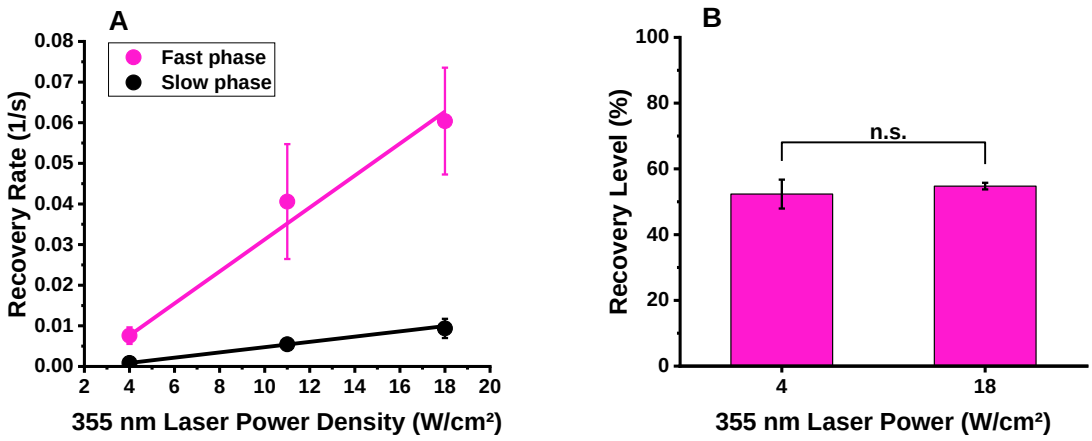

Figure S7: (A) Rates of off-to-on switching of rsEGFP2 at CT as a function of 355 nm power density extracted from bi-exponential fits of 3 independent switching measurements. The straight lines show linear fits to extracted rates as a function of laser power density. (B) On state recovery level for two different 355 nm laser power densities. For pre-on-to-off switching, 488 nm laser light of 1.0 kW/cm² was used for all measurements. n.s: not significant.

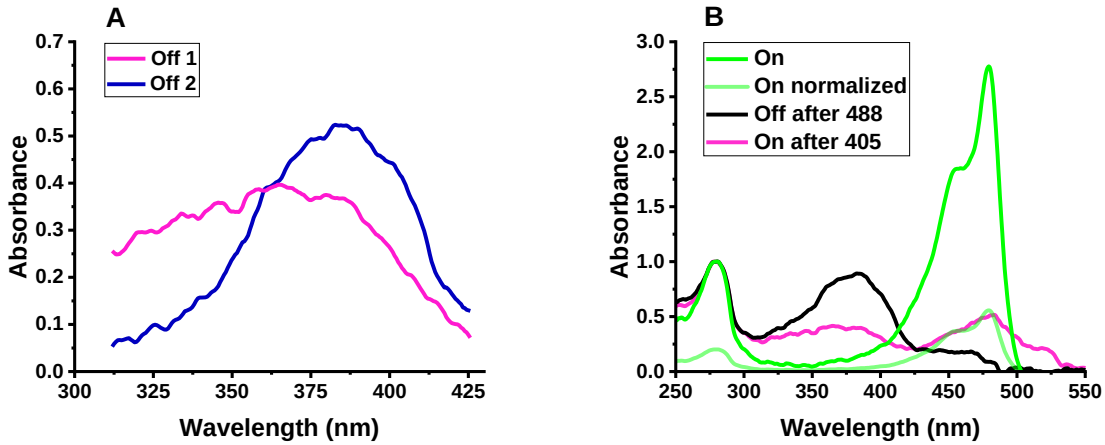

Figure S8: (A) Estimated Off_1 and Off_2 absorption spectra extracted by computation of difference spectra. Scaling of the spectra incorporates relative populations in Off_1 and Off_2 (B) Absorption spectrum of rsEGFP2 in the on-state (green, and normalized version in light green), in the off-state (black) and in the recovered on-state after preliminary off- and on-switching (magenta). The absorption spectrum of Off_1 was obtained by subtracting the normalized on-state spectrum from the recovered on-state spectrum. The Off_2 absorption spectrum was obtained by subtracting Off_1 from the off-state spectrum.

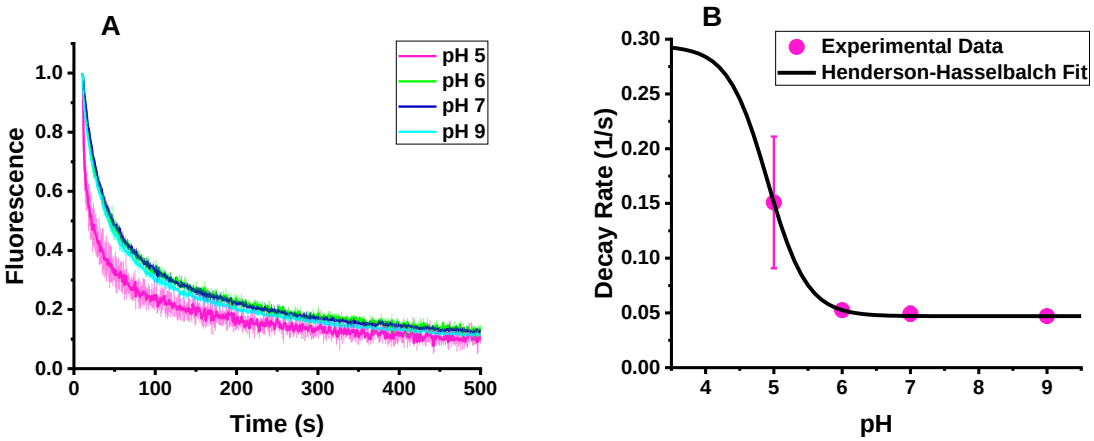

Figure S9: pH dependence of rsEGFP2 off-switching at CT. (A) off-switching curves at different pH values (488 nm laser light, 1.0 kW/cm²). Fluorescence levels are calculated by integration of the fluorescence emission spectra in the 495-630 nm spectral range. (B) Decay rates corresponding to the fast phase of on-to-off switching, as a function of pH and extracted from bi-exponential fits of 3 independent switching measurements. The dark curve shows a fit with a Henderson-Hasselbalch function.

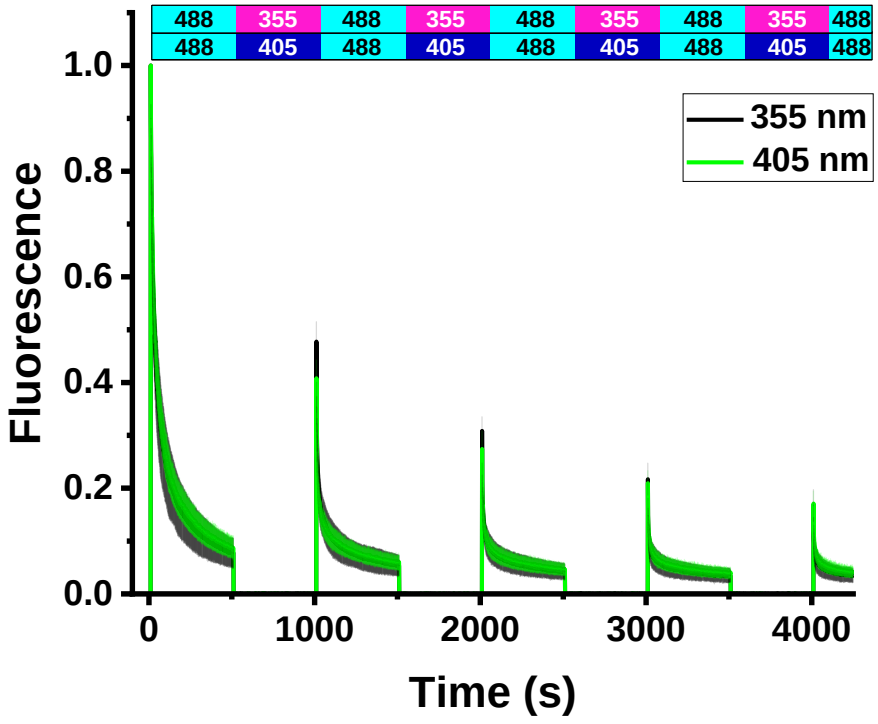

Figure S10: Fluorescence photofatigue switching curves of rsEGFP2 at CT, corresponding to the absorbance photofatigue data shown in Fig. 4. Fluorescence was calculated by integration of the fluorescence emission spectra in the 495-630 nm spectral range. Back and forth switching was performed with 488 nm (1.0 kW/cm²) and either 405 nm (0.2 kW/cm², green) or 355 nm (0.01 kW/cm², black) laser light, corresponding to the illumination schemes shown in the upper bars. Fluorescence was normalized to 1 at the start of acquisition. The mean ± s.d. of n = 3 measurements is shown.

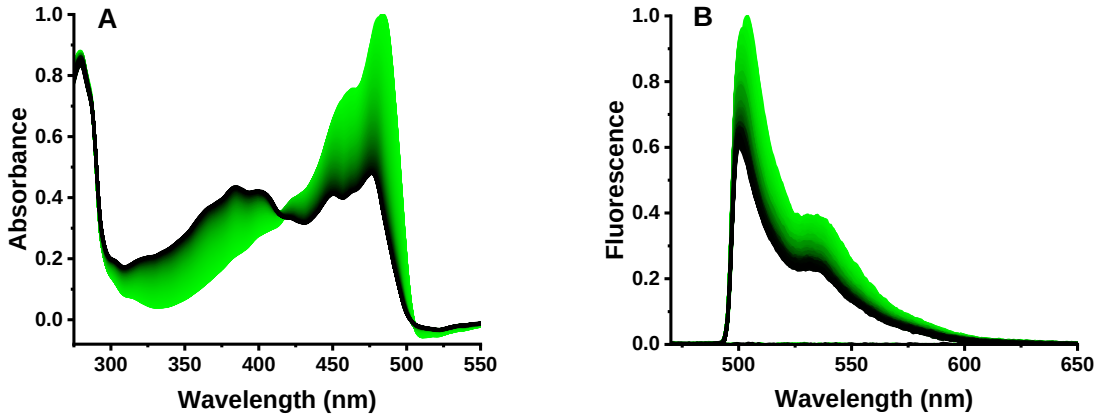

Figure S11: On-to-off photoswitching (green-to-black) of an rsEGFP2 crystal at 110 K with 488 nm laser light (0.05 kW/cm²) for 700 s monitored by (A) absorption and (B) fluorescence emission microspectrophotometry. Spectra were normalized to 1 at the highest value of the first spectrum.

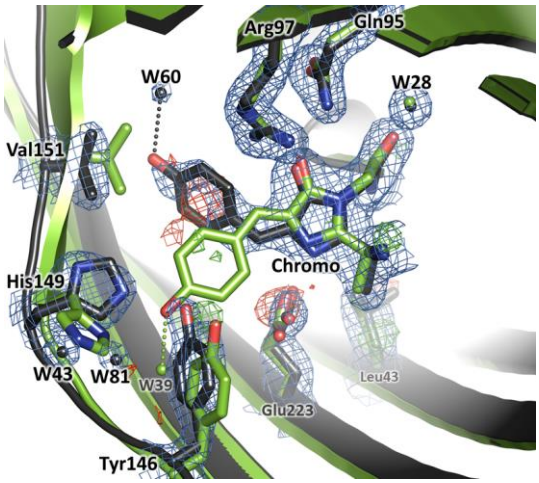

Figure S12: Crystallographic view of rsEGFP2 switching at RT (control experiment). Refined models of the chromophore and surrounding residues of rsEGFP2 are shown in the cis on state (green carbons and water molecules) and in the trans off state (dark grey carbons and water molecules).

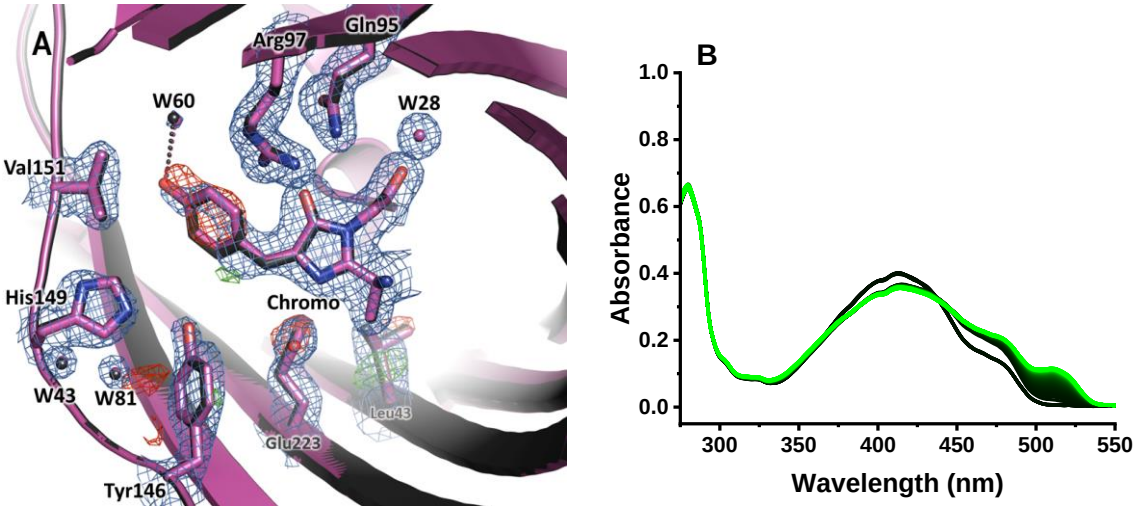

Figure S13: (A) Refined models of the chromophore and surrounding residues of rsEGFP2 in its trans off state switched at RT by 488 nm illumination (3.4 W/cm²) (dark grey carbons and water molecules) and in the same state followed by 405 nm illumination (14 W/cm² for 180 s) at CT (purple carbons and water molecules, PDB model 8AHB). Both structures nearly perfectly overlap, so that only the second one is visible. The 2Fobs-Fcalc electron density map contoured at 1σ (blue) and the Fobs-Fcalc difference electron density maps contoured at ±3 σ (red: negative, green: positive) of the RT-switched state followed by 405 nm illumination at 110K are shown. (B) Off-to-on switching (black-to-green) by 405 nm illumination was monitored in crystalline rsEGFP2 by absorption microspectrophotometry. The absorbance spectra were normalized at the protonated peak as in Fig. 1E.

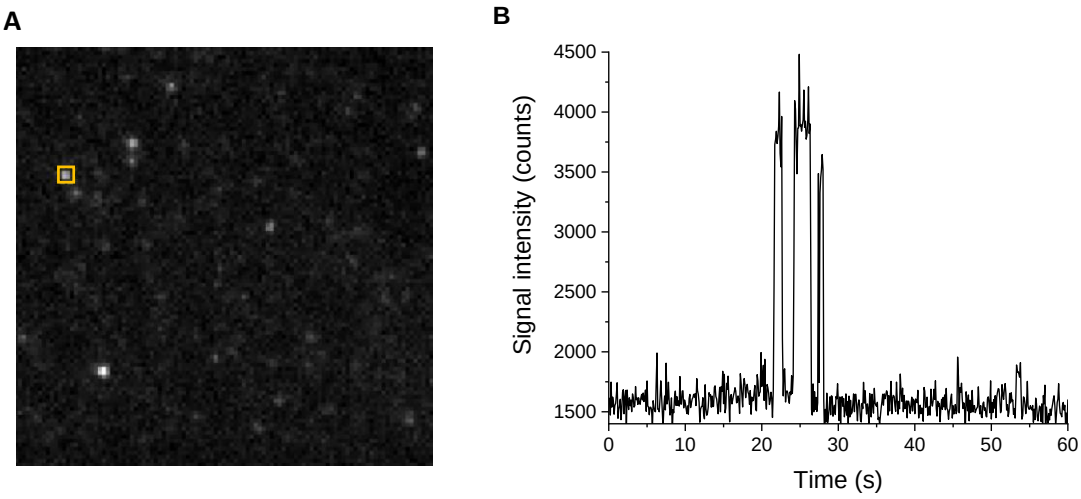

Figure S14: Single-molecule data collection on rsEGFP2 at CT. A: example of a single frame with individual localizations of rsEGFP2 molecules. B: intensity trace during acquisition corresponding to the single molecule highlighted in yellow in A.

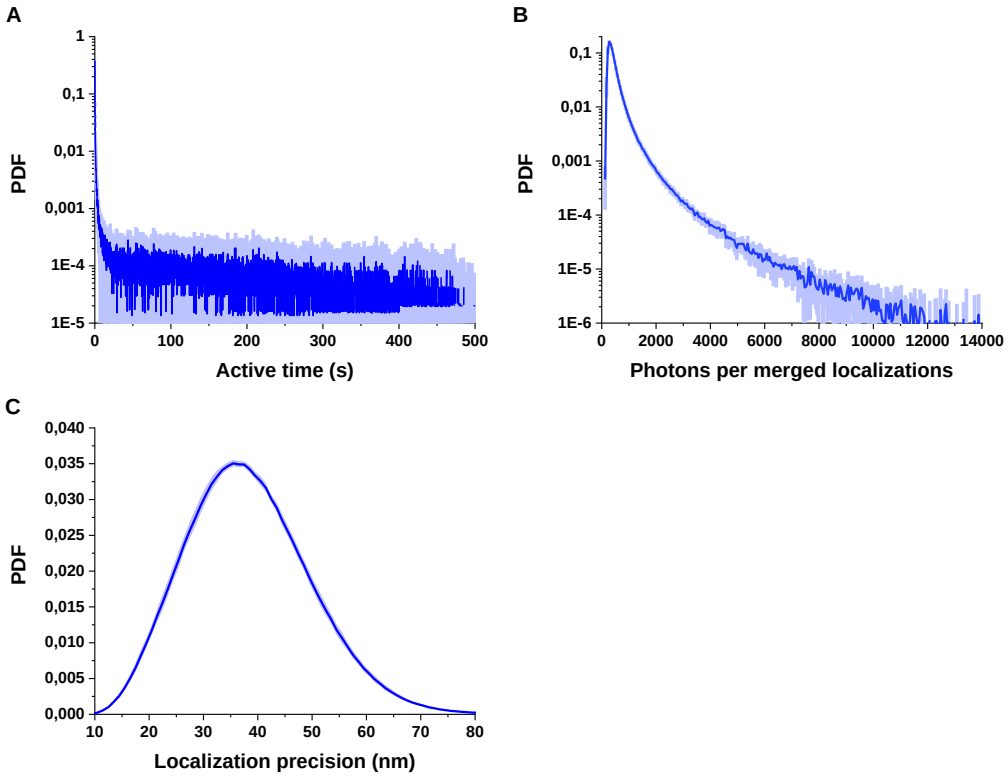

Figure S15: (A) active time (sum of on- and off-times), (B) photon budget and (C) localization precision probability density functions extracted from CT single-molecule measurements.

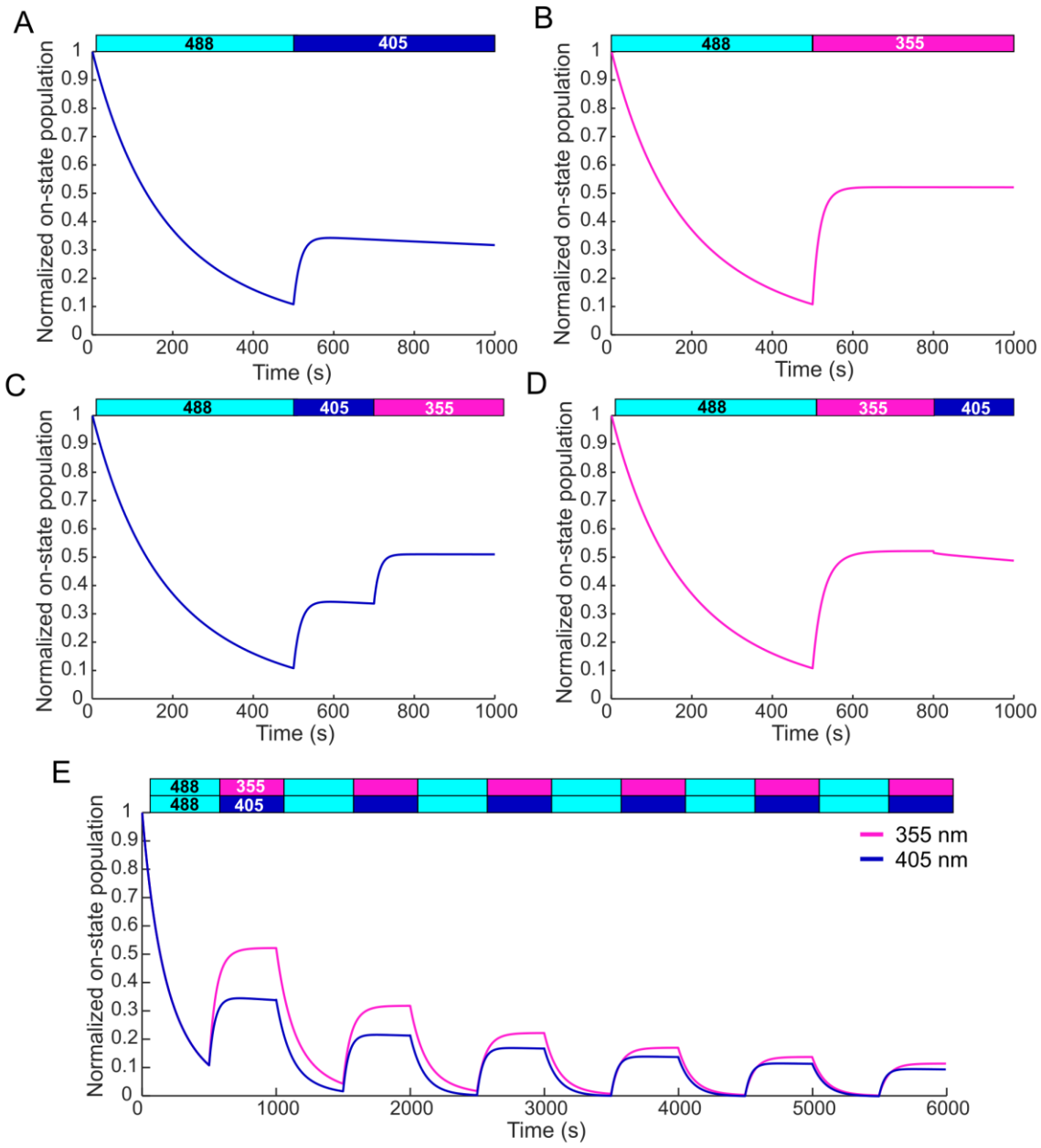

Figure S16: Ensemble simulations of rsEGFP2 photoswitching at CT. A: Off-switching by 500 W/cm2 488 nm light followed by on-switching by 500 W/cm2 405 nm light. B: Off-switching by 500 W/cm2 488 nm light followed by on-switching by 30 W/cm2 355 nm light. C: Off-switching by 500W/cm2 488 nm light followed by sequential on-switching by 500 W/cm2 405 nm light and 30 W/cm2 355 nm light. D: Off-switching by 500 W/cm2 488 nm light followed by sequential on-switching by 20 W/cm2 355 nm light and 500 W/cm2 405 nm light. E: Photofatigue switching curves under 500 W/cm2 488 nm light and 20 W/cm2 355 nm or 100 W/cm2 405 nm light.

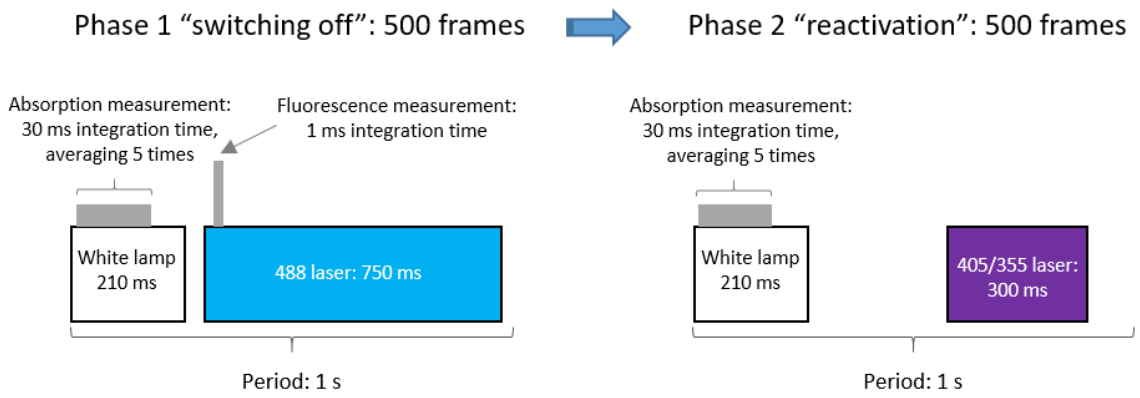

Figure S17: Illumination scheme employed in microspectrophotometry experiments at CT. During 750 ms of a 1 s period (75% duty cycle) a 488 nm laser was used to switch off the rsEGFP2 molecules, repeated for 500 frames. During the second phase, a 405 nm / 355 nm laser was applied for 300 ms (30% duty cycle), in order to reactivate the molecules, repeated for typically 500 frames. Before laser illumination a white lamp was switched on to measure the absorption of the protein. See methods, section “Solution sample illumination”.

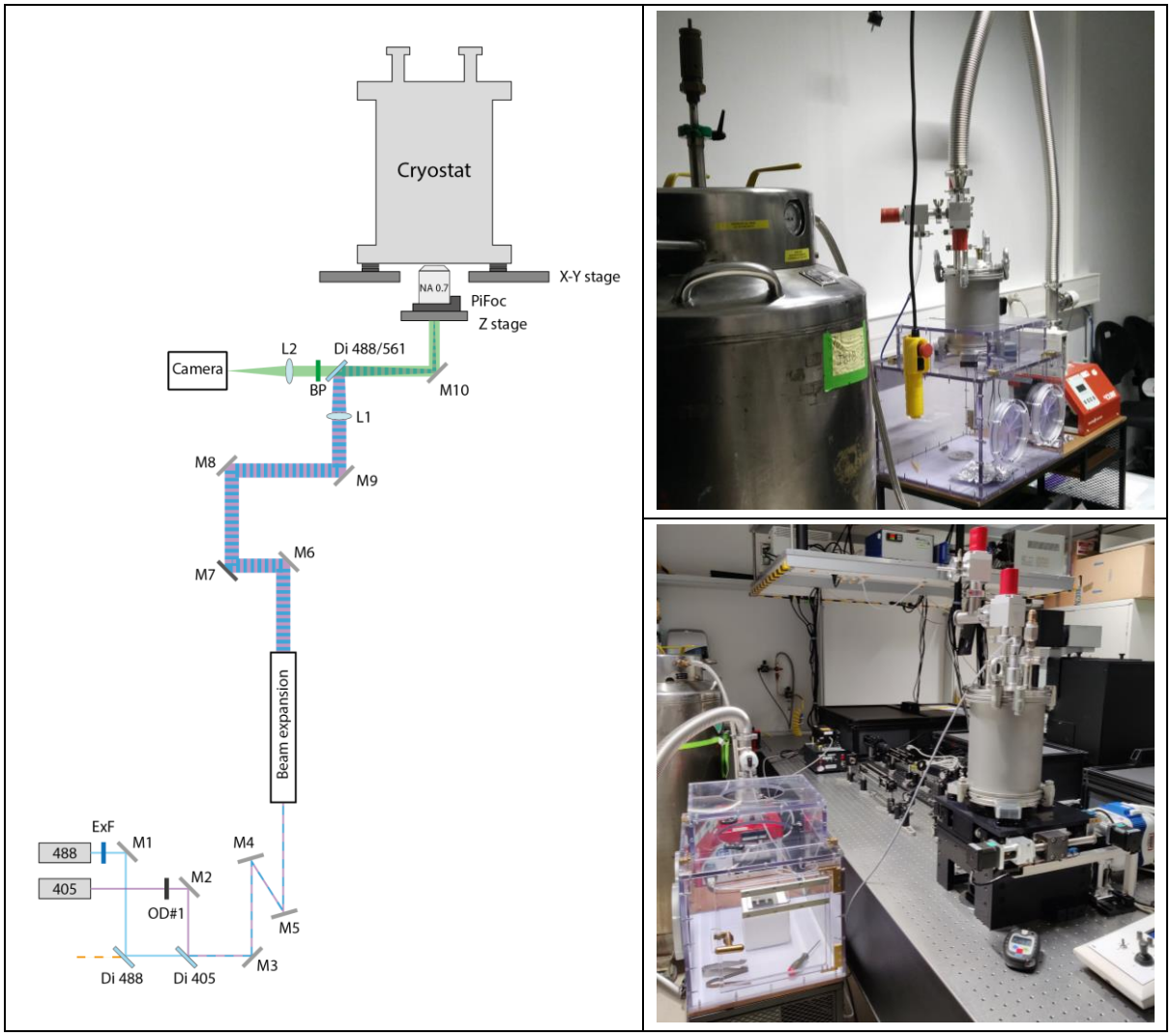

Figure S28: Schematic illustration and photos of the "cryoPALM" setup. Laser beams at 488 nm (LBX-488-200, Oxxius) and 405 nm (06-MLD 200mW, Cobolt) are first combined together with help of a single-edge 405 nm dichroic mirror (DMLP425, Thorlabs), then expended eight times with a set of achromatic lenses (Thorlabs) and focused with L1 (AC254-300-A-ML, Thorlabs) on the back focal plane of the 60x air objective (LUCPLFLN60X/0.70, Olympus) to produce a wide-field epi illumination of the protein sample mounted in a cryostat. The emission signal is separated from the excitation light with a Di03-R488/561-t1 dichroic mirror (Semrock) and further filtered with a FF01-525/45 band-pass filter (Semrock). The image is finally focused onto an Evolve 512 EM-CCD (Photometrics) camera using an AC508-180-A-ML lens (Thorlabs). A neutral density filter can be inserted into the 405 nm laser beam path for precise adjustment of very low activation laser power. M1 - M10: broadband dielectric mirrors (BB1-E02, Thorlabs).

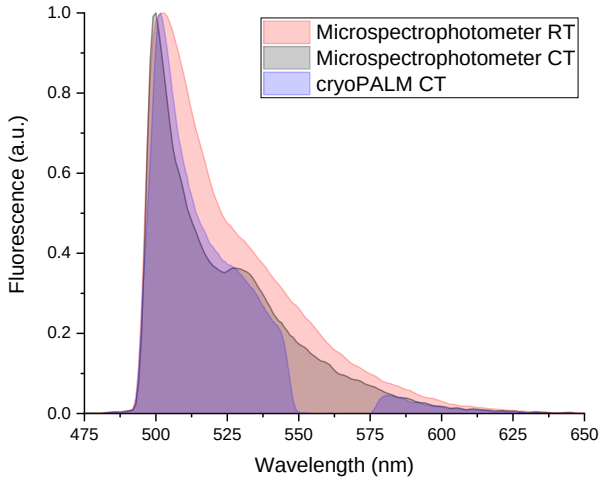

Figure S19: Fluorescence spectra comparison for measurements done on the micro-spectrophotometer at RT and CT in capillaries and on the cryoPALM setup working with protein-coated cover glasses. The gap in the later one corresponds to the 561 nm reflection band of the Di03-R488/561-t1 dichroic mirror.

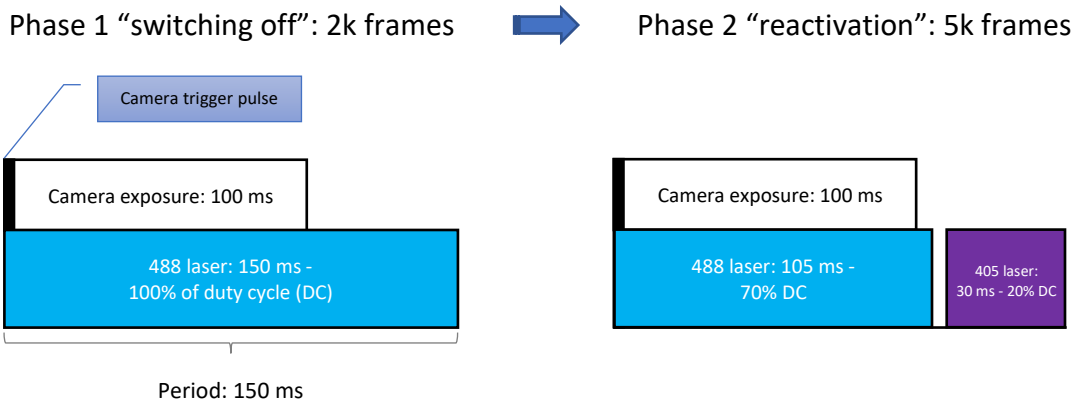

Figure S20: Illumination scheme employed in single-molecule experiments at CT. During 2000 frames a 488 nm laser was used to switch off the rsEGFP2 molecules and enter the single-molecule regime. During the second phase (5000 frames), a 405 nm laser was added to reactivate the molecules (after the camera exposure to not interfere with image readout).

Supplementary Tables

Table S1. Quantum yields and thermal rates in s^{-1} used for simulations of rsEGFP2 photoswitching at CT.

	On1	**On2**	**Off1**	**Off2**	**Offsl_1**	**Offsl_2**	**Bleached**
On1	-	-	1.3e-8	-	2.6e-5	-	1.7e-8
On2	-	-	-	7.1e-8	-	2.6e-5	7.9e-9
Off1	2.1e-5	-	-	-	-	-	1.2e-5
Off2	-	1.7e-6	-	-	-	-	1.0e-7
Offsl_1	11.0*	-	-	-	-	-	-
Offsl_2	-	11.0*	-	-	-	-	-

* Thermal rates

Note: Quantum yields and rates are estimations rather than exact calculations.

Table S2. Data collection and refinement statistics of Crystal 1 (off-switching at CT).

Crystal 1	***Position 1, Initial state***	***Position 2, Cryo-switched off***
Pre-illumination	None	488 nm, 110K
PDB accession code	Not deposited	8AHA
Beamline	ESRF ID30A-3 (MASSIF-3)	ESRF ID30A-3 (MASSIF-3)
Wavelength (Å)	0.9677	0.9677
Resolution range (Å)	42.35-2.32 (2.403-2.32)	46.32-2.38 (2.465-2.38)
Space group	P 21 21 21	P 21 21 21
Unit cell dimensions (a, b, c) (Å)	52.46, 60.77, 71.75	52.40, 60.75, 71.58
Unit cell angles (α, β, γ) (°)	90.0, 90.0, 90.0	90.0, 90.0, 90.0
Total reflections	134796 (13901)	124380 (12739)
Unique reflections	10390 (1021)	9604 (941)
Multiplicity	13.0 (13.6)	13.0 (13.5)
Completeness (%)	99.78 (100.00)	99.88 (100.00)
Mean I/sigma(I)	8.44 (2.31)	11.44 (2.23)
Wilson B-factor (Å²)	34.31	33.76
R-merge	0.2258 (1.441)	0.2481 (1.453)
R-meas	0.2352 (1.498)	0.2583 (1.51)
R-pim	0.0649 (0.4044)	0.07113 (0.4082)
CC1/2	0.993 (0.754)	0.996 (0.714)
CC*	0.998 (0.927)	0.999 (0.913)
Reflections used in refinement	10381 (1022)	9600 (941)
Reflections used for R-free	508 (46)	490 (43)
R-work	0.1943 (0.2272)	0.1857 (0.1997)
R-free	0.2436 (0.3260)	0.2251 (0.3601)
CC(work)	0.937 (0.880)	0.951 (0.886)
CC(free)	0.929 (0.694)	0.918 (0.599)
Number of non-hydrogen atoms	2008	2008
macromolecules	1886	1886
ligands	60	60
solvent	62	62
Protein residues	237	237
RMS(bonds)	0.008	0.008
RMS(angles)	1.04	1.01
Ramachandran favored (%)	97.00	97.85
Ramachandran allowed (%)	3.00	2.15
Ramachandran outliers (%)	0.00	0.00
Rotamer outliers (%)	0.00	0.48

Clashscore	3.69	2.11
Average B-factor (Å²)	36.80	36.21
macromolecules	35.89	35.29
ligands	65.03	65.59
solvent	36.88	35.51

Statistics for the highest-resolution shell are shown in parentheses.

Table S3. Data collection and refinement statistics of Crystal 2 (back-switching at CT after off-switching at RT).

Crystal 2	***Position 1, RT-switched off***	***Position 2, RT-switched off + cryo-switched on***
Pre-illumination	488 nm, RT	488 nm, RT + 405 nm, 110K
PDB accession code	Not deposited	8AHB
Beamline	ESRF ID30B	ESRF ID30B
Wavelength (Å)	0.9763	0. 9763
Resolution range (Å)	46.40-1.82 (1.885-1.82)	46.44-1.79 (1.858-1.79)
Space group	P 21 21 21	P 21 21 21
Unit cell dimensions (a, b, c) (Å)	51.43, 61.78, 70.26	51.67, 61.76, 70.44
Unit cell angles (α, β, γ) (°)	90.0, 90.0, 90.0	90.0, 90.0, 90.0
Total reflections	228965 (10899)	254080 (14673)
Unique reflections	20581 (1724)	21607 (2020)
Multiplicity	11.1 (5.7)	11.8 (7.3)
Completeness (%)	98.41 (85.14)	99.36 (94.43)
Mean I/sigma(I)	9.59 (0.31)	10.87 (0.45)
Wilson B-factor	36.04	34.59
R-merge	0.1465 (3.939)	0.1268 (3.356)
R-meas	0.1534 (4.348)	0.1326 (3.616)
R-pim	0.04481 (1.785)	0.03823 (1.315)
CC1/2	0.998 (0.155)	0.999 (0.237)
CC*	1 (0.519)	1 (0.619)
Reflections used in refinement	20356 (1724)	21589 (2018)
Reflections used for R-free	1018 (86)	1081 (101)
R-work	0.1959 (0.5422)	0.1921 (0.4730)
R-free	0.2418 (0.5371)	0.2195 (0.4800)
CC(work)	0.962 (0.374)	0.964 (0.606)
CC(free)	0.961 (0.503)	0.959 (0.555)
Non-hydrogen atoms	2030	2030
macromolecules	1902	1902
ligands	40	40
solvent	88	88
Protein residues	235	235
RMS(bonds)	0.006	0.006
RMS(angles)	0.95	0.92
Ramachandran favored (%)	99.13	99.13
Ramachandran allowed (%)	0.87	0.87
Ramachandran outliers (%)	0.00	0.00
Rotamer outliers (%)	1.90	1.90
Clashscore	3.67	2.62
Average B-factor	39.61	39.37
macromolecules	38.92	38.66
ligands	63.26	63.66
solvent	43.69	43.61

Statistics for the highest-resolution shell are shown in parentheses.

ChemPhysChem

Research Article
doi.org/10.1002/cphc.202200192

Chemistry Europe
European Chemical Societies Publishing

www.chemphyschem.org

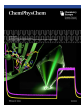

Rational Control of Off-State Heterogeneity in a Photoswitchable Fluorescent Protein Provides Switching Contrast Enhancement**

Virgile Adam[+,[a]] Kyprianos Hadjidemetriou[+,[a]] Nickels Jensen[+,[b]] Robert L. Shoeman[+,[c]] Joyce Woodhouse[+,[a]] Andrew Aquila,[d] Anne-Sophie Banneville,[a] Thomas R. M. Barends,[c] Victor Bezchastnov,[c] Sébastien Boutet,[d] Martin Byrdin,[a] Marco Cammarata,[e] Sergio Carbajo,[d] Nina Eleni Christou,[a] Nicolas Coquelle,[a] Eugenio De la Mora,[a] Mariam El Khatib,[a] Tadeo Moreno Chicano,[a] R. Bruce Doak,[c] Franck Fieschi,[a] Lutz Foucar,[c] Oleksandr Glushonkov,[a] Alexander Gorel,[c] Marie Luise Grünbein,[c] Mario Hilpert,[c] Mark Hunter,[d] Marco Kloos,[c] Jason E. Koglin,[d] Thomas J. Lane,[d] Mengning Liang,[d] Angela Mantovanelli,[a] Karol Nass,[c] Gabriela Nass Kovacs,[c] Shigeki Owada,[f, g] Christopher M. Roome,[c] Giorgio Schirò,[a] Matthew Seaberg,[d] Miriam Stricker,[c] Michel Thépaut,[a] Kensuke Tono,[f, g] Kiyoshi Ueda,[h] Lucas M. Uriarte,[i] Daehyun You,[h] Ninon Zala,[a] Tatiana Domratcheva,*[c, j] Stefan Jakobs,[b] Michel Sliwa,[i] Ilme Schlichting,[c] Jacques-Philippe Colletier,[a] Dominique Bourgeois,*[a] and Martin Weik*[a]

Reversibly photoswitchable fluorescent proteins are essential markers for advanced biological imaging, and optimization of their photophysical properties underlies improved performance and novel applications. Here we establish a link between photoswitching contrast, one of the key parameters that dictate the achievable resolution in nanoscopy applications, and chromophore conformation in the non-fluorescent state of rsEGFP2, a widely employed label in REversible Saturable OpticaL Fluorescence Transitions (RESOLFT) microscopy. Upon illumination, the *cis* chromophore of rsEGFP2 isomerizes to two distinct *off*-state conformations, *trans1* and *trans2*, located on either side of the V151 side chain. Reducing or enlarging the side chain at this position (V151A and V151L variants) leads to single *off*-state conformations that exhibit higher and lower switching contrast, respectively, compared to the rsEGFP2 parent. The combination of structural information obtained by serial femtosecond crystallography with high-level quantum chemical calculations and with spectroscopic and photophysical

[a] *Dr. V. Adam,[+] Dr. K. Hadjidemetriou,[+] Dr. J. Woodhouse,[+] Dr. A.-S. Banneville, Dr. M. Byrdin, Dr. N. Eleni Christou, Dr. N. Coquelle, Dr. E. De la Mora, Dr. M. El Khatib, Dr. T. Moreno Chicano, Prof. Dr. F. Fieschi, Dr. O. Glushonkov, A. Mantovanelli, Dr. G. Schirò, M. Thépaut, N. Zala, Dr. J.-P. Colletier, Dr. D. Bourgeois, Dr. M. Weik*
Univ. Grenoble Alpes, CEA, CNRS, Institut de Biologie Structurale, F-38044 Grenoble, France
E-mail: dominique.bourgeois@ibs.fr
weik@ibs.fr

[b] *Dr. N. Jensen,[+] Prof. Dr. S. Jakobs*
Department of NanoBiophotonics, Max Planck Institute for Multidisciplinary Sciences, Göttingen, Germany and University Medical Center of Göttingen, Clinic for Neurology, Göttingen, Germany
and
Fraunhofer Institute for Translational Medicine and Pharmacology ITMP, Göttingen, Germany

[c] *Dr. R. L. Shoeman,[+] Dr. T. R. M. Barends, Dr. V. Bezchastnov, Prof. Dr. R. Bruce Doak, Dr. L. Foucar, A. Gorel, Dr. M. L. Grünbein, M. Hilpert, Dr. M. Kloos, Dr. K. Nass, Dr. G. Nass Kovacs, C. M. Roome, M. Stricker, Dr. T. Domratcheva, Prof. Dr. I. Schlichting*
Max-Planck-Institut für medizinische Forschung, Jahnstrasse 29, 69120 Heidelberg, Germany
E-mail: t.domratcheva@lcc.chem.msu.ru

[d] *Dr. A. Aquila, Dr. S. Boutet, Prof. Dr. S. Carbajo, Dr. M. Hunter, Dr. J. E. Koglin, Dr. T. J. Lane, Dr. M. Liang, Dr. M. Seaberg*
Linac Coherent Light Source (LCLS), SLAC National Accelerator Laboratory, 2575, Sand Hill Road, Menlo Park, CA 94025, USA

[e] *Dr. M. Cammarata*
Department of Physics, UMR UR1-CNRS 6251, University of Rennes 1, Rennes, France

[f] *Dr. S. Owada, Dr. K. Tono*
RIKEN SPring-8 Center, Sayo, Japan

[g] *Dr. S. Owada, Dr. K. Tono*
Japan Synchrotron Radiation Research Institute, 1-1-1 Kouto, Sayo-cho, Sayo-gun, Hyogo 679-5198, Japan

[h] *Prof. Dr. K. Ueda, Dr. D. You*
Institute of Multidisciplinary Research for Advanced Materials, Tohoku University, Sendai 980-8577, Japan

[i] *Dr. L. M. Uriarte, Dr. M. Sliwa*
Univ. Lille, CNRS, UMR 8516, LASIR, Laboratoire de Spectroscopie pour les Interactions, la Réactivité et l'Environnement, Lille 59000, France

[j] *Dr. T. Domratcheva*
Department of Chemistry, Lomonosov Moscow State University, Moscow 119991, Russia

[+] *These authors contributed equally to this work*

[**] *A previous version of this manuscript has been deposited on a preprint server (DOI: https://doi.org/10.1101/2021.11.05.462999)*

Supporting information for this article is available on the WWW under https://doi.org/10.1002/cphc.202200192

data determined *in vitro* suggests that the changes in switching contrast arise from blue- and red-shifts of the absorption bands associated to *trans1* and *trans2*, respectively. Thus, due to elimination of *trans2*, the V151A variants of rsEGFP2 and its superfolding variant rsFolder2 display a more than two-fold higher switching contrast than their respective parent proteins, both *in vitro* and in *E. coli* cells. The application of the rsFolder2-V151A variant is demonstrated in RESOLFT nanoscopy. Our study rationalizes the connection between structural and photophysical chromophore properties and suggests a means to rationally improve fluorescent proteins for nanoscopy applications.

Introduction

Reversibly switchable fluorescent proteins (RSFPs[1,2]) are photochromic markers that are key to multiple super-resolution microscopy (nanoscopy) schemes including RESOLFT[3–5], NL-SIM (Non Linear Structured Illumination Microscopy[6]), SOFI (Super resolution Optical Fluctuation Imaging[7]) and multicolor PALM (Photo Activated Localization Microscopy[8]). They are also central tools in contrast enhancing approaches such as OLID (Optical Lock-In Detection microscopy[9]) and in single channel multicolor approaches such as OPIOM (Out-of-Phase Imaging after Optical Modulation[10]). With the exception of Dreiklang[5] and its variant SPOON,[11] RSFPs typically switch between a fluorescent *on*- and a non-fluorescent *off*-state through light-induced *cis-trans* isomerization of their p-hydroxybenzylidene imidazolinone chromophore.[1,12,13] Depending on whether the same wavelength that induces fluorescence switches the RSFP from the *on*- to the *off*-state or *vice versa*, they are said to be negative or positive, respectively.[14] At neutral pH, the chromophore of negative RSFPs (such as rsEGFP2 and its rsFolder variants studied here) is generally *cis*-anionic in the *on*-state and *trans*-protonated in the *off*-state, although exceptions have been reported in rsGamillus.[15] *Off*-switching is promoted by illumination with wavelengths near the fluorescence excitation maximum (typically 488 nm) while *on*-switching requires illumination in the near UV region (typically 405 nm, Figure 1a).

In all nanoscopy applications relying on RSFPs as labels, image quality and the achievable spatial resolution are mainly determined by the following photophysical characteristics:[14] i) the fluorescence brightness, being defined as the product of the extinction coefficient of the *on*-state and the fluorescence quantum yield, ii) the ensemble switching speed, *i.e.* the time required to switch the ensemble from the *on*- to the *off*-state, or *vice versa*, iii) the switching fatigue, being defined as the fraction of an RSFP ensemble being photobleached per full switching cycle, and iv) the switching contrast, that is, the ratio between the fluorescence signal after *on*-switching and the residual signal after *off*-switching. Such residual fluorescence after *off*-switching mainly originates from back switching of the *off*-state chromophore by the *off*-switching light.[16] Among these characteristics, a high switching contrast is most critical for achieving high spatial resolution, and engineering efforts have thus been recently conducted to maximize it.[15,17] If we neglect the possibility that the chromophore is not fully in the fluorescent *cis*-anionic state after *on*-switching,[18] the switching contrast is a function of the *on*-to-*off* and *off*-to-*on* switching quantum yields and the extinction coefficients of both the *on*- and *off*-states at the *off*-switching wavelength (see eq. 1 in the Results section). In recent experimental[19,20] and computational[21] studies, it was proposed that the switching contrast is controlled by the relative stability of RSFPs in their *on*- and *off*-states *via* the number of hydrogen bonds between the chromophore and the protein pocket and its water molecules in each state. Here, focusing on rsEGFP2 and its rsFolder variants, we expand this view by showing how different conformations of the *off*-state chromophore modulate switching contrast, opening the door to rational optimization of RSFPs for enhanced nanoscopy applications.

rsEGFP2 (Figure 1a) has been generated based on EGFP and is widely applied in RESOLFT microscopy thanks to its fast maturation and favorable balance between fluorescence brightness, switching quantum yields, photofatigue resistance and switching contrast.[22] Recently, evidence for conformational heterogeneity in the *off*-state of rsEGFP2 at room temperature was provided by serial femtosecond crystallography (SFX), where in addition to the major *trans* state (*trans1* conformer), a hitherto unobserved *trans* isomer (*trans2* conformer) was observed,[23] which displays different twist and tilt dihedral angles (ϕ and τ dihedral angles; see also Supplementary table S3), protein environment and H-bonding network (Supplementary Figure S1). Interestingly, cryo-crystallographic synchrotron data revealed a similar *trans2* isomer upon *off*-switching of an rsEGFP2 variant containing a monochlorinated chromophore when crystals with a contracted unit cell were examined, whereas a conformation similar to *trans1* was populated in crystals with a larger unit cell.[24] *Trans1* and *trans2* conformers are located on either side of the V151 side chain (Supplementary Figure S1), a residue that needs to transiently retract for the chromophore to switch between its *cis* and *trans* conformations (see supplementary movie in[25]) as suggested by time-resolved SFX.[25] To start addressing the role of this residue in photoswitching, a variant with more space was generated by mutating V151 to an alanine.[25] During the preliminary photophysical characterization[25] neither the switching contrast or the structure of the rsEGFP2-V151A variant was analyzed nor was the rsEGFP2-V151L control with a more bulkier side chain generated.

The *trans2* conformation in rsEGFP2 is also very similar to the *trans* conformation observed in the *off*-state of rsFolder, a superfolding variant of rsEGFP2 that harbors a phenylalanine instead of a tyrosine at position 146 and that was designed to facilitate RESOLFT microscopy in "hostile" environments such as the bacterial periplasm.[26] Strikingly, rsFolder has a much lower switching contrast than rsEGFP2 and rsFolder2, a single mutant of rsFolder with a tyrosine at position 146 and thus the same chromophore pocket as rsEGFP2.[26] This observation suggests a possible link between the presence of *trans2* and a reduced switching contrast, raising the intriguing hypothesis that

removal of the *trans2* fraction in rsEGFP2 could further enhance its switching contrast.

Here, we investigate the structural *off*-state heterogeneity in rsEGFP2 and eliminated it in V151A and V151L variants by shortening or lengthening the amino-acid side chain at position 151, respectively. The V151A variant exhibits only the *trans1* conformation and a substantially higher switching contrast compared to the rsEGFP2 parent, whereas the V151L variant shows only the *trans2* conformation and a lower contrast. The effects of the V151A and V151L mutations on the switching contrast are reproduced in rsFolder2. We show that changes in switching contrast between the investigated variants mainly result from differences in extinction coefficients of the corresponding *off*-states at the *off*-switching illumination wavelength. Furthermore, we postulate rapid exchange dynamics between *trans1* and *trans2* in parental rsEGFP2 and in rsFolder2 and suggest that the achieved equilibrium depends on environmental factors, a notion we refer to as "photoswichting fragility". Finally, we show that the V151A variants maintain their gain in switching contrast *in vivo* and investigate the potential of rsFolder2-V151A for RESOLFT nanoscopy.

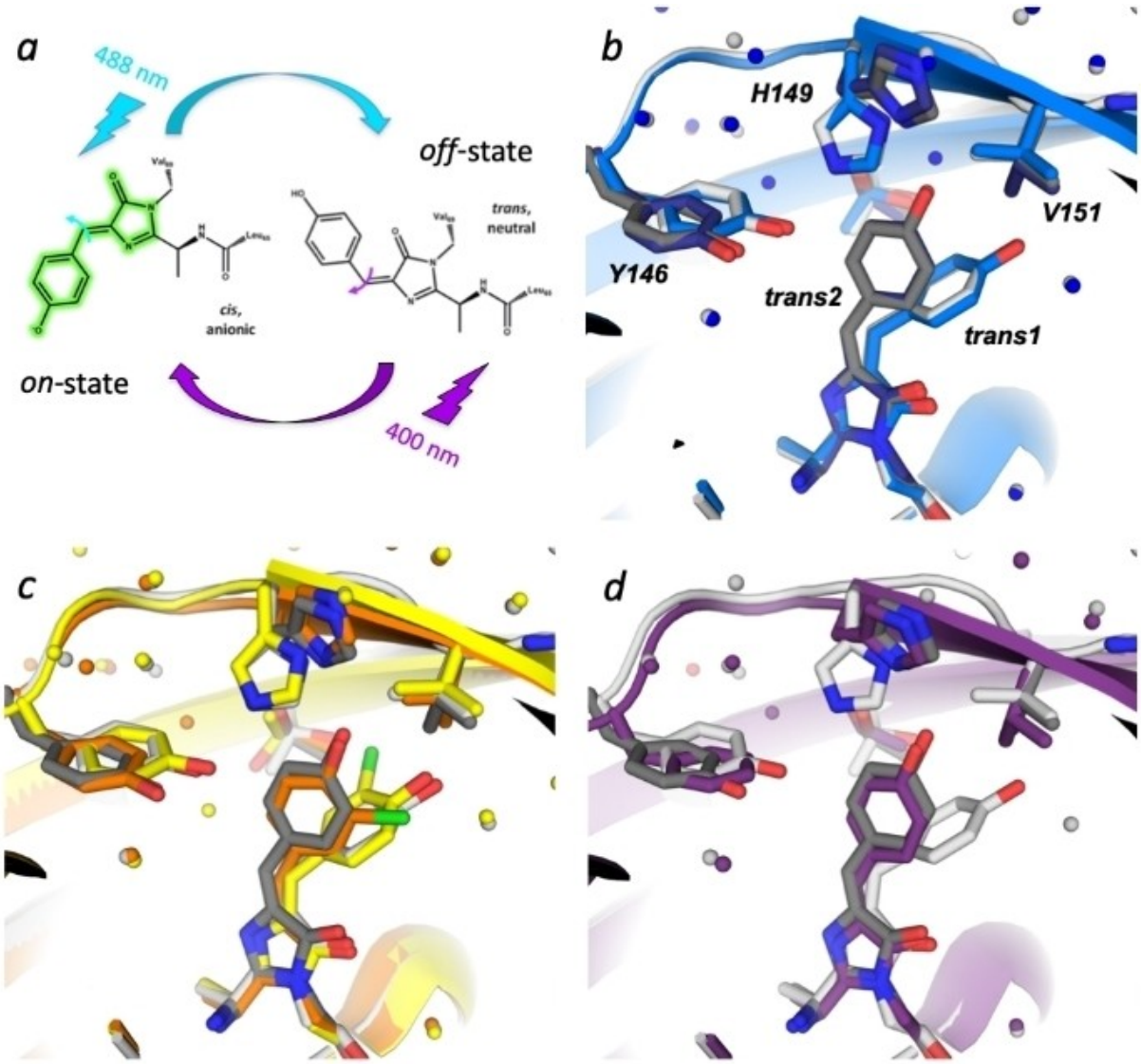

Figure 1. Photoswitching and *off*-state conformations in parental rsEGFP2. (*a*) rsEGFP2 can be photoswitched from the fluorescent *on*-state (anionic *cis* chromophore) to the non-fluorescent *off*-state (neutral trans chromophore) by illumination with 488 nm light, and back by illumination with 405 nm light. Photoswitching involves chromophore isomerization (blue and purple arrows on chromophore methylene bridge) and a change in protonation state of the phenol group. (*b*) Structures of parental rsEGFP2 in its *off*-state solved from RT SFX data. *Off*-state models of parental rsEGFP2 solved from RT SFX data earlier (PDB entry 6T39[23]) and in this work (PDB entry 7O7U). *Trans1* and *trans2* are occupied at 40% (light grey) and 30% (dark grey) in parental rsEGFP2 (this work) and at 65% (light blue) and 25% (dark blue) in 6T39, respectively. (*c*, *d*) *Off*-state models of parental rsEGFP2 solved from RT SFX data in this work (light and dark grey), overlaid with *trans* conformations in synchrotron structures of rsEGFP2 containing a monochlorinated chromophore[24] solved from crystals with looser (yellow) and tighter (orange) crystal packings[24] (*c*) and with the *off*-state model of rsFolder (PDB entry 5DU0[26]) in purple (*d*).

Results

Structural Heterogeneity in the *off*-State of Parental rsEGFP2

In order to corroborate the observation of a second *trans* isomer in parental rsEGFP2,[23] a follow-up SFX experiment was carried out at the Linac Coherent Light Source (LCLS) using microcrystals of parental rsEGFP2 of the same crystal batch used earlier.[23,25] The *on*-state crystals were photoswitched by 488 nm light[27] and the room-temperature (RT) structure of the resulting *off*-state solved at 1.7 Å resolution (PDB entry 7O7U; see SI for details). Both *trans1* and *trans2* chromophore conformations are again present (Figure 1b, Supplementary Figure S2). They agree well with those observed earlier,[23] as well as with those observed in cryo-crystallographic structures of an rsEGFP2 variant containing a monochlorinated chromophore[24] (Figure 1c, Supplementary table S3). The *trans2* conformation is similar to the one adopted by rsFolder in its *off*-state[26] (Figure 1d).

Structural Heterogeneity Bisected in the *off*-States of rsEGFP2-V151A and -V151L Variants

Given that the *trans1* and *trans2* chromophore conformations lie on either side of the V151 side chain (Figure 1b–d), we reasoned that this residue could also control the *off*-state heterogeneity. In addition to the rsEGFP2 variant with a shortened side chain (V151A[25]), one with an enlarged (V151L) side chain was therefore generated and non-fluorescent *off*-state structures of both solved from RT SFX data collected at the SPring-8 Angstrom Compact free electron LAser (SACLA) from microcrystals after 488 nm light illumination[27] (Figure 2, Supplementary Figure S3, Supplementary table S2). The *off*-state structures (V151A: PDB entry 7O7X, V151L: PDB entry 7O7W) display only one chromophore conformation: *trans1* for V151A (Figure 2a) and *trans2* for V151L (Figure 2b). Absorption spectroscopy indicates that about 85% and 77% of microcrystalline rsEGFP2-V151A and -V151L chromophores have switched from the *on*- to the *off*-state, respectively (for details see Supplementary Figure S4 and its legend). *Trans1* and *trans2* chromophore conformations were modelled at 80% (75%) occupancy in rsEGFP2-V151A (V151L) and the residual *cis* conformer at 20% (25%). Spectroscopic and crystallographic *on*- and *off*-state occupancies are thus consistent. In addition to differences in chromophore conformations, the *off*-states of the two variants also differ in their His149 and Tyr146 conformations. In the V151A variant His149 forms a hydrogen bond with Tyr146 and the *trans1* chromophore forms a hydrogen bond with a water molecule (distance: 2.7 Å, Supplementary Figure S1c, Figure 2a), whereas in the V151L variant His149 is hydrogen bonded to the *trans2* chromophore (distance of 2.5 Å between the chromophore phenol group and His149ND1; Supplementary Figure S1b, Figure 2b). Synchrotron cryo-crystallography structures of rsEGFP2-V151A (*off*-state: PDB entry 7O7C, *on*-state: PDB entry 7O7D) and -V151L (*off*-state: PDB entry 7O7H, *on*-state: PDB entry 7O7E) also feature a *trans1* and *trans2* chromophore in their *off*-state, respectively (Supplementary Figure S5b, d) and a *cis* chromophore in the *on*-state (Supplementary Figure S5a, c).

Overall, the RT SFX structures strongly suggest that the conformational *off*-state heterogeneity (*trans1*, *trans2*) seen in parental rsEGFP2 is eliminated in the rsEGFP2-V151A and -V151L variants, with *trans1* being occupied in the former and *trans2* in the latter. Thus, the residue at position 151 controls the *off*-state chromophore conformations (for a discussion of the modulation of conformational off-state heterogeneity see Supplementary Text S4).

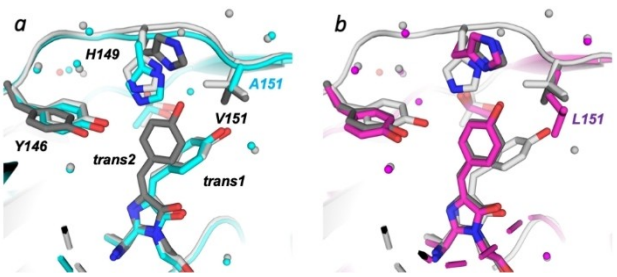

Figure 2. Structures of rsEGFP2 and its V151A and V151L variants in their *off*-states solved from RT SFX data. *Off*-state models of (a) rsEGFP2-V151A (cyan; PDB entry 7O7X) and (b) -V151L (purple; PDB entry 7O7W) variants are superimposed on the model of parental rsEGFP2 in the *off*-state solved from RT SFX data (PDB entry 7O7U), featuring *trans1* in light grey and *trans2* in dark grey. *Trans1* and *trans2* are occupied at 80% and 75% in rsEGFP2 V151A and V151L, respectively. The *cis* conformers were removed for clarity.

Occupancies of *trans1* and *trans2* Conformations in Parental rsEGFP2 and rsFolder2 are Sensitive to Experimental Conditions

A puzzling observation is that the relative occupancies of the *trans1* and *trans2* conformations differ in *off*-state crystal structures of rsEGFP2 determined from three different SFX data sets, although the same batch of microcrystals was used (Supplementary text S1). In addition, attempts to observe the *trans2* conformation in macrocrystals of parental rsEGFP2 upon RT illumination at various intensities by synchrotron cryo-crystallography remained unsuccessful (see Supplementary text S2). In contrast, the rsFolder2 *off*-state structure determined by synchrotron cryo-crystallography (PDB entry 7AMF) showed residual occupancy of the *trans2* chromophore in addition to a mainly occupied *trans1* (Supplementary Figure S6), similarly to the parental rsEGFP2 structures determined by RT SFX. These results suggest that relative occupancies of the two *off*-state conformations may change depending on even subtle differences in experimental conditions (see also[24]) or possibly the age of the crystalline proteins. In contrast, the rsEGFP2-V151A and -V151L structures in their *off*-states determined by SFX (Figure 2) are similar to those derived from cryo-crystallographic data we collected from macrocrystals at the European Synchrotron Radiation Facility (ESRF) (Supplementary table S1; Supplementary Figure S5).

Determination of Switching Contrast, Switching Quantum Yields and Extinction Coefficients of rsEGFP2, rsFolder2 and Their Variants Embedded in Polyacrylamide Gels

To explore a possible correlation between the *off*-state chromophore conformations and the switching contrast, we measured the switching kinetics of rsEGFP2-V151A, rsEGFP2-V151L and parental rsEGFP2 that contain either *trans1*, *trans2*, or both conformations, respectively. We also investigated rsFolder and rsFolder2, as well as the two variants rsFolder2-V151A and rsFolder2-V151L.

We embedded the seven investigated variants in polyacrylamide gels and recorded their fluorescence switching curves under laser illumination at 488 nm, using a wide field fluorescence microscope (Figure 3). The switching contrast was calculated as the ratio of the initial fluorescence in the *on*-state after illumination at 405 nm divided by the residual steady-state fluorescence after *off*-switching with 488 nm light (Table 1). We found that for both rsEGFP2 and rsFolder2 the switching contrast is reduced (× ~0.33) in the V151L variants and increased (× ~2.6) in the V151A variants compared to the parent proteins. The switching contrasts measured in the V151L variants (~15) are similar to that of rsFolder (~20), whereas that measured for both V151A variants exceeds 100.

To explore the underlying reason for the modified switching contrasts, we examined the photoswitching kinetics of all variants in more detail. Neglecting the slow thermal relaxation in RSFPs (~hour range) in view of the timescale of our experiments (~second range), the switching contrast *SC* at wavelength λ can be approximated by:

$$SC(\lambda) \simeq \frac{k_{on\rightarrow off}}{k_{off\rightarrow on}} = \frac{\varepsilon_{\lambda,on} \times Q_{on-to-off}}{\varepsilon_{\lambda,off} \times Q_{off-to-on}} \quad (1)$$

where $k_{on\rightarrow off}$ and $k_{off\rightarrow on}$ are the *on*-to-*off* and *off*-to-*on* switching rates, $Q_{on\text{-}to\text{-}off}$ and $Q_{off\text{-}to\text{-}on}$ are the *on*-to-*off* and *off*-to-*on* switching quantum yields, respectively, and $\varepsilon_{\lambda,on}$ and $\varepsilon_{\lambda,off}$ are the extinction coefficients of both the *on* and *off* states at the *off*-switching wavelength, respectively. Eq. 1 thus results from the photochemically-driven equilibrium between *on* and *off* states, assuming that the *off* states do not fluoresce. Changes in the switching contrast can thus be due to changes in switching quantum yields[19,20] and/or extinction coefficients of the *on*- and/or *off*-states. For the proteins in the present study, the *off*-switching wavelength is 488 nm. Whereas $\varepsilon_{488,on}$ was measured using the Ward method[28] $Q_{on\text{-}to\text{-}off}$, $Q_{off\text{-}to\text{-}on}$, $\varepsilon_{488,off}$ values were calculated by fitting the experimental fluorescence switching curves (Figure 3) with a kinetic model (see Supplementary methods section and Supplementary text S3). Overall, the dominating effect underlying variations between the observed switching contrasts in the studied variants follows from significant differences in *off*-to-*on* (rather than *on*-to-*off*) switching brightness at 488 nm (Table 1): the V151A variants switch *on* significantly less efficiently at 488 nm than the parent proteins, while the V151L variants switch *on* much more efficiently. The observed differences in the *off*-to-*on* switching brightness are mainly due to differences in $\varepsilon_{488,off}$ (reduced ~2.4 fold in rsEGFP2-V151A, and increased ~1.9 fold in rsEGFP2-V151L compared to parental rsEGFP2) and only to a minor extend to differences in *off*-to-*on* switching quantum yields (Table 1). Note that absolute values of *off*-to-*on* switching quantum yields are notoriously difficult to determine, as evidenced by the spread in values determined in different laboratories (e.g. for rsEGFP2 in solution, values of 0.12[29] and 0.34[26] have been published). Yet, values determined under identical conditions in the same laboratory should be comparable. It is thus striking that similar *off-to-on*-switching quantum yields were measured here on rsEGFP2 (0.23) and rsEGFP2-V151A (0.25) embedded in polyacrylamide gels, but a two-fold increase of the quantum yields for the proteins in solution has been reported by us earlier (0.40 and 0.77 for rsEGFP2 and rsEGFP2-V151A, respectively[25]). Unlike data in Table 1, the value

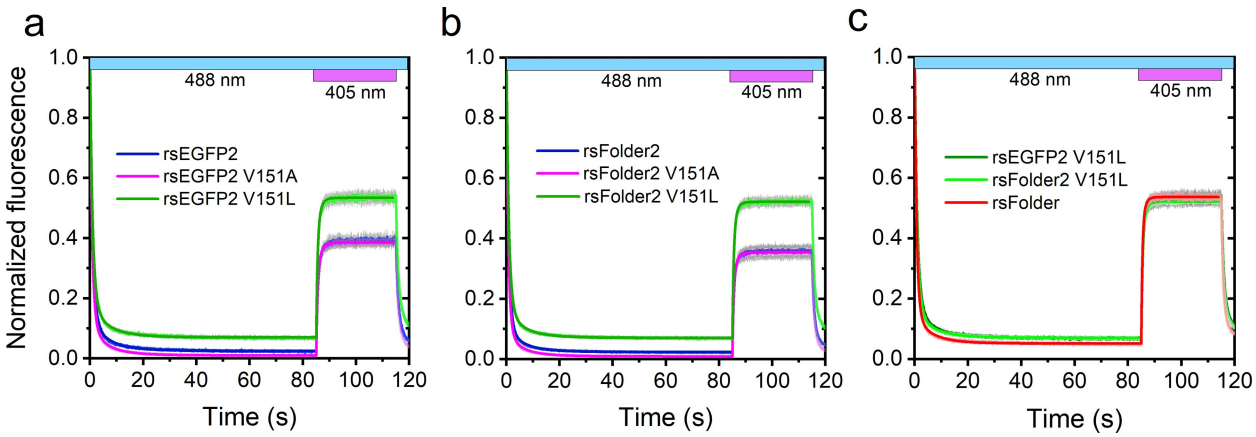

Figure 3. Fluorescence switching curves. (*a*, *b*) Fluorescence switching curves for rsEGFP2 and rsFolder2 proteins together with their V151A and V151L variants. (*c*) Switching curve for rsFolder compared to V151L variants of rsEGFP2 and rsFolder2. Data obtained from *in-vitro* measurements of purified proteins, embedded in polyacrylamide gel (pH 8.0), on an epifluorescence microscope using 488 nm (0.27 W/cm^2) illumination throughout data acquisition, and additional 405 nm (0.03 W/cm^2) during *off*-to-*on* switching. Pale colors stand for the mean values calculated from six measurements with standard deviations shown in grey, whereas dark solid lines represent the fits from the used kinetic model.

Table 1. Photophysical parameters obtained *in vitro*.

	rsEGFP2	rsEGFP2-V151A	rsEGFP2-V151L	rsFolder2	rsFolder2-V151A	rsFolder2-V151L	rsFolder
Absorption max. anionic (on) [nm]	482	483	483	483	484	483	479
Absorption max. neutral (off) [nm]	403	397	405	397	397	400	402
Absorption max. switched (off) [nm]	409	406	417	413	410	418	413
on-to-*off*-switching brightness[a,b] [$M^{-1}\,cm^{-1}$]	563 ± 13	673 ± 9	415 ± 18	690 ± 28	827 ± 48	455 ± 15	441 ± 13
on-to-*off*-switching quantum yield, $Q_{on\text{–}to\text{–}off}$	$9.3\times10^{-3}\pm0.2\times10^{-3}$	$11.4\times10^{-3}\pm0.2\times10^{-3}$	$6.5\times10^{-3}\pm0.3\times10^{-3}$	$10.0\times10^{-3}\pm0.4\times10^{-3}$	$14.1\times10^{-3}\pm0.8\times10^{-3}$	$6.5\times10^{-3}\pm0.2\times10^{-3}$	$7.3\times10^{-3}\pm0.2\times10^{-3}$
off-to-*on*-switching brightness[c] [$M^{-1}\,cm^{-1}$]	5807 ± 233	6590 ± 134	8713 ± 193	6054 ± 173	6852 ± 198	8979 ± 210	7877 ± 125
off-to-*on* -switching brightness[d] [$M^{-1}\,cm^{-1}$]	14.9 ± 0.9	6.8 ± 0.8	35.4 ± 1.2	16.9 ± 1.1	7.4 ± 0.5	39.3 ± 1.7	26.0 ± 0.8
off-to-*on* switching quantum yield, $Q_{off\text{–}to\text{–}on}$	$2.3\times10^{-1}\pm0.09\times10^{-1}$	$2.5\times10^{-1}\pm0.05\times10^{-1}$	$2.9\times10^{-1}\pm0.06\times10^{-1}$	$1.5\times10^{-1}\pm0.04\times10^{-1}$	$2.2\times10^{-1}\pm0.06\times10^{-1}$	$2.7\times10^{-1}\pm0.06\times10^{-1}$	$2.4\times10^{-1}\pm0.04\times10^{-1}$
$\varepsilon_{max,on}$ [$M^{-1}\,cm^{-1}$]	65474	62284	68295	72675	61091	74470	71871
$\varepsilon_{488,on}$ [$M^{-1}\,cm^{-1}$]	60807	59090	63851	69124	58798	70254	59509
$\varepsilon_{488,off}$ [$M^{-1}\,cm^{-1}$]	65 ± 3	27 ± 3	122 ± 3	111 ± 6	34 ± 2	145 ± 5	110 ± 3
$\varepsilon_{max,off}$ [$M^{-1}\,cm^{-1}$]	25758	26694	33333	42434	32267	37079	38518
$\varepsilon_{405,off}$ [$M^{-1}\,cm^{-1}$]	25349	26670	29987	39841	31473	33061	36137
off-to-*on* thermal recovery time [hours]	4.5	65	10	25	75	13	69
Switching contrast [fold-change][e]	43 ± 5	119 ± 21	15 ± 1	46 ± 3	125 ± 11	15 ± 1	20 ± 1
Fluorescence brightness	20952	16194	19123	24709	12829	33511	21561
Fluorescence quantum yield	0.32 ± 0.02	0.26 ± 0.01	0.28 ± 0.01	0.34 ± 0.01	0.21 ± 0.01	0.45 ± 0.04	0.30 ± 0.01
Maturation time [min]	39.1 ± 4.2	116.7 ± 3.3	90.8 ± 7.7	70.8 ± 6.6	157.7 ± 2.3	119.7 ± 60.3	77.2 ± 5.3
pKa	5.9	6.4	5.7	5.8	6.4	5.9	5.5

[a] Switching brightness refers to the product (switching quantum yield × extinction coefficient). [b] Off switching brightness at 488 nm [c] On switching brightness at 405 nm. [d] On switching brightness at 488 nm. [e] Experimentally measured switching contrast, *i.e.* ratio of the measured fluorescence at the beginning and at the end of the 488 nm illumination period. This experimental switching contrast is always higher than the ratio of *on-off* and *off-on* switching brightnesses. This stems from the fact that the reported minor dark state harbors a population of nonfluorescent molecules and therefore provides additional contrast (supplementary Figure S8). All parameters were determined by measurements on protein in solution at pH 7.5 except switching brightness, switching quantum yield and switching contrast values that were extracted from measurements on protein in polyacrylamide gel at pH 8.0. Values obtained from at least three independent measurements for each variant. ND: Not Determined

for rsEGFP2-V151A in[25] was determined from a single measurement and we suspect that an unidentified experimental flaw attributed to a laser power density calibration error lead to the erroneously high value (0.77) that should thus be discarded. Compared to rsEGFP2 and rsFolder2, the behavior of rsFolder is similar to that of the V151L variants. We note that the V151A variants are characterized by a lower fluorescence brightness than their parents (Table 1).

Overall, our results suggest that the higher and lower switching contrasts of the V151A and V151L variants relative to the parent proteins, respectively, are mainly due to lower absorptions of 488 nm light ($\varepsilon_{488,off}$) by the *trans1* chromophore in V151A and to higher absorption of the *trans2* chromophore in V151L.

UV-Visible Absorption Spectroscopy on rsEGFP2, rsFolder2 and Their Variants in Solution

The differences in $\varepsilon_{488,off}$ determined from fitting the experimental fluorescence switching curves (Table 1) can be rationalized by comparing UV-visible absorption spectra of rsEGFP2, rsFolder2 and their V151A and V151L variants in their *on*- and *off*-states, respectively (Figure 4). Indeed, we consistently observed that the maximum of the *off*-state spectra of the V151A variants are blue shifted, and the spectra of the V151L variants red shifted relative to those of the parent proteins (Table 1). In the V151A variants, the blue shifted *off*-state absorbance band leads to a lower residual extinction coefficient at 488 nm ($\varepsilon_{488,off}$), resulting in less *on*-state contamination after *off*-switching (Figure 4) and thus to an increased switching contrast. In contrast, the red shifted *off*-state absorbance band in the V151L variants leads to a higher extinction coefficient at 488 nm, more *on*-state contamination and a lower contrast. Interestingly, a shoulder at 440 nm is visible in the *off*-state absorbance spectra of rsEGFP2-V151L, rsFolder2-V151L and rsFolder (Figure 4) that cannot be attributed to residual absorbance of the *on*-state. This shoulder is also visible in *off*-state absorption spectra of microcrystalline rsEGFP2-V151L (Supplementary Figure S4b).

We also recorded absorption spectra along *on*-to-*off* switching under alternating 488 nm illumination for all variants in the solution state. An isosbestic point (Supplementary Figure S7) was always observed, suggesting a homogenous *off*-state, not only for the V151A and V151L variants, but also for the parent proteins. Likewise, all our fluorescent switching curves (Supplementary Figure S8) displayed a similar trend, with no sign of more complex kinetics in the parent proteins compared to the V151A and V151L variants.

Quantum Chemical Calculation Analysis of Chromophore Conformations in Parental rsEGFP2

So far, we implicitly assumed that the *trans1* and *trans2* conformations observed in the crystal structures occur in the proteins in solution, and hence, the blue- and red-shifted absorption could be attributed to *trans1* and *trans2* chromophores, respectively. To test this assumption, the absorption spectra of the *trans1* and *trans2* conformers were characterized by quantum chemistry calculations. Starting from the SFX structure of parental rsEGFP2 (PDB entry 6T39[23]), the geometries of models featuring *trans1* and *trans2* chromophore conformations in their respective protein environment (*i.e. trans1* being H-bonded to a water molecule and *trans2* to His149; Figure 5a) were optimized. The planarity of the chromophore remained similar to the experimentally derived one (Supplementary table S3) with *trans1* being rather distorted from the planar configuration in contrast to *trans2* (Figure 5a). The two configurations also differ in the length of the phenolic OH bond and bonds of the conjugated system indicating a stronger binding of the phenolic proton concomitant with a reduced π-conjugation in *trans1* as compared to *trans2*. The energy cross sections computed for the phenolic OH bond stretching (Figure 5b) demonstrate a shape typical for the

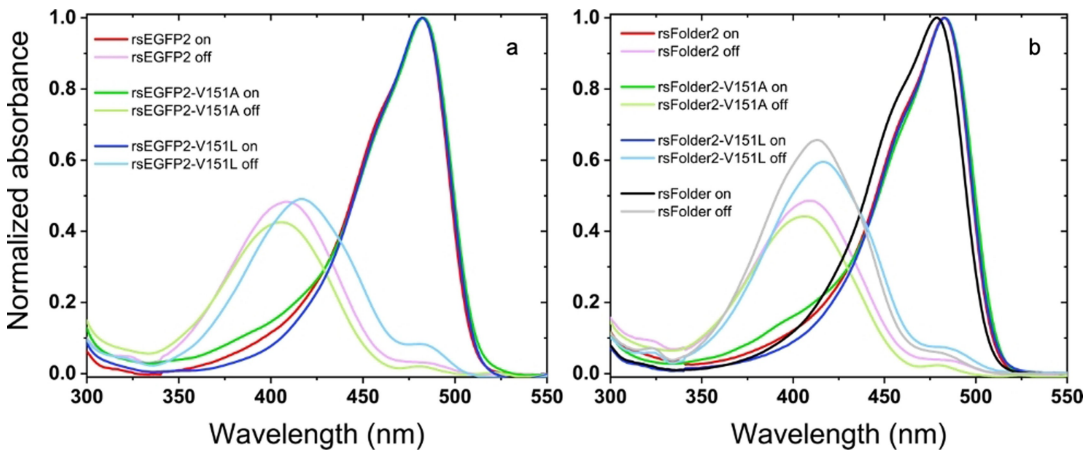

Figure 4. Absorption spectra of fluorescent proteins presented in this study in their fluorescent *on*-state (dark colors) and non-fluorescent *off*-state (dim colors) in solution. (*a*) rsEGFP2 and its variants rsEGFP2-V151A and rsEGFP2-V151L, (*b*) rsFolder2 and its variants rsFolder2-V151A and rsFolder2-V151L and rsFolder. Spectra are normalized relatively to the respective *on* state spectra and are measured in HEPES buffer at pH 7.5.

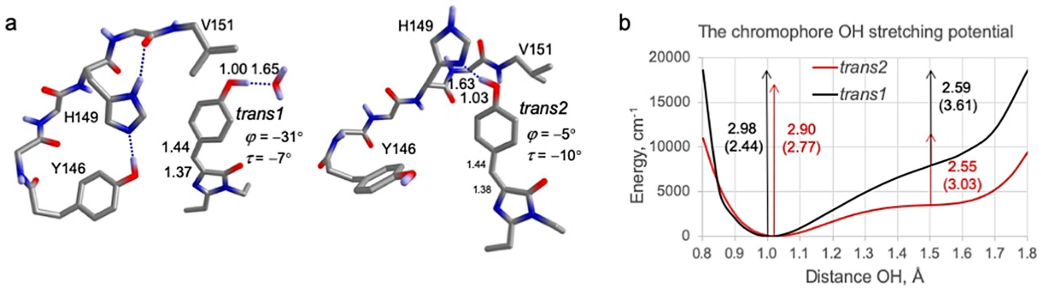

Figure 5. Quantum chemical calculations of *trans1* and *trans2* within parental rsEGFP2. (*a*) Fragments of the chromopore models and selected distances (Å) and angles in the optimized geometries. (*b*) The OH stretching energies. Vertical arrows indicate the S_0–S_1 excitation energies (eV) and transition dipole moments (in brackets; Hartree*Bohr). The decrease of the S_0–S_1 energy along the OH stretching coordinate is demonstrated. The effect of the OH-stretching potentials, showing strong anharmonicity, on the S_0–S_1 vibronic band structure potentially explaining the observed spectral shift is demonstrated in Supplementary Figure S9.

protonated p-hydroxybenzylidene imidazolinone chromophore interacting with a proton acceptor[30] and confirm a stronger proton binding in *trans1*. Consistent with reduced π-conjugation, the S_0–S_1 energy is higher for *trans1* than for *trans2* (Figure 5b, Supplementary table S4), suggesting a blue-shifted absorption maximum for the former. The enhanced proton binding in *trans1* could be linked to a substantial electronic coupling of 15 meV between *trans1* chromophore and electron donor Tyr146. The coupling is facilitated by a H-bond between His149 and Tyr146. The *trans2* chromophore is H-bonded with His149 itself, and its electronic coupling with Tyr146 is reduced to 0.5 meV. The absorption band shapes obtained with a quantum-mechanical model considering the one-dimensional OH-stretching potential (Supplementary Figure S9 and Supplementary table S5) also suggest a blue shifted absorption band of *trans1* compared to *trans2*.

Geometry optimization and excitation energy calculations were performed for the *trans1* and *trans2* models with alanine and leucine, respectively, at position 151. Similar distorted and planar geometries of *trans1* and *trans2*, respectively, were found in these models (Supplementary Figure S10 and Supplementary table S3). Further, the calculations confirmed that the S_0–S_1 excitation energy is higher for *trans1* compared to *trans2* independent of the residue at position 151 (Supplementary table S4). Hence, our calculations suggest an increase of the excitation energy for *trans1* in comparison to *trans2*, consistent with the blue-shifted absorption band assigned to *trans1*, which we correlate with the increased out of plane distortion and increased proton binding of *trans1*. The calculations thus corroborate our assumption that the *trans1* and *trans2* conformers are adopted both *in crystallo* and in solution.

Determination of *in vivo* Switching Contrasts of rsEGFP2, rsFolder2 and Their Variants and RESOLFT Experiments on rsFolder2-V151A

To investigate the *in vivo* switching properties of rsEGFP2, rsFolder2 and their variants at light intensities similar to those typically utilized in RESOLFT nanoscopy, we recorded switching curves on *E. coli* colonies expressing the respective proteins using high light intensities (Figure 6a, b). The determined contrasts of rsEGFP2-V151A (109) and rsFolder2-V151A (119) increased and that of rsEGFP2-V151L (6) decreased with respect to parental rsEGFP2 (28) and rsFolder2 (22), in line with the results obtained with low light intensities *in vitro* (Table 1). We

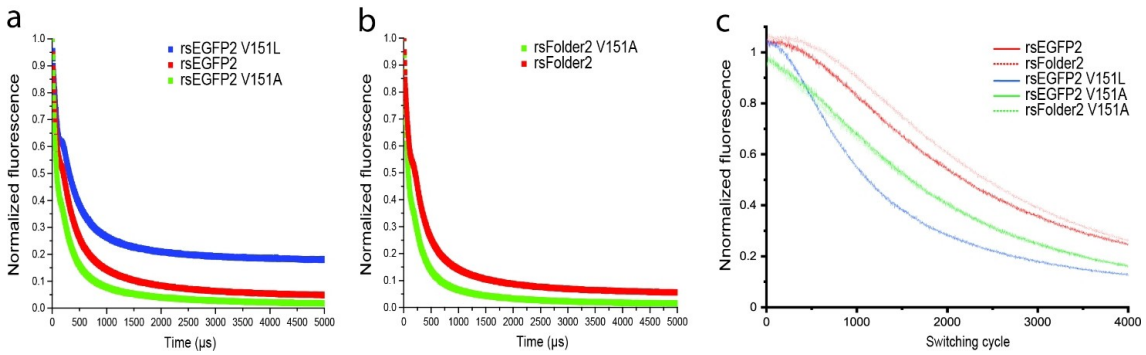

Figure 6. Switching kinetics and switching fatigue of rsEGFP2, rsEGFP2-V151A, rsEGFP2-V151L, rsFolder2 and rsFolder2-V151A. Comparison of the *off* switching curve of rsEGFP2, rsEGFP2-V151A and rsEGFP2-V151L (*a*), as well as rsFolder2 and rsFolder2-V151A (*b*). Switching fatigue measurements of the five proteins (*c*). All graphs were recorded on living *E. coli* colonies using high light intensities.

also compared the switching fatigue of parental rsEGFP2 and rsFolder2 and their variants. To this end, the fluorescence of *E. coli* colonies was switched *on* and *off* 4000 times and the maximal fluorescence of the *on*-state was recorded for every switching cycle (Figure 6c). While rsEGFP2 and rsFolder2 could be switched more than 2000 times before their fluorescence was reduced to 50% of the initial brightness, the V151A variants could be switched ~1500 times. Based on *in vivo* switching properties, both V151A variants appeared to be suitable for RESOLFT nanoscopy.

For investigating the usefulness for RESOLFT imaging, we decided to concentrate on rsFolder2-V151A, as this variant showed the highest photoswitching contrast *in vitro* (Table 1) and *in vivo*, and could be particularly useful because of its superfolding properties. A fusion protein of the cytoskeletal protein Keratin with rsFolder2-V151A was expressed in cultured human HeLa cells and imaged on the RESOLFT microscope. While the resulting image shows the expected clear improvement in resolution compared to the confocal counterpart (Figure 7), its resolution of ~60 nm is comparable to the one of previous RESOLFT recordings on the same microscope using parental rsEGFP2,[31] as judged by the full width at half maximum (FWHM) of line profiles across small Keratin-rsFolder2-V151A filaments. Hence, despite the increased switching contrast of the V151A variant, evidenced *in vitro* (Table 1) and *in vivo* (Figure 6), the recorded images do not show a significant increase in resolution compared to the parent protein. We mainly attribute this result to the lower molecular and cellular brightnesses of these variants compared to the parents (Table 1).

Discussion

Correlation between *off*-State Conformations, Switching Contrast and Absorbance Spectra

We establish a link between the switching contrast and *off*-state occupancy of the *trans1* or *trans2* chromophore conformations in rsEGFP2 and rsFolder2 variants by combining our structural and photophysical results. For the *trans1* conformer (V151A variants), the switching contrast is high, whereas the *trans2* conformer (V151L variants) leads to a lower contrast. Parental rsEGFP2 and rsFolder2, exhibiting *trans1/trans2 off*-state heterogeneity (see Supplementary text S4), display an intermediate contrast (Table 1). The quantitative evaluation of fluorescence switching kinetics and the *off*-state absorbance spectra of the investigated variants strongly suggest that the main contribution to modulation of the switching contrast arises from red- and blue-shifted absorption maxima of the *off*-state in the V151L and V151A variants, respectively. This observation correlates with the differences in twist and tilt dihedral angles of the chromophore in *trans1* and *trans2*, as well as in its local environment, that tune the energy gap between the S_0 and S_1 electronic states as shown by our high-level quantum chemistry calculations. The red-shift of the experimental absorption maximum of the rsEGFP2-V151L *off*-state was reproduced computationally (Figure 5b) and is consistent with the more extended electron delocalization in the near-planar chromophore of its *trans2* conformation compared to *trans1* (Figure 5a). The less planar *trans1* chromophore conformation might result from stabilization of the protonated form by charge transfer from Tyr146, activated by H-bonding to His149, that is absent for *trans2*. Of note, based on the calculation of ratiometric absorption spectra between the *on* and *off* states for the three rsEGFP2 variants (Supplementary Figure S11), we do not expect an increase in switching contrast by employing illumination at red-shifted wavelengths.

When linking structural and spectroscopic results, we rely on the assumption that the *off*-state heterogeneity observed in crystals of parental rsEGFP2 and rsFolder2 is maintained in solution. Our high-level quantum chemistry calculations justify this assumption. Yet, the presence of isosbestic points in the absorbance spectra along *off*-switching (Supplementary Figure S7) and detection of a single long-lived *off*-state in our fluorescence-based switching curves (Supplementary Figure S12) indicate a homogeneous *off*-state in solution. These findings are consistent if we postulate a fast exchange between

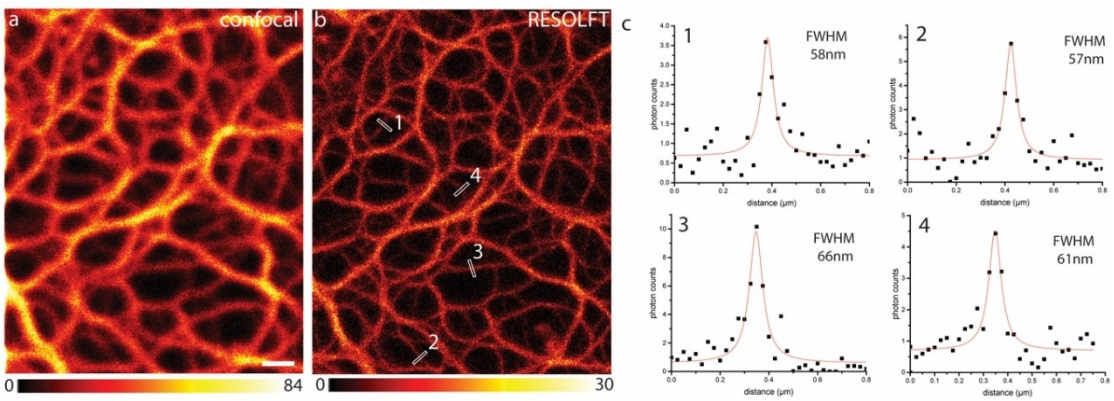

Figure 7. RESOLFT imaging using rsFolder2-V151A. Comparison of a confocal (*a*) and RESOLFT (*b*) recording of a HeLa cell expressing Keratin-rsFolder2-V151A. Line profiles were taken at the indicated positions and the FWHM was determined on the fitted functions (*c*). Scale bar: 1 µm. The color maps indicate the actual photon counts.

trans1 and *trans2* in parental rsEGFP2 and rsFolder2 in solution, occurring on timescales faster than detectable (~0.1 s) in our absorbance and switching kinetics measurements. Our measurements in solution thus capture the average photophysical behavior between those of *trans1* and *trans2*, giving rise to an apparently homogeneous *off*-state. The postulated fast exchange contrasts the assumption by Chang *et al* that *trans* conformations are locked on the second time scale (see Supplementary information S3 in[24]).

Photoswitching Fragility in Parental rsEGFP2 and rsFolder2

The differential *trans2* occupancies found in *off*-state structures of rsEGFP2 determined by RT SFX under identical buffer conditions on microcrystals of the same batch but of different age and with varying illumination conditions (Supplementary text S1), as well as the absence of *trans2* in flash-cooled parental rsEGFP2 macrocrystals (Supplementary Figure S13) and its presence in rsFolder2 (Supplementary text S2, Supplementary Figure S6), suggest that experimental and environmental parameters determine to which extent *trans2* gets populated in parental rsEGFP2 and rsFolder2. We suggest that this is the result of a low, environmentally dependent, barrier in the protein conformational energy landscape[32] separating access to, or exchange between, *trans1* and *trans2*, a notion that we refer to as "*switching fragility*". Yet, the experimental conditions that would reproducibly control heterogeneity in the *off*-states of rsEGFP2 and rsFolder2 have not been identified. Alternatively, or additionally, conformational heterogeneity of the *cis* chromophore in the *on*-state could be at the origin of the observed *off*-state heterogeneity.

Photoswitching fragility in parental rsEGFP2 or rsFolder2 may have consequences for imaging applications, when labels are addressed to various cellular locations with potentially different physicochemical environments. These different environments (e.g. viscosity, ionic strength, or nature of a fusion protein) could lead to different levels of heterogeneity and variability in switching contrast (beyond that expected from pH induced effects[15]). Such variability is expected to be alleviated in rsFolder, the V151L variants, and the high switching contrast V151A variants so that they may be considered as more "robust" than their parents.

In conclusion, this work establishes a causal relationship between the occupancy of two *off* conformations in rsEGFP2 and rsFolder2 and the achievable switching contrast, essentially through absorbance shifts of the *off*-switched chromophore. A point mutation is sufficient to enforce single *trans* conformations in the *off*-state. These had also been observed in more or less densely packed crystals of *off*-state variants containing a monochlorinated chromophore.[24] *Trans1* seems to be favoured in a more spacious chromophore pocket (V151A variant (this work) and in crystals with a less contracted unit cell[24]) and *trans2* in a more constricted pocket (V151L variant (this work) and in crystals with a contracted unit cell[24]). The rsEGFP2- and rsFolder2-V151A variants, containing only the *trans1* conformer, exhibit greatly enhanced switching contrasts as compared to their parents, both *in vitro* and *in vivo*. Due to a loss in fluorescence brightness of these variants, however, the optical resolution obtained by RESOLFT nanoscopy on Keratin-rsFolder2-V151A filaments did not significantly increase compared to previous studies using either parental rsFolder2 or rsEGFP2. In the future, it would be interesting to investigate whether an optimum illumination wavelength exists, possibly deviating from the employed 488 nm light, that would further enhance the switching contrast to a point overcompensating the observed loss in brightness of the *on* form. Our rsEGPF2-V151A and rsFolder2-V151A variants constitute promising leads for the next-generation RSFPs, for which the fluorescence brightness has to be increased while maintaining the enhanced switching contrast described here.

Acknowledgments

We thank Elke de Zitter for critically commenting on the manuscript. The XFEL experiments were carried out at BL2-EH3 of SACLA with the approval of the Japan Synchrotron Radiation Research Institute (JASRI; Proposal No. 2018 A8026; 27–29 July 2018) and at the CXI beamline at the LCLS (Proposal No. LM47 (23–27 June 2016) and LR38 (22–26 February 2018). We warmly thank the SACLA and LCLS staff for assistance. Use of the LCLS, SLAC National Accelerator Laboratory, is supported by the U.S. Department of Energy, Office of Science, Office of Basic Energy Sciences under Contract no. DE-AC02-76SF00515. Part of the sample injector used at LCLS for this research was funded by the National Institutes of Health, P41 GM103393, formerly P41RR001209. We acknowledge support from the Max Planck Society. The study was supported by travel grants from the CNRS (GoToXFEL) to MW, an ANR grant to MW, MC, MSl (BioXFEL), an ANR grant to DB (grant no. ANR-17-CE11-0047-01), a PhD fellowship from Lille University to LMU and an MENESR – Univ. Grenoble Alpes fellowship to KH. This work was partially carried out at the platforms of the Grenoble Instruct-ERIC center (IBS and ISBG; UMS 3518 CNRS-CEA-UGA-EMBL) within the Grenoble Partnership for Structural Biology (PSB). Platform access was supported by FRISBI (ANR-10-INBS-05-02) and GRAL, a project of the University Grenoble Alpes graduate school (Ecoles Universitaires de Recherche) CBH-EUR-GS (ANR-17-EURE-0003). The IBS acknowledges integration into the Interdisciplinary Research Institute of Grenoble (IRIG, CEA).

Conflict of Interest

The authors declare no conflict of interest.

Data Availability Statement

The data that support the findings of this study are openly available in the Protein Data Bank, https://www.wwpdb.org/, PDB ID codes 7O7D, 7O7C, 7O7E, 7O7H, 7AMB, 7AMF, 7O7U, 7O7V, 7O7X, 7O7W.

Keywords: nanoscopy · photoswitchable fluorescent proteins · serial femtosecond crystallography · switching contrast · quantum chemistry

[1] D. Bourgeois, V. Adam, *IUBMB Life.* **2012**, *64*, 482–491.
[2] K. Nienhaus, G. U. Nienhaus, *ACS Nano* **2016**.
[3] M. Hofmann, C. Eggeling, S. Jakobs, S. W. Hell, *Proc. Natl. Acad. Sci. USA* **2005**, *102*, 17565–17569.
[4] T. Grotjohann, I. Testa, M. Leutenegger, H. Bock, N. T. Urban, F. Lavoie-Cardinal, K. I. Willig, C. Eggeling, S. Jakobs, S. W. Hell, *Nature* **2011**, *478*, 204–208.
[5] T. Brakemann, A. C. Stiel, G. Weber, M. Andresen, I. Testa, T. Grotjohann, M. Leutenegger, U. Plessmann, H. Urlaub, C. Eggeling, M. C. Wahl, S. W. Hell, S. Jakobs, *Nat. Biotechnol.* **2011**, *29*, 942–947.
[6] M. G. L. Gustafsson, *Proc. Natl. Acad. Sci. USA* **2005**, *102*, 13081–13086.
[7] T. Dertinger, R. Colyer, G. Iyer, S. Weiss, J. Enderlein, *Proc. Nat. Acad. Sci.* **2009**, *106*, 22287.
[8] H. Shroff, C. G. Galbraith, J. A. Galbraith, H. White, J. Gillette, S. Olenych, M. W. Davidson, E. Betzig, *Proc. Nat. Acad. Sci.* **2007**, *104*, 20308.
[9] G. Marriott, S. Mao, T. Sakata, J. Ran, D. K. Jackson, C. Petchprayoon, T. J. Gomez, E. Warp, O. Tulyathan, H. L. Aaron, E. Y. Isacoff, Y. Yan, *Proc. Natl. Acad. Sci. USA* **2008**, *105*, 17789–17794.
[10] J. Quérard, R. Zhang, Z. Kelemen, M.-A. Plamont, X. Xie, R. Chouket, I. Roemgens, Y. Korepina, S. Albright, E. Ipendey, M. Volovitch, H. L. Sladitschek, P. Neveu, L. Gissot, A. Gautier, J.-D. Faure, V. Croquette, T. Le Saux, L. Jullien, *Nat. Commun.* **2017**, *8*, 969.
[11] Y. Arai, H. Takauchi, Y. Ogami, S. Fujiwara, M. Nakano, T. Matsuda, T. Nagai, *ACS Chem. Biol.* **2018**, *13*, 1938–1943.
[12] M. Andresen, M. C. Wahl, A. C. Stiel, F. Grater, L. V. Schafer, S. Trowitzsch, G. Weber, C. Eggeling, H. Grubmuller, S. W. Hell, S. Jakobs, *Proc. Natl. Acad. Sci. USA* **2005**, *102*, 13070–13074.
[13] M. Andresen, A. C. Stiel, S. Trowitzsch, G. Weber, C. Eggeling, M. C. Wahl, S. W. Hell, S. Jakobs, *Proc. Natl. Acad. Sci. USA* **2007**, *104*, 13005–13009.
[14] N. A. Jensen, I. Jansen, M. Kamper, S. Jakobs in *Reversibly Switchable Fluorescent Proteins for RESOLFT Nanoscopy, Vol.* (Eds.: T. Salditt, A. Egner, D. R. Luke), Springer International Publishing, Cham, **2020**, pp.241–261.
[15] H. Shinoda, K. Lu, R. Nakashima, T. Wazawa, K. Noguchi, T. Matsuda, T. Nagai, *Cell Chem. Biol.* **2019**, *26*, 1469–1479 e1466.
[16] D. Ruhlandt, M. Andresen, N. Jensen, I. Gregor, S. Jakobs, J. Enderlein, A. I. Chizhik, *Commun. Biol.* **2020**, *3*, 627.
[17] X. Zhang, M. Zhang, D. Li, W. He, J. Peng, E. Betzig, P. Xu, *Proc. Natl. Acad. Sci. USA* **2016**, *113*, 10364–10369.
[18] N. E. Christou, K. Giandoreggio-Barranco, I. Ayala, O. Glushonkov, V. Adam, D. Bourgeois, B. Brutscher, *J. Am. Chem. Soc.* **2021**, *143*, 7521–7530.
[19] E. De Zitter, D. Thédié, V. Mönkemöller, S. Hugelier, J. Beaudouin, V. Adam, M. Byrdin, L. Van Meervelt, P. Dedecker, D. Bourgeois, *Nat. Methods* **2019**, *16*, 707–710.
[20] E. De Zitter, J. Ridard, D. Thédié, V. Adam, B. Lévy, M. Byrdin, G. Gotthard, L. Van Meervelt, P. Dedecker, I. Demachy, D. Bourgeois, *J. Am. Chem. Soc.* **2020**, *142*, 10978–10988.
[21] D. Morozov, G. Groenhof, *Angew. Chem. Int. Ed.* **2016**, *55*, 576–578; *Angew. Chem.* **2016**, *128*, 586–588.
[22] T. Grotjohann, I. Testa, M. Reuss, T. Brakemann, C. Eggeling, S. W. Hell, S. Jakobs, *eLife* **2012**, *1*, e00248.
[23] J. Woodhouse, G. Nass Kovacs, N. Coquelle, L. M. Uriarte, V. Adam, T. R. M. Barends, M. Byrdin, E. de la Mora, R. Bruce Doak, M. Feliks, M. Field, F. Fieschi, V. Guillon, S. Jakobs, Y. Joti, P. Macheboeuf, K. Motomura, K. Nass, S. Owada, C. M. Roome, C. Ruckebusch, G. Schirò, R. L. Shoeman, M. Thepaut, T. Togashi, K. Tono, M. Yabashi, M. Cammarata, L. Foucar, D. Bourgeois, M. Sliwa, J.-P. Colletier, I. Schlichting, M. Weik, *Nat. Commun.* **2020**, *11*, 741.
[24] J. Chang, M. G. Romei, S. G. Boxer, *J. Am. Chem. Soc.* **2019**, *141*, 15504–15508.
[25] N. Coquelle, M. Sliwa, J. Woodhouse, G. Schirò, V. Adam, A. Aquila, T. R. M. Barends, S. Boutet, M. Byrdin, S. Carbajo, E. De la Mora, R. B. Doak, M. Feliks, F. Fieschi, L. Foucar, V. Guillon, M. Hilpert, M. S. Hunter, S. Jakobs, J. E. Koglin, G. Kovacsova, T. J. Lane, B. Lévy, M. Liang, K. Nass, J. Ridard, J. S. Robinson, C. M. Roome, C. Ruckebusch, M. Seaberg, M. Thepaut, M. Cammarata, I. Demachy, M. Field, R. L. Shoeman, D. Bourgeois, J.-P. Colletier, I. Schlichting, M. Weik, *Nat. Chem.* **2018**, *10*, 31–37.
[26] M. El Khatib, A. Martins, D. Bourgeois, J. P. Colletier, V. Adam, *Sci. Rep.* **2016**, *6*, 18459.
[27] G. Schiro, J. Woodhouse, M. Weik, I. Schlichting, R. L. Shoeman, *J. Appl. Crystallogr.* **2017**, *50*, 932–939.
[28] W. W. Ward in *Properties of the coelenterate green-fluorescent proteins. Bioluminescence and chemiluminescence: basic chemistry and analytical applications.*, Vol. xxviii (Ed. M. A. D. a. W. D. McElroy), New York, Academic Press, **1981**, pp. 782.
[29] S. Duwé, E. De Zitter, V. Gielen, B. Moeyaert, W. Vandenberg, T. Grotjohann, K. Clays, S. Jakobs, L. Van Meervelt, P. Dedecker, *ACS Nano* **2015**, *9*, 9528–9541.
[30] J. Langeland, N. W. Persen, E. Gruber, H. V. Kiefer, A. M. Kabylda, A. V. Bochenkova, L. H. Andersen, *ChemPhysChem* **2021**, *22*, 833–841.
[31] S. Schnorrenberg, T. Grotjohann, G. Vorbrüggen, A. Herzig, S. W. Hell, S. Jakobs, *eLife* **2016**, *5*, e15567.
[32] H. Frauenfelder, S. G. Sligar, P. G. Wolynes, *Science* **1991**, *254*, 1598–1603.

Manuscript received: March 22, 2022
Revised manuscript received: June 25, 2022
Version of record online: August 12, 2022

ChemPhysChem

Supporting Information

Rational Control of Off-State Heterogeneity in a Photoswitchable Fluorescent Protein Provides Switching Contrast Enhancement**

Virgile Adam[+], Kyprianos Hadjidemetriou[+], Nickels Jensen[+], Robert L. Shoeman[+], Joyce Woodhouse[+], Andrew Aquila, Anne-Sophie Banneville, Thomas R. M. Barends, Victor Bezchastnov, Sébastien Boutet, Martin Byrdin, Marco Cammarata, Sergio Carbajo, Nina Eleni Christou, Nicolas Coquelle, Eugenio De la Mora, Mariam El Khatib, Tadeo Moreno Chicano, R. Bruce Doak, Franck Fieschi, Lutz Foucar, Oleksandr Glushonkov, Alexander Gorel, Marie Luise Grünbein, Mario Hilpert, Mark Hunter, Marco Kloos, Jason E. Koglin, Thomas J. Lane, Mengning Liang, Angela Mantovanelli, Karol Nass, Gabriela Nass Kovacs, Shigeki Owada, Christopher M. Roome, Giorgio Schirò, Matthew Seaberg, Miriam Stricker, Michel Thépaut, Kensuke Tono, Kiyoshi Ueda, Lucas M. Uriarte, Daehyun You, Ninon Zala, Tatiana Domratcheva,* Stefan Jakobs, Michel Sliwa, Ilme Schlichting, Jacques-Philippe Colletier, Dominique Bourgeois,* and Martin Weik*

Rational control of off-state heterogeneity in a photoswitchable fluorescent protein provides switching contrast enhancement

Authors: Dr. Virgile Adam[1,#], Dr. Kyprianos Hadjidemetriou[1,#], Dr. Nickels Jensen[2,#], Dr. Robert L. Shoeman[3, #], Dr. Joyce Woodhouse[1,#], Dr. Andrew Aquila[4], Dr. Anne-Sophie Banneville[1], Dr. Thomas R. M. Barends[3], Dr. Victor Bezchastnov[3], Dr. Sébastien Boutet[4], Dr. Martin Byrdin[1], Dr. Marco Cammarata[5], Prof. Dr. Sergio Carbajo[4], Dr. Nina Eleni Christou[1], Dr. Nicolas Coquelle[1], Dr. Eugenio De la Mora[1], Dr. Mariam El Khatib[1], Dr. Tadeo Moreno Chicano[1], Prof. Dr. R. Bruce Doak[3], Prof. Dr. Franck Fieschi[1], Dr. Lutz Foucar[3], Dr. Oleksandr Glushonkov[1], Alexander Gorel[3], Dr. Marie Luise Grünbein[3], Mario Hilpert[3], Dr. Mark Hunter[4], Dr. Marco Kloos[3], Dr. Jason E. Koglin[4], Dr. Thomas J. Lane[4], Dr. Mengning Liang[4], Angela Mantovanelli[1], Dr. Karol Nass[3], Dr. Gabriela Nass Kovacs[3], Dr. Shigeki Owada[6,7], Christopher M. Roome[3], Dr. Giorgio Schirò[1], Dr. Matthew Seaberg[4], Miriam Stricker[3], Michel Thépaut[1], Dr. Kensuke Tono[6,7], Prof. Dr. Kiyoshi Ueda[8], Dr. Lucas M. Uriarte[9], Dr. Daehyun You[8], Ninon Zala[1], Dr. Tatiana Domratcheva[3,10,*], Prof. Dr. Stefan Jakobs[2], Dr. Michel Sliwa[9], Prof. Dr. Ilme Schlichting[3], Dr. Jacques-Philippe Colletier[1], Dr. Dominique Bourgeois[1,*], Dr. Martin Weik[1,*]

Supplementary material

Supplementary Methods

Site-directed mutagenesis, purification and spectroscopic characterisation of parent proteins (rsEGFP2 and rsFolder2) and their V151A and V151L variants

The primers for V151A and V151L substitutions were 5′-CAACAGCCACAACGCCTATATCATGGCC-3′ and 5′-CTACAACAGCCACAACCTCTATATCATGGCCG-3′, respectively, for rsEGFP2 and 5′-CAGCCACAACGCGTACATCACC-3′ and 5′-CAGCCACAACCTGTACATCACCG-3′, respectively, for rsFolder2. Mutagenesis, transformation, expression and purification were performed as described in [1]. Absorption spectra were recorded using a Jasco V-630 UV/VIS spectrophotometer (Easton, USA). Emission spectra were measured either with a Jasco FP-8500spectrofluorometer (Easton, USA) or with a CCD-based microspectrophotometer (AvaSpec-ULS2048, Avantes, Eerbeek, The Netherlands) coupled with optic fibres to a cuvette holder and photoinduced fluorescence switching cycles were measured as described earlier [2].

Microcrystal growth of rsEGFP2 and its V151A and V151L variants, injection for SFX data collection and pre-illumination to induce on-to-off switching

rsEGFP2, rsEGFP2-V151A and rsEGFP2-V151L microcrystals (3 × 3 × 3 μm^3) were generated by the batch method and employing microseeding as described earlier [1, 3]. The final protein, precipitant, salt and buffer concentrations were 20 mg/ml, 2 M ammonium sulfate, 20 mM NaCl, 120 mM HEPES pH 8, respectively. Purification and microcrystallization of rsEGFP2, rsEGFP2-V151A and rsEGFP2-V151L took place in April 2015, October 2017 and February 2018, respectively. The rsEGFP2 microcrystal batch was the same as the one used for earlier SFX experiments [1, 3]. Prior to injection, sedimented rsEGFP2 microcrystals (but not those of the V151A and V151L variants) were resuspended in 100 mM HEPES pH 8, 2.5 M ammonium sulphate and 5 – 10 % (v/v) of finely crushed rsEGFP2 microcrystals were added to reduce aggregation of microcrystals and the resulting clogging of the injector tubing. All microcrystal suspensions were filtered through a 20-µm stainless-steel filter using a sample loop and a manually-driven syringe. They were loaded into a stainless-steel sample syringe, which was then installed on an anti-settling device [4] onto a Peltier element-cooled (20°C) syringe holder. Crystals were injected at flow rates between 30 – 40 µL min^{-1} with a gas dynamic virtual nozzle (GDVN [5]), using sample capillaries with an inner diameter of 75 µm. For *off*-state data collections, rsEGFP2 microcrystals were injected at a concentration of 20-30% (v/v) into the microfocus vacuum chamber of the CXI instrument [6] at the LCLS (proposal LM47, 23 – 27 June 2016) and those of the V151A and V151L variants at 6.6 % (v/v) into the helium-filled *Diverse Application Platform for hard X-ray Diffraction in SACLA* (DAPHNIS [7]) chamber on the BL2 – EH3 experimental station of SACLA [8] (SACLA 2018A8026, 27 – 29 July 2018). For *on*-state data collection of the rsEGFP2-V151A variant, the sample was injected at 5 % (v/v) into the microfocus vacuum back-chamber of the CXI instrument at the LCLS (proposal LR38, 22 – 26 February 2018).

For *off*-state data collections, microcrystals were pre-illuminated during transit from the sample syringe to the injector with 488 nm laser light (200 mW nominal power, 25 ms transit time, 300 W / cm^2) within a custom made device [9] to switch them from the resting *on*-state to the *off*-state (Figure 1a). The pre-illumination efficiency, *i.e*. the residual amount of remaining *on*-state was checked by absorption spectroscopy using a Nanodrop 2000c spectrometer. The spectra after 488 nm illumination contain contributions from *off*- and *on*-state chromophores and are distorted by scattering effects. They were modeled by a sum of two Gaussians (Gaussian 1 at 400 nm and Gaussian 2 at 482 nm) and an exponential function, respectively. Baseline distortions due to scattering were subtracted and the spectrum smoothened with a Savitzky-Golay filter and normalized at 280 nm (Supplementary figures S4 and S14). The absorbance of Gaussian 2 at 482 nm relative to the absorbance at 482 nm of the

spectrum before 488 nm illumination (assumed to correspond to 100% *on*-state) represents the pre-illumination efficiency. In the case of rsEGFP2-V151A (Supplementary figure S4a) and V151L (Supplementary Figure S4b), 85% and 77% (accuracy is estimated to be around 10%) were switched to the *off*-state, respectively, and 15% and 23% remained in the *on*-state, respectively. For parental rsEGFP2 (LCLS experiment LM47), only 66% were switched to the *off*-state and 34% remained in the *on*-state (Supplementary figure S14a), *i.e.* less than during our earlier SFX experiments [1, 3], where 90% [1] and 84% (SACLA experiment in 2015 (2015A8031[3]) (Supplementary figure S14b) of parental rsEGFP2 was switched to the *off*-state. We noticed after the LM47 experiment on rsEGFP2 that the SMA fiber within the high-performance liquid chromatography (HPLC) tee union of the pre-illumination device (see Figure 2 in [9]) was dirty or damaged, leading to a 50% drop in laser power at the sample position. For the SACLA 2018A8026 experiment on the V151A and V151L variants, a new version of the pre-illumination device was engineered (Shoeman *et al.*, unpublished).

RT SFX data collection and online monitoring

SFX data on parental rsEGFP2 in the *off*-state were acquired with the CSPAD detector [10] operating in a dual-gain mode in the microfocus vacuum chamber of the CXI instrument at the LCLS operating at 120 Hz, with X-ray pulses of 35 fs in length and a photon energy of nominally 9.1 keV (LM47). The X-ray beam was focused to 1 – 2 μm (FWHM). rsEGFP2-V151A *on*-state data (LR38) were collected in the vacuum backchamber of CXI (focus 5 – 10 μm (FWHM); photon energy 9.8 keV). SFX data on rsEGFP2 V151A and V151L variants in their *off*-states were collected on the BL2 – EH3 experimental station (hutch temperature ca 27 - 29ºC, but sample syringe on cooled (20°C) Peltier element) using X-ray pulses (nominal photon energy 7.6 keV, pulse length ≤ 10 fs) at a repetition rate of 30 Hz. The X-ray beam was focused to 1.3 μm (H) × 1.4 μm (V) (FWHM), the pulse energy was ~400 μJ. Data were acquired with the octal-MPCCD detector with eight sensor modules positioned 50 mm away from the sample. The CFEL–ASG Software Suite (CASS [11]) was used for online monitoring of diffraction data, such as diffraction resolution, hit rate, fraction of multiple hits and pixel saturation.

SFX data processing

NanoPeakCell [12] was used for the on- and off-line hit finding. Hit-finding parameters were adjusted after visual inspection of the first diffraction patterns using the NanoPeakCell graphical interface.

For rsEGFP2, rsEGFP2-V151A in the *on*- and the *off*-state, and rsEGFP2-V151L in the *off*-state, 80 605, 17 538, 10 794 and 4 930 images were indexed, respectively (Table S2). The CrystFEL suite [13] was used for further data processing. The data were indexed with *Mosflm* and integrated using v.0.6.2 for parent rsEGFP2, v.0.6.3 for rsEGFP2-V151A in the *on*-state and v.0.7.0 for rsEGFP-V151A and rsEGFP2-V151L in the *off*-state. Merging was performed using CrystFEL v.0.8.0 with the Monte Carlo algorithm, *process_hkl*, for the parental rsEGFP2 *off*-state dataset and with *partialator* using the xsphere partiality model with one cycle of scaling and post-refinement for all rsEGFP2-variant datasets. A resolution cut-off of 1.7, 1.9, 1.95, 2.1 Å was chosen based on SNR, Rsplit and CC* statistics (Table S2) for parent rsEGFP2, rsEGFP2-V151A in the *on*-state, and rsEGFP2-V151A and rsEGFP2-V151L in the *off*-state, respectively.

SFX structure solution and refinement

The SFX structures were phased by molecular replacement with *Phaser* [14]. As a search model was used the SFX *off*-state structure of the parental rsEGFP2 (PDB entry 6T39 [3]) for structures of rsEGFP2 in the *off*-state (PDB entry 7O7U), and of rsEGFP2-V151A (PDB entry 7O7X) and -V151L (PDB entry 7O7W) in the *off*-state. The SFX parental rsEGFP2 *on*-state structure (PDB entry 5O89 [1]) was used as a search model for the structure of rsEGFP2-V151A in the *on*-state (PDB entry 7O7V).

Refinement included positional and isotropic individual B-factor refinement in reciprocal space in Refmac5 [15] for all structures. Model building and real space refinement were performed in *Coot* [16]. Initially, the chromophore had been omitted from the model and subsequently included and modelled as described below. Once the chromophore had been included, its position and isotropic individual B-factors were refined in reciprocal space, while the protein moiety remained fixed. All the structures were superposed to the SFX parental rsEGFP2 *off*-state structure (PDB entry 6T39 [3]) using the CCP4 program *superpose* which is a structural alignment tool based on secondary structure matching.

For rsEGFP2 in the *off*-state, the chromophores were modelled in a *trans1* conformation at 70% occupancy and the *on*-state *cis* conformation at 30% according to spectroscopy (Supplementary figure S14a). The resulting $F_{obs} - F_{calc}$ map showed a positive peak indicating the presence of *trans2* (Supplementary figure S2a). When the occupancy of *cis*, *trans2* and *trans1* were set to 30%, 30% and 40% occupancy the resulting $F_{obs} - F_{calc}$ map was featureless in the chromophore region (Supplementary figure S2b). That a considerable fraction (30%) of the chromophore was in the *trans2* conformation was also confirmed by a $F_{obs} - F_{calc}$ map in

which the hydroxybenzylidene moiety was omitted (Supplementary figure S2c). We note that the chromophore occupancies were different from the ones in parental rsEGFP2 in the *off*-state reported earlier (6T39 [3], 10% *cis*, 25% *trans2* and 65% *trans1*), in agreement with spectroscopy (Supplementary figure S14).

For rsEGFP2-V151A in the *on*-state, the *cis* chromophore of parent rsEGFP2 was included at 100% occupancy.

For rsEGFP2-V151A in the *off*-state the chromophore was first modelled at 100% occupancy in the *trans1* conformation of the parent rsEGFP2 (PDB entry 7O7U) resulting in negative $F_{obs} - F_{calc}$ peaks on the chromophore and the side chains of Tyr146 and H149 (not shown). Then, the chromophore (*cis*) and Tyr146 and H149 conformations of the rsEGFP2-V151A SFX *off*-state model (PDB entry 7O7X) were added and their occupancies set manually. Several cycles of positional and isotropic individual B-factor refinements in reciprocal space were carried out. No major features remained in the resulting $F_{obs} - F_{calc}$ map when the *cis* and *trans1* chromophores were occupied at 20 and 80%, respectively (Supplementary figure S3b), in accordance we spectroscopy (Supplementary figure S4a) that indicated 85% of the molecules were switched to the *off*-state.

For rsEGFP2-V151L in the *off*-state the *trans2* chromophore of parental rsEGFP2 (PDB entry 7O7U) and the *cis* chromophore of the rsEGFP2-V151L cryo-MX *on*-state model (PDB entry 7O7E) were inserted and their respective occupancies varied manually. The resulting $F_{obs} - F_{calc}$ map was featureless when the *cis* and *trans2* chromophores were occupied at 25 and 75%, respectably (Supplementary figure S3c), in accordance we spectroscopy (Supplementary figure S4b) that indicated 77% of the molecules were switched to the *off*-state.

Crystallization of rsEGFP2-V151A and -V151L for synchrotron cryo-crystallography

For V151L, crystallization was carried out by vapor diffusion with hanging drops in 24-well plates. The well solution was composed of 100 mM HEPES pH 7.8 - 8.4 and 1.7 - 2.4 M ammonium sulfate for a total volume of 500 µl. Drops were prepared at 20 °C by mixing 2 µl from the well with 2 µl of protein solution at 10 mg/ml in 50 mM HEPES pH 7.5, 50 mM NaCl. Crystals appeared within a few days and continued growing during a few weeks to reach their final size.

For V151A, crystallization trials were first assessed following the same procedure using the same conditions than for V151L but without success (drops remained clear even after several days). A cross-seeding approach was then adopted. First, V151A crystals were generated by vapor diffusion in sitting drops on 24-well plates using seeds of parental rsEGFP2.

The well solution was composed of 100 mM HEPES pH 8, 2 M ammonium sulfate. Drops were prepared at 20 °C by mixing 10 µl of protein solution at 10 mg/ml, 50 mM HEPES pH 7.5, 50 mM NaCl with 10 µl of solution at 2 M ammonium sulfate, 100 mM HEPES pH 8 containing parental rsEGFP2 seeds diluted 1/1000 (v/v). Crystals appeared after a few days and were used for generating seeds that were used to crystallize V151A on 24-well plates using the vapor diffusion method in hanging drops. The well solution was composed of 100 mM HEPES pH 8, and 1.8 - 2.4 M ammonium sulfate concentration. Drops were prepared by mixing 2 µl of protein solution at 10 mg/ml, 50 mM HEPES pH 7.5, 50 mM NaCl with 2 µl containing V151A seeds in 2 M ammonium sulfate, 100 mM HEPES pH 8. Crystal appeared and reached their final size within a few days. Generation of V151A macrocrystals without seeding was achieved only after V151A structures had already been determined.

In crystallo photoswitching, synchrotron data collection and processing of rsEGFP2-V151A and -V151L variants

For structure determination of the rsEGFP2-V151A variant in its *on*-state, a macrocrystal (200 × 20 × 20 µm^3) grown in 2.2 M ammonium sulfate, 100 mM HEPES pH 8 was harvested with a cryo-loop and soaked for a few seconds in a cryo-solution composed of 2 M ammonium sulfate, 100 mM HEPES pH 8, 20% glycerol (the same cryo-solution was used for all crystal preparations presented here). Then the crystal was flash-cooled in liquid nitrogen. For structure determination of V151A in the *off*-state a macrocrystal (150 × 10 × 10 µm^3) grown in the same condition was exposed to 488 nm laser-light, guided through a fiber, for around one minute at room temperature (RT) directly in the drop where it grew until the crystal turned colorless. The crystal was then harvested with a cryo-loop and soaked in the cryo-solution before being flash-cooled. For structure determination of the rsEGFP2-V151L variant in its *on*-state, a macrocrystal (300 × 100 × 100 µm^3) grown in 1.7 M ammonium sulfate, 100 mM HEPES pH 7.8, 10 mg/ml was harvested with a cryo-loop and soaked in the cryo-solution before being flash-cooled in liquid nitrogen. For structure determination of V151L in the *off*-state, the same procedure than for V151A was applied. A macrocrystal (150 × 50 × 50 µm^3) grown in 1.8 M ammonium sulfate, 100 mM HEPES pH 8.2, 10 mg/ml protein was exposed to 488 nm laser-light for around one minute at RT as described above and then soaked in the cryo-solution before being flash-cooled.

X-ray crystallographic oscillation data were collected at 100 K on ID29 [17] at the European Synchrotron Radiation Facility (ESRF, Grenoble, France) operating in 7/8

multibunch mode at an X-ray wavelength of 0.976 Å (12.7 keV) and with a beamsize of 30 µm × 30 µm. Data were recorded with a Pilatus 6M detector (Dectris). For rsEGFP2-V151A in the *on*-state, 1 050 frames were recorded with an oscillation range of 0.10 ° and an exposure time of 0.037 s per frame with a photon flux of 1.6×10^{11} ph/s at 5% transmission. For rsEGFP2-V151A in the *off*-state, 547 frames were recorded (oscillation range 0.15 °, exposure time 0.039 s per frame, photon flux 2.8×10^{11} ph/s, 9.94 % transmission). For rsEGFP2 V151L in the *on*-state, 794 frames were recorded (oscillation range 0.15 °, exposure time 0.1 s per frame, photon flux 2.2×10^{10} ph/s, 1.27 % transmission). For rsEGFP2 V151L in the *off*-state, 950 frames were recorded (oscillation range 0.10 °, exposure time 0.037 s per frame, photon flux 2.8×10^{10} ph/s, 9% transmission). Images were indexed and intensities were integrated and merged using XDS [18].

Molecular replacement and structure refinement of rsEGFP2-V151A and -V151L synchrotron cryo-data

For both states of the two variants, molecular replacement was performed with *Phaser* [14] using the cryo-structure of parental rsEGFP2 in the fluorescent *on*-state as a starting model (PDB entry: 5DTX [19]). Manual model building was performed in *Coot* [16] and refinement with the *Phenix* suite [20] included positional and isotropic individual B factor refinement. *PyMOL* [21] was used to produce all figures. For the structure of the *on*-state of rsEGFP2-V151A (PDB entry 7O7D), the occupancy of the phenol of the chromophore and the imidazole of H149 was fixed to 0.9 before final cycles of refinement were carried out. For the *off*-state structure of rsEGFP2-V151L (PDB entry 7O7H), the chromophore, H149 and L151 were modeled in alternate conformations.

We note that *on*-state crystal structures of the rsEGFP2-V151A variant have been determined by both synchrotron cryo-crystallography (PDB entry 7O7D, Supplementary table S1; Supplementary figure S5a) and RT SFX (PDB entry 7O7V, Supplementary figure S3a) and the one of the V151L variant only by synchrotron cryo-crystallography (PDB entry 7O7E, Supplementary table S1, Supplementary figure S5c).

Crystallization, synchrotron cryo-crystallographic data collection and structure solution and refinement of rsFolder2 in its on- and off-states

rsFolder2 was crystallized at a concentration of ~12 mg/ml using the vapor diffusion method, against a reservoir consisting in 20% PEG 3350, 100 mM Tris pH 8.5 and 20 mM

NaCl. Thick plate-shaped crystals appeared after 3-4 days at 20 ºC. Before harvesting, crystals were cryo-protected using mother liquor solution supplemented with 15% glycerol and then cryo-cooled in liquid nitrogen. To obtain the *off*-state structure, crystals were illuminated for 5 s with an optical fiber connected to a 488 nm laser just before harvesting. X-ray diffraction data collection was performed at beamline ID30a-3 (MASSIF-3) of the ESRF at 100 K, using 0.97 Å wavelength X-rays and a Pilatus3 2M detector (Dectris Ltd.). Data processing was carried out with XDS [18], and merged data were phased by molecular replacement with Phaser [14], within the CCP4i2 suite [22], using as search model the rsFolder *on*-state structure (PDB entry 5DTZ [19]). Final models were obtained after successive refinement rounds (maintaining isotropic B-factors) with Refmac5 [15], with manual model building in-between cycles using *Coot* [16]. For the *on*-state structure (PDB entry 7AMB), a fully occupied *cis* chromophore was found in the active site, as expected. In the case of the *off*-state structure (PDB entry 7AMF), initially only the *cis* and *trans1* conformers were modelled. After a round of refinement, there was a faint indication of the presence of the *trans2* conformer as a weak positive peak in the $F_{obs} - F_{calc}$ map. This evidence was clearer when the NCS averaged difference map (four monomers in the asymmetric unit) was calculated with *Coot* (Supplementary figure S6 b). The *trans2* conformation was modelled in each of the monomers and then refined together with the *cis* and *trans1* conformations. Occupancies for the different conformers were set manually according to electron density in the $2F_{obs} - F_{calc}$ and $F_{obs} - F_{calc}$ maps, and then assessed after refinement to make sure there were no further peaks in the $F_{obs} - F_{calc}$ map. Validation of the structures was performed using Molprobity [23], JCSG QC-check server, and the validation tools within *Coot* as well as the PDB validation service.

Crystallization, in crystallo photoswitching at various illumination intensities, synchrotron data collection and processing of parental rsEGFP2

Crystals of parental rsEGFP2 were prepared as previously described [19]. Crystals were then individualized within crystallization trays and exposed to controlled power densities of 488 nm laser light (0.1, 0.2, 0.4 and 0.8 W/cm²) during 30 s. Crystals were then immediately cryoprotected in the mother liquor solution supplemented by 15% glycerol, mounted on microloops and flash-cooled in liquid nitrogen. X-ray data collections was performed at the ID29 beamline at the European Synchrotron Radiation Facility (ESRF, Grenoble, France) operating in 7/8 multibunch mode at an X-ray wavelength of 0.976 Å (12.7 keV), with a beamsize of 30 µm × 30 µm and recorded with a Pilatus 6M detector (Dectris).

Fluorescence microscopy

Ensemble fluorescence microscopy data were acquired on a custom-made setup based on an Olympus IX81 inverted microscope equipped with a x100 1.49 NA oil-immersion apochromatic objective lens (Olympus, Japan). Widefield illumination was achieved by focusing the diode-pumped solid state 405-nm (CrystaLaser, USA) and 488-nm (Spectra Physics, USA) laser beams to the back focal plane of the objective. Intensities of laser illuminations at the sample were tuned by an acousto-optical tunable filter (AOTF, AA Opto Electronic, France). Fluorescence images were acquired with an Evolve 512 back-illuminated EMCCD camera (Photometrics, USA) controlled by the Metamorph software (Molecular Devices, USA).

Fluorescent-protein (FP) immobilization on a polyacrylamide gel

Five µL of purified RSFP at ~12 mg/ml concentration was mixed with 50 µL of 30% polyacrylamide (PAA) solution with 43 µL of Tris at pH 8.0. PAA polymerization was initiated by adding 1 µL of 10% APS (ammonium persulfate) and 1 µL TEMED (Tetramethylethylenediamine). Twenty five µL of the FP-containing PAA was then spread between two glass coverslides separated by a calibrated spacer (Gene Frame 25 µl (1.0 × 1.0 cm) AB-0576 Thermo Scientific) thoroughly cleaned using a UV ozone cleaning system (HELIOS 500, UVOTECH Systems) to form a uniform 200 µm thick layer, and let to harden at room temperature for 5 minutes.

Ensemble-level switching experiments

Ensemble level switching experiments were based on measuring the evolution of fluorescence emission. The illumination scheme for driving *off*- and *on*-switching in all variants was the following: first, samples were submitted to 0.086 W/cm² of 405-nm light for 2.5 s, so as to maximize the population of proteins in the *on*-state. *Off*-switching was performed by recording 1700 EMCCD frames of 25 ms exposure at 20 Hz with dark periods of 25 ms in between frames. During frame exposure, actinic light at 488 nm (0.27 W/cm²) also served as excitation light to readout fluorescence. *On*-switching was performed by recording 600 frames using the same scheme, except that the dark periods of 25 ms in between frames were replaced by illumination at 405 nm (0.03 W/cm^2). Thus, FPs were first *off*-switched for 85 s under 488 nm light, and subsequently switched-*on* by 405 nm light, in the presence of 488 nm light, for 30 s. The laser power at the sample position was measured with a calibrated power meter (S170C sensor and PM100D console, Thorlabs), and laser power densities were estimated from

a Gaussian fit of the laser profiles that were recorded with fluorescent coverslides (92001, Autofluorescent Plastic Slides, Chroma). Each variant was measured three times from at least three independently prepared samples.

Extraction of switching curves

Analysis of switching cycles was performed on a small region of 5 × 5 pixels (0.38 μm²) located at the region of maximum laser intensity, so as to ensure homogenous illumination. Of note, considering the thickness of the FP samples (200 μm), which exceeds the depth of field of the employed X100 objective (~500 nm), the signal analyzed in this small region contained residual contributions from out-of-focus FPs submitted to lower illumination intensities. This out-of-focus effect was corrected by estimating the contribution of FPs located elsewhere than in the selected region. This contribution was based on estimating the depth-dependent point spread function (PSF) of the microscope objective according to a Gibson & Lanni model using the PSF generator plug-in of Fiji version 1.52p. In this way, the fluorescence signal recorded at position (x0, y0) of the EMCCD detector of a molecule positioned at (x, y, z) can be calculated using the PSF at position z, centered at (x, y). The overall contributions of all molecules at positions (x, y) (*i.e.* out of the small selected central region), over the whole depth of the sample, to the recorded signal at (x0, y0) (*i.e.* within the selected central region) is then obtained by integrating contributions in the x, y and z dimensions. Because at each (x, y) the illuminating laser power density is known (and assumed to be constant over z), the switching kinetics of molecules at (x, y) can be modelled. Thus, in the central region, the observed switching kinetics is the sum of the signals of all molecules in the sample with their own switching kinetics, weighted by the fraction of those signals reaching the central region. Since this central recorded region was chosen to correspond to the region of peak laser intensity, the out of focus contribution essentially brings in signal from molecules that experience slower switching kinetics. Consequently, the overall switching kinetics in the central region is slower than if no out-of-focus effect took place. Neglecting the out-of-focus effect would then result in underestimating the extracted switching quantum yields. Corrections for this effect modified the yields by ~10%. Of note, the relative values of the extracted yields from one variant to another was not affected. Thus the main conclusions of the study are independent of the out-of-focus correction procedure described here.

Determination of switching quantum yields and extinction coefficients $\varepsilon_{488,off}$

On-to-*off* and *off*-to-*on* photoswitching parameters were derived from global fitting of both *off*-switching and *on*-switching phases of the switching cycles with a kinetic model that includes, in addition to the *on*- and *off*-states, a short-lived reversible dark states that can be accessed from the *on*-state (supplementary figure S15). This short-lived dark state needed to be invoked to account for the strongly biphasic *off*-switching decay curves. Due to the strong photofatigue resistance of all tested variants, photobleaching was assumed to not contribute to the first photoswitching cycle studied here. Thus the evolution of the various species can be described as follows:

$$\frac{d[ON]}{dt} = -(k_1 + k_3) \times [ON] + k_2 \times [OFF] + k_4 \times [DARK]$$

$$\frac{d[OFF]}{dt} = -k_2 \times [OFF] + k_1 \times [ON]$$

$$\frac{d[DARK]}{dt} = -k_4 \times [DARK] + k_3 \times [ON]$$

with, during the *on-off* switching phase:

$$k_1 = \alpha \times \varepsilon_{488,on} \times Q_{on-to-off} \times P_{488} \times \lambda_{488}$$

$$k_2 = \alpha \times \varepsilon_{488,off} \times Q_{off-to-on} \times P_{488} \times \lambda_{488}$$

$$k_3 = \alpha \times \varepsilon_{488,on} \times Q_{on-to-dark} \times P_{488} \times \lambda_{488}$$

$$k_4 = \alpha \times \varepsilon_{488,dark} \times Q_{dark-to-on} \times P_{488} \times \lambda_{488}$$

and, during the *off-on* switching phase:

$$k_1 = \alpha \times \varepsilon_{488,on} \times Q_{on-to-off} \times P_{488} \times \lambda_{488} + \alpha \times \varepsilon_{405,on} \times Q_{on-to-off} \times P_{405} \times \lambda_{405}$$

$$k_2 = \alpha \times \varepsilon_{488,off} \times Q_{off-to-on} \times P_{488} \times \lambda_{488} + \alpha \times \varepsilon_{405,off} \times Q_{off-to-on} \times P_{405} \times \lambda_{405}$$

$$k_3 = \alpha \times \varepsilon_{488,on} \times Q_{on-to-dark} \times P_{488} \times \lambda_{488} + \alpha \times \varepsilon_{405,on} \times Q_{on-to-dark} \times P_{405} \times \lambda_{405}$$

$$k_4 = \alpha \times \varepsilon_{488,dark} \times Q_{dark-to-on} \times P_{488} \times \lambda_{488} + \alpha \times \varepsilon_{405,dark} \times Q_{dark-to-on} \times P_{405} \times \lambda_{405}$$

where ε ($M^{-1}cm^{-1}$) is the extinction coefficient of the considered species at the specified wavelength, Q is the switching quantum yield between the specified states, λ (nm) is the wavelength, P (W/cm^2) is the laser power density and α is a multiplication factor given by:

$$\alpha = \frac{Ln(10) \times 10^{-6}}{N_A \times h \times c}$$

where N_A is the Avogadro number, h is the Planck constant and c is the speed of light.

The fitting model also took into account the effect of switching *during* the integration time of the EMCCD, which can be non-negligible for the fast-switching proteins studied here. Using measured laser power densities and molar extinction coefficients of the *on*-state proteins obtained by the Ward method (see below) as input, the global fitting of both the *on*-to-*off* and the *off*-to-*on* phases of the switching cycles allowed retrieving the $Q_{on-to-off}$ and $Q_{off-to-on}$ switching quantum yields, as well as the extinction coefficient $\varepsilon_{488,off}$ of the *off*-state at 488 nm that largely dictates the experimentally observed switching contrast. Of note, the procedure allowed extracting values for $Q_{on-to-dark}$, and the products $Q_{dark-to-on} \times \varepsilon_{488,dark}$ and $Q_{dark-to-on} \times \varepsilon_{405,dark}$. $\varepsilon_{405,on}$ was given an arbitrary value of 1000 $M^{-1}cm^{-1}$ for all variants (the choice of this value did not influence the results significantly). Fitting was realized with a custom-made routine based on the lsqcurvefit method in Matlab.

Measurement of absorption spectra before and during photoswitching

Purified proteins of rsEGFP2, rsFolder2 and their related variants V151A and V151L were adjusted in concentration to ~0.5 OD at their maximum anionic peak absorption in a 100 mM HEPES buffer, pH 7.5. These samples were placed in a quartz cuvette at room temperature in a CCD-based microspectrophotometer [2] equipped with a square diffuser within the excitation path to achieve homogeneous illumination. Before acquiring each spectrum, the sample was pre-exposed to 405-nm laser light for ~5 s (~88 mW/cm²) to maximize the *on*-state. Photoswitching data was obtained by alternating laser illuminations at 488 nm (~25 mW, 730 ms) and synchronized spectrometer acquisition with white lamp probing (70 ms).

Determination of off-to-on thermal recovery time

After switching the RSFPs to their off state by constant illumination at 488 nm, their thermal relaxation was probed by monitoring the absorption as a function of time for 1 to 5 days. Diluted proteins (50 µl) were placed at 20°C in a 50-µl cuvette within a CCD-based spectrometer (AvaSpec-ULS2048, Avantes, Eerbeek, The Netherlands) coupled with optic fibres to a cuvette holder. Absorption spectra were measured every 10 minutes (or 20 minutes for slower mutants) thanks to a pulse of white light synchronised to the spectrophotometer acquisition.

Determination of maturation time

RSFP were overexpressed in *E. coli* BL21(DE3), transformed to express fluorescent proteins and plated. Three colonies for each RSFP were transferred in individual flasks containing 100 mL LB medium and allowed to grow for 4 hours before IPTG-induction. The agitation (230 rpm, 37°C) was further pursued for 1 hour to allow the overexpression of RSFPs and to ensure the exponential growth log phase of bacteria. Protein synthesis was then stopped by the addition of chloramphenicol (300 µg/mL) and 100 µL of each culture was deposited within a 96-cell plate. Absorption and emission points were recorded every 5 min using a Biotek Synergy H4 microplate reader (Winooski, VT, USA) under agitation and controlled temperature at 37°C. Absorption at 600 nm was used to normalize the emission values that were obtained using excitation at 485 ± 20 nm and emission and 528 ± 20 nm. Maturation time was evaluated by fitting a logarithmic model and determining the half-time of each fluorescence increase.

Measurement of switching kinetics and switching fatigue in vivo

The measurements of switching kinetics and switching fatigue under conditions comparable to RESOLFT nanoscopy conditions were performed on *E. coli* colonies using an automated microscope. Fluorescent proteins were freshly expressed in bacteria grown on LB agar plates containing 0.02% L-Arabinose for 20 h at 37°C using the pBAD expression system and *E. coli* Top10 cells. The *E. coli* colonies were irradiated with laser light of 405 nm for 2 ms (to switch RSFPs completely to the *on*-state) and of 488 nm for 5-20 ms (to switch RSFPs completely to the *off*-state). A 20-fold objective (numerical aperture (NA) 0.4) was used to focus light onto the colonies with power of 5 mW (488 nm) and 1.5 mW (405 nm). The fluorescence was detected with a photomultiplier tube. For measurement of the switching kinetics, the proteins were switched *on* and *off* ten times consecutively, the average of the ten *off* switching curves was calculated for every colony and then normalized to the initial colony brightness. The graphs in figure 6 represent the average of 20 colonies, respectively. For quantification of switching fatigue, the colonies were switched *on* and *off* completely for 4000 times consecutively and the fluorescence intensity of the first time point of every *off*-switching step was used for quantification of the colony brightness in the respective switching cycle. The data was normalized to the initial colony brightness. The graphs represent the average of 10 colonies, respectively.

RESOLFT microscopy

HeLa cells were transfected with the plasmid pKeratin-rsFolder2-V151A using TurboFect^{TM} according to the manufactures' instructions. Imaging was performed 20 h after transfection in DMEM without phenol red (Thermo Fisher Scientific, Waltham, MA, USA) at room temperature. RESOLFT microscopy was performed using a customized 1C RESOLFT QUAD scanning microscope (Abberior Instruments, Göttingen, Germany) equipped with a 100X oil immersion objective (NA 1.4). The RESOLFT image was recorded by applying the following three illumination steps at each scanning position. First, proteins were transferred to the *on*-state by illuminating with 405-nm light for 15 µs with an power of 2 µW. Second, the proteins in the periphery of the focal spot were transferred to the *off*-state using a doughnut-shaped beam of 488 nm light with an intensity of 15 µW for 520 µs. Finally, residual *on*-state proteins at the centre of the spot were excited for 30 µs with 8 µW 488 nm light. In the last step, fluorescence was detected using a SPCM-AQRH-13 photon counting module (Excelitas Technologies, Waltham, MA, USA) with a HC 550/88 detection filter. Power values were measured in the back focal aperture of the objective lens. The scanning step size was set to 25 nm. A line accumulation of 2 was used. The corresponding confocal image was taken accordingly without the *off*-switching step. The full width half maximum (FWHM) of keratin filaments (Figure 7) was determined by averaging three adjacent line profiles at the indicated positions in the raw data image and fitting with a Lorentz curve using Origin 9.1.

Quantum chemical calculations

The Firefly program version 8.0 (http://classic.chem.msu.su/gran/firefly/index.html), which is partially based on the US GAMESS code [24], was used to perform quantum-chemistry calculations. Geometry optimization and OH-stretching energy cross sections were computed with the B3LYP-D3 method [25]. The excitation spectrum and electronic couplings were computed with the XMCQDPT2 method [26]. To estimate the S_0-S_1 energy and transition moments, the SA3-CASSCF(2e,2MO) zero-order wave function was used (two electrons in two molecular orbitals of the chromophore were correlated and state averaging was performed for three states), whereas to compute electronic coupling using the generalized Mulliken-Hush method [27] the SA4-CASSCF(4e,3MO) zero-order wave function (the active space was extended to four electrons in three molecular orbitals by additionally including the occupied orbital of Tyr146; four states were included in state averaging) was used in the XMCQDPT2 calculations. The cc-pvdz basis set [28] was used throughout. The geometries of the cluster models were optimized starting from the coordinates of parental rsEGFP2 (PBD 6T39 [3]). To model the active sites containing *trans1* and *trans2* chromophore geometries the subsets of

coordinates labelled as A and C, respectively, were selected from the PBD file. Figure 5 presents the results of the rsEGFP2 active-site models comprised of 283 atoms. The cluster models included the following fragments of the chromophore-containing site: Thr63-Leu70, Gln95, Arg97, Tyr146-Tyr152, Ser164, Gln184, Asn186, Thr204-Ser206, Glu223 and water molecules. The ionisable groups were set as follows: Arg97 protonated, chromophore neutral, Glu223 neutral, His149 neutral (δN-H for *trans1* and εN-H for *trans2*), hence, the cluster model has a net charge +1. During geometry optimization, the coordinates of selected atoms from the cluster boundary were kept constant. The OH stretching potentials of the chromophore phenolic group were computed starting from the optimized geometries by changing the coordinates of the H atom, whilst all other coordinates were kept as in the optimized structure. At the optimized geometries and geometries with the phenolic OH distance 1.5 Å, excitation energies were computed. To model the band shape of the S_0-S_1 transition, active-site models of a reduced size were employed (for details see caption of Supplementary figure S9). To obtain the A151 and L151 models, the V151 side chain was modified accordingly, and similar computations as for the rsEGFP2 cluster models were performed.

Supplementary Text

Supplementary text S1: Occupancies of trans1 and trans2 off-state chromophore conformations in parental rsEGFP2 determined from data collected during three different SFX experiments

Occupancies of chromophore conformations differ in *off*-state structures determined from data collected during three different SFX experiments, *i.e.* 10%, 90% and 0% [1], 10%, 65% and 25% [3], 30%, 40% and 30% (present work) for *cis*, *trans1* and *trans2*, respectively (Supplementary figure S2). The conversion efficiency differed in the latter two SFX experiments as assessed by absorption spectroscopy (Supplementary figure S14), with 10% [3] and 20% (present work) of the molecules remaining in the *on*-state, suggesting that illumination conditions may modulate the *trans1/trans2* ratio. Alternatively, aging of the crystalline proteins might be at the origin of *trans2* being increasingly populated in *off*-state structures of parental rsEGFP2 determined by SFX under identical buffer conditions on microcrystals of the same batch (0% in May 2015 [1], 25% in July 2015 [3] and 30% in June 2016 (present work)).

Supplementary text S2: Synchrotron cryo-crystallography of parental rsEGFP2 crystals following RT illumination

To study conformational *off*-state heterogeneity by synchrotron cryo-crystallography, macrocrystals of parental rsEGFP2 in their *on*-state were illuminated with 488 nm light at RT at various intensities for 30 s, flash-cooled and the resulting structures determined (Supplementary figure S13). With increasing illumination intensity, the occupancy of the *trans1* chromophore conformation increased at the expense of the *cis* conformation, yet the *trans2* conformation was never observed. This suggests that *trans2* does not build up to the same extent in parental rsEGFP2 macrocrystals, or is eliminated upon flash cooling.

Supplementary text S3: Analysis of photoswitching curves

We first observed that *on*-to-*off* switching of all investigated variants exhibits a biphasic behavior (Supplementary figure S8), suggesting the transient build-up of a short-lived dark state of potentially different spectroscopic and/or structural nature as compared to the *off*-states associated with *trans1* and *trans2* investigated in the present study. Such additional dark states were previously observed in other RSFPs and in photoconvertible FPs [29], and may involve a twisted *cis* configuration of the chromophore with rapid thermally induced relaxation, but their exact nature will need to be investigated in future studies.

The V151A variants switch *off* slightly more efficiently upon illumination at 488 nm than the parent proteins (*off*-switching rate increased by +20%), and the V151L variants less efficiently (-30%). This appears to be mostly an effect of moderate differences in *off*-switching quantum yields. Upon illumination at 405 nm, the V151A variants switch *on* about as efficiently as the parent proteins (*on*-switching brightness increased by +13 %), while the V151L mutants switch *on* more efficiently (+50%), mostly originating from a higher *on*-switching quantum yields in the V151L variants. The reduced *on*-to-*off* switching quantum yield in the V151L variants might be attributed to the presence of the bulky leucine raising the excited state energy barrier between the *on*- and *off*-states.

Supplementary text S4: Modulation of conformational off-state heterogeneity

In addition to the well documented *trans1* conformation of the *off*-state chromophore [1, 19], a second conformation, *trans2*, has been reported for crystalline parental rsEGFP2 [3, 30]. Here, we confirm the observation of *trans2* in parental rsEGFP2 (Figure 1) and provide evidence for its existence in rsFolder2 (Supplementary figure S6). We show that the occupancy of *trans1* and *trans2* conformations can be controlled by modifying the steric constraints imposed by the side-chain of residue 151, a residue retracting transiently during *off*-to-*on* photoswitching [1]. Upon *on*-to-*off* switching, only *trans1* forms in the rsEGFP2-V151A variant, whereas only *trans2* seems to be occupied in the V151L variant (Figure 2).

Interestingly, only the *trans2* conformation is observed in rsFolder, although it has a valine at position 151 [19]. rsFolder displays a phenylalanine at position 146 instead of a tyrosine in rsEGFP2 and rsFolder2 that cannot form an H-bond to the critical His149 in the *off*-state [3, 19]. Consequently, it seems plausible that His149 is free to form an H-bond with the protonated *off*-state chromophore that during on-to-*off* switching then adopts the *trans2* conformer, instead of the *trans1* conformer that is not H-bonded to His149 in rsEGFP2 and rsFolder2. On the other hand, rsGreen0.7 [31] features a phenylalanine at position 146, like rsFolder, but an alanine at position 151, and its *off*-state shows essentially the *trans1* conformer. Thus, access to *trans1* or *trans2* is controlled by residues located either on the *cis* or the *trans* sides of the chromophore pocket, although it appears that the presence of an alanine at position 151 has a dominant effect on the presence of the *trans1* isomer.

Supplementary tables and figures

Table S1 : Cryo-crystallographic synchrotron data collection and refinement statistics of rsEGFP2-V151A, rsEGFP2-V151L and rsFolder2 structures in their *on*- and *off*-states solved from

Data collection and processing						
Dataset	rsEGFP2 V151A *on*	rsEGFP2 V151A *off*	rsEGFP2 V151L *on*	rsEGFP2 V151L *off*	rsFolder2 *on*	rsFolder2 *off*
PDB entry	7O7D	7O7C	7O7E	7O7H	7AMB	7AMF
Illumination (488 nm)	No	Yes	No	Yes	No	Yes
Space group	$P2_12_12_1$	$P2_12_12_1$	$P2_12_12_1$	$P2_12_12_1$	C2	C2
Unit cell parameters						
a (Å)	60.0	51.2	51.1	51.3	142.3	142.3
b (Å)	62.1	60.3	62.5	61.2	134.5	134.9
c (Å)	69.4	66.6	70.4	70.3	51.6	51.7
β (°)					106.1	106.0
Collected frames	1050	547	794	950	3700	3700
Observations	166,004 (12,182)*	89,498 (6,540)	91,956 (14,602)	84,740 (13,701)	389,403 (15,763)	408,905 (19,013)
Resolution (Å)	46.28 - 1.4 (1.44-1.4)	40.57 - 1.55 (1.59-1.55)	41.38 - 1.8 (1.91-1.8)	46.16 - 1.7 (1.81-1.7)	47.94 – 1.63 (1.66-1.63)	48.07 -1.63 (1.66-1.63)
R_{meas} (%)	4.8 (42.5)	4.5 (60.6)	6.5 (46.6)	4.7 (42.8)	6.5 (73.0)	7.2 (80.7)
$CC_{½}$ (%)	99.9 (85.3)	99.9 (70.7)	99.9 (91.6)	99.9 (87.1)	99.9 (74.7)	99.8 (67.9)
I/σI	17.26 (3.23)	14.82 (2.26)	14.17 (2.72)	15.5 (2.9)	13.2 (1.8)	10.3 (1.5)
Completeness (%)	97.4 (96.7)	97.0 (98.4)	98.3 (98.3)	97.2 (98.5)	99.7 (99.7)	99.8 (99.5)
Multiplicity	3.9 (3.9)	3.0 (3.0)	4.3 (4.3)	3.5 (3.5)	3.5 (3.1)	3.5 (3.3)
Refinement statistics						
Resolution (Å)	46.28 - 1.4 (1.43-1.40)	40.57 - 1.55 (1.60-1.55)	41.38 - 1.8 (1.88-1.80)	46.16 - 1.7 (1.77-1.70)	47.98 – 1.63	48.12- 1.63
Number of reflections	42,980 (2,669)	29,619 (2,528)	21,205 (2,482)	24,184 (2,539)	115,478 (2000)	116,053 (2000)
R_{free} (%)	17.90 (25.39)	19.61 (28.60)	20.76 (29.05)	19.70 (26.05)	19.0	18.4
R_{work} (%)	15.21 (21.80)	16.40 (24.46)	15.92 (24.97)	15.70 (22.17)	15.1	15.5
Number of protein atoms	2,066	2,096	1,977	2,129	8,108	8,190
Number of solvent atoms	353	275	317	298	1014	949
B-factor protein ($Å^2$)	16.11	19.12	29.12	29.66	24.97	25.44
r.m.s.d bond lengths (Å)	0.006	0.008	0.006	0.01	0.011	0.012
r.m.s.d angles (°)	0.902	0.997	0.847	1.031	1.764	1.996
Ramachandran favored (%)	99.12	98.68	98.70	97.84	98.22	98.35
Ramachandran allowed (%)	0.88	1.32	1.30	2.16	1.67	1.54
Ramachandran outliers (%)	0.00	0.00	0.00	0.00	0.11	0.11
Rotamer outliers (%)	1.29	1.28	1.79	2.08	2.10	2.84
C-beta outliers	0	0	0	0	2	0
Clashscore	4.32	5.66	3.29	5.81	8.24	9.24

* Values in brackets correspond to the highest resolution shell

Table S2 : RT SFX data collection and refinement statistics of the structures of rsEGFP2 and its V151A and V151L variants in their *off*-states

Dataset	Parental rsEGFP2 *off*	rsEGFP2-V151A *on*	rsEGFP2-V151A *off*	rsEGFP2-V151L *off*
PDB entry	7O7U	7O7V	7O7X	7O7W
Data collection and processing				
Space group	$P2_12_12_1$	$P2_12_12_1$	$P2_12_12_1$	$P2_12_12_1$
Unit cell parameters a (Å) b (Å) c (Å)	 51.7± 0.1 63.1 ± 0.2 73.5 ± 0.2	 51.9± 0.2 62.7 ± 0.3 72.0 ± 0.4	 51.8 ± 0.2 62.7 ± 0.2 71.6 ± 0.3	 51.8 ± 0.2 62.9 ± 0.2 71.9 ± 0.3
Collected frames				
Hits				
Indexed images	80,605	17,538	10,794	4,930
Resolution (Å)	17– 1.70 (1.74 – 1.70)	24 – 1.9 (1.95 – 1.90)	24– 1.95 (2.00 – 1.95)	24– 2.10 (2.15 –2.10)
Observations	22,894,347 (991,284)	2,916,477 (100,602)	2,044,776 (75,714)	778,314 (28,668)
Unique reflections	27,394 (1,810)	19,739 (1,293)	18,181 (1,176)	14,734 (958)
R_{split}[#] (%)	6.8 (56.3)	6.3 (73.6)	7.7 (58.4)	14.0 (53.4)
CC*	0.999 (0.924)	0.999 (0.891)	0.999 (0.904)	0.996 (0.891)
I / σ(I)	10.0 (1.9)	7.8 (1.4)	7.0 (1.8)	4.9 (1.9)
Completeness (%)	100 (100)	100 (100)	100 (100)	100 (100)
Multiplicity	835 (548)	148 (78)	112 (64)	53 (30)
Refinement statistics				
Refinement strategy	Classical refinement	Classical refinement	Classical refinement	Classical refinement
Resolution (Å)	17– 1.70 (1.74 – 1.70)	24 – 1.9 (1.95 – 1.90)	31 – 1.95 (2.00 – 1.95)	31– 2.10 (2.15 –2.10)
Number of reflections	26368 (2,661)	19,091 (2,543)	17,600 (2,739)	14,284 (2,661)
R_{free}	21.5 (38.0)	19.2 (27.14)	20.1 (31.0)	21.3 (22.0)
R_{work}	18.0 (37.0)	14.9 (21.16)	15.7 (26.0)	17.3 (29.0)
Number of protein atoms	2,443	2005	2,182	2,193
Number of ligand atoms	60	20	40	40
Number of water atoms	177	111	125	58
B-factor protein ($Å^2$)	22.81	48.5	43.41	38.97
r.m.s.d. bond lengths (Å)	0.01	0.01	0.008	0.008
r.m.s.d. angles (°)	1.728	1.609	1.547	1.566
Ramachandran favoured	97.00	97.90	97.83	97.41
Ramachandran allowed	3.00	2.10	2.17	2.59
Ramachadran outliers	0.00	0.00	0.00	0.00
Rotamer outliers	4.01	1.80	1.22	0.81
C-beta outliers	0	0	0	0
Clashscore	6.23	2.51	5	6.78

Table S3 : Chromophore dihedral angles from crystallographic models and after computational geometry optimization

Method	Protein	State	PDB ID	Conformer	[*] φ (°)	[#] τ (°)
Synchrotron cryo-crystallography	rsEGFP2-V151A	*off*-state	7O7C	*cis*	174	-166
			7O7C	*trans1*	-54	16
		on-state	7O7D	*cis*	174	-166
	rsEGFP2-V151L	*off*-state	7O7H	*cis*	171	-169
			7O7H	*trans2*	7	-3
		on-state	7O7E	*cis*	171	-169
	rsFolder2	*on*-state	7AMB	*cis*	175	-178
		off-state	7AMF	*cis*	170	-176
			7AMF	*trans1*	-44	17
			7AMF	*trans2*	7	-4
	Cl-rsEGFP2 [30]	*on*-state	6PFR	expanded *cis*	167	-166
			6PFS	contracted *cis*	142	-169
		off-state	6PFT	expanded *trans*	-32[$]	2
			6PFU	contracted *trans*	43	-30
RT SFX	rsEGFP2	*off*-state	7O7U	*cis*	168	-167
			7O7U	*trans1*	-48	7
			7O7U	*trans2*	7	-4
	rsEGFP2-V151A	*off*-state	7O7X	*cis*	173	-172
			7O7X	*trans1*	-50	9
		on-state	7O7V	*cis*	178	-170
	rsEGFP2-V151L	*off*-state	7O7W	*cis*	173	-151
			7O7W	*trans2*	10	-18
Comput. B3LYP-D3 geometry optimization	rsEGFP2	*off*-state	(6T39)[&]	*trans1*	-31	-5
		off-state	(6T39)[&]	*trans2*	-7	-10
	rsEGFP2-V151A	*off*-state	(6T39)[&]	*trans1*	-27	-6
	rsEGFP2-V151L	*off*-state	(6T39)[&]	*trans2*	-8	-10

[*]CA2-CB2-CG2-CD2 (for numbering see Supplementary figure 16c in [1])

[#]C2-CA2-CB2-CG2

[$]CA2-CB2-CG2-CD1 (due to the flip of the chromophore around CB2-CG2 in PDB ID 6PFT)

[&]starting coordinates of the computational models were taken from PDB 6T39

Table S4. Results of XMCQDPT2 excited-state calculations comparing *trans1* and *trans2*. The calculations employed the SA3-CASSCF(2e,2MO) and SA4-CASSCF(4e,3MO) (indicated as CT[a)]) zero-order approximation.

Chromophore conformation	Geometry	Excitation energy (eV) and transition dipole moment (Hartree*Bohr, indicated in brackets) of S_0-Sn		
		S_0-S_1	S_0-S_2 (CT Y149)	S_0-S_3
Trans1	V151, S_0-min	2.98 (2.44)	-	5.07 (0.60)
	V151, R(O-H)=1.5 Å	2.59 (2.61)	-	4.82 (0.50)
	A151, S_0-min	2.98 (2.50)	-	5.06 (0.65)
	V151, S_0-min, CT[a)]	2.82 (2.67)	3.92(0.05)	5.00 (0.69)
Trans2	V151, S_0-min	2.90 (2.77)	-	4.95 (2.76)
	V151, R(O-H)=1.5 Å	2.55 (3.03)	-	4.71 (0.61)
	L151, S_0-min	2.86 (2.78)	-	4.94 (0.75)
	V151, S_0-min, CT[a)]	2.78 (3.00)	4.74 (0.002)	5.04 (0.79)

a) The SA4-CASSCF(4e,3MO) calculations.

Table S5. Vibrational energy levels (cm^{-1}) relative to the S_0-min[a)] energy and energies of the vibronic transition computed for one-dimensional electronic potentials presented in Supplementary figure S9. In brackets, the energies are presented in eV to facilitate comparison with figure S9c.

Chromophore conformation	S_0 state		S_1 state		S_0-S_1 vibronic transitions	
Trans1	S_0-min[a)]	0	VEE[b)]	24071 (2.98 eV)		
	v=0	1724	*v*=0	24390	0-0	22666 (2.81 eV)
	v=1	4333	*v*=1	25655	0-1	23931 (2.97 eV)
	v=2	6146	*v*=2	27211	0-2	25487 (3.16 eV)
	v=3	7952	*v*=3	28936	0-3	27212 (3.37 eV)
	v=4	9867	*v*=4	30833	0-4	29109 (3.61 eV)
	v=5		*v*=5	32902	0-5	31178 (3.87 eV)
Trans2	S_0-min[a)]	0	VEE [b)]	23445 (2.91 eV)		
	v=0	965	*v*=0	22027	0-0	21062 (2.61 eV)
	v=1	1541	*v*=1	23194	0-1	22229 (2.76 eV)
	v=2	2472	*v*=2	24196	0-2	23231 (2.88 eV)
	v=3	3575	*v*=3	25237	0-3	24272 (3.01 eV)
	v=4	4836	*v*=4	26476	0-4	25511 (3.16 eV)

a) $S_{0\text{-min}}$ indicates the minimum-energy geometry in the S_0 state;
b) VEE stands for vertical excitation energy.

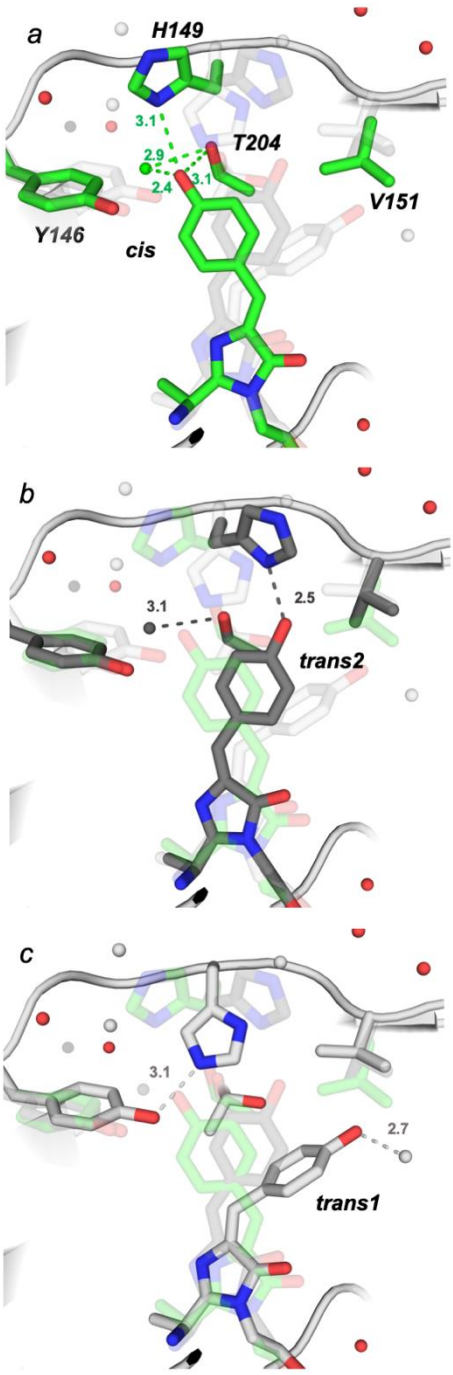

Supplementary figure S1: Environment of the chromophore in its *cis* (a; green), *trans2* (b; dark grey) and *trans1* (c; light grey) conformation in the parental rsEGFP2 *off*-state structure (PDB entry 7O7U). Water molecules belonging to all three chromophore conformations are shown in red. Hydrogen-bond lengths are in Ångstrom.

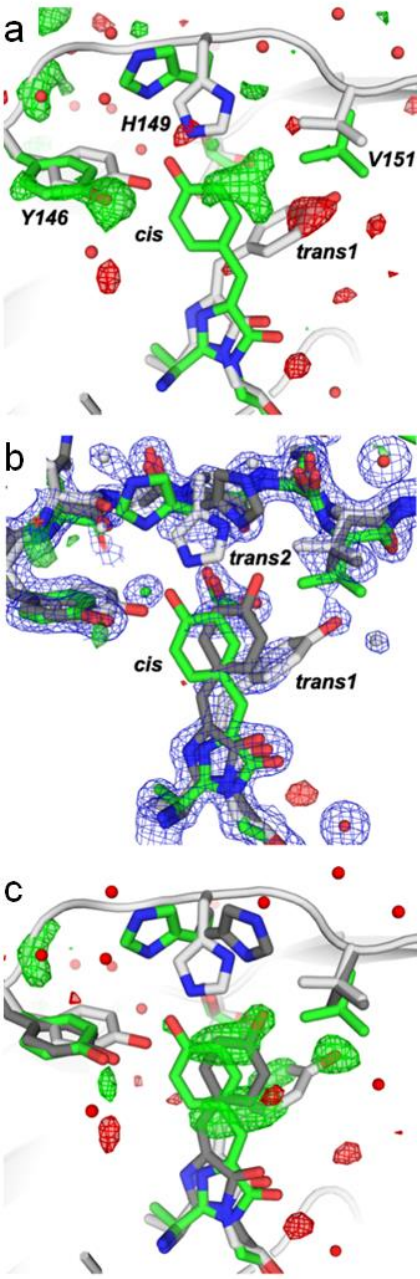

Supplementary figure S2: Structure of parental rsEGFP2 in its *off*-state solved from RT SFX data. (a) Residual $F_{obs} - F_{calc}$ map (green, 3σ ; red, -3σ) of the parental rsEGFP2 in the *off*-state calculated with a model containing a *cis* (light green) and a *trans1* chromopore (light grey) at an occupancy of 30 and 70%, respectively. (b) Final model of parental rsEGFP2 in the *off*-state (PDB entry 7O7U) with occupancies of *cis* (green), *trans1* (light grey) and *trans2* (dark grey) chromophore conformations of 30%, 40% and 30%, respectively. Superimposed are the 2 $F_{obs} - F_{calc}$ (blue, 1 σ) and $F_{obs} - F_{calc}$ (green, 3 σ ; red, -3 σ) maps. (c) $F_{obs} - F_{calc}$ omit map (hydroxybenzylidene moiety omitted from the model; green, 3 σ ; red, -3 σ), overlaid with the model of parental rsEGFP2 in the *off*-state (PDB entry 7O7U).

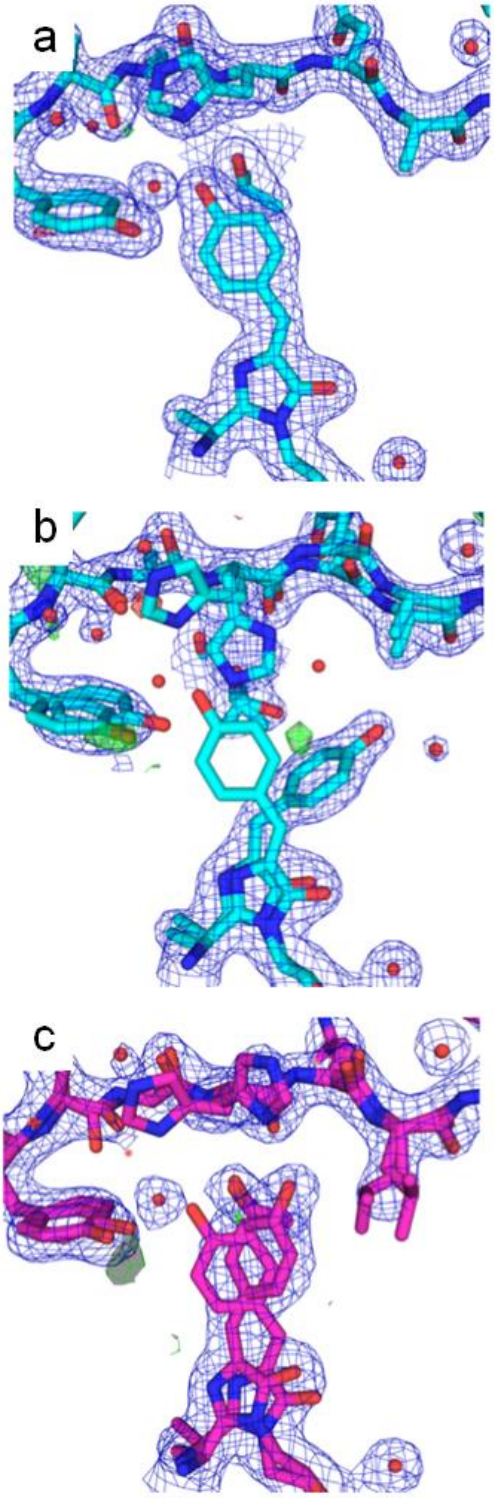

Supplementary figure S3: Zoom on the chromophore (p-hydroxybenzylidene imidazolinone, p-HBI) region in crystal structures of (a) the rsEGFP2-V151A variant in its *on*- (PDB entry 7O7V) and (b) *off*-state (PDB entry 7O7X) and (c) the V151L variant in its *off*-state (PDB entry 7O7W) solved from SFX data collected at room temperature. $2F_{obs} - F_{calc}$ (1σ) and $F_{obs} - F_{calc}$ (+/- 3σ) electron density maps are shown in blue and green/red, respectively.

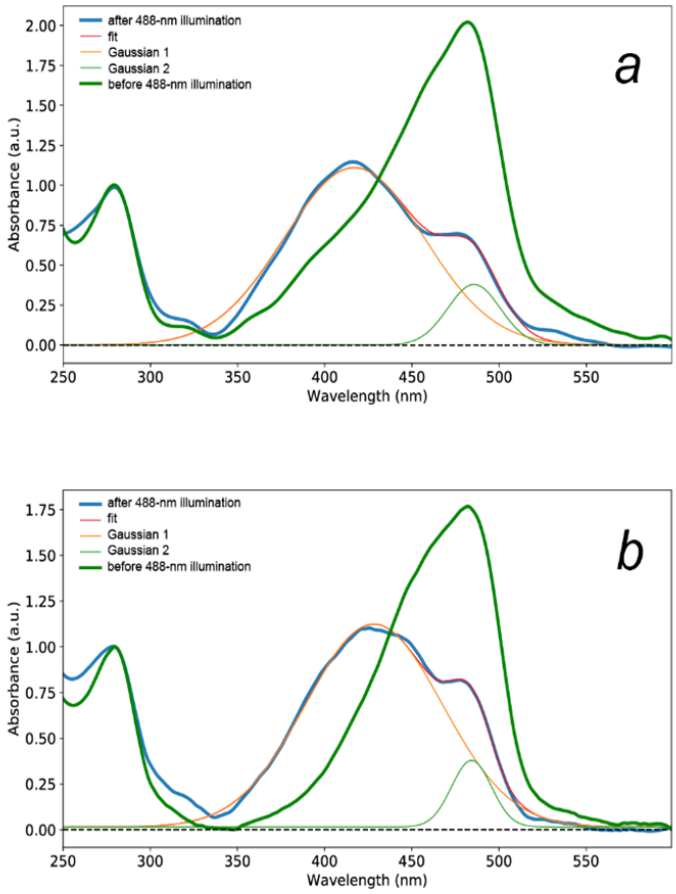

Supplementary figure S4: Absorption spectra of rsEGFP2-V151A (*a*) and -V151L (*b*) microcrystals before (green) and after having been pre-illuminated (blue) at a laser power of nominally 200 mW within a custom-made device [9] during an SFX experiment at SACLA (July 2018) after background subtraction, smoothening with a Savitzky-Golay filter and normalization at 280 nm. The spectrum after 488 nm illumination was modeled by a sum of two Gaussians (Gaussian 1 at 400 nm shown in orange and Gaussian 2 at 482 nm shown in light green). The absorbance of Gaussian 2 at 482 nm relative to the absorbance at 482 nm of the spectrum before 488 nm illumination (assumed to correspond to 100% *on*-state) indicates that 85% (77%) were switched to the *off*-state for rsEGFP2-V151A (V151L) and 15% (23%) remained in the *on*-state.

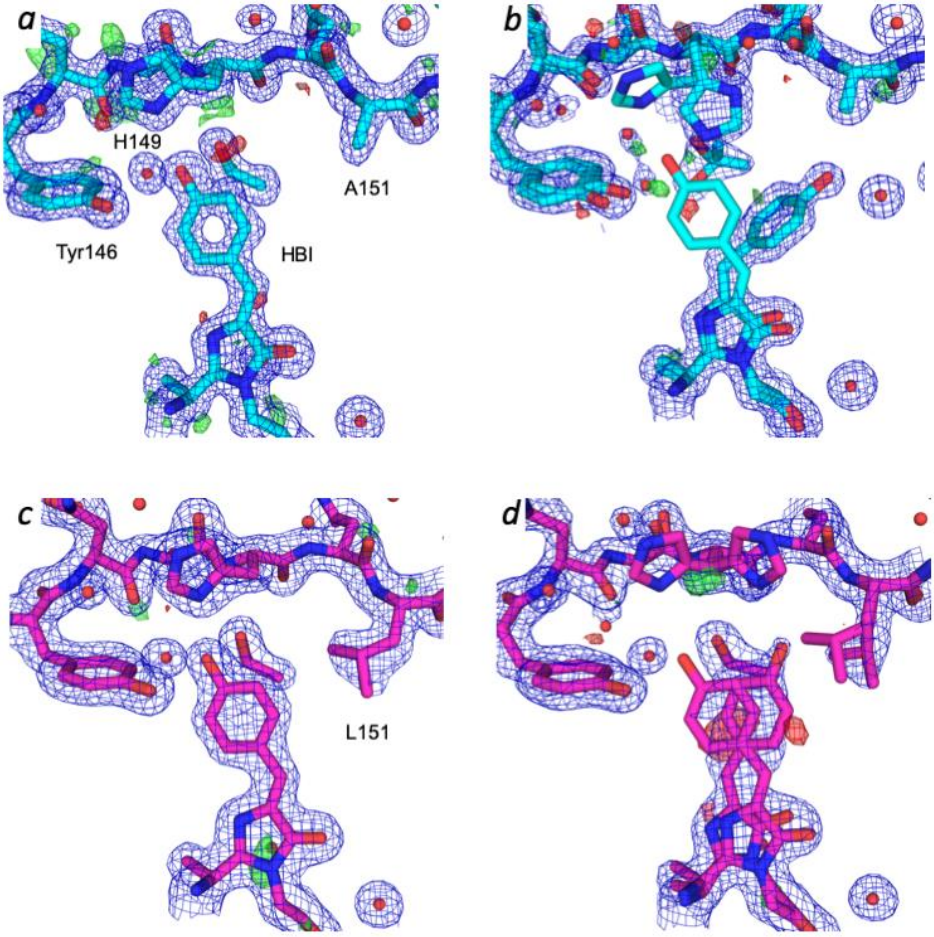

Supplementary figure S5: Zoom on the chromophore (p-hydroxybenzylidene imidazolinone, p-HBI) region in crystal structures of rsEGFP2 variants V151A (cyan) and V151L (purple) in their *on*- and *off*-states solved from synchrotron data collected at cryo-temperature. (*a, b*) Electron density maps (mesh) and models of the rsEGFP2-V151A variant in the (*a*) *on*- (PDB entry 7O7D) and (*b*) *off*-state (PDB entry 7O7C). (*c, d*) Electron density maps (mesh) and models of the rsEGFP2-V151L variant in the (*c*) *on*- (PDB entry 7O7E) and (*d*) *off*-state (PDB entry 7O7H). In (*d*) an alternate conformation of the chromophore corresponding to the *cis* isomer of the *on*-state remains in the *off*-state. $2F_{obs}$-F_{calc} (1 σ) and F_{obs}-F_{calc} (+/- 3 σ) electron density maps are shown in blue and green/red, respectively.

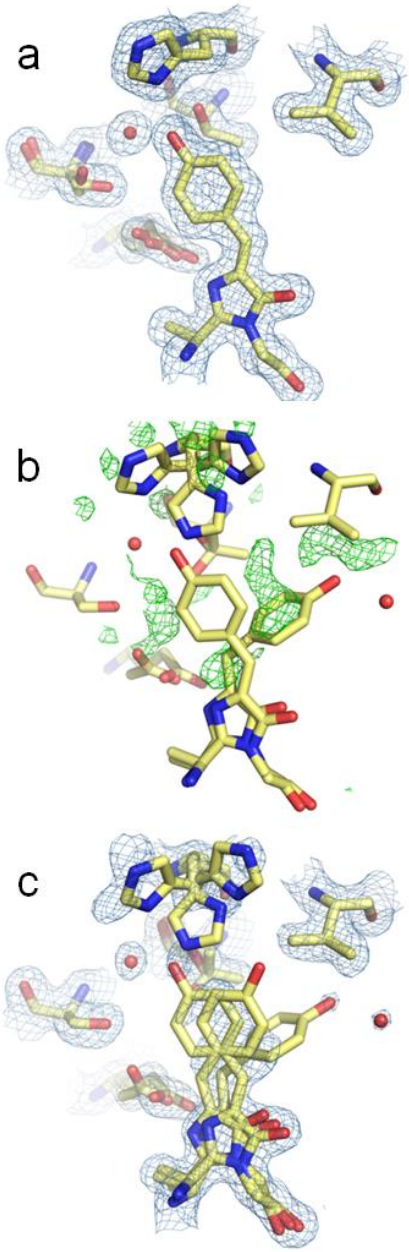

Supplementary figure S6: rsFolder2 *on*- and *off*-state structures featuring evidence for a low occupancy *trans2* conformation in monomer A, derived from synchrotron cryo-crystallographic data. Electron density $2F_{obs}$-F_{calc} maps are shown as a blue mesh at 1σ and the F_{obs}-F_{calc} difference map is shown as a green mesh at 3 σ. (a) Active site environment for the *on*-state structure (PDB entry 7AMB), with a fully occupied *cis* chromophore. (b) active site for the *off*-structure, where only *cis* and *trans1* conformers have been included in the model for refinement. NCS averaged difference map is shown in green, indicating the presence of the *trans2* conformer. (c) refined *off*-state model (PDB entry 7AMF) for monomer A, with *cis* (60%), *trans1* (30%) and *trans2* (10%).

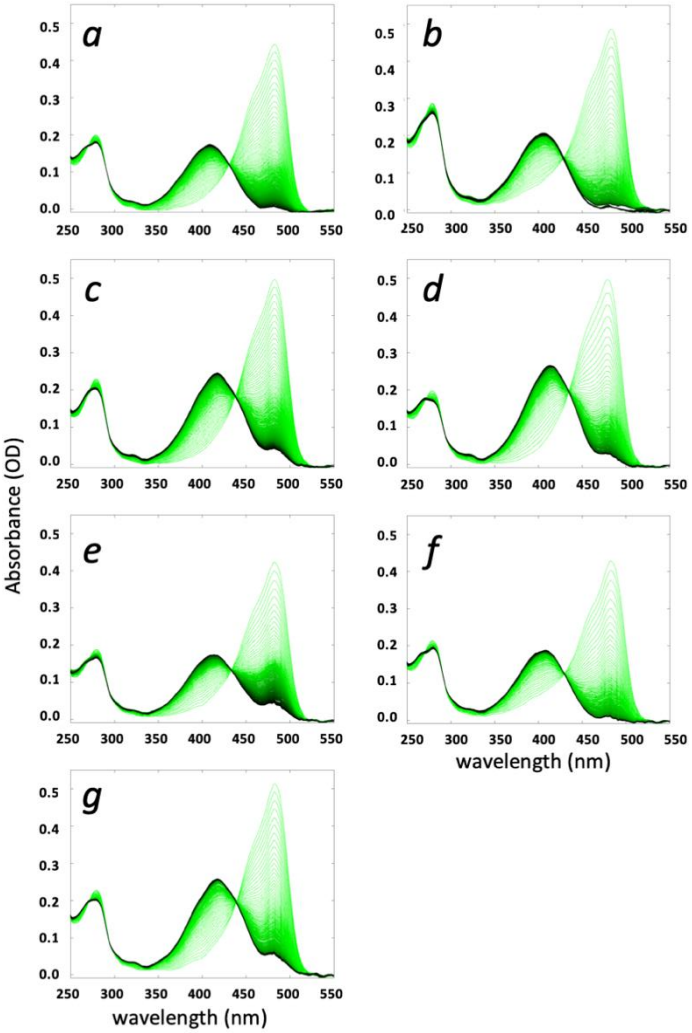

Supplementary figure S7: Absorption spectra along *on*-to-*off* photoswitching of the RSFPs presented in this study measured in solution in HEPES buffer at pH 7.5. Photoswitching series of spectra are color-coded from light green (*on*) to black (*off*) for rsEGFP2 (a), rsEGFP2-V151A (b), rsEGFP2-V151L (c), rsFolder (d), rsFolder2 (e), rsFolder2-V151A (f) and rsFolder2-V151L (g).

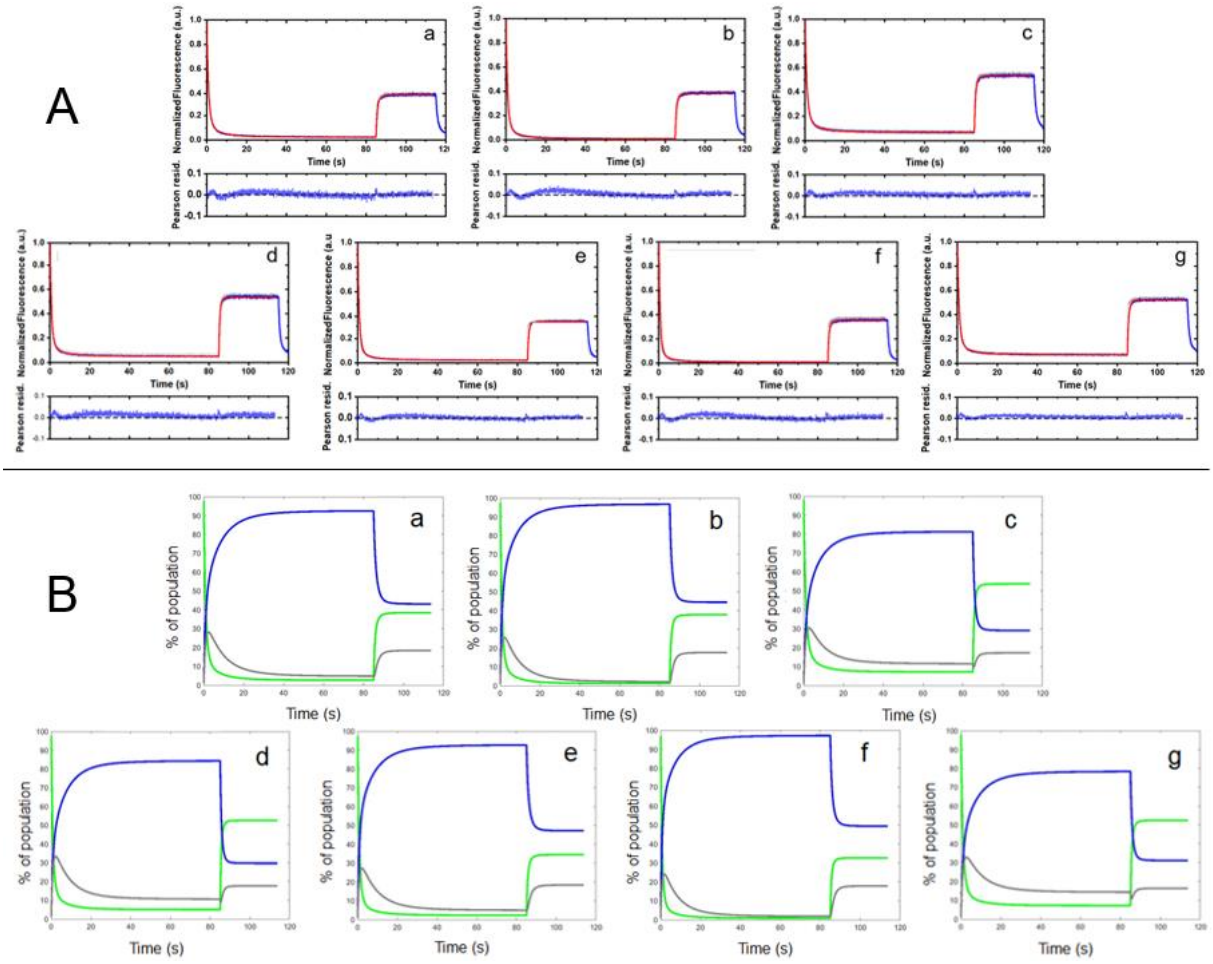

Supplementary figure S8: Switching curves (A) and concentration plots (B) for rsEGFP2 (a), rsEGFP2-V151A (b), rsEGFP2-V151L (c), rsFolder (d), rsFolder2 (e), rsFolder2-V151A (f) and rsFolder2-V151L (g).

A: Fluorescence switching curves. The mean of six measurements is represented in blue with a standard deviation in grey. Data was fitted with a model (red) that includes an additional dark state. Pearson residuals below each graph demonstrate the goodness of fit.

B: Concentration plots. The percentage of protein population are shown in the *on*-state (green), the *off*-state (blue) and in the additional dark state (grey) along the switching cycle. The fluorescence profile of the full switching cycle was fitted with a kinetic model including two reversible dark-states.

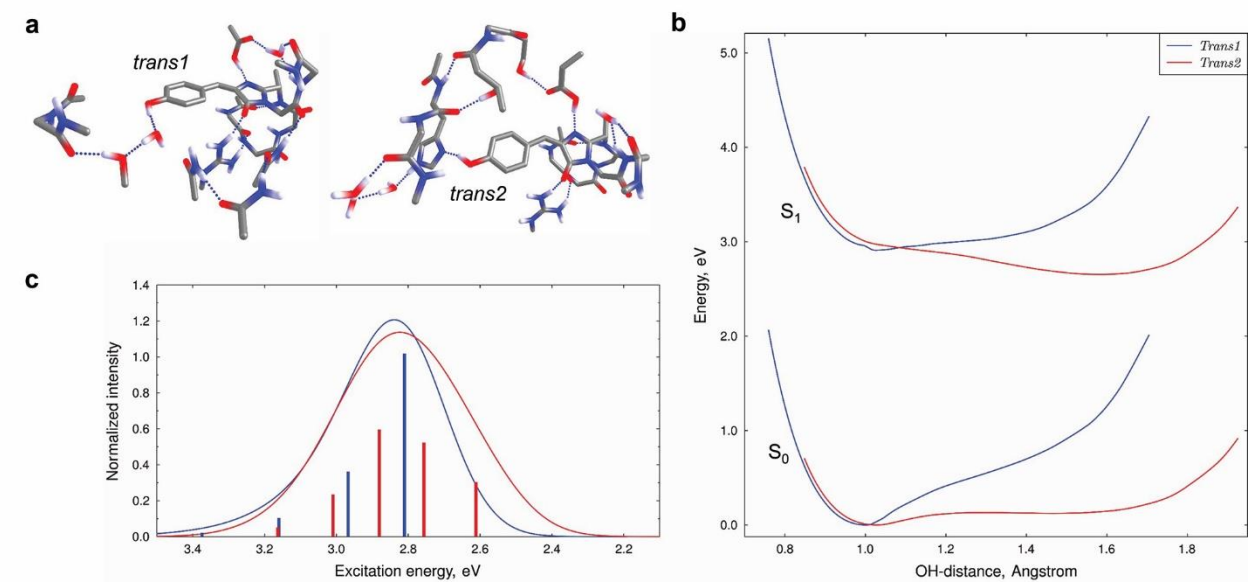

Supplementary figure S9. The phenolic group OH-stretching potentials in the ground and excited states and corresponding vibronic band of the S_0-S_1 transition. Panel (a) demonstrates models of the chromophore in the *trans1* and *trans2* configurations employed in computations. Panel (b) presents the S_0 and S_1 energies computed with the XMCQDPT2-SA3-CASSCF(2e,2MO) method at the geometries obtained by performing relaxed OH-stretching energy scans in the ground state utilizing the B3LYP-D3/cc-pvdz method. The S_1 energies demonstrate that electronically excited *trans2* chromophore undergoes deprotonation. The S_0 and S_1 OH-stretching potentials were used to simulate the vibronic band shown in panel (c). The energies and probability density of vibrational states were computed for the one-dimensional potentials presented in panel (b) using a numerical procedure. The resulting energies of vibronic transitions are collected in Supplementary table S5. The intensities of vibronic transitions were normalized to the S_0-S_1 transition dipole moments computed with the XMCQDPT2-SA3-CASSCF(2e,2MO) method at the S_0-min equilibrium geometries optimized with the B3LYP-D3/cc-pvdz method. The simulated spectral bands were obtained by broadening the computed stick spectra with Gaussian functions (1000 cm^{-1} FWHM). Panel (c) demonstrates that the red-shifted band predicted for *trans2* isomer results from lowering the 0-0 transition energy (2.6 eV and 2.8 eV for *trans2* and *trans1*, respectively).

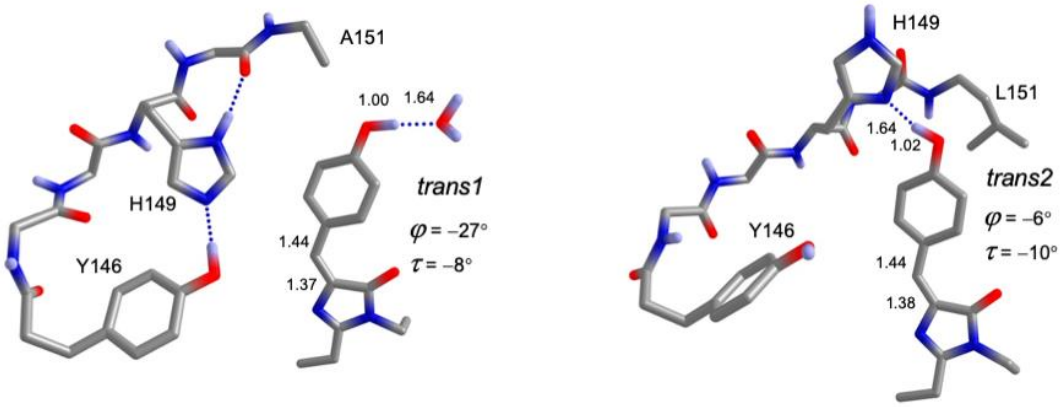

Supplementary figure S10: Optimized geometries obtained for the active sites containing the V151A (left) and V151L (right) substitutions. The initial coordinates of the atoms were obtained by substituting the Val151 side chain of parental rsEGFP2 (PDB entry 6T39 [3]) by Ala or Leu side chains. The geometry was optimized with the B3LYP-D3/cc-pvdz method. At the optimized geometries, the excitation energies were computed with the XMCQDPT2/cc-pvdz method (SA3-CASSCF(2,2) wave function). The excitation energies and transition moments are compared with those obtained for rsEGFP2 active-site models are presented in Supplementary table S4.

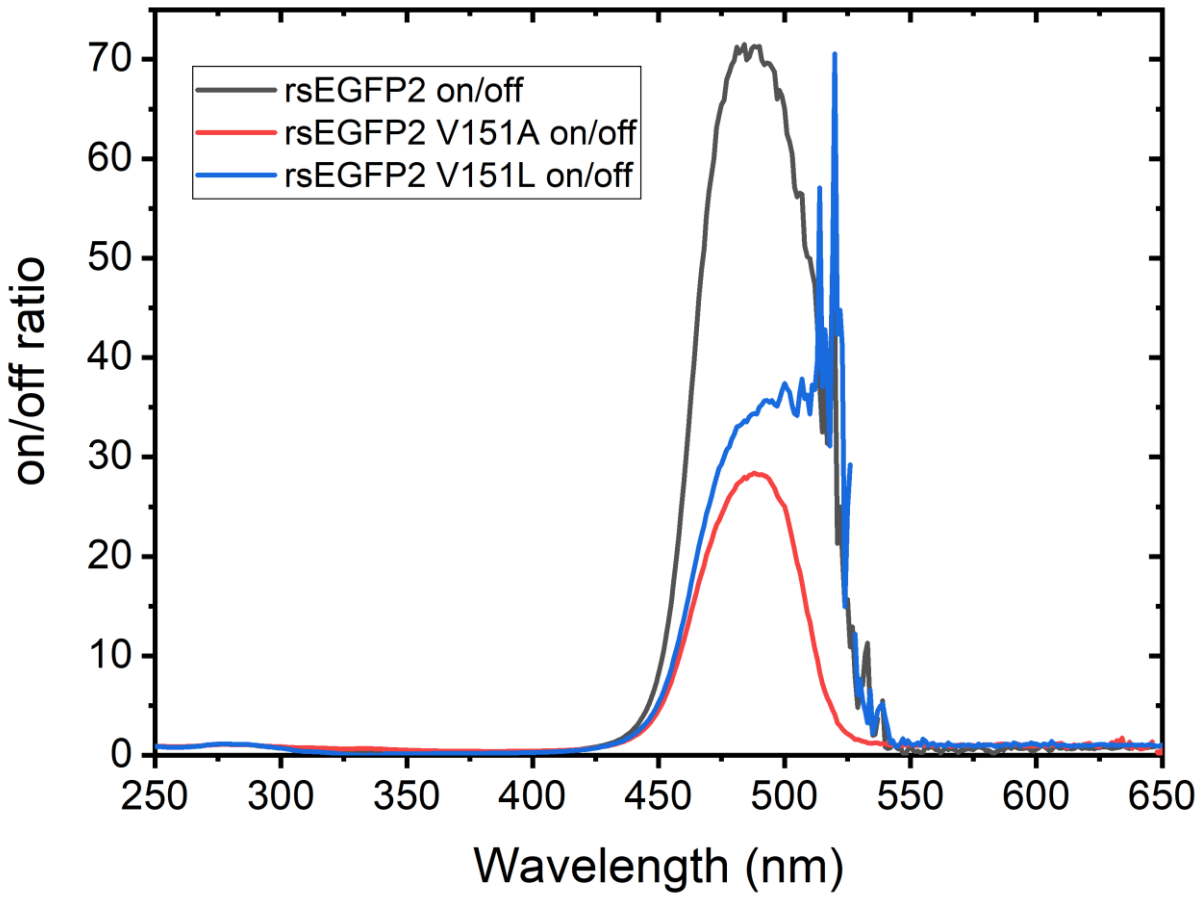

Supplementary figure S11: Ratiometric absorption spectra for the different variants. It can be seen that a significant improvement in switching contrast, assuming wavelength independent photoswitching quantum yields, is not expected at wavelengths red shifted relative to 488 nm (despite the fact that at wavelengths > ~520 nm the noise prevents a reliable comparison).

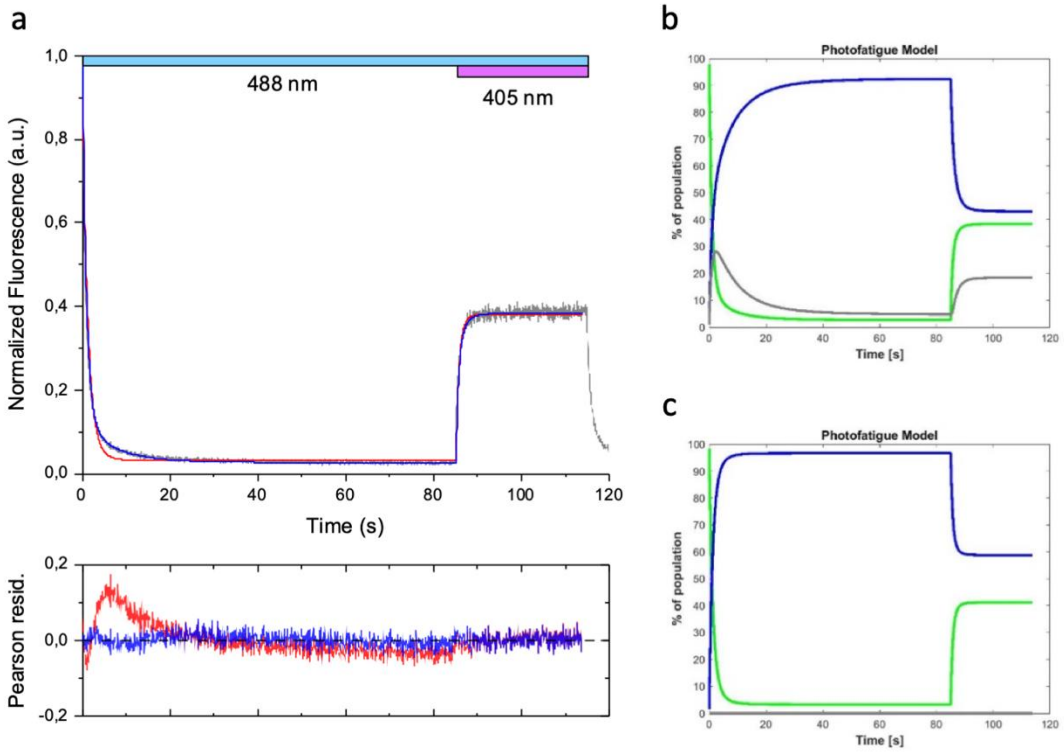

Supplementary figure S12: Additional dark state during photoswitching of parent rsEGFP2. (a) Fitted switching profiles using a model that includes (blue) or does not include (red) an additional dark state, overlaid on experimental switching profile (grey); Pearson residuals for each fit (bottom panel). (b, c) Fitted populations along time for both models (*on*-state in green, *off*-state in blue and the additional dark state in grey).

.

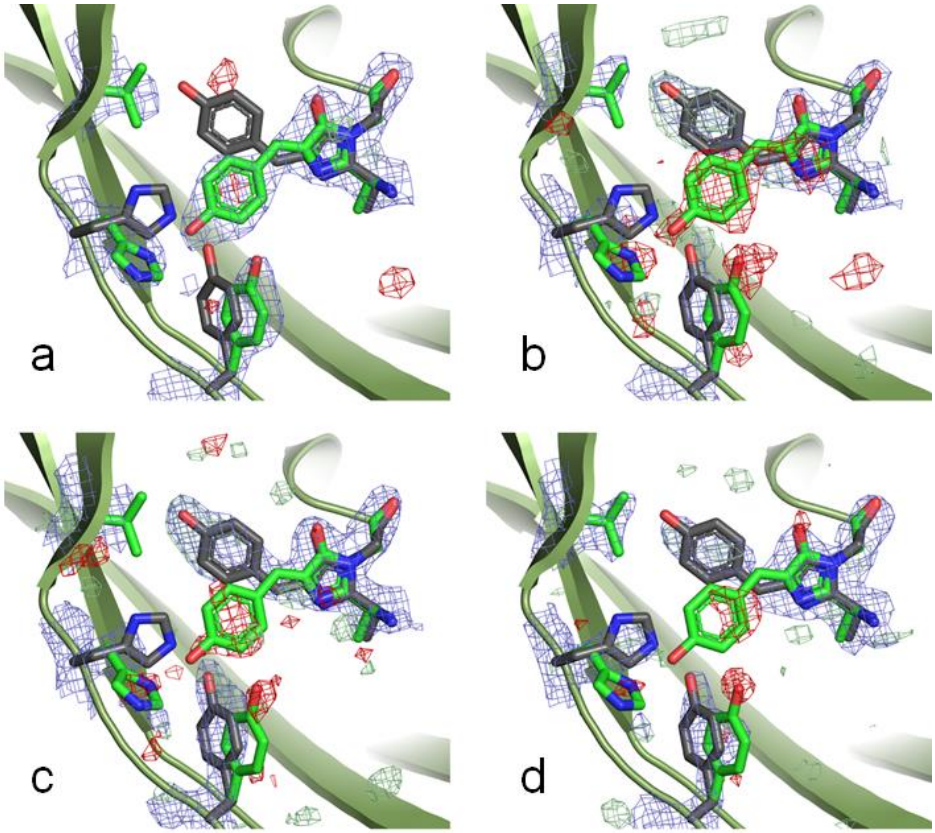

Supplementary figure S13: Synchrotron cryo-structures and electron density maps of rsEGFP2 photoswitched at different power densities. Each crystal was photoswitched during ~30 s at 100 mW/cm² (a), 200 mW/cm² (b), 400 mW/cm² (c) or 800 mW/cm² (d) and immediately cryoprotected and flash-cooled. $2F_{obs} - F_{calc}$ electron density maps (blue) are shown at 1.5 σ, $F_{obs} - F_{calc}$ difference electron density maps are shown at 3 σ (green) and -3σ (red).

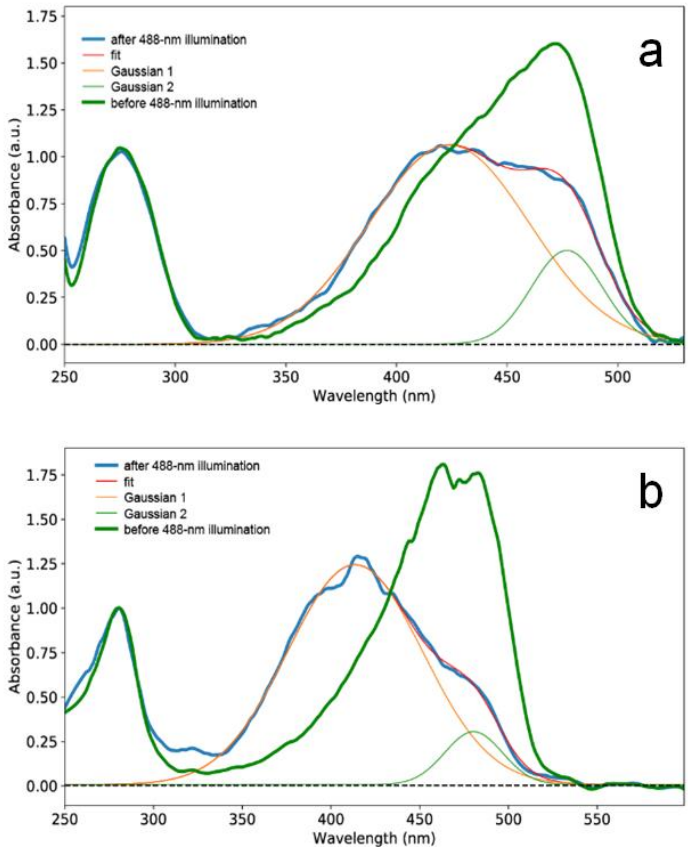

Supplementary figure S14: Absorption spectra of parental rsEGFP2 microcrystals before (green) and after having been pre-illuminated (blue) at a laser power of nominally 200 mW within a custom-made device [9] during SFX experiments at the LCLS in June 2016 (LM47) (a) and at SACLA in July 2015 [3] (b) after background subtraction, smoothening with a Savitzky-Golay filter and normalization at 280 nm. The spectrum after 488 nm illumination was modeled by a sum of two Gaussians (Gaussian 1 at 400 nm and Gaussian 2 at 482 nm). The absorbance at 482 nm as fitted by Gaussian 2 relative to the absorbance at 482 nm of the spectrum before 488 nm illumination (assumed to correspond to 100% *on*-state) indicates that 66% (84%) were switched to the *off*-state in panel a (b) and 34% (16%) remained in the *on*-state.

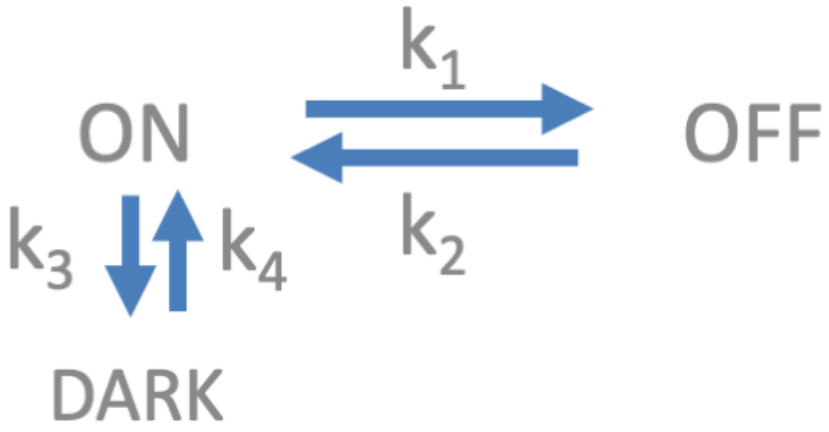

Supplementary figure S15: Kinetic scheme used to fit the switching data

References

[1] N. Coquelle, M. Sliwa, J. Woodhouse, G. Schirò, V. Adam, A. Aquila, T. R. M. Barends, S. Boutet, M. Byrdin, S. Carbajo, E. De la Mora, R. B. Doak, M. Feliks, F. Fieschi, L. Foucar, V. Guillon, M. Hilpert, M. S. Hunter, S. Jakobs, J. E. Koglin, G. Kovacsova, T. J. Lane, B. Lévy, M. Liang, K. Nass, J. Ridard, J. S. Robinson, C. M. Roome, C. Ruckebusch, M. Seaberg, M. Thepaut, M. Cammarata, I. Demachy, M. Field, R. L. Shoeman, D. Bourgeois, J.-P. Colletier, I. Schlichting, M. Weik, *Nature Chemistry* **2018**, *10*, 31-37.

[2] M. Byrdin, D. Bourgeois, *Spectroscopy Europe* **2016**, *28*, 14-17.

[3] J. Woodhouse, G. Nass Kovacs, N. Coquelle, L. M. Uriarte, V. Adam, T. R. M. Barends, M. Byrdin, E. de la Mora, R. Bruce Doak, M. Feliks, M. Field, F. Fieschi, V. Guillon, S. Jakobs, Y. Joti, P. Macheboeuf, K. Motomura, K. Nass, S. Owada, C. M. Roome, C. Ruckebusch, G. Schirò, R. L. Shoeman, M. Thepaut, T. Togashi, K. Tono, M. Yabashi, M. Cammarata, L. Foucar, D. Bourgeois, M. Sliwa, J.-P. Colletier, I. Schlichting, M. Weik, *Nature Communications* **2020**, *11*, 741.

[4] L. Lomb, J. Steinbrener, S. Bari, D. Beisel, D. Berndt, C. Kieser, M. Lukat, N. Neef, R. L. Shoeman, *Journal of Applied Crystallography* **2012**, *45*, 674-678.

[5] U. Weierstall, J. C. Spence, R. B. Doak, *The Review of scientific instruments* **2012**, *83*, 035108.

[6] M. Liang, G. J. Williams, M. Messerschmidt, M. M. Seibert, P. A. Montanez, M. Hayes, D. Milathianaki, A. Aquila, M. S. Hunter, J. E. Koglin, D. W. Schafer, S. Guillet, A. Busse, R. Bergan, W. Olson, K. Fox, N. Stewart, R. Curtis, A. A. Miahnahri, S. Boutet, *Journal of synchrotron radiation* **2015**, *22*, 514-519.

[7] K. Tono, E. Nango, M. Sugahara, C. Song, J. Park, T. Tanaka, R. Tanaka, Y. Joti, T. Kameshima, S. Ono, T. Hatsui, E. Mizohata, M. Suzuki, T. Shimamura, Y. Tanaka, S. Iwata, M. Yabashi, *Journal of synchrotron radiation* **2015**, *22*, 532-537.

[8] M. Yabashi, H. Tanaka, T. Ishikawa, *Journal of synchrotron radiation* **2015**, *22*, 477-484.

[9] G. Schiro, J. Woodhouse, M. Weik, I. Schlichting, R. L. Shoeman, *Journal of Applied Crystallography* **2017**, *50*, 932-939.

[10] G. Blaj, P. Caragiulo, G. Carini, S. Carron, A. Dragone, D. Freytag, G. Haller, P. Hart, J. Hasi, R. Herbst, S. Herrmann, C. Kenney, B. Markovic, K. Nishimura, S. Osier, J. Pines, B. Reese, J. Segal, A. Tomada, M. Weaver, *Journal of synchrotron radiation* **2015**, *22*, 577-583.

[11] L. Foucar, *Journal of Applied Crystallography* **2016**, *49*, 1336-1346.

[12] N. Coquelle, A. S. Brewster, U. Kapp, A. Shilova, B. Weinhausen, M. Burghammer, J.-P. Colletier, *Acta Crystallographica Section D* **2015**, *71*, 1184-1196.

[13] T. White, *Acta Crystallographica Section D* **2019**, *75*.

[14] A. J. McCoy, R. W. Grosse-Kunstleve, P. D. Adams, M. D. Winn, L. C. Storoni, R. J. Read, *Journal of Applied Crystallography* **2007**, *40*, 658-674.

[15] G. N. Murshudov, P. Skubak, A. A. Lebedev, N. S. Pannu, R. A. Steiner, R. A. Nicholls, M. D. Winn, F. Long, A. A. Vagin, *Acta crystallographica. Section D, Biological crystallography* **2011**, *67*, 355-367.

[16] P. Emsley, B. Lohkamp, W. G. Scott, K. Cowtan, *Acta Crystallographica Section D* **2010**, *66*, 486-501.

[17] D. de Sanctis, A. Beteva, H. Caserotto, F. Dobias, J. Gabadinho, T. Giraud, A. Gobbo, M. Guijarro, M. Lentini, B. Lavault, T. Mairs, S. McSweeney, S. Petitdemange, V. Rey-

Bakaikoa, J. Surr, P. Theveneau, G. A. Leonard, C. Mueller-Dieckmann, *Journal of synchrotron radiation* **2012**, *19*, 455-461.
[18] W. Kabsch, *Acta crystallographica. Section D, Biological crystallography* **2010**, *66*, 133-144.
[19] M. El Khatib, A. Martins, D. Bourgeois, J. P. Colletier, V. Adam, *Scientific reports* **2016**, *6*, 18459.
[20] P. V. Afonine, R. W. Grosse-Kunstleve, N. Echols, J. J. Headd, N. W. Moriarty, M. Mustyakimov, T. C. Terwilliger, A. Urzhumtsev, P. H. Zwart, P. D. Adams, *Acta Crystallographica Section D* **2012**, *68*, 352-367.
[21] W. L. DeLano, *San Carlos, CA, USA: DeLano Scientific* **2002**.
[22] L. Potterton, J. Agirre, C. Ballard, K. Cowtan, E. Dodson, P. R. Evans, H. T. Jenkins, R. Keegan, E. Krissinel, K. Stevenson, A. Lebedev, S. J. McNicholas, R. A. Nicholls, M. Noble, N. S. Pannu, C. Roth, G. Sheldrick, P. Skubak, J. Turkenburg, V. Uski, F. von Delft, D. Waterman, K. Wilson, M. Winn, M. Wojdyr, *Acta Crystallographica Section D* **2018**, *74*, 68-84.
[23] C. J. Williams, J. J. Headd, N. W. Moriarty, M. G. Prisant, L. L. Videau, L. N. Deis, V. Verma, D. A. Keedy, B. J. Hintze, V. B. Chen, S. Jain, S. M. Lewis, W. B. Arendall Iii, J. Snoeyink, P. D. Adams, S. C. Lovell, J. S. Richardson, D. C. Richardson, *Protein Science* **2018**, *27*, 293-315.
[24] M. W. Schmidt, K. K. Baldridge, J. A. Boatz, S. T. Elbert, M. S. Gordon, J. H. Jensen, S. Koseki, N. Matsunaga, K. A. Nguyen, S. Su, T. L. Windus, M. Dupuis, J. A. Montgomery Jr, *Journal of Computational Chemistry* **1993**, *14*, 1347-1363.
[25] aA. D. Becke, *The Journal of Chemical Physics* **1993**, *98*, 5648-5652; bC. Lee, W. Yang, R. G. Parr, *Physical Review B* **1988**, *37*, 785-789; cS. Grimme, J. Antony, S. Ehrlich, H. Krieg, *J Chem Phys* **2010**, *132*, 154104.
[26] A. A. Granovsky, *J Chem Phys* **2011**, *134*, 214113.
[27] R. J. Cave, M. D. Newton, *Chemical Physics Letters* **1996**, *249*, 15-19.
[28] D. E. Woon, T. H. D. Jr., *The Journal of Chemical Physics* **1995**, *103*, 4572-4585.
[29] aE. De Zitter, J. Ridard, D. Thédié, V. Adam, B. Lévy, M. Byrdin, G. Gotthard, L. Van Meervelt, P. Dedecker, I. Demachy, D. Bourgeois, *Journal of the American Chemical Society* **2020**, *142*, 10978-10988; bE. De Zitter, D. Thédié, V. Mönkemöller, S. Hugelier, J. Beaudouin, V. Adam, M. Byrdin, L. Van Meervelt, P. Dedecker, D. Bourgeois, *Nature Methods* **2019**, *16*, 707-710; cR. Berardozzi, V. Adam, A. Martins, D. Bourgeois, *J Am Chem Soc* **2016**, *138*, 558-565.
[30] J. Chang, M. G. Romei, S. G. Boxer, *J Am Chem Soc* **2019**, *141*, 15504-15508.
[31] S. Duwé, E. De Zitter, V. Gielen, B. Moeyaert, W. Vandenberg, T. Grotjohann, K. Clays, S. Jakobs, L. Van Meervelt, P. Dedecker, *ACS nano* **2015**, *9*, 9528-9541.